UNIVERSIDADE DE LISBOA
FACULDADE DE CIÊNCIAS

An exotic Universe: from dark energy to wormholes

" Documento Definitivo"

Doutoramento em Astronomia e Astrofísica

Bruno Jorge Castelo Branco de Barros

Tese orientada por:
Doutor Nelson Nunes
Doutor Tiago Barreiro

Documento especialmente elaborado para a obtenção do grau de doutor

2020

UNIVERSIDADE DE LISBOA

FACULDADE DE CIÊNCIAS

Ciências
ULisboa

An exotic Universe: from dark energy to wormholes

Doutoramento em Astronomia e Astrofísica

Bruno Jorge Castelo Branco de Barros

Tese orientada por:

Doutor Nelson Nunes

Doutor Tiago Barreiro

Júri:

Presidente:

- Doutor José Manuel Nunes Vicente Rebordão, Investigador Coordenador e Presidente do Departamento de Física da Faculdade de Ciências da Universidade de Lisboa

Vogais:

- Doutor Sante Carloni, Ricercatori a tempo determinato da Scuola Politecnica da Università di Genova (Itália)
- Doutor Alvaro de La Cruz-Dombriz, Senior Lecturer da Faculty of Science da University of Cape Town (África do Sul)
- Doutor Tiago Manuel Duarte Marques Barreiro, Professor Auxiliar da Escola de Ciências Económicas e das Organizações da Universidade Lusófona (Orientador)
- Doutora Noemi Frusciante, Investigadora Júnior da Faculdade de Ciências da Universidade de Lisboa

Documento especialmente elaborado para a obtenção do grau de doutor

Trabalho financiado pela Fundação para a Ciência e a Tecnologia através da bolsa de doutoramento PD/BD/128018/2016

2020

(Come chocolates, pequena;

Come chocolates!

Olha que não há mais metafísica no mundo senão chocolates.

Olha que as religiões todas não ensinam mais que a confeitaria.

Come, pequena suja, come!

Pudesse eu comer chocolates com a mesma verdade com que comes!

Mas eu penso e, ao tirar o papel de prata, que é de folhas de estanho,

Deito tudo para o chão, como tenho deitado a vida.)

From *Tabacaria*,

by Álvaro de Campos (Fernando Pessoa)

Acknowledgments

I would like to express my gratitude to some people that have contributed, directly or indirectly, to the completion of this PhD. First, to my supervisors, Nelson Nunes and Tiago Barreiro, for all the motivation and constant help when any problem arose throughout these arduous, but stimulating, four years. To all the IA Cosmology group members, or people that were part of it during these years, in particular, Francisco Lobo, Noemi Frusciante, Ippocratis Saltas, Ismael Tereno, José Pedro Mimoso, Lara Sousa, Daniele Vernieri, Martina Vicinanza, Ángeles Moliné, António da Silva and Alberto Rozas-Fernández. To my fellow office colleagues, Rita Neves, Ismael Ayuso, Francisco Cabral, Diogo Castelão and Cédric Pereira, for all the good times. To the genuine care, unconditional friendship, and all the literature matters, a tender gratitude to Víctor da Fonseca. To Vasco Ferreira for all the good conversations, chess games and, hopefully, what is still yet to come. To Sante Carloni for the academic support and presence during my PhD evaluations. To João Lin Yun for all the guidance. I would also like to thank my external collaborators, in particular, Tomi Koivisto, Luca Amendola, Tiberiu Harko and Bogdan Dănilă for the scientific contribution, and the Heidelberg group for hosting me. To Elsa for all the emotional and intellectual support. To my long lasted friends from Forte da Casa (and Vialonga), whose presence have helped me to preserve my sanity and welfare. Finally to my father, for giving me care and shelter during these years, and to my family.

This PhD was financially supported by Fundação para a Ciência e a Tecnologia (FCT, Portugal) through the grant PD/BD/128018/2016.

Resumo

A presente tese explora teorias modificadas da relatividade geral e as suas aplicações na cosmologia e gravitação. Esta dissertação centra-se maioritariamente em modelos de energia escura conduzidos por campos escalares acoplados a matéria escura. No estudo destes modelos, serão apresentadas algumas possíveis respostas para problemas que o modelo padrão da cosmologia actual enfrenta. São feitas previsões para missões futuras que nos permirão desvendar alguns mistérios do lado escuro do Universo. São também exploradas formulações alternativas à relatividade geral, no âmbito de aliviar o problema actual da discrepância entre diferentes observações relativamente ao parametro cosmológico $f\sigma_8$, que o modelo ΛCDM enfrenta. Serão também estudados túneis no espaço tempo, extendendo a relatividade geral pela adição de um novo campo tensorial exótico. Será apresentada uma teoria efetiva modificada da gravidade onde a singularidade inicial, prevista pelo modelo padrão, é substituída por um ressalto cósmico. No primeiro capítulo, o leitor encontra uma breve introdução à relatividade geral e as principais motivações para extendê-la.

O segundo capítulo propõe um novo modelo de energia escura acoplada a uma componente de matéria sem pressão, onde a interação é mediada pelo termo cinético de um campo escalar descrito por um Lagrangeano do tipo k-essence. É apresentada a ação para a teoria, e as equações de campo juntamente com as relações de conservação para as componentes que interagem entre si. O modelo é seguidamente particularizado para uma teoria que considera um campo de quintessência canónico, cineticamente acoplado a uma espécie de matéria escura, a partir de um termo da forma $X^\alpha \mathcal{L}_m$, onde $X = \frac{1}{2} g^{\mu\nu} \partial_\mu \phi \partial_\nu \phi$ representa a energia cinética do campo escalar ϕ. É feita uma análise de sistemas dinâmicos às equações do movimento, onde são encontrados os pontos fixos e é feito o estudo da sua estabilidade. Uma novidade bastante aliciante deste modelo é a presença de um regime *scaling* durante a evolução do Universo, que pode ser utilizado como resposta ao problema da coincidência cósmica. Como demonstrado, este comportamento é apenas possível devido à emergência de dois novos pontos fixos, quando o acoplamento cinético está presente. É analisada a dinâmica do *background* da cosmologia, onde as equações são numericamente evoluídas, e é estudada a influência da interação no comportamento dos principais parâmetros cosmológicos, como a densidade de energia de cada espécie, parâmetro de Hubble e equação de estado. Finalmente, é apresentado um constrangimento para a o acoplamento, a partir de observações da missão Planck, e é discutido alternativas para aliviar este valor limite.

O terceiro capítulo começa por escrever a ação para um campo escalar canónico ϕ con-

siderando acoplamentos conformes a uma componente de matéria escura. Estes acoplamentos são motivados por transformações conformes, $\tilde{g}_{\mu\nu} = e^{-\kappa\beta\phi} g_{\mu\nu}$, e podem ser igualmente escritos (no referencial de Einstein) com um termo da forma $e^{-\kappa\beta\phi}\mathcal{L}_m$. A particularidade deste modelo, em contraste com os modelos semelhantes já estudados na literatura, é o facto de a expansão do *background* ser forçada a reproduzir a mesma dinâmica que no modelo ΛCDM. É feita uma análise detalhada do *background*, com foco nos desvios causados pela parâmetro de acoplamento β. Depois, são escritas as equações para as perturbações das componentes de matéria (matéria escura mais bariões) no limite de pequenas escalas na *gauge* Newtoniana. Estas são numericamente evoluídas, sendo possível identificar o efeito da interação no crescimento das flutuações de matéria, em particular no parâmetro $f\sigma_8$ que pode ser testado directamente com dados de estrutura de larga escalar no Universo tardio. É feita uma análise de *likelihood* a partir de dados de distorções espaciais no desvio para o vermelho. Os resultados são comparados com as previsões do modelo padrão, e é discutido como este modelo em particular pode aliviar a presente tensão entre dados experimentais do Universo tardio *vs* dados do Universo primitivo. É feita uma previsão da sensibilidade de duas missões futuras, concretamente, Euclid e SKA, relativamente ao número de estruturas a serem detectadas. O próximo passo baseia-se em evoluir as perturbações de segunda ordem da matéria com o objectivo de estudar a dinâmica do colapso esférico e o número de estruturas que são formadas a um dado redshift e com um certo intervalo de massa. Finalmente, é feita uma breve previsão relativamente à expectativa de observação de enxames de galáxias observados por dois rastreios, conduzidos pelo *South Pole Telescope* e pela missão *eROSITA*.

O capítulo 4, apresenta uma formulação alternativa à relatividade geral, onde a gravidade é mediada por um objecto geométrico entitulado não-metricidade, em vez de curvatura, num espaço plano e sem torsão. A ação da teoria é dada tal que a dinâmica das componentes é exactamente a mesma que no modelo padrão ao nível do background. Como é mostrado, irão emergir desvios ao nível linear, onde as perturbações da matéria podem ser suprimidas ou realçadas dependendo do parâmetro livre da teoria. Seguidamente é feita uma análise de *likelihood* semelhante à do capítulo 2, considerando dados de distorções espaciais no desvio para o vermelho. Os resultados são comparados entre si, perante três modelos distintos, sendo um deles o modelo ΛCDM.

O capítulo 5 estuda soluções das equações de Einstein para túneis no espaço-tempo, chamados buracos de verme ou *wormholes*, suportados por um campo tensorial, especificamente uma 3-forma. É dada a ação da teoria e são deduzidas as equações de campo. A construção meticulosa

das componentes da forma diferencial é feita especificamente para a métrica em questão. As equações do movimento são evoluídas onde é dada ênfase ao tópico das condições de energia. Especificamente, é mostrado que é possível a formação de *wormholes* onde a matéria "normal" obedece às condições de energia clássicas. Nestes casos, é a 3-forma que absorve toda a exoticidade, e que é responsável por manter a garganta do *wormhole* aberta, violando assim as condições de energia.

Finalmente, no sexto capítulo, são estudadas teorias de gravidade modificadas, especificamente, gravidade modificada de *Gauss-Bonnet*. Um dos problemas do modelo padrão da cosmologia, é o facto de possuir uma singularidade inicial, aquando da criação do espaço-tempo. Uma possível solução para esta dificuldade é dada por uma descrição effectiva da teoria de *Loop Quantum Cosmology*, onde a singularidade inicial é substituída por um ressalto, ou, formalmente, um *bounce*. Neste capítulo, é construído um Lagrangeano geral, dentro de teorias de gravidade modificadas de *Gauss-Bonnet*, onde a equação de Friedmann emergente é a mesma que na teoria effectiva de *Loop Quantum Cosmology*, substituindo assim a singularidade inicial por um *bounce* cósmico. Para isso, é utilizada uma técnica, denominada redução de ordem, que trata o modelo como uma teoria efetiva, permitindo escrever os termos geométricos de ordem superior em função dos campos de matéria, nas equações de campo. Assim, é possível descartar os graus de liberdade adicionais não desejados, que usualmente estão presentes em teorias da gravidade com equações de campo de ordem superior a 2.

As notas finais podem ser encontradas no capítulo 7.

Palavras-chave: Energia escura acoplada – Colapso esférico – Buracos de verme – Não-metricidade – Cosmologias ressalto

Abstract

This thesis deals with extensions of General Relativity and their application to Cosmology and Gravitation. The introduction and main motivations of this essay can be found on Chapter 1.

The second chapter proposes a dark energy model driven by a scalar field kinetically coupled to matter. The dynamics of the system are analysed through dynamical systems techniques. The background is evolved and the solutions are meticulously studied, focusing on the influence of the coupling on the cosmological parameters. Through the Planck constraints, it is derived an upper bound on the coupling parameter.

Chapter three is devoted to the analysis of a conformally coupled quintessence model in which the background expansion is set to mimic a ΛCDM evolution. Both the background and linear perturbations are analysed. The growth of structures is tested against redshift space distortions data. The spherical collapse and cluster number counts are explored, and we shed some light on the possibility to distinguish between theoretical models with regard to two surveys.

An alternative formulation of General Relativity, where gravity is mediated by nonmetricity, on a flat and torsion free spacetime is exposed on the fourth Chapter. The background dynamics are set to follow the same evolution as in the standard model of Cosmology. The linear matter perturbations are evolved and the $f\sigma_8$ parameter is tested against large scale observations in the late Universe.

Chapter five introduces a 3-form field to the Einstein-Hilbert action in the context of gravitation. Specifically, it is found wormhole solutions where the ordinary matter fields are able to coexist throughout spacetime without violating the classical energy conditions. On such scenario, the 3-form field is responsible for holding the throat of the wormhole open.

On Chapter six the gravitational Lagrangian for modified Gauss-Bonnet gravity is reconstructed, such that the Friedmann equation of a bouncing Universe is recovered.

Keywords: Interacting dark energy – Redshift space distortions – Wormholes – Nonmetricity – Bouncing Cosmology

Contents

Acknowledgments . . . iii

Resumo . . . v

Abstract . . . ix

List of Tables . . . xii

List of Figures . . . xv

1 Introduction: An exotic Universe **1**

1.1 General relativity and the ΛCDM model . . . 2

1.2 Caveats of the ΛCDM model . . . 5

1.3 Published works . . . 9

2 Dark energy: kinetic couplings **11**

2.1 Model . . . 14

2.1.1 Particular cases . . . 16

2.2 Quintessence field with coupling $f \propto X^{\alpha}$ . . . 17

2.3 Dynamical analysis . . . 19

2.4 Cosmological solutions . . . 26

3 Coupled quintessence with a ΛCDM background **35**

3.1 Nonminimal couplings and conformal transformations . . . 36

3.2 Background . . . 39

3.3 Perturbations and the σ_8 tension . . . 44

3.4 Spherical collapse and number counts . . . 55

3.5 Observing $\mathcal{N}$ with eROSITA and the SPT . . . 66

4 The σ_8 tension in the light of Q-gravity **69**

4.1 Model . . . 73

4.2 Analysis and results 76

5 Exotic fluids in gravitation: 3-form Wormholes 81

5.1 Wormholes and energy conditions 83

5.2 3-forms 89

5.3 Model 90

5.4 Solutions 94

5.4.1 Case I 94

5.4.2 Case II 95

6 Bouncing cosmology in modified Gauss-Bonnet gravity 99

6.1 Model 101

6.2 Solutions 105

7 Final remarks 109

Bibliography 115

A Kinetically coupled dark energy 145

A.1 FLRW background 148

B Connection decomposition 149

List of Tables

2.1 Fixed points of the system (2.3.9) and (2.3.10), respective relative energy densities and equation of state parameters. 22

2.2 Existence regions of the fixed points regarding the system (2.3.9) and (2.3.10) and whether they feature accelerated expansion. 23

3.1 Best fit values for β and σ_8, number of fitted parameters (dof) and respective χ^2 and $\tilde{\chi}^2$ values. 51

4.1 Best fit values for M (in units of H_0) and σ_8, number of fitted parameters (N_{fp}) and respective χ^2 and AIC_c values. 78

5.1 Energy conditions for a fluid with $T_{\mu\nu} = \text{diag}(\rho, p_1, p_2, p_3)$. 87

List of Figures

2.1 Phase space of the system of equations (2.3.9),(2.3.10), for $\lambda = 1$, with different values of the coupling α (respective title). Black dots denote the fixed points (with labels inside referenced to Table 2.1). The shaded region depicts the accelerated expansion area, i.e. where the condition $w_{\text{eff}} < -1/3$ is met. 25

2.2 Top panel: evolution of the energy densities, ρ, for different values of the coupling (see legend), along redshift, with $\lambda = 0.2$, in regard to the model presented in Sec.2.4. Bottom panel: deviation on the energy density of dark matter relative to the uncoupled case ($\alpha = 0$), *i.e.* $\Delta\rho_c = \rho_c - \tilde{\rho}_c$, where $\tilde{\rho}_c = \rho_c(\alpha = 0)$. 29

2.3 Ratio of the energy densities of cold dark matter and dark energy along the redshift z, for different values of the coupling (see legend), in regard to the model presented in Sec.2.4, with $\lambda = 0.2$. A scaling regime is characterised by a constant value, *i.e.* $\rho_c/\rho_\phi =$ constant. 30

2.4 Coupling strength parameter along the redshift z, for different values of α (see legend), with $\lambda = 0.2$, in regard to the model presented in Sec.2.4. 31

2.5 Top panel: evolution of the relative energy densities (cosmic abundances), Ω, for different values of the coupling (see legend), along the redshift z, with $\lambda = 0.2$, in regard to the model presented in Sec.2.4. Bottom panel: deviations on the Hubble rate relative to the uncoupled case ($\alpha = 0$), *i.e.* $\Delta H = H - \tilde{H}$, where $\tilde{H} = H(\beta = 0)$. 32

2.6 Evolution of the equation of state parameters, w_{eff} and w_ϕ, along redshift, for different coupling values (see legend), with $\lambda = 0.2$, in regard to the model presented in Sec.2.4. 33

3.1 Top panel: evolution of the energy densities, ρ, for different values of the coupling (see legend), along redshift, in regard to the model presented in Sec.3.2. Bottom panel: deviation on the energy density of dark matter relative to the uncoupled case ($\beta = 0$), *i.e.* $\Delta\rho_c = \rho_c - \rho_{cdm}$. 42

3.2 Evolution of the relative energy densities (cosmic abundances), Ω, for different values of the coupling (see legend), along redshift, in regard to the model presented in Sec.3.2. 43

3.3 Evolution of the equation of state parameters, $w_{\rm eff}$ and w_ϕ, along redshift, for different coupling values (see legend), in regard to the model presented in Sec.3.2. 44

3.4 Top: evolution of the total matter (CDM + baryons) density contrast for different values of the coupling. Bottom: Difference of the dark matter perturbation in comparison with the uncoupled model (ΛCDM). 49

3.5 Function $f\sigma_8$ for ΛCDM (solid line) and different values of β (see legend) fixing a value of $\sigma_8(0) = 0.818$ [139]. The observational data points are taken from Refs. [148–162] and are summarised in Table II of Ref. [163]. 50

3.6 Constraints on β and σ_8: 1σ and 2σ regions and respective marginalised curves for the coupled quintessence model. A dot denotes the best fit value on the two parameter space. 52

3.7 Error bars corresponding to the generated mock data regarding the future SKA (blue) and Euclid (red) missions [166]. The curves presented are the same as in Fig. 3.5. 53

3.8 Forecast on the future constraints for β and σ_8 from the mock data generated for SKA and Euclid missions. The two lines represent the 1σ and 2σ regions (darker to lighter), present in Fig. 3.6, and the two small ellipses show the 1σ and 2σ regions expected from the points of Fig. 3.7. 54

3.9 Linear (gray), δ_L, and nonlinear (black), δ_{NL}, CDM density contrast versus redshift. Solutions of Eqs. (3.2.13) and (3.4.6) for $\beta = 0$ (solid), $\beta = 0.05$ (dashed) and $\beta = 0.08$ (dotted) with $\delta_{in} = 9 \times 10^{-4}$. 59

3.10 Linear density contrast at collapse, δ_c, versus redshift of the collapse, z_c, for $\beta = 0$ (solid), $\beta = 0.05$ (dashed) and $\beta = 0.08$ (dotted). 60

3.11 Comoving number of dark matter halos with masses within $10^{14}h^{-1}M_{\odot} < M < 10^{16}h^{-1}M_{\odot}$ for the Press-Schechter (left panel) and the Sheth-Tormen (right panel) mass functions, with $\beta = 0$ (solid), $\beta = 0.05$ (dashed) and $\beta = 0.08$ (dotted). 61

3.12 Press-Schechter mass function, Eq. (3.4.8), for $M = 10^{14}\, h^{-1}M_{\odot}$ with $\beta = 0$ (solid), $\beta = 0.05$ (dashed) and $\beta = 0.08$ (dotted). 62

3.13 Integrated number of dark matter halos with masses within $10^{14}h^{-1}M_{\odot} < M < 10^{16}h^{-1}M_{\odot}$. Solution of Eq. (3.4.13) with $\beta = 0$ (solid), $\beta = 0.05$ (dashed) and $\beta = 0.08$ (dotted). 63

3.14 Comoving number of dark matter halos with masses within $10^{14}h^{-1}M_{\odot} < M < 10^{16}h^{-1}M_{\odot}$ calculated from the Press-Schechter mass function for the uncoupled case (solid) and $\beta = 0.05$ (dotted) with $\sigma_8 = 0.811$ (black) and $\sigma_8 = 0.75$ (gray). 64

3.15 Difference of the comoving number of dark matter halos with masses within $10^{14}h^{-1}M_{\odot} < M < 10^{16}h^{-1}M_{\odot}$, between the ST Eq. (3.4.14) and the PS mass function Eq. (3.4.8), for $\beta = 0$ (solid), $\beta = 0.05$ (dashed) and $\beta = 0.08$ (dotted). 65

3.16 Estimate on the number of galaxy clusters for the SPT SZ survey (left) and expected number of clusters along redshift for the eROSITA (right), for $\beta = 0$ (solid), $\beta = 0.05$ (dashed) and $\beta = 0.08$ (dotted). 67

3.17 Difference on the expected number of galaxy clusters from ΛCDM, for the SPT (left) and eROSITA (right) surveys, for $\beta = 0.05$ (dashed) and $\beta = 0.08$ (dotted). 68

4.1 Top panel: derivative of the density contrast, δ', for $M = -2$ (dotted), ΛCDM (solid) and $M = 1$ (dashed). M values are in H_0 units. Bottom: Deviations on the effective gravitational constant with respect to ΛCDM, for the same values of the coupling. 75

4.2 Evolution of $f\sigma_8$ given the best fit values for ΛCDM (solid), $F(Q) = Q + M\sqrt{Q}$ (dashed) and $M^2 = 8\Lambda$ (dotted). Data points can be found in Table I of Ref. [238]. 76

4.3 Constraints on M and σ_8: contours for the 1σ and 2σ regions, with the respective marginalised curves for $F(Q) = Q + M\sqrt{Q}$. A circle denotes the best fit value. The vertical lines denote the reference models: ΛCDM (solid) with a square marker on the best fit and for $M^2 = 8\Lambda$ (dashed) with a triangle marker on the best fit. 79

4.4 Likelihood for σ_8 (curves) and respective 1σ interval (shaded region), for the models (dashed lines) labelled on top of each panel. Planck reference in solid red lines. 80

5.1 Rotation of the surface $z(r)$ given by Eq. (5.1.6) with the choice of the shape function $b = r_0^2/r$. 86

5.2 Energy densities (left panel) and NEC profile (right panel) for the form field (solid) and for the matter sources (dashed), regarding the specific choice given by Eqs. (5.4.1)-(5.4.2) with $\beta = -1/2$, $\Phi_0 = -6.3$, $\alpha = 1$, $\zeta_0 = 1$, $\gamma = 3$ and $C = 0$. 95

5.3 Energy densities (thick) and NEC profiles (thin) for the form field (solid) and the matter sources (dashed) for the choices in Eqs. (5.4.1)-(5.4.2) and Eq. (5.4.4) and . Left panel: $\beta = 1$, $\Phi_0 = -1$, $\alpha = 1$ and $C = -0.1$. Right panel: $\beta = -1/2$, $\Phi_0 = -2$, $\alpha = 1$ and $C = 0$. 96

5.4 Solutions for $\zeta(r)$, regarding the two solutions of Eqs. (5.4.1)-(5.4.2) and Eq. (5.4.4) for: $\beta = -1/2$, $\Phi_0 = -2$, $\alpha = 1$ and $C = 0$ (solid) and $\beta = 1$, $\Phi_0 = -1$, $\alpha = 1$ and $C = -0.1$ (dot dashed). 97

Chapter 1

Introduction: An exotic Universe

He values my understanding and talents more highly than my heart, but I am proud of the latter only. It is the sole source of everything of our strength, happiness, and misery. All the knowledge I possess everyone else can acquire, but my heart is exclusively my own.

From *The Sorrows of Young Werther*,

by Johann Wolfgang von Goethe

This thesis gathers the work conducted along a PhD specialized in cosmological physics. It encompasses several different subjects of cosmology and Gravitation. We will journey through very small scales in the Universe, studying tunnels in spacetime known as wormholes, to the very large scales, analysing models of dark energy interacting with dark matter. Throughout this excursion, we will study an alternative model of general relativity (GR) which lies not on the curvature of spacetime, but another different geometrical object, for describing gravitational phenomena. Finally, we will find ourselves on the very beginning of the Universe, right after the Big Bang, where a model that replaces the initial singularity by a cosmic bounce will be presented. You may now ask: how is it possible for such different matters to be gathered on a single thesis, where in principle they all should share a common ground? And that is indeed a pertinent question. Note that there is however an underlying concept linking all these studies: *extensions and alternatives to general relativity*. This is the main focus of this thesis: to explore extensions of GR and study their applications to cosmology and gravitation. There is however a price to pay for gathering such diverse subjects in a single essay. Mainly, the impossibility to expose each detail every time a subject is introduced without comprising a fair amount of pages while sill providing a light reading. Thus, this thesis ensembles a collection of articles

published along this PhD whilst giving a brief introduction of each topic every time a new subject is introduced. But let us first focus on what do we mean by extending GR and why would someone feel compelled to consider such alternatives. First, let us discuss how GR came to be.

1.1 General relativity and the ΛCDM model

In 1915 Albert Einstein presented us with a geometrical theory of gravity, *general relativity*. For more than two centuries, up until that time we would rely on Newton's notion of forces between objects to describe gravitational phenomena. Despite the success of Newton's theory, the nature of these forces was never fully understood. Newton's law of gravitation (which is not in fact universal) failed however to describe the motion of objects near strong gravitational sources, such as the sun. General relativity, on the other hand, was able to give a satisfactory answer to this problem, accounting for the inexplicable precession of the perihelion of Mercury. In the early 1900's, Einstein was motivated by a thought experiment, trying to generalize special relativity, which then culminated on the *equivalence principle*. This principle lies on the hypothesis that one observer can not distinguish between falling in a gravitational field (such as the earth) or travelling at a constant acceleration. Locally, these two scenarios are actually equivalent. The universality of this principle, and the fact that in the 1900's Bernhard Riemann already had developed Riemannian geometry, led Einstein to formulate GR as a geometrical theory of gravity. This theory describes gravity as a geometrical aspect of spacetime. In the words of John Wheeler: *"Spacetime tells matter how to move and matter tells spacetime how to curve"*. An expedition led by Eddington in 1919 finally provided us with the observational evidence for the theory of GR.

The stage in which GR acts upon is a pseudo Riemannian space $(\mathcal{M}, g_{\mu\nu})$, consisting of a 4-dimensional smooth manifold $\mathcal{M}$ and a metric tensor $\mathbf{g}$, which we will mostly in general denote it by its components $g_{\mu\nu}$. The manifold $\mathcal{M}$ is endowed with a covariant derivative (or connection) ∇_μ with components characterized by the Christoffel symbols, $\Gamma^\mu{}_{\alpha\beta}$, constructed following the assumption that the connection is torsion-free and metric compatible, *i.e.* $\Gamma^\mu{}_{\alpha\beta} = \Gamma^\mu{}_{\beta\alpha}$ and $\nabla_\mu g_{\alpha\beta} = 0$, respectively. Note that the connection coefficients encode the equivalence between inertial and gravitational forces, which is germane to the equivalence principle.

Without further ado, let us introduce the Einstein field equations, our best theory hitherto to describe gravitational phenomena:

$$G_{\mu\nu} = \kappa^2 T_{\mu\nu} \,, \tag{1.1.1}$$

where $\kappa^2 = 8\pi G/c^4$, with G being Newton's constant, first accurately measured by Henry Cavendish in 1798, c the speed of light, $T_{\mu\nu}$ are the energy-momentum tensor components of the matter fields, and $G_{\mu\nu}$ the components of the Einstein tensor. The latter tensor describes the geometrical aspect of spacetime as it is a function of the metric, its first and second order derivatives, *i.e.* $G_{\mu\nu} = G_{\mu\nu}(g_{\mu\nu}, \partial_\alpha g_{\mu\nu}, \partial_\alpha \partial_\beta g_{\mu\nu})$. Actually, Lovelock's theorem [1, 2] guarantees that, in four spacetime dimensions, the only geometrical tensor, say $A_{\mu\nu}$, that can be constructed from the metric $g_{\mu\nu}$, its first and (linear dependent on the) second derivatives, while remaining symmetric ($A_{\mu\nu} = A_{\nu\mu}$) and divergence free ($\nabla_\alpha A_{\mu\nu} = 0$), is

$$A_{\mu\nu} = \alpha G_{\mu\nu} + \Lambda g_{\mu\nu}\,, \tag{1.1.2}$$

with α and Λ being arbitrary constants. This is simply the Einstein tensor plus, what is usually called, a *cosmological constant* term, which will be dealt with more detail further ahead. The divergenceless character of the Einstein tensor implies the conservation of energy and momentum, expressed through:

$$\nabla_\mu T^{\mu\nu} = 0\,. \tag{1.1.3}$$

The Einstein field equations can be derived by an action principle through the following statement:

$$\mathcal{S} = \int \omega_g \left(\frac{R}{2\kappa^2} - 2\Lambda\right) + \mathcal{S}_m(g_{\mu\nu}, \psi, \nabla\psi)\,, \tag{1.1.4}$$

where $\omega_g = \sqrt{|\det g_{\mu\nu}|}d^4x$ is the metric volume form[1], R the Ricci scalar, $\mathcal{S}_m$ denotes the matter action, with ψ standing for a collective representation of the matter fields[2], minimally coupled to our massless spin-2 field $g_{\mu\nu}$. Variation of the action Eq. (1.1.4) with respect to the metric $g_{\mu\nu}$ yields the field equations

$$G_{\mu\nu} + \Lambda g_{\mu\nu} = \kappa^2 T_{\mu\nu}\,, \tag{1.1.5}$$

where

$$G_{\mu\nu} = R_{\mu\nu} - \frac{1}{2} g_{\mu\nu} R\,, \tag{1.1.6}$$

with $R_{\mu\nu}$ being the components for the Ricci tensor[3].

[1] The determinant of the metric tensor will also be denoted simply by g.

[2] Formally, ψ stands for any arbitrary set of sections of the frame bundle, associated to our connection ∇ on the principal fiber bundle (see Refs. [3–5]).

[3] See Ref. [6] for a detailed book on general relativity.

The metric field $g_{\mu\nu}$ of general relativity carries two degrees of freedom (dof), the needed parameters to describe the physical states associated with the theory. To understand this, one needs to say some words with regard to a geometrical identity, called the Bianchi identity, and with gauge freedom. To start off, since $g_{\mu\nu}$ is a symmetric tensor, one naively starts with 10 dof (the independent components of $g_{\mu\nu}$). The divergentless character of the Einstein tensor culminates on a geometrical relation of utmost importance, known as the Bianchi identities:

$$\nabla_\alpha R^\alpha{}_\mu = \frac{1}{2}\nabla_\mu R\,. \tag{1.1.7}$$

These are a set of four constraints which set dependencies among the equations, and kill four degrees of freedom. The last four dof are killed by gauge freedom. This concept is at the very heart of every gauge theory, and carries with it the fact that the action is completely oblivious to the coordinates we choose (sometimes this concept is referred to as general covariance). This is, however, much more profound, as it is related with a group of symmetries which leave the theory invariant, expressed in terms of diffeomorphisms. Let us not extend much in this regard, but simply consider a diffeomorphism (more concretely an automorphism) $\phi : \mathcal{M} \to \mathcal{M}$. Then, diffeomorphism invariance states that given a solution of the field equations, say $(\mathcal{M}, g_{\mu\nu}, \psi)$, then acting ϕ upon our objects, *e.g.* $x^\mu \to \phi(x^\mu)$, the "transformed" solution is still a solution of our theory, *i.e.* $(\mathcal{M}, \phi^* g_{\mu\nu}, \phi^*\psi)$ is still a solution (where $\phi^*\psi$ denotes the pullback of ψ by ϕ, *i.e.* $\phi^*\psi = \psi \circ \phi$). Generally, one says that a given theory is $G-$invariant when $\phi \in G \subseteq$ Diff$(\mathcal{M})$. This leaves us with a total of $10 - 4 - 4 = 2$ dof.

Lovelock's theorem guarantees that the action Eq. (1.1.4) is the only action that gives second order equations of motion for the metric[4]. Thus, if one wishes to study modifications of GR, it is inevitable to introduce extra degrees of freedom. These extensions can be achieved in several ways. First, one may consider theories encompassing more than four spacetime dimensions. These however, are very hard to measure and, even in higher dimensional theories a four dimensional model should naturally emerge in an effective low energy limit. Other ways to consider deviations from GR is to consider higher order field equations or break diffeomorphism invariance. This thesis will not focus on any of these options, but rather on a (maybe) simpler one: add extra fields beyond the metric, thus preserving the second order field equations and diffeomorphism invariance. But we have yet to tackle the crucial question: Why to consider

[4]Higher order equations of motion are usually plagued by instabilities related with the ground state of the theory not being bounded. This is known as *Ostrogradsky instability* [7].

extensions of GR in the first place? To do so, let us then present the most accepted model for cosmological physics and discuss some relevant puzzles within it.

The standard model of cosmology, the ΛCDM model, stands upon the shoulders of GR, and encompasses three major sectors to describe the observed properties of our Universe: two dark components, specifically dark energy (DE) and cold dark matter (CDM), and ordinary matter, consisting of the standard model particles. The ΛCDM model is supported by a fair amount of experiments, such as the cosmic microwave background (CMB) and the distribution of large scale structures in the Universe [8, 9].

Predictions from the Big Bang Nucleosynthesis and observations from the cosmic microwave background suggest the existence of a non-baryonic dark component, named *dark matter*, which does not interact at all with the electromagnetic field. The first hint towards the existence of dark matter dates back to 1933 when Zwicky observed that ordinary matter was not sufficient to account for the velocities of galaxies in the Coma cluster [10]. Later on, in the 70's, there was further evidence of the existence of DM, through the observation of rotational curves of galaxies [11]. Today, we estimate that dark matter has a contribution of around 25% for the total budget of the Universe, in contrast with the minute 5% for ordinary matter. The remaining 70% of the Universe's composition comes from an unknown exotic source, dubbed *dark energy*, on which the most part of this thesis is focused. Thus, some more words with regard to DE, along with some related problems within the standard model of cosmology should be stated.

1.2 Caveats of the ΛCDM model

In 1917 Einstein introduced in his field equations a cosmological constant Λ [12], as presented in Eq. (1.1.5), to counterbalance the gravitational pull of matter and thus (ironically) to describe a static Universe. However, in 1927, a Belgian mathematician (and catholic priest), Georges Lemaître, provided theoretical evidence for an expanding Universe. Two years later, an American astronomer, Edwin Hubble, confirmed this thesis by observing that the recessional velocity of galaxies nearby our local system [13] increases as they get further away from the Earth (today known as Hubble-Lemaître law). After realizing this, Einstein said that the introduction of the cosmological constant was one of his "greatest blunders".

Much later on, in 1998, two independent teams [14, 15] observed that *the expansion of our Universe is accelerating*, based on various observations of Type Ia supernovae. Quoting this study directly [14]:

"Different lightcurve fitting methods, SN Ia subsamples, and prior constraints unanimously favor eternally expanding models with positive cosmological constant (i.e., $\Omega_\Lambda > 0$) and a current acceleration of the expansion (i.e.,$q_0 < 0$)."

and [15]:

"..., only currently accelerating universes fit the data well."

Results from these experiments shook our primal knowledge, were later on strongly supported by several other probes and observations, and finally resulted in a Physics Nobel prize in 2011. So, there must be some sort of exotic substance which counteracts gravity and accelerates the expansion. Hence we witnessed the rebirth of Λ. Up to this day, the cosmological constant, which baptized the ΛCDM model, is the simplest candidate to the dark energy component, and it has been successful in explaining most cosmological observations. However there are two major conceptual problems in regard to Λ (see sections 6.3 and 6.4 of Ref. [16]).

The cosmological constant acts as a component with constant energy density throughout time, and with a negative pressure capable of counterbalancing the gravitational pull of matter and thus accelerate the expansion. It is common to associate the cosmological constant Λ to the vacuum energy density of empty space. That is, it accounts for the contributions from all the particle fields fluctuating around their ground state. The lowest possible energy state of a quantum harmonic oscillator, called the ground state, or zero-point function, is simply given by $E_0 = \hbar\omega/2$, where ω is the frequency of the oscillator (remember that $E_n = \hbar\omega(n + 1/2)$). This means that even in the ground state, the quantum oscillator still fluctuates with a small variance, in contrast with its classical analogue; otherwise the Heisenberg uncertainty principle would be violated. Quantum Field Theory suggests that all standard model particles, *i.e.* fermions (matter fields) and bosons (force carriers), have a characteristic zero-point function. As a simple approach, one can envision the empty space as a collection of all of these harmonic oscillators (of all the particle fields) oscillating around the ground state, $E_0 = \hbar/2 \sum_i \omega_i$, where the frequencies can be written in terms of the corresponding wave vector, *i.e.* $\omega_i = \sqrt{k_i^2 + m^2}$. On the $k-$space continuum, one may write the energy density ($\rho_0 = E_0/V$) of the vacuum, by summing over all the possible modes,

$$\rho_0 = \frac{\hbar}{2} \int_0^\infty \sqrt{k^2 + m^2} \frac{d^3k}{(2\pi)^3} \,, \tag{1.2.1}$$

just to realize that it diverges, predicting an infinite value for the zero-point energy density. At this point, one usually assumes that new physics should arise once some cut-off scale, $k_{\max}$, is

reached. Thus, assuming the integral to be dominated by the modes $k \gg m$, one is left with

$$\rho_0 \approx \frac{k_{\max}^4}{16\pi^2}, \tag{1.2.2}$$

and assuming $k_{\max} = m_{pl}$, we can estimate,

$$\rho_0 \approx 10^{74}\,\mathrm{GeV}^4\,. \tag{1.2.3}$$

This has indeed been proposed as a natural motivation for the cosmological constant, $T^{\Lambda}{}_{\mu\nu} = -\rho_0\, g_{\mu\nu}$. However, obervations suggest a value for this density of around $\rho_\Lambda \approx 10^{-47}\,\mathrm{GeV}^4$, which is about 121 orders of magnitude lower than the estimated vacuum energy Eq. (1.2.3). This tremendous discrepancy between the theoretical value for the zero-point function and the observed value for Λ, is known as the *cosmological constant problem* [17]. Note that from quantum chromodynamics it is possible to set a different energy scale for this cut-off, however the value is still around 40 orders of magnitude higher than the observed one.

Another cosmic puzzle of the ΛCDM model, associated also with Λ is the *cosmic coincidence problem* [18]. In a nutshell, it consists of the following question: how likely is it that we are currently living in such specific epoch of the history of the Universe, where the dark energy and dark matter energy densities are the same order of magnitude, *i.e.* $\rho_\Lambda/\rho_{CDM} \approx \mathcal{O}(1)$ at the present? The rate at which the cosmic components evolve with time depends on the nature of each species. Measurements of the cosmological constant tell us that in the past, its energy density should have had a very small value - much smaller than the energy scales of typical particles (a *fine tuning* problem) and only nearly 14 billion years latter does DE become of a comparable size as the other components. Why now?

There are still other conundrums related with the dark sector of the standard model of cosmology. Ground and space-based experiments are currently reaching levels of precision without precedent. With such sensitivity, it is possible to detect discrepancies between different observations. Early and late time experiments seem to present tensions on their cosmological observables, in particular, for the present rate at which the Universe is expanding, H_0 [19, 20], and the growth rate of structures, $\sigma_8 - S_8$ [21]. In fact, there is a tension of 4.4σ on the background observed value of H_0 between the Cosmic Microwave Background measurements [8] and the Cepheid variable-calibrated Type Ia supernovae [22]. As for observations on structure formation, large scale observations of weak lensing and redshift distortions, suggest a lower

clustering rate when compared with the Planck values [23–28]. Naturally, the dark components' nature is sensible to these values, for example, a higher density of dark energy hampers structure formation by counteracting the collapse of matter. Neither dark matter or dark energy have yet been observed in laboratory experiments. There exist other small-scale puzzles that the current ΛCDM model has not yet been able to give a satisfactory answer (such as [29]).

These problems motivate cosmologists to extend theories beyond the standard model and test their consistency against observations. One approach is to promote dark energy to a dynamical entity. This can be achieved either through a modification of gravity itself [30–33] or by adding new extra fields, such as scalar fields, to the action of the theory [34, 35]. When dealing with models of dark energy driven by scalar fields, it is common to refer to them as *quintessence models*[5]. These fields were first proposed in the context of dark energy in Ref. [36].

Around 60% of this thesis is concerned with dark energy and formation of structure physics through interacting scalar fields. Adding higher order exotic fields to GR in the context of gravitation occupies 18% of this essay and 22% is dedicated to modifications/alternatives to the geometrical part of the theory. In particular, Chapters 2 and 3 deal with models of dark energy with canonical scalar fields, which are allowed to interact with dark matter. The background cosmology is analysed, and, additionally, in Chapter 3, the linear and nonlinear perturbations are evolved, the latter in the context of the spherical collapse and cluster number counts, and the pertubative parameters are tested against observational data. Chapter 4 studies an alternative model of modified gravity in the light of the σ_8 tension, where the matter perturbations are evolved and a likelihood data analysis is performed. As this thesis also deals with deviations from GR in the context of gravitation, Chapter 5 explores the consequences of adding extra dynamical fields, specifically 3-form fields, in wormhole geometries. The field equations are evolved and the energy conditions are analysed. In Chapter 6 a modified gravity model is exposed, in particular modified Gauss-Bonnet gravity, in the light of attaining bouncing cosmological solutions. To do so, we resorted to an order-reduction technique which enables one to get rid of the spurious degrees of freedom, usually present in higher order theories of gravity. The final remarks can be found in Chapter 7.

Note that all the models exposed in this thesis can be naively appreciated as modifications to the Einstein field equations, either to the gravity side or to the matter sector, as an attempt to

[5]In ancient Greece, Aristotle added a fifth element (*"quinta essentia"* in Latin) - aside from the usual four (air, fire, water and earth) - an aether, which would permeate all the entire Universe; *"there is in nature some bodily substance other than the formations we know, prior to them all and more divine than they"* (Aristotle, *On the Heavens*, 350 BC).

alleviate some of the problems of the standard model of cosmology. Chapters 2, 3 and 5 deal with models comprising exotic fluids in the theory (in particular scalar and 3-form fields), sourcing the energy momentum tensor, while Chapters 4 and 6 consider modifications/alternatives to the geometrical aspect of Einstein's gravity.

1.3 Published works

The work conducted along this PhD resulted on the following articles published on refereed journals:

1. Bruno J. Barros, Tiago Barreiro, Tomi Koivisto and Nelson J. Nunes, *Phys. Dark Univ. 30 (2020) 100616*, "TESTING $F(Q)$ GRAVITY WITH REDSHIFT SPACE DISTORTIONS", arXiv: 2004.07867 [gr-qc].

2. Bruno J. Barros, Bogdan Dănilă, Tiberiu Harko and Francisco S. N. Lobo, *Eur. Phys. J. C 80, 617 (2020)*, "BLACK HOLE AND NAKED SINGULARITY GEOMETRIES SUPPORTED BY THREE-FORM FIELDS", arXiv: 2004.06605 [gr-qc].

3. Bruno J. Barros, Elsa M. Teixeira and Daniele Vernieri, *Annals Phys. 419 (2020) 168231*, "BOUNCING COSMOLOGY IN $f(R, \mathcal{G})$ GRAVITY BY ORDER REDUCTION", arXiv: 1907.11732 [gr-qc].

4. Bruno J. Barros, Tiago Barreiro and Nelson J. Nunes, *Phys. Rev. D 101, 023502 (2020)*, "SPHERICAL COLLAPSE IN COUPLED QUINTESSENCE WITH A ΛCDM BACKGROUND", arXiv: 1907.10083 [astro-ph].

5. Bruno J. Barros, *Phys. Rev. D 99, 064051 (2019)*, "KINETICALLY COUPLED DARK ENERGY", arXiv: 1901.03972 [gr-qc].

6. Bruno J. Barros and Francisco S. N. Lobo, *Phys. Rev. D 98, 044012 (2018)*, "WORMHOLE GEOMETRIES SUPPORTED BY THREE-FORM FIELDS", arXiv: 1806.10488 [gr-qc].

7. Bruno J. Barros, Luca Amendola, Tiago Barreiro and Nelson J. Nunes, *JCAP 01 (2019) 007*, "COUPLED QUINTESSENCE WITH A ΛCDM BACKGROUND: REMOVING THE σ_8 TENSION", arXiv: 1802.09216 [astro-ph].

This thesis is based on all of these works except number 2. Since this thesis is based on these articles, some sentences might be quoted *verbatim* the original works.

Chapter 2

Dark energy: kinetic couplings

Oh, if I had done nothing simply from laziness! Heavens, how I should have respected myself, then. I should have respected myself because I should at least have been capable of being lazy; there would at least have been one quality, as it were, positive in me, in which I could have believed myself. Question: What is he? Answer: A sluggard; how very pleasant it would have been to hear that of oneself! It would mean that I was positively defined, it would mean that there was something to say about me. 'Sluggard' - why, it is a calling and vocation, it is a career. Do not jest, it is so. I should then be a member of the best club by right, and should find my occupation in continually respecting myself. I knew a gentleman who prided himself all his life on being a connoisseur of Lafitte. He considered this as his positive virtue, and never doubted himself. He died, not simply with a tranquil, but with a triumphant conscience, and he was quite right, too. Then I should have chosen a career for myself, I should have been a sluggard and a glutton, not a simple one, but, for instance, one with sympathies for everything sublime and beautiful. How do you like that?

From *Notes from the Underground*,
by Fyodor Dostoevsky

This section is based on Ref. [37].

Promoting dark energy to a dynamical field interacting with the other matter species may alleviate some of the problems related to the standard model. This can be understood through the following argument:

- *Coincidence problem:* As it will become clear further on, a scalar field cosmology might generate the so-called scaling solutions. These can hide the presence of a dark energy field throughout time, when its energy density may be large, or at least close to the order of the

one of matter, whilst small at present times. This would generate a natural mechanism (independent of initial conditions), to explain the fact that today the energy densities of dark energy and matter are of the same order; in fact this holds not only near the present, but throughout a much larger period of the history of our Universe. Note that this effect is impossible to achieve with Λ as its energy density is always constant throughout time.

- H_0 *tension:* As the evolution of the cosmic fluids, for example in scalar field cosmology, is modified in relation to the standard model ones, this will directly impact the rate at which the Universe expands (through the Friedmann equation). Thus, the theoretical predictions for the Hubble rate, in particular for H_0, in such models will be different than in standard ΛCDM, which may be useful to tackle the present discrepancy between early and local measurements of H_0.

- σ_8 *tension:* As we will show in Chapter 3, an interaction within the dark sector naturally influences the dynamics of the perturbations on the coupled matter component. In particular, a fifth-force mediated by the scalar degree of freedom arises, accompanied by additional friction terms. These effects will impact the clustering rate of matter, therefore resulting in different predictions for the value of σ_8 at present times. This can be used to tailor a specific model to address the σ_8 tension between CMB experiments and local measurements of redshift space distortions and weak lensing.

The three arguments above motivate the description of dark energy as a dynamical field [34, 35]. This was first proposed in Ref. [36]. Soon after, it were put forward [36, 38] models where this dark energy scalar field interacts with the other particles. However, throughout the literature most models concerning interacting dark energy either lay out the coupling at the level of the field equations [39–43] or it naturally emerges in scalar-tensor theories when performing a conformal transformation [44]. The Lagrangian formalism regarding coupled quintessence models was examined in Refs. [45, 46] assuming that the matter species are coupled to a field dependent function. An interacting model in which the mass of the dark matter particles varies with the value of the quintessence field ϕ through a Yukawa coupling was studied in Ref. [47]. The action for the cases where dark matter is described in terms of a wave function for $1/2$-spin particles and for scalar dark matter was presented. Quantum fluctuations and the stability of quintessence theories were examined in Ref. [48] for the noninteracting case and considering couplings to fermions only. The analysis of interacting models within the general Horndeski

Lagrangian was explored in Ref. [49], where the action allowing for scaling solutions was derived.

Throughout nature, most species naturally interact with one another. Therefore it is not unreasonable to assume that kinetic terms may also influence the dynamics of other constituents. This intimate relation has been explored in several works in the literature. For example, mimetic models [50, 51] with interactions involving field derivatives have been proposed in Refs. [52, 53]. These consider derivatives of the mimetic field, representing dark matter, linearly coupled to the matter current, at the level of the action. By assuming a shift symmetry, the mimetic field is forced to present derivative couplings to the matter species, not directly involving the field value. Derivative couplings in quintessence theories were first mentioned in Ref. [54]. Linear interactions of the field's derivative to the four-velocity of the fluid u_μ were explored, considering terms of the form $u^\mu \nabla_\mu \phi$. These scalar-fluid models make use of the Brown's formalism [55] and assume derivative couplings as linear interactions of the field derivative to the vector-density particle-number flux, J^μ (related with the fluid's four velocity u^μ), of matter [56, 57]. A dynamical system analysis was conducted in Ref. [58] and the study of perturbations and formation of structures in Ref. [59]. Nonminimal kinetic couplings to curvature were introduced in Refs. [60, 61]. One consequence was the existence of solutions leading to late time accelerated expansion of the Unvierse. Disformally coupled theories [62–65] generalize the concept of conformal transformation, alowing the metric rescaling to depend also on the kinetic term of the scalar field, by means of a disformal transformation such that the rescaled metric is $\tilde{g}_{\mu\nu} = C(\phi) g_{\mu\nu} + D(\phi) \partial_\mu \phi \partial_\nu \phi$ [66]. Hence, the metric felt by the matter fields is intimately connected with the field's velocity when $D(\phi) \neq 0$. The spherical collapse and cluster counts in disformally coupled theories were studied in Ref. [67]. A generalization of derivative couplings in scalar-fluid theories can be found on the last pages of Ref. [59].

In this chapter, a generalized form for interacting dark energy models is proposed, by allowing a scalar field ϕ with a k-essence Lagrangian density $P(\phi, X)$, to kinetically couple to matter, where $X := -\frac{1}{2}\partial^\mu \phi \partial_\mu \phi$ is the kinetic term. Accordingly, it is assumed that the term X can couple directly to the matter fields at the level of the action. The interaction is mediated by a general function $f(\phi, X)$ in the matter action. The cosmological field equations are derived and solved for a specific model and it is shown how the presence of the coupling allows for early scaling solutions followed by a period of accelerated expansion, when the f function depends solely on the kinetic term. With the aid of dynamical systems techniques, the influence of the

coupling on the overall cosmological dynamics is examined. The scaling regime, useful to alleviate the cosmic coincidence problem, is only possible due to the emergence of two new critical points that emerge when the coupling is active. Using constraints from the Planck data, it is possible to find an upper bound for the coupling. It is shown how this theory encapsulates a vast amount of dark energy models present in the literature *hitherto*.

2.1 Model

Let us consider a Universe filled by two components, consisting of one scalar field ϕ interacting with a matter fluid, with Lagrangian densities $\mathcal{L}_\phi$ and $\tilde{\mathcal{L}}_m$ respectively. The total action minimally coupled to Einstein's gravity of the proposed theory is:

$$\mathcal{S} = \int \omega_g \left[\frac{R}{2\kappa^2} + P(\phi, X) + f(\phi, X)\tilde{\mathcal{L}}_m(g_{\mu\nu}, \psi) \right] , \tag{2.1.1}$$

where ψ stands for the matter fields and $f := f(\phi, X)$ entails the information regarding the interaction between the species. The novelty of this work is the fact that f is allowed to depend on $X := -\frac{1}{2}\partial^\mu\phi\partial_\mu\phi$. Note that the Lagrangian of the scalar source is a general k-essence [68–73] function, $\mathcal{L}_\phi = P(\phi, X)$.

We find the modified field equations through the variation of the action Eq. (2.1.1) with respect to the metric $g^{\mu\nu}$, yielding,

$$\frac{1}{8\pi G}G_{\mu\nu} = T^{(\phi)}_{\mu\nu} + f\,\tilde{T}^{(m)}_{\mu\nu} + f_{,X}\tilde{\mathcal{L}}_m\partial_\mu\phi\partial_\nu\phi\,, \tag{2.1.2}$$

with

$$T^{(\phi)}_{\mu\nu} := -2\frac{\delta\mathcal{L}_\phi}{\delta g^{\mu\nu}} + \mathcal{L}_\phi g_{\mu\nu} \quad \text{and} \quad \tilde{T}^{(m)}_{\mu\nu} := -2\frac{\delta\tilde{\mathcal{L}}_m}{\delta g^{\mu\nu}} + \tilde{\mathcal{L}}_m g_{\mu\nu} \tag{2.1.3}$$

being the energy-momentum tensors regarding the i-th species. In order to avoid extensive expressions we use the notation $P := P(\phi, X)$. By considering couplings that depend on the kinetic term of the scalar field, a new interaction term arises – the last one on the right-hand side of Eq. (2.1.2) – in the Einstein equations. As will be shown, this affects the contracted Bianchi identities, and thus has an impact on the overall dynamics of the Universe.

It is possible to write the equations for the current model in a more intuitive and familiar

form, by defining the object

$$\mathcal{L}_m(g_{\mu\nu}, \psi, \phi, X) := f(\phi, X)\tilde{\mathcal{L}}_m(g_{\mu\nu}, \psi)\,, \tag{2.1.4}$$

which defines an effective matter Lagrangian, encapsulating the effects of the coupling *per se*. Thus, we have the following relation for the stress-tensors:

$$\begin{aligned} T^{(m)}_{\mu\nu} &= -2\frac{\delta\mathcal{L}_m}{\delta g^{\mu\nu}} + \mathcal{L}_m g_{\mu\nu} \\ &= f\,\tilde{T}^{(m)}_{\mu\nu} - 2\tilde{\mathcal{L}}_m\frac{\delta f}{\delta g^{\mu\nu}} \\ &= f\,\tilde{T}^{(m)}_{\mu\nu} + f_{,X}\tilde{\mathcal{L}}_m\partial_\mu\phi\partial_\nu\phi\,, \end{aligned} \tag{2.1.5}$$

where a prime denotes a derivative, *i.e.* $f_{,X} := \partial f/\partial X$, and we may recast the field equations, Eq.(2.1.2), more conveniently as

$$\frac{1}{\kappa^2}G_{\mu\nu} = T^{(\phi)}_{\mu\nu} + T^{(m)}_{\mu\nu}\,. \tag{2.1.6}$$

Variation of the action Eq. (2.1.1) with respect to ϕ holds the equations of motion for the scalar source (See appendix A for details):

$$P_{,\phi} + P_{,X}\Box\phi - 2P_{,X\phi}X - P_{,XX}A = -Q\,, \tag{2.1.7}$$

where $A = \partial^\alpha\phi\partial_\beta\phi\nabla_\alpha\partial^\beta\phi$, $\Box\phi = \nabla_\mu\partial^\mu\phi$ is the d'Alembert operator, and the coupling is defined as

$$Q = \mathcal{L}_m\left[\frac{f_{,\phi}}{f} + \frac{f_{,X}}{f}\left(\Box\phi + \partial^\alpha\phi\frac{\nabla_\alpha\mathcal{L}_m}{\mathcal{L}_m} + \frac{f_{,X}}{f}A + 2\frac{f_{,\phi}}{f}X\right) - 2\frac{f_{,X\phi}}{f}X - \frac{f_{,XX}}{f}A\right]\,. \tag{2.1.8}$$

Conservation of the total energy-momentum tensor is declared by the contracted Bianchi identities,

$$\nabla_\mu G^\mu_\nu = 0 \quad \Rightarrow \quad \nabla_\mu\left(T^{(\phi)\,\mu}_{\quad\ \nu} + T^{(m)\,\mu}_{\quad\ \nu}\right) = 0\,. \tag{2.1.9}$$

However, each component is not individually conserved due to the energy flow stemming from

the interaction object f. The conservation relations take the form:

$$\nabla_\mu T^{(\phi)\,\mu}_{\ \ \nu} = -Q\,\nabla_\nu \phi, \tag{2.1.10}$$

$$\nabla_\mu T^{(m)\,\mu}_{\ \ \nu} = Q\,\nabla_\nu \phi, \tag{2.1.11}$$

with Q given by Eq.(2.1.8).

Note that all the equations derived so far are completely independent of the choice of $g_{\mu\nu}$, and thus are valid on any background.

In the literature, it is common to impose the couplings at the level of the conservation relations [74–81], that is, by fixing the term on the right-hand side of Eqs. (2.1.10) and (2.1.11). Coupled models considering noncanonical scalar fields have been studied in Refs. [82–84], allowing for interactions with nonlinear terms of $\dot{\phi}$ [85], where a dot denotes derivative with respect to cosmic time, *i.e.* $\dot{\phi} := \partial\phi/\partial t$. In this work, however, the coupling is imposed in the action, through the choice of f. The conservation relations for the individual interacting species naturally emerge *a posteriori* from this choice. The $f := f(\phi)$ cases for a canonical and a a tachyon scalar field were analysed in Ref. [45] and Ref. [86], respectively.

Since the publication of this work [37], several works in the literature considering generalizations or applications of this present model have been conducted. Relevant examples are the study of an Horndeski Lagrangian for the scalar field using the Schutz-Sorkin action for matter [87], the study of perturbations and their corresponding stability [88], the general form for the Lagrangian which allows for scaling solutions [89] and an interacting Multi-Proca vector dark energy model [90].

2.1.1 Particular cases

By fixing $f = 1$ in the total action Eq.(2.1.1), and thus neglecting the coupling, we recover the k-essence models already meticulously examined in the literature [68–73]. Furthermore, by assuming a canonical scalar field, *i.e.* $P(\phi, X) = X - V(\phi)$, with V the scalar potential, the theory reduces to standard quintessence models, describing dark energy with a noninteracting scalar degree of freedom [18]. In this case, setting $f := f(\phi)$ to be an arbitrary function of ϕ, gives rise to coupled quintessence models [38], analised in, *e.g.* Ref. [45].

Let us now assume that our matter species in pressureless. We may then write [91, 92]

$\mathcal{L}_m = T^{(m)\,\alpha}{}_{\alpha} = -\rho_m$, which results in a pressureless perfect fluid form for stress-energy tensor:

$$T^{(m)}_{\mu\nu} = \rho_m u_\mu u_\nu \,, \tag{2.1.12}$$

where u_μ is the four-velocity vector, defined such as $u_\mu u^\mu = -1$. In this framework, it is interesting to notice that, if $f = f(\phi)$, the conservation Eqs.(2.1.10) and (2.1.11) become:

$$\nabla_\mu T^{(\phi)\,\mu}_{\ \ \nu} = \frac{f_{,\phi}}{f}\rho_m \nabla_\nu \phi \,, \tag{2.1.13}$$

$$\nabla_\mu T^{(m)\,\mu}_{\ \ \nu} = -\frac{f_{,\phi}}{f}\rho_m \nabla_\nu \phi \,, \tag{2.1.14}$$

with $Q = \rho_m f_{,\phi}/f$. Indeed, these are the equations describing scalar-tensor theories [93] after performing a conformal transformation and switching to the Einstein frame (see 3.1), with the following conformal factor

$$\tilde{g}_{\mu\nu} = f(\phi)^2 g_{\mu\nu} \,. \tag{2.1.15}$$

Through the choice $f(\phi) = e^{C\phi}$, with C being a constant, we recover $Q = C\rho_m$ [38, 94, 95]. The case $C = C(\phi)$ was studied in Ref. [96].

2.2 Quintessence field with coupling $f \propto X^\alpha$

Having presented the underlying formalism, in this section we follow to solve the field equations for a specific cosmological setting. The accelerated expansion is driven by a quintessence field, with $P(\phi, X) = X - V(\phi)$, coupled to a cold (pressureless) dark matter component with $\mathcal{L}_m = -\rho_c$, where ρ_c denotes its energy density. Note that since couplings to standard model fields are tighly constrained by observational data [97–102], it is common practice to couple the scalar degree of freedom to dark matter, whose Lagrangian form is still unknown. Therefore, the total action is

$$\mathcal{S} = \int \omega_g \left[\frac{R}{2\kappa^2} + \overbrace{X - V(\phi)}^{=\mathcal{L}_\phi} + \underbrace{f(X)\tilde{\mathcal{L}}_m}_{=\mathcal{L}_m = -\rho_c} \right] . \tag{2.2.1}$$

We stand upon a flat Friedmann–Lemaître–Robertson–Walker (FLRW) spacetime, describing an homogeneous and isotropic Universe, with line element,

$$ds^2 = -dt^2 + a(t)^2 \delta_{ij} dx^i dx^j \,, \tag{2.2.2}$$

where $a(t) =: a$ is the scale factor, a function of cosmic time t. Regarding the scalar field potential, we assume an exponential form,

$$V = V_0\, e^{-\kappa\lambda\phi}\,, \tag{2.2.3}$$

with V_0 being the scale of the potential, a constant with dimensions of [Mass]^4, and the stifness of the potential is given in terms of the dimensionless constant λ. This choice for the potential has been shown to produce cosmological scaling solutions [34, 94, 103, 104].

Finally, we close the system by specifying the coupling function to be solely dependent on the kinetic term,

$$f = \left(\kappa^2 X\right)^{\alpha}\,, \tag{2.2.4}$$

where now $X = \frac{1}{2}\dot{\phi}^2$ and α is a constant dictating the strength of the kinetic interaction. We recover the uncoupled quintessence model [105] for $\alpha = 0$. The factor κ^2 in Eq. (2.2.4) simply renders the function f dimensionless in the total action Eq. (2.1.1)[1]. From Eq. (2.1.8) with the choice in Eq. (2.2.4) we have,

$$Q = -\rho_c \frac{\alpha}{X}\left(\Box\phi + \frac{A}{X} + \partial^\nu\phi\frac{\partial_\nu\rho_c}{\rho_c}\right)\,. \tag{2.2.5}$$

The energy density and pressure of the quintessence field are defined as:

$$\rho_\phi = -T^{(\phi)0}{}_0 = \frac{1}{2}\dot{\phi}^2 + V\,, \tag{2.2.6}$$

$$p_\phi = T^{(\phi)1}{}_1 = T^{(\phi)2}{}_2 = T^{(\phi)3}{}_3 = \frac{1}{2}\dot{\phi}^2 - V\,, \tag{2.2.7}$$

respectively ,with Eq. (2.1.3),

$$T^{(\phi)}_{\mu\nu} = \partial_\mu\phi\partial_\nu\phi + g_{\mu\nu}\mathcal{L}_\phi\,. \tag{2.2.8}$$

The equation of state parameter for the field is defined as,

$$w_\phi = \frac{p_\phi}{\rho_\phi} = \frac{\frac{1}{2}\dot{\phi}^2 - V}{\frac{1}{2}\dot{\phi}^2 + V}\,. \tag{2.2.9}$$

[1]Remember that, in natural units, $[\kappa] = M^{-1}$, $[\mathcal{L}] = M^4$, $[H] = M$, and for quintessence models $[\phi] = M$.

The species are then set to follow the evolution:

$$\ddot{\phi} + 3H\dot{\phi} + V_\phi = Q\,, \tag{2.2.10}$$

$$\dot{\rho}_c + 3H\rho_c = -\dot{\phi}Q\,, \tag{2.2.11}$$

with $H := \dot{a}/a$ being the Hubble function, $V_\phi = dV/d\phi$, and the interaction term Eq.(2.2.5), using Eqs.(2.2.5), (2.2.10) and (2.2.11), becomes

$$Q = 2\alpha\rho_c \frac{3H\dot{\phi} - \lambda V}{\dot{\phi}^2 + 2\alpha\left(\rho_c + \dot{\phi}^2\right)}\,. \tag{2.2.12}$$

The cosmic evolution is subjected to the Friedmann constraint, the 00-component of the field equations Eqs. (2.1.6), describing the expansion rate of the Universe,

$$\frac{3}{\kappa^2}H^2 = \rho_c + \rho_\phi\,. \tag{2.2.13}$$

2.3 Dynamical analysis

The use of dynamical systems techniques in cosmology is of great importance [105] since it enables us to shed some light on the overall behaviour of the solutions for the field equations without the need to actually solve them. In the literature they have been applied to a wide variety of subjects raging from modified gravity [106] to dynamical dark energy models [34]. In this subsection we follow to study the cosmology of 2.2 with the aid of dynamical systems. For simplicity, and without loss of generality, we set $\kappa^2 = 1$.

We start by defining the following set of dimensionless, expansion normalised, variables [107]:

$$x^2 := \frac{\dot{\phi}^2}{6H^2}\,, \quad y^2 := \frac{V}{3H^2}\,, \quad z^2 := \frac{\rho_m}{3H^2}\,. \tag{2.3.1}$$

Then, it is possible to write the system (2.2.10) and (2.2.11), as a system of first order differential

equations:

$$x' = -x\left(3 + \frac{H'}{H}\right) + \sqrt{\frac{3}{2}}\left(\lambda y^2 + \frac{Q}{3H^2}\right) , \tag{2.3.2}$$

$$y' = -y\left(\sqrt{\frac{3}{2}}\lambda x + \frac{H'}{H}\right) , \tag{2.3.3}$$

$$z' = -z\left(\frac{3}{2} + \frac{H'}{H} + \frac{Qx}{\sqrt{6}H^2 z^2}\right) , \tag{2.3.4}$$

where a prime represents derivatives with respect to $N := \ln a$, and

$$\frac{H'}{H} = -\frac{3}{2}\left(1 + w_{\text{eff}}\right) , \tag{2.3.5}$$

with

$$w_{\text{eff}} = x^2 - y^2 \tag{2.3.6}$$

the effective equation of state parameter. The acceleration condition is verified when $w_{\text{eff}} < -1/3$. The equation of state parameter for the ϕ-field reads

$$w_\phi = \frac{p_\phi}{\rho_\phi} = \frac{x^2 - y^2}{x^2 + y^2} . \tag{2.3.7}$$

Equation (2.2.13) can be recast into

$$1 = x^2 + y^2 + z^2, \tag{2.3.8}$$

and is used to replace z in Eqs. (2.3.2), (2.3.3) and (2.3.4), reducing the dimensionality of the system:

$$x' = \frac{3}{2}x\left(x^2 - y^2 - 1\right) + \sqrt{\frac{3}{2}}\left[\lambda y^2 + \alpha\,\frac{\sqrt{6}x - \lambda y^2}{x^2 + \alpha\left(1 + w_{\text{eff}}\right)}(1 - x^2 - y^2)\right] , \tag{2.3.9}$$

$$y' = \frac{3}{2}y\left(1 + x^2 - y^2 - \sqrt{\frac{2}{3}}\lambda x\right) . \tag{2.3.10}$$

The interaction term Q is now rewritten within this setting as,

$$\frac{Q}{\rho_c} = \alpha\,\frac{\sqrt{6}x - \lambda y^2}{x^2 + \alpha\left(1 + w_{\text{eff}}\right)} . \tag{2.3.11}$$

Accordingly, when $\alpha = 0$ one reproduces the system studied in Ref. [94].

We restrict ourselves to the case where α is non-negative, that is $\alpha \geqslant 0$. This assumption stems from the fact that the coupling function in Eq. (2.2.4), $f \propto \dot{\phi}^{2\alpha}$, diverges for $(\alpha < 0) \wedge (\dot{\phi} = 0)$, and in addition the coupling term, Eq. (2.3.11), is singular for negative values of α along the hyperbola

$$y^2 = 1 + x^2 \left(1 + \frac{1}{\alpha}\right) , \tag{2.3.12}$$

giving rise to an ill-defined phase space.

The analysis of the fixed points of the system is essential to our study. These correspond to equilibrium states possessed by the Universe in some phase of its history. To examine them, we will focus on three important properties: existence, stability and whether they are capable of featuring a Universe with accelerated expansion. Existence is simply manifested through the Friedmann equation, by the condition $0 \leqslant \Omega_\phi = x^2 + y^2 \leqslant 1$ (a disk on the x-y plane), and requiring these points to be real-valued. As mentioned earlier, we have an accelerated critical point if $w_{\text{eff}} = x^2 - y^2 < -1/3$.

Let us consider a system of first order coupled (possibly nonlinear) differential equations

$$\dot{\mathbf{x}} = f(\mathbf{x}) , \tag{2.3.13}$$

with $\mathbf{x} = (x_1, \dots, x_n) \in \mathbb{R}^n$. A critical point (also called fixed or equilibrium point), $\mathbf{x}^c$ is a point where the system remains constant, *i.e.* $\dot{\mathbf{x}}^c = f(\mathbf{x}^c) = 0$. Note that the dimension of the vector $\mathbf{x}$ encodes the number of variables that span the phase space of the system. Say, for example, that $\dot{\phi}$ is a dynamical variable ($x_i = \dot{\phi}$). Thus, a critical point would have to satisfy the condition $\ddot{\phi} = 0$. This means that the kinetic energy of the ϕ field at this critical point remains constant (but ϕ is still evolving). To study the behaviour of the system, we are, however, interested in the study of the trajectories nearby this equilibria, since the points *per se* have no physical meaning. This may be done through linear stability theory. Consider a small perturbation of each variable around a critical point $\mathbf{x}^c$, that is, $\mathbf{x} = \mathbf{x}^c + \delta\mathbf{x}$. Now, we may Taylor expand Eq. (2.3.13) to first order

$$\dot{\mathbf{x}} = f(\mathbf{x}^c + \delta\mathbf{x}) = f(\mathbf{x}^c) + \mathbf{J}|_{x^c} \cdot \delta\mathbf{x} , \tag{2.3.14}$$

where $\mathbf{J} = \partial f_i / \partial x_j$ is the Jacobian matrix of f. Since at the fixed point, $f(\mathbf{x}_c) = 0$, we have at

Table 2.1: Fixed points of the system (2.3.9) and (2.3.10), respective relative energy densities and equation of state parameters.

Point	x_c	y_c	Ω_ϕ	$w_{\rm eff}$	w_ϕ
(A)	0	0	0	0	$-$
(B$^\pm$)	± 1	0	1	1	1
(C)	$\frac{\lambda}{\sqrt{6}}$	$\sqrt{1-\frac{\lambda^2}{6}}$	1	$\frac{\lambda^2}{3}-1$	$\frac{\lambda^2}{3}-1$
(D$^\pm$)	$\pm\sqrt{\frac{\alpha}{1+\alpha}}$	0	$\frac{\alpha}{1+\alpha}$	$\frac{\alpha}{1+\alpha}$	1
(E)	$\sqrt{\frac{3}{2}}\frac{1+2\alpha}{\lambda(1+\alpha)}$	$\sqrt{\frac{3-2\alpha(1+\alpha)(\lambda^2-6)}{2\lambda^2(1+\alpha)^2}}$	$\frac{3-\alpha(1+\alpha)(\lambda^2-12)}{\lambda^2(1+\alpha)^2}$	$\frac{\alpha}{1+\alpha}$	$\frac{\lambda^2\alpha(1+\alpha)}{3-\alpha(1+\alpha)(\lambda^2-12)}$

linear order $\dot{\delta\mathbf{x}} = \mathbf{J}\cdot\delta\mathbf{x}$, which has a general solution

$$\delta\mathbf{x} = \sum_{i=1}^{n} a_i v_i e^{\lambda_i t}\,, \tag{2.3.15}$$

near the fixed points, with λ_i and v_i being the eigenvalues and (respective) eigenvectors of $\mathbf{J}$ at x^c, and a_i constant coefficients (set by the initial conditions). Therefore, we note that if all the λ_i are negative, then all the perturbations decay, and we say that the critical point is *stable*. If all the eigenvalues are positive, then the perturbations grow and we call x^c an *unstable* critical point. Finally if some λ_i are positive and other negative, then the perturbations grow along given directions and decay over others (along the directions of the respective eigenvectors), and we say the point is a *saddle*. The *Hartman-Grobman theorem* [108] guarantees that the linear approximation is effective in expressing the dynamical behaviour of the nonlinear system, near the critical points. We refer the reader to [105, 107] for technical details and applications of dynamical systems to dark energy and modified gravity. A detailed description of dynamical systems goes beyond the scope of this thesis.

The dynamical analysis can be simplified by the symmetries of our system. Inspecting Eqs. (2.3.9) and (2.3.10) we note that the system is invariant under the reflection $y \to -y$ and time reversal $t \to -t$. Hence, we will only study the upper half disk, $y \geqslant 0$, in our analysis. An additional symmetry, namely $(x, \lambda) \to (-x, -\lambda)$ tells us that the phase space is completely characterised by non-negative values of λ.

In Table 2.1 we report on the critical points of the system of equations (2.3.9) and (2.3.10), together with the values of the energy density and equation of state parameters. Table 2.2 depicts

Table 2.2: Existence regions of the fixed points regarding the system (2.3.9) and (2.3.10) and whether they feature accelerated expansion.

Point	Existence	Acceleration
(A)	$\forall\, \alpha, \lambda$	No
(B$^{\pm}$)	$\forall\, \alpha, \lambda$	No
(C)	$0 < \lambda^2 \leqslant 6$	$\lambda^2 < 2$
(D$^{\pm}$)	$\forall\, \alpha, \lambda$	No
(E)	$3\frac{1+2\alpha}{1+\alpha} \leqslant \lambda^2 \leqslant 3\frac{4\alpha(1+\alpha)+1}{2\alpha(1+\alpha)}$	No

the parameter space in which the fixed points exist and feature accelerated expansion. We follow to give a more detailed analysis on the nature of each fixed point.

- **Point (A):** The fixed point $(x_c, y_c) = (0, 0)$, stands for a matter dominated Universe, $\Omega_m = 1$, and exists for all values of λ and α. Without an interaction, that is $\alpha = 0$, this fixed point has a saddle nature, attracting the trajectories along the x-axis and repelling them towards the y-axis. On the other hand, when we turn on the coupling, $\alpha \neq 0$, this point acquires a repulsive nature. This explicitly shows how the presence of the kinetic interaction may alter the dynamical behaviour of this critical point. Point (A) is not able to feature accelerated expansion.

- **Point (B$^{\pm}$):** Both these fixed points correspond to a Universe totally dominated by the kinetic energy of the scalar field, with $\Omega_\phi = x^2 = 1$. The equation of state describes a stiff fluid with $w_{\text{eff}} = w_\phi = 1$, and thus, acceleration is never achieved. These two points are never stable. Critical point (B$^+$) is a saddle for $\lambda < \sqrt{6}$ ($\lambda > -\sqrt{6}$ for (B$^-$)) and a repeller otherwise.

- **Point (C):** This is a well known critical point that is present in scalar field models of dark energy and inflation [34, 109]. It corresponds to a dark energy dominated solution with $\Omega_\phi = 1$. It exists for $\lambda^2 \leqslant 6$. However if the coupling is switched on, $\alpha \neq 0$, we also need to ensure that the parameter Q, Eq. (2.3.11), is well defined. This is achieved by imposing $\lambda \neq 0$ for its existence condition when $\alpha \neq 0$. When $\alpha = 0$, this point is stable for $\lambda^2 < 3$.

However, for $\alpha \neq 0$, the stability region can be generalised to

$$\lambda^2 < 3\frac{1+2\alpha}{1+\alpha}. \tag{2.3.16}$$

This is a new feature of considering a kinetic coupling: the region in which (C) is an attractor can be enlarged by α. This fixed point is a repeller when $\lambda^2 > 6$ and a saddle otherwise. Acceleration is achieved for $\lambda^2 < 2$.

- **Point ($D^{\pm}$):** These are novel critical points which arise solely in the presence of the kinetic interaction. They are always present in the phase space and describe a scaling regime. This (matter) scaling regime is characterised by the fact that the energy density of the scalar field, while being subdominant, evolves proportionally to - *scales with* - the matter component, *i.e.* $\rho_\phi = C\rho_m$ during this regime. For critical points $D^{\pm}$, we have $C = \alpha$. Scaling solutions arise in some models beyond the standard ΛCDM [110], and are of great importance since they can alleviate the cosmic coincidence problem by hiding the presence of a scalar field throughout an early period of the cosmic history, where its energy density may be large, albeit small at present times. In the current work, this early scaling regime can only be achieved in the presence of the coupling, $\alpha \neq 0$, absent in the standard uncoupled model. Points ($D^{\pm}$) will play a major role in the next subsection when finding solutions to the field equations by making use of the scaling behaviour. These fixed points coincide with the points ($B^{\pm}$) in the limit $\alpha \to \infty$, and with (A) when $\alpha \to 0$. Acceleration is never achieved since $w_{\rm eff} = \frac{\alpha}{1+\alpha}$. Stability, however, is verified if

$$\lambda > \sqrt{6 + \frac{3}{2\alpha(1+\alpha)}}, \tag{2.3.17}$$

for point (D^{+}),

$$\lambda < -\sqrt{6 + \frac{3}{2\alpha(1+\alpha)}}, \tag{2.3.18}$$

for (D^{-}), and they acquire a saddle nature otherwise.

- **Point (E):** This critical point is also present in the uncoupled case, $\alpha = 0$, [105], but here it is generalised with a dependence on α. It describes a scaling regime with $\Omega_\phi = \frac{3-\alpha(1+\alpha)(\lambda^2-12)}{\lambda^2(1+\alpha)^2}$. This fixed point is always stable and it does not generate acceler-

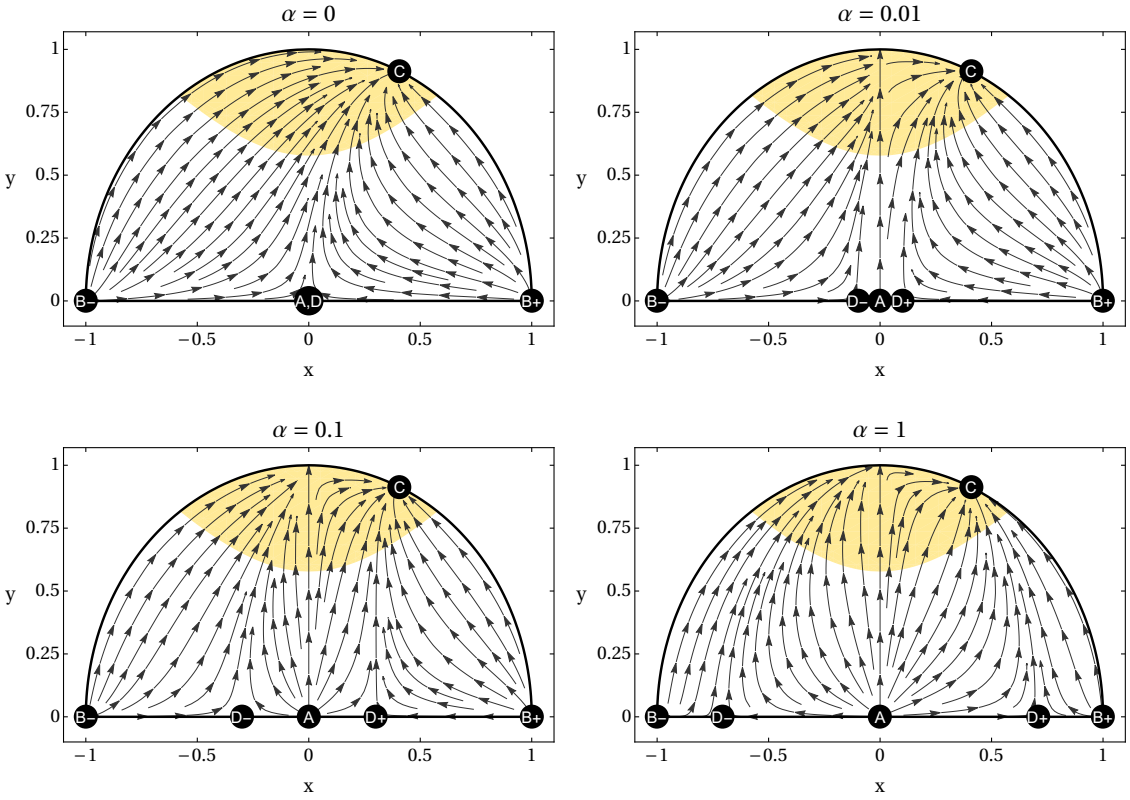

Figure 2.1: Phase space of the system of equations (2.3.9),(2.3.10), for $\lambda = 1$, with different values of the coupling α (respective title). Black dots denote the fixed points (with labels inside referenced to Table 2.1). The shaded region depicts the accelerated expansion area, i.e. where the condition $w_{\text{eff}} < -1/3$ is met.

ated expansion.

Note that in the presence of an interaction, when $x = 0$, Eq. (2.3.9) turns into $x' = 0$. This means that, when we switch on the kinetic coupling, *i.e.* $\alpha \neq 0$, we have a slicing of the phase space, at the axis $x = 0$, into two invariant sets[2] (see Ref. [107]), $x < 0$ and $x > 0$: if any orbit is found in this region at some time instant, then it will always remain there. This means that, assuming an expanding Universe, that is $H > 0$, the ϕ field will always evolve in the same direction: $\text{sgn}(\dot{\phi})$ never changes for any physical orbit. The orbit on the $x = 0$ axis (also an invariant set itself), joining the points $(x, y) = (0, 0)$ and $(0, 1)$, follows a Λ + CDM evolution, with a noninteracting pressureless matter species and a cosmological constant. In such case, the energy density $\rho_\Lambda = \rho_\phi = V =$ constant. Hence, any initial condition satisfying $x_i = 0$ will inevitably mimic a ΛCDM cosmology, portraying a transition from a matter dominated epoch into a potential totally dominated Universe, $(x, y) \to (0, 1)$. This final stage, represents a

[2]Consider the dynamical system $\dot{x} = f(x)$. A set $X \subset \mathbb{R}$ is called invariant (in f), if at some instant t^*, any tragectory $x(t^*) \in X \Rightarrow x(t) \in X, \ \forall t \geqslant t^*$.

cosmological constant governed solution, with $w_\phi = w_{\rm eff} = -1$, and $\Omega_\phi = y^2 = 1$. Since the sign of x does not change in any physical orbit, if one aims at reaching the future attractor (C) with an initial condition satisfying $x_i < 0$, then $\lambda < 0$ should also be verified. This guarantees that (C) lies on the $x < 0$ plane of the phase space. Invariance under the transformation $(x, \lambda) \mapsto (-x, -\lambda)$ guarantees that by simultaneously changing the signs of x_i and λ, the same cosmology is attained.

The only fixed point which is stable and generates accelerated expansion is point (C). Hence, we will rely on this equilibrium state, a dark energy governed solution (see Table 2.1), to be our future attractor candidate. There is, however, the risk of points (E) and ($\mathrm{D}^\pm$) being competing attractors for certain values of our parameters λ and α whilst not featuring accelerated expansion. But it turns out that the parametric window for λ where (C) generates acceleration (which is our aim) is outside the regions of existence of point (E) and stability of ($\mathrm{D}^\pm$), so we do not have to worry.

The critical points ($\mathrm{D}^\pm$) emerge every time there is an interaction, *i.e.* $\alpha \neq 0$. They emerge near the origin for small values of α (remember that $\mathrm{D}^\pm \xrightarrow{\alpha \to 0} \mathrm{A}$), and are shifted along the x-axis, until they coincide with ($\mathrm{B}^\pm$) when the interaction is strong (that is $\mathrm{D}^\pm \xrightarrow{\alpha \to \infty} \mathrm{B}^\pm$). This effect is depicted in Fig.2.1. Since point (D) is a saddle, we can naturally exit the early scaling regime and reach the accelerating attractor (C). Thus, we are able to reproduce solutions which at late times are described by the heteroclinic orbits connecting (D)→(C) (more rigorously, trajectories passing sufficiently close to these points).

Some last words should be mentioned. The dynamical analysis conducted in this section is only valid for a Universe filed with ϕ and a pressureless matter component. As in the next section we will look at solutions for a Universe filled with all cosmological fluids (including relativistic fluids), this analysis is only valid at late times when radiation is negligible.

2.4 Cosmological solutions

The aim of this section is to find numerical solutions for this kinetically interacting theory. To that end, we have modified CLASS [111–114] to include a scalar field interacting with dark matter through Eq. (2.2.4). In addition we also consider baryons and radiation with energy-momentum tensors described by a perfect fluid:

$$T^{(i)}_{\mu\nu} = \rho_i(1 + w_i)u^{(i)}_\mu u^{(i)}_\nu - \rho_i w_i g_{\mu\nu}\,, \tag{2.4.1}$$

where $w_b = 0$ for baryons and $w_r = 1/3$ for radiation. As previously stated, since couplings to standard model fields are tightly constrained by observational data, we assume baryons and radiation to be noninteracting:

$$\nabla_\mu T^{(b)\mu}_{\ \ \nu} = \nabla_\mu T^{(r)\mu}_{\ \ \nu} = 0\,. \tag{2.4.2}$$

The main focus of this work is to study the influence of the kinetic coupling on the dynamics of the cosmological parameters. Thus, we will present the numerical results for a fixed value of λ and vary the coupling, quantified by α. Firstly, because we observe that the effect of varying λ, for a fixed α, always follows the same trend, independently of the value of α. Second, because the effect of varying the stiffness of the potential, λ, has been already extensively studied in the literature [34, 115].

CLASS uses for the time variable conformal time, η, which is related to cosmic time through $d\eta = dt/a$. Thus, we write the metric Eq. (2.2.2) in terms of conformal time,

$$ds^2 = a(\eta)^2 \left(-d\eta^2 + \delta_{ij} dx^i dx^j\right)\,, \tag{2.4.3}$$

conformally related to Minkowski space.

The equations governing the background dynamics of our FLRW Universe become:

$$\phi'' + 2\mathcal{H}\phi' + a^2 V_\phi = a^2 Q\,, \tag{2.4.4}$$

$$\rho_c' + 3\mathcal{H}\rho_c = -Q\phi'\,, \tag{2.4.5}$$

$$\rho_b' + 3\mathcal{H}\rho_b = 0\,, \tag{2.4.6}$$

$$\rho_r' + 4\mathcal{H}\rho_r = 0\,, \tag{2.4.7}$$

where $\mathcal{H} = a'/a = aH = \dot{a}$ is the conformal Hubble rate, a prime now denotes derivative with respect to conformal time (not N), and

$$Q = 2\alpha\rho_c \frac{3\mathcal{H}\phi' + a^2 V_\phi}{2\alpha a^2 \rho_c + (1+2\alpha)\,\phi'^2}\,. \tag{2.4.8}$$

The energy density and pressure of the ϕ field are:

$$\rho_\phi = -T^{(\phi)0}{}_0 = \frac{\phi'^2}{2a^2} + V\,, \tag{2.4.9}$$

$$p_\phi = T^{(\phi)1}{}_1 = T^{(\phi)2}{}_2 = T^{(\phi)3}{}_3 = \frac{\phi'^2}{2a^2} - V\,, \tag{2.4.10}$$

respectively, and the Hubble flow follows the Friedmann constraint,

$$\frac{3a^2}{\kappa^2}\mathcal{H}^2 = \rho_\phi + \rho_m + \rho_r\,, \tag{2.4.11}$$

where we have defined the total matter density $\rho_m = \rho_b + \rho_c$.

The initial conditions are given deep in a radiation dominated epoch, at which $z_i = 10^{14}$ (z denotes redshift, defined as $1 + z = a_0/a$ with the value of the scale factor today set as $a_0 = 1$). We note that the initial conditions for ϕ and ϕ' only influence the time at which ρ_ϕ enters the scaling regime, and therefore has little influence over the cosmic evolution. The scale of the potential V_0 is used as a shooting parameter in order to get the present abundance of dark energy, $\Omega^0_\phi = \Omega^0_\Lambda$, as predicted by the latest Plank data [8]. Hence, we follow to fix $\phi_i = \phi(z_i) = \phi'_i = \phi'(z_i) = 10^{-2}$ and vary α so as to study the influence of the coupling on the cosmological parameters.

On the top panel of Fig. 2.2 the evolution of the energy densities ρ_i for each species is shown, with $\lambda = 0.2$. We note that when the coupling is switched on, $\alpha \neq 0$, an early scaling regime is attained, due to the new scaling critical points ($\mathrm{D}^\pm$) (studied in Sec. 2.3), whereas for $\alpha = 0$ this is not possible. We observe that the scalar source enters the scaling regime deep in the radiation epoch, around $z \approx 10^{10}$, with $\rho_c/\rho_\phi = 1/\alpha$ (see Table 2.1). This trend is depicted in Fig. 2.3.

Notice from Eqs (2.4.5), that the term which expresses the direction of the energy flow within the dark sector is $Q\phi'$: when $Q\phi' > 0$ energy is transferred from the dark matter source into the ϕ field, and when $Q\phi' < 0$ it is the quintessence field which grants energy into dark matter. The evolution of the coupling strength, $Q\phi'/\rho_c$, is depicted in Fig. 2.4. We notice that this term is always positive, since the values of ϕ' throughout the cosmic history always verify $\phi' > \kappa\lambda V/3\mathcal{H} \Leftrightarrow Q > 0$ (see Eq. (2.2.12) remembering that $\alpha > 0$). Therefore, dark matter grants energy to the ϕ field from cosmic ancient times until today. Since we impose that the energy density of dark energy today is the same independently of α (as mentioned, this is achieved by varying the shooting parameter V_0), the dark matter component must start with a larger energy density for increasing α (since it will give more energy to DE when the coupling is

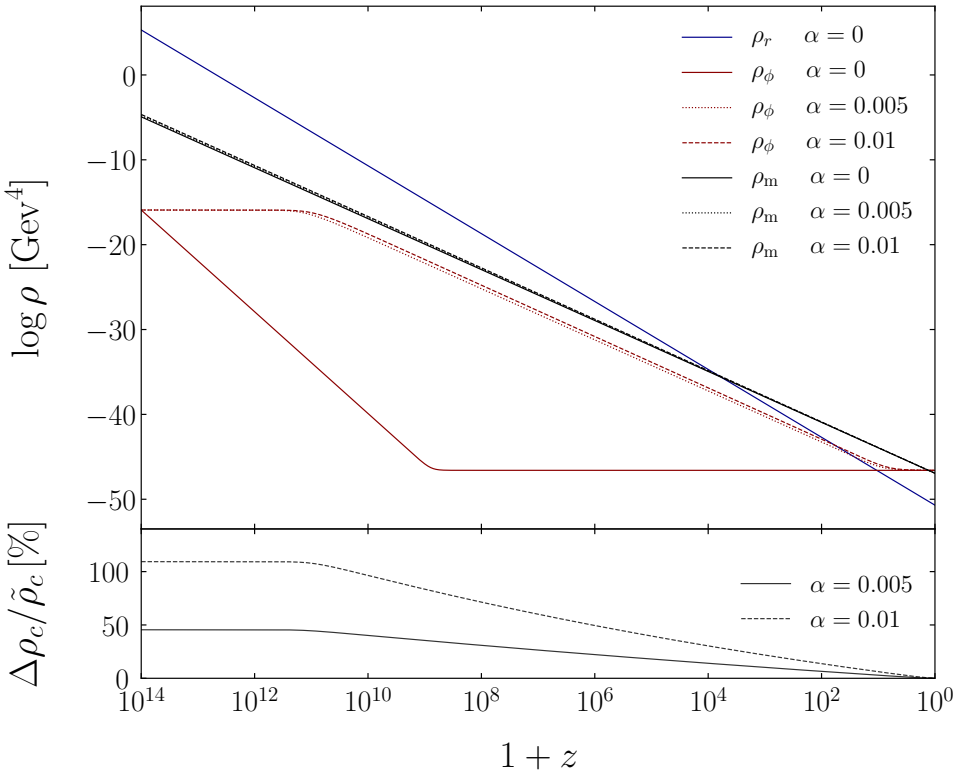

Figure 2.2: Top panel: evolution of the energy densities, ρ, for different values of the coupling (see legend), along redshift, with $\lambda = 0.2$, in regard to the model presented in Sec.2.4. Bottom panel: deviation on the energy density of dark matter relative to the uncoupled case ($\alpha = 0$), *i.e.* $\Delta\rho_c = \rho_c - \tilde{\rho}_c$, where $\tilde{\rho}_c = \rho_c(\alpha = 0)$.

stronger), which then decreases with time, as energy is lost for the ϕ field. This is shown on the bottom plot of Fig. 2.2, where we notice that for an interaction of $\alpha = 0.01$ the dark matter starts the simulation with approximately twice the value of DE compared with the uncoupled case. Naturally, as ρ_c increases with larger values of α, this will set the matter-radiation equality earlier in the cosmic history. This can be seen in Fig. 2.5, where the relative energy densities (cosmic abundances) for each species and for different values of the coupling (see respective legend) have been plotted. However, as the ϕ field is acquiring energy from the coupled matter component, at late times this effect becomes prominent, and dark energy starts to dominate earlier in the cosmic history. The bottom panel of the same figure, shows the deviations of the Hubble rate for each coupled model when compared with the uncoupled case: $\Delta H = H - \tilde{H}$, where a tilde denotes the noninteracting ($\alpha = 0$) case. Obviously, while radiation dominates the cosmic expansion, there is no deviation on H, since we have assumed radiation to be noninteracting. However, when matter becomes non-negligible, around $z \approx 10^6$, models with higher couplings acquire higher values for the expansion rate, since we have more DM for the same amount of radiation

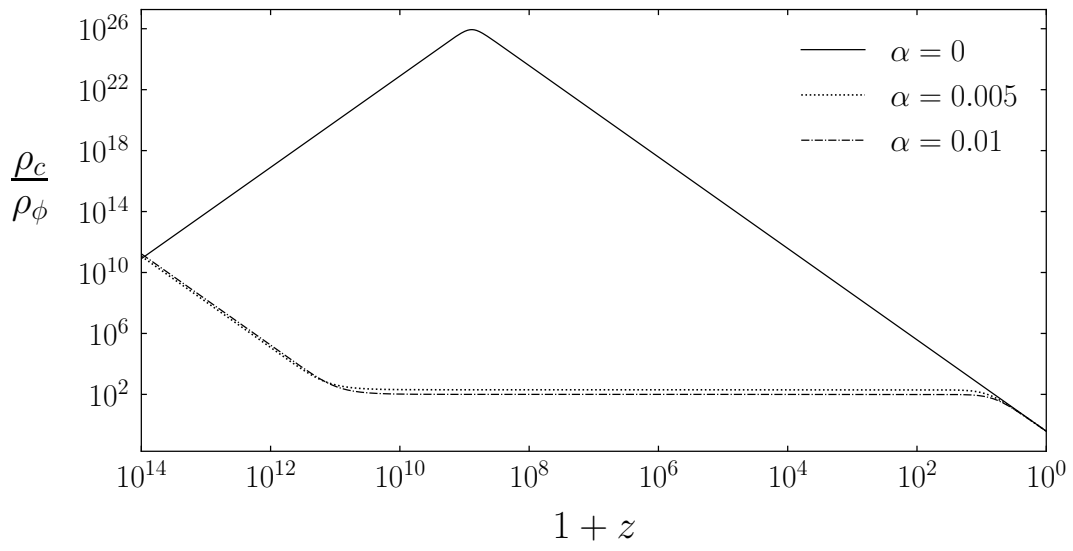

Figure 2.3: Ratio of the energy densities of cold dark matter and dark energy along the redshift z, for different values of the coupling (see legend), in regard to the model presented in Sec.2.4, with $\lambda = 0.2$. A scaling regime is characterised by a constant value, *i.e.* $\rho_c/\rho_\phi =$ constant.

on both models.

The dynamics of the equation of state parameters for the field, w_ϕ, and for the total effective budget, $w_{\rm eff}$ are shown in Fig. 2.6. According to Table 2.1, we observe that during the scaling regime the field behaves as a stiff fluid, $w_\phi = 1$, as its potential is negligible in contrast with its kinetic energy, $V \ll \phi'^2$ (see Eq. (2.3.7)). One may define an effective equation of state for the field, $w_\phi^{\rm eff}$, and for dark matter, $w_c^{\rm eff}$, by rewriting Eqs. (2.4.4) and (2.4.5) as

$$\rho'_\phi + 3\mathcal{H}\rho_\phi\left(1 + \overbrace{w_\phi - \frac{Q\phi'}{3\mathcal{H}\rho_\phi}}^{=:w_\phi^{\rm eff}}\right) = 0\,, \tag{2.4.12}$$

$$\rho'_c + 3\mathcal{H}\rho_c\left(1 + \underbrace{\frac{Q\phi'}{3\mathcal{H}\rho_c}}_{=:w_c^{\rm eff}}\right) = 0\,, \tag{2.4.13}$$

which accounts for the influence of the coupling. During the scaling regime, $\rho_c = \rho_\phi/\alpha \Rightarrow \rho'_c = \rho'_\phi/\alpha$, thus, from Eqs. (2.4.12) and (2.4.13), $w_c^{\rm eff} = w_\phi^{\rm eff}$ at the scaling. Now, we have

$$w_\phi^{\rm eff} = w_\phi - \underbrace{\frac{Q\phi'}{3\mathcal{H}\rho_c}}_{=w_c^{\rm eff}} \overbrace{\frac{\rho_c}{\rho_\phi}}^{=1/\alpha} \Rightarrow w_\phi^{\rm eff} = w_\phi - \frac{w_c^{\rm eff}}{\alpha}\,, \tag{2.4.14}$$

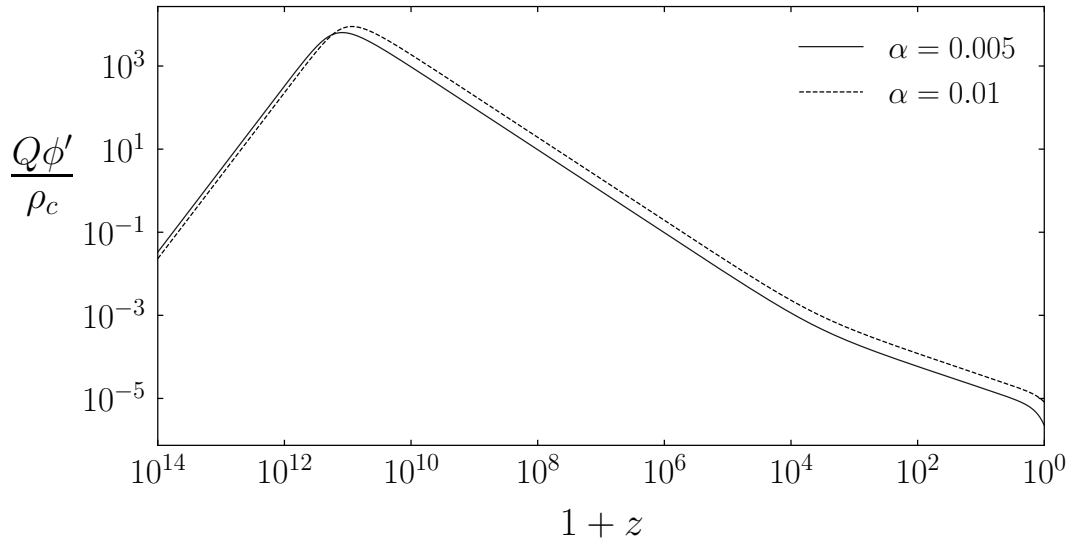

Figure 2.4: Coupling strength parameter along the redshift z, for different values of α (see legend), with $\lambda = 0.2$, in regard to the model presented in Sec.2.4.

and since $w_c^{\text{eff}} = w_\phi^{\text{eff}}$ at the scaling, we arrive at,

$$w_\phi = w_c^{\text{eff}} \left(1 + \frac{1}{\alpha}\right), \qquad \text{at the scaling.} \tag{2.4.15}$$

For a ϕCDM Universe (scalar field + cold dark matter), which was the case studied in the dynamical analysis on Sec. 2.3, we would have $w_\phi^{\text{eff}} = w_c^{\text{eff}} = w_{\text{eff}} = p_\phi/(\rho_\phi + \rho_c)$.

Still on Fig. 2.6, we note that the effective equation of state, w_{eff}, during radiation domination is $w_{\text{eff}} \approx w_r = 1/3$. During matter domination, $w_{\text{eff}} \approx \alpha/(1+\alpha)$ (see Table 2.1) during the scaling. Eventually the field exits the scaling regime, dark energy starts to dominate, and ϕ approaches the attractor where $w_{\text{eff}} \approx \lambda^2/3 - 1$. The Universe starts to accelerate later on for larger values of α. This is because, for a stronger interaction, the field leaves the scaling regime, where $w_\phi = 1$, later, and thus, its impact on the total equation of state is less pronounced. As a consequence, when the Universe starts to accelerate ($w_{\text{eff}} < -1/3$), it will accelerate slower. This can be verified since, for the same z, w_{eff} has a larger value as α grows. This latter trend may be more intuitively understood by inspecting the deceleration parameter $q := -\ddot{a}a/\dot{a}^2$. However, one would quickly realise that this is simply w_{eff} disguised, since

$$\frac{H'}{H} = -\frac{3}{2}\left(1 + w_{\text{eff}}\right) = -\left(1 + q\right) . \tag{2.4.16}$$

To finalise this chapter, let us briefly mention that it is known [116, 117] that the presence of

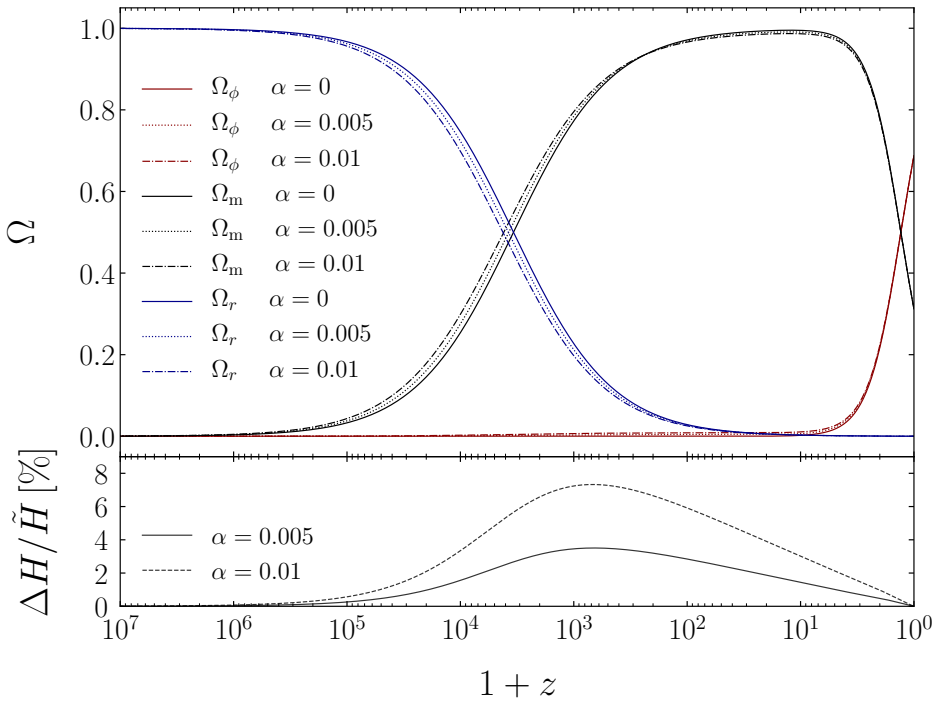

Figure 2.5: Top panel: evolution of the relative energy densities (cosmic abundances), Ω, for different values of the coupling (see legend), along the redshift z, with $\lambda = 0.2$, in regard to the model presented in Sec.2.4. Bottom panel: deviations on the Hubble rate relative to the uncoupled case ($\alpha = 0$), *i.e.* $\Delta H = H - \tilde{H}$, where $\tilde{H} = H(\beta = 0)$.

a considerable amount of early dark energy can significantly affect the position of the cosmic microwave background peaks. This early dark energy contribution can be constrained by experiments such as CMB lensing and small-scale measurements. Specifically, an upper bound of $\Omega_\phi < 0.0036$ was found at 95% confidence level (for Planck TT,TE,EE+lowP+BSH), from the Planck 2015 data [117]. In this work, this translates into a bound on the parameter α, since during the scaling regime, the energy of the scalar field depends solely on this coupling parameter, $\Omega_\phi = \alpha/(1+\alpha)$ (Table 2.1). Therefore, we find that $\alpha < 0.0036$. Satisfying this inequality guarantees that the dark energy imprints are negligible during matter domination. On the other hand, note that early dark energy models may present larger expansion rates at early times [118], and therefore have been used to alleviate the H_0 tension [119]. The bound found for α may be alleviated if one shifts the early scaling regime towards latter times, where the constraints for Ω_ϕ are not so stringent (see Fig.11 of Ref. [117]). In that case, by avoiding the Planck constraints, one way to further test the model at lower redshifts could be through measurements of the Hubble rate, such as quasar distances, from their X-ray and ultraviolet emission [120]; it was found 4σ deviations from ΛCDM by considering data for $z > 1.4$ (see Fig.3 of Ref. [120]). Furthermore, one expects the future space-based interferometer eLisa [121] to be able to constrain early and

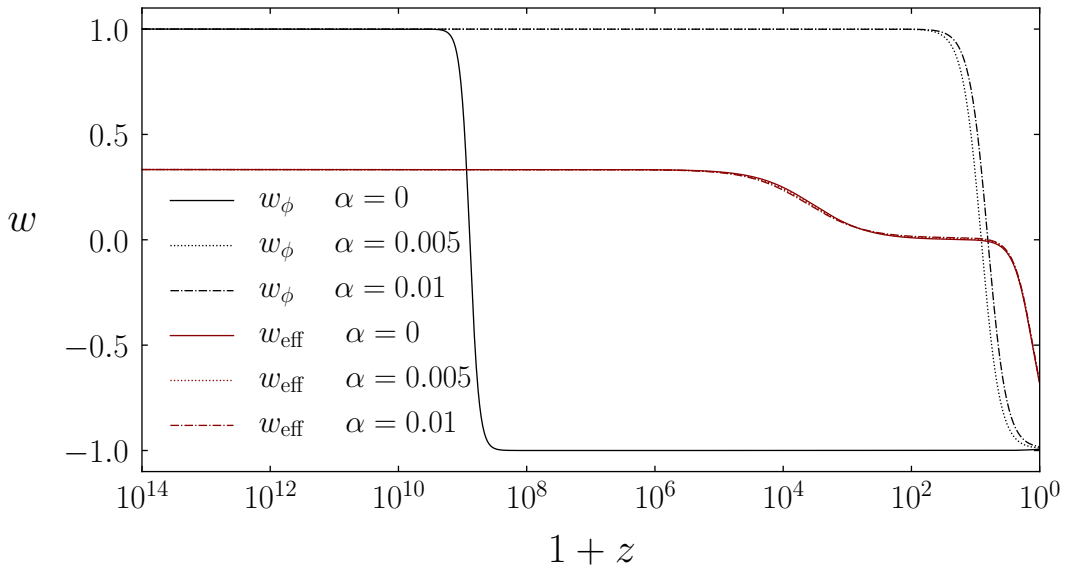

Figure 2.6: Evolution of the equation of state parameters, $w_{\rm eff}$ and w_ϕ, along redshift, for different coupling values (see legend), with $\lambda = 0.2$, in regard to the model presented in Sec.2.4.

interacting dark energy models at redshifts $1 < z < 8$ [122, 123], with data coming from gravitational wave standard sirens.

Chapter 3

Coupled quintessence with a ΛCDM background

Oh you, who have never heard the voice of heaven, who think man destined only to live this little life and die in peace; you, who can resign in the midst of populous cities your fatal acquisitions, your restless spirits, your corrupt hearts and endless desires.

From *Discourse on the Origin of Inequality Among Men*,
by Jean Jacques Rousseau

This chapter is based on Refs. [124] and Ref. [125].

At present, the ΛCDM model features a tension between CMB experiments and redshift space distortions on the amplitude of the matter power spectrum at the scale of $8h^{-1}$ Mpc, denoted σ_8, [23–28]. The lower clustering rate predicted by Planck data against large scale observations is a well known problem of the standard model of cosmology. There have been proposals to alleviate or solve this problem through, for example, modified theories of gravity [126, 127]. These models alter the dynamical behaviour of the matter perturbations in contrast with the standard ΛCDM, consequently making it possible to obtain values of σ_8 that are compatible with data.

In this chapter, a coupled quintessence model, with a particular feature imposed *a priori*, is proposed to alleviate the σ_8 tension. Although the theory can be recast into a particular case of the general model presented in Chapter 2 as we will see, in Sec. 3.1 the details regarding the motivation for the nonminimal coupling to matter are presented, stemming from conformal transformations. This possibility had already been briefly mentioned in Sec. 2.1.1. The background

and perturbations are then analysed in Secs. 3.2 and 3.3, together with the analysis on the σ_8 parameter. The nonlinear matter perturbations and the spherical collapse are then studied in the last section, Sec. 3.4.

3.1 Nonminimal couplings and conformal transformations

One common approach to introduce a nonminimal coupling in the matter sector is by assuming that matter experiences a different metric, say $\tilde{\mathbf{g}}$, than the one according to which ϕ propagates, $\mathbf{g}$. These two different metrics can be related through a Weyl scaling stemming from a conformal transformation (see Section 7.6.2 of Ref. [128]). Specifically, given a Riemannian space $(\mathcal{M}, \mathbf{g})$, consisting of a smooth manifold $\mathcal{M}$ endowed with a metric $\mathbf{g}$, a conformal tranformation ζ is a diffeomorphism

$$\begin{aligned} \mathcal{M} &\xrightarrow{\ \zeta\ } \mathcal{M} \\ x^\mu &\longmapsto \tilde{x}^\mu = \zeta(x^\mu) \end{aligned} \tag{3.1.1}$$

such that $\zeta^* \mathbf{g} = \Omega^2(x^\mu)\, \mathbf{g}$; that is, a change of coordinates that leaves the metric invariant up to a conformal factor Ω^2. Note that the trivial case $\Omega = 1$ simply represents an isometry. In scalar-tensor theories of gravity (see section 3.2 of Ref. [33]) the conformal factor is mediated by a scalar field ϕ naturally present in the theory, *i.e.* $\Omega(x^\mu) = \Omega[\phi(x^\mu)]$. It is then common to evoke a given theory $\mathcal{S}\,[\mathbf{g}, \phi, \psi]$ (where ψ portray the matter fields) in one of two physically meaningful representations, or as it customary to say, two different frames, which portray the same underlying theory but with distinct interpretations for gravitational phenomena. One spacetime, say, $(\mathcal{M}, \mathbf{g})$, is known as the Einstein frame if the scalar degree of freedom is minimally coupled to gravity, $\mathcal{L}_g = \mathcal{L}_g(\mathbf{g})$, but nonminimally coupled to matter, $\mathcal{L}_m = \mathcal{L}_m(\mathbf{g}, \phi, \psi)$. In the other frame, $(\mathcal{M}, \tilde{\mathbf{g}})$, with $\tilde{\mathbf{g}} = \Omega^2 \mathbf{g}$, dubbed the Jordan frame, ϕ is minimally coupled to matter, $\mathcal{L}_m = \mathcal{L}_m(\mathbf{g}, \psi)$, and nonminimally coupled to gravity, $\mathcal{L}_g = \mathcal{L}_g(\mathbf{g}, \phi)$. This nonminimal coupling to gravity, in the so-called Jordan frame, can be interpreted as a varying gravitational constant, and was introduced in 1961 by Carl H. Brans and Robert H. Dicke (known as Brans-Dicke theory) [129] as an effort to integrate Mach's principle within GR. We refer the reader to Ref. [130] to see the details on scalar-tensor cosmology. One may then write the action for a given theory in a given frame, and map it to another one simply by means of a Weyl scaling, $\mathbf{g} \mapsto \tilde{\mathbf{g}} = \Omega^2 \mathbf{g}$. A discusion regarding the equivalence of both frames, and some concepts within them, can be

found in, for example, Refs. [131, 132].

Let us then write the following total action in the Einstein frame:

$$\mathcal{S} = \int \omega_g \left(\frac{R}{2\kappa^2} - \frac{1}{2} g^{\mu\nu} \partial_\mu \phi \partial_\nu \phi - V \right) + \mathcal{S}_m \left[\tilde{g}_{\mu\nu}, \psi \right] . \tag{3.1.2}$$

In this framework the matter fields propagate in geodesics laid out by the metric $\tilde{g}_{\mu\nu}$, associated to $g_{\mu\nu}$ through a general Weyl scaling

$$\tilde{g}_{\mu\nu} = \Omega(\phi)^2 g_{\mu\nu} . \tag{3.1.3}$$

The reader is referred to section 2.1 of Ref. [133] for the mathematical *apparatus* of conformal transformations. In essence, the propagation of the matter fields is affected by the dynamics of ϕ, as $\mathcal{S}_m$ depends on ϕ through Eq. (3.1.3).

Varying the action Eq. (3.1.2) with respect to $g^{\mu\nu}$ yields the following field equations:

$$R_{\mu\nu} + \frac{1}{2} g_{\mu\nu} R = \kappa^2 \, T^{(\mathrm{eff})}_{\mu\nu} , \tag{3.1.4}$$

where the effective energy-momentum tensor is defined as

$$T^{(\mathrm{eff})}_{\mu\nu} = T^{(\phi)}_{\mu\nu} + T^{(m)}_{\mu\nu} , \tag{3.1.5}$$

with

$$T^{(\phi)}_{\mu\nu} = \partial_\mu \phi \partial_\nu \phi - g_{\mu\nu} \left(g^{\alpha\beta} \partial_\alpha \phi \partial_\beta \phi + V \right) , \tag{3.1.6}$$

$$T^{(m)}_{\mu\nu} = -\frac{2}{\sqrt{|g|}} \frac{\delta \mathcal{S}_m}{\delta g^{\mu\nu}} . \tag{3.1.7}$$

The contracted Bianchi identities give the following conservation relations for the stress-energy tensors (see Chapter 2 of Ref. [133] or Appendix D of Ref. [6]):

$$\nabla_\mu T^{(\phi)\mu}_{\ \ \ \nu} = -T^{(m)} \nabla_\nu \left(\ln \Omega \right) , \tag{3.1.8}$$

$$\nabla_\mu T^{(m)\mu}_{\ \ \ \nu} = T^{(m)} \nabla_\nu \left(\ln \Omega \right) , \tag{3.1.9}$$

where $T^{(m)}$ is the trace of matter's energy-momentum tensor. Since the conformal factor is

mediated by ϕ, as defined in Eq. (3.1.3), *i.e.* $\Omega = \Omega(\phi)$, we may write instead:

$$\nabla_\mu T^{(\phi)\mu}_{\ \ \nu} = -\frac{\Omega_{,\phi}}{\Omega} T^{(m)} \nabla_\nu \phi \,, \tag{3.1.10}$$

$$\nabla_\mu T^{(m)\mu}_{\ \ \nu} = \frac{\Omega_{,\phi}}{\Omega} T^{(m)} \nabla_\nu \phi \,, \tag{3.1.11}$$

where $\Omega_{,\phi} = \partial\Omega/\partial\phi$. Note that while the total energy-momentum tensor is conserved, each invividual species is not. There is a flow of energy between matter and the scalar field mediated by the conformal factor $\Omega(\phi)$. This is germane to the fact that we have considered the action in Eq. (3.1.2) in the Einstein frame, where the scalar degree of freedom is uncoupled to gravity but *nonminimally* coupled to matter. For obvious reasons, this specific form of interactions, as defined in Eqs. (3.1.10) and (3.1.11), are referred to as *conformal couplings*.

In this current work, we will focus on the case where $\Omega = e^{-\kappa\beta\phi}$, with β being a constant governing the strenght of the interaction between the two components. Therefore, Eqs. (3.1.10) and (3.1.11) can be expressed as,

$$\nabla_\mu T^{(\phi)\mu}_{\ \ \nu} = -\nabla_\mu T^{(m)\mu}_{\ \ \nu} = \kappa\beta\, T^{(m)} \nabla_\nu \phi \,. \tag{3.1.12}$$

Rewriting the action Eq. (3.1.2) in the Jordan frame, through the transformation $g_{\mu\nu} \mapsto e^{-\kappa\beta\phi} g_{\mu\nu}$, would result in a gravitational Lagrangian nonminimally coupled to ϕ as $R \to e^{-\kappa\beta\phi} R$ (see section 8.4 of Ref. [16]). This particular form of the coupling can be found, for example, in string theory as a low-energy matter coupling of the dilaton field [134, 135], although in the original formulation, the exponential term is universally coupled to the entire matter sector in the action.

Note that the theory described by the action Eq. (3.1.2), with the transformation $g_{\mu\nu} \mapsto \Omega(\phi)^2 g_{\mu\nu}$, resulting in the fluid relations Eq. (3.1.12), is a specific case of the model described in the last chapter, Eq. (2.1.1), with $f(\phi, X) = \Omega(\phi) = e^{-\kappa\beta\phi}$.

Finally, note that the coupling to the matter species in Eq. (3.1.2) needs not to be universal to all the components [136]. Different fluids may experience different metrics:

$$\mathcal{S} = \int \omega_g \left(\frac{R}{2\kappa} - \frac{1}{2} g^{\mu\nu} \partial_\mu\phi \partial_\nu\phi - V \right) + \sum_i \mathcal{S}_i \left[\tilde{g}^i_{\mu\nu}, \psi_i \right] \,, \tag{3.1.13}$$

thus resulting on different conservation relations for each species; different Ω_i are associated with each species, where $\Omega = 1$ denotes the absence of a coupling.

As mentioned in the last chapter, as couplings to standard model fields are tightly constrained,

for example by Solar System observations, it is common to assume that only the DM component couples to the scalar degree of freedom. Thus, in this chapter, we rely on such an assumption. Additionally we also consider noninteracting radiation and baryons. Thus, the cosmology of the present *coupled quintessence* model upon which this section is based, is determined by the following set of equations:

$$\frac{1}{\kappa^2}G_{\mu\nu} = T^{(\phi)}_{\mu\nu} + T^{(c)}_{\mu\nu} + T^{(b)}_{\mu\nu} + T^{(r)}_{\mu\nu}\,, \tag{3.1.14}$$

$$\nabla_\mu T^{(\phi)\mu}_{\ \ \nu} = -\kappa\beta\,\rho_c \nabla_\nu \phi\,, \tag{3.1.15}$$

$$\nabla_\mu T^{(c)\mu}_{\ \ \nu} = \kappa\beta\,\rho_c \nabla_\nu \phi\,, \tag{3.1.16}$$

$$\nabla_\mu T^{(b)\mu}_{\ \ \nu} = 0\,, \tag{3.1.17}$$

$$\nabla_\mu T^{(r)\mu}_{\ \ \nu} = 0\,, \tag{3.1.18}$$

where the stress tensors are defined according to Eq. (2.4.1), with $w_c = w_b = 0$, $w_r = 1/3$ and Eq. (2.3.7) for w_ϕ. Note that the scalar potential $V(\phi)$ is left unspecified as it will be automatically determined by an assumption explained in the following section.

3.2 Background

Under a flat cosmology, described by Eq. (2.2.2), the system of equations Eqs. (3.1.14)-(3.1.18), render the background to follow

$$\ddot{\phi} + 3H\dot{\phi} + V_{,\phi} = \kappa\beta\rho_c\,, \tag{3.2.1}$$

$$\dot{\rho}_c + 3H\rho_c = -\kappa\beta\dot{\phi}\rho_c\,, \tag{3.2.2}$$

$$\dot{\rho}_b + 3H\rho_b = 0\,, \tag{3.2.3}$$

$$\dot{\rho}_r + 4H\rho_r = 0\,, \tag{3.2.4}$$

with the Friedmann equation

$$\frac{3}{\kappa^2}H^2 = \rho_\phi + \rho_c + \rho_b + \rho_r\,. \tag{3.2.5}$$

We can immediately integrate Eq. (3.2.2), yielding the following evolution equation for the

energy density of dark matter:

$$\rho_c = \rho_c^* a^{-3} e^{-\kappa\beta\phi}\,, \tag{3.2.6}$$

where ρ_c^* is an integration constant.

At this point, several studies in the literature [38, 94] follow to fix a specific form for the potential V and numerically solve the equations. Here, instead of fixing V, we assume a particular relation, which *a posteriori* determines V. The assumption is that the background expansion follows a ΛCDM evolution

$$H^2 = H_s^2\,, \tag{3.2.7}$$

where H^2 is the Hubble rate for the coupled quintessence model, given by Eq.(3.2.5), and H_s^2 is the standard Hubble rate, defined in the context of the ΛCDM model, with uncoupled cold dark matter and a cosmological constant,

$$H_s^2 = \frac{\kappa^2}{3}(\rho_\Lambda + \rho_{cdm} + \rho_b + \rho_r)\,, \tag{3.2.8}$$

with $\rho_{cdm} = \rho_{cdm}^0 a^{-3}$, being $\rho_{cdm}^0 = \rho_{cdm}(a=1)$ the present energy density of CDM. Through this assumption, the background predictions become indistinguishable from the standard model ones; supernovae type Ia distances will remain unaltered as the luminosity distance depends only on the Hubble rate. Similarly, for baryonic acoustic oscillations, the observables are given in terms of $H(z)$ only [137]. When compared against observational data, most of the proposed quintessence models in the literature are constrained to be extremely close to ΛCDM. Therefore, we are interrested in studying if, by fixing the background to exactly follow the dynamics of ΛCDM, distinctive deviations arise at the perturbation level. Note that we only assume that the Hubble rates coincide, which doesn't necessarily amount to the same evolution for the individual species. A similar behaviour at the background level was also proposed in Ref. [138], however in a different fashion: by considering an interaction depending on the velocities of DM and DE the authors are able to hide the effect of the coupling at large scales, and only at small scales does the interaction manifest itself.

Through Eq. (3.2.7), we are able to find the underlying form of V that assures the validity of $H = H_s$, Eq. (3.2.7):

$$V = \frac{1}{2}\dot{\phi}^2 + \rho_\Lambda\,, \tag{3.2.9}$$

and the energy densities for the dark components can be written, respectively, as:

$$\rho_\phi = \rho_\Lambda + \dot{\phi}^2 \,, \tag{3.2.10}$$

$$\rho_c = \rho_{cdm} - \dot{\phi}^2 \,. \tag{3.2.11}$$

Note that the assumption Eq. (3.2.7) completely fixes the potential through Eq. (3.2.9), resulting on a single free parameter for the theory, the coupling β, and none associated to the potential (such as, for example λ in the model presented in Sec. 2.2). Taking the derivative with respect to ϕ of Eq. (3.2.9) and substituting in Eq. (3.2.1) we find the background equation of motion for the scalar field which renders the background to follow a ΛCDM evolution,

$$2\ddot{\phi} + \dot{\phi}\,(3H + \kappa\beta\dot{\phi}) - \kappa\beta\rho_{cdm} = 0 \,. \tag{3.2.12}$$

We can write Eq. (3.2.12) in terms of derivatives with respect to the number of e-folds $N = \ln a$, i.e. $\phi' := \partial\phi/\partial N = \dot{\phi}/H$, such that

$$2\phi'' + \phi'\left(3 + 2\frac{H'}{H} + \kappa\beta\phi'\right) - \frac{3}{\kappa}\beta\,\Omega_{cdm} = 0 \,, \tag{3.2.13}$$

where

$$\frac{H'}{H} = -\frac{1}{2}\left(3 + \Omega_r - 3\,\Omega_\Lambda\right) \,. \tag{3.2.14}$$

Note that in the absence of interaction, $\beta = 0$, Eq. (3.2.7) turns into $\rho_\phi = \rho_\Lambda$, thus we recover a pure ΛCDM evolution for every species. Curiously, from Eqs. (3.2.10) and (3.2.11) we observe that when the coupling is switched on, $\beta \neq 0$, the energy density of dark matter can only be smaller than its ΛCDM counterpart, with the opposite holding for dark energy. Eq. (3.2.10) tells us that for a certain value of β, at a given redshift z, the energy density of the field will exceed that of Λ by $\dot{\phi}^2(z)$, with the opposite holding to DM, according to Eq. (3.2.13). Kindly note that since Eq. (3.2.13) is symmetric under the reflection $(\beta, \dot{\phi}) \mapsto (-\beta, -\dot{\phi})$, we will choose to conduct our analysis considering only the case $\beta \geqslant 0$.

We follow to numerically solve Eq. (3.2.13), which here completely determines the background evolution. We start the simulations in a radiation dominated epoch, at $z_i \approx 10^6$, and assume that initially the relative energy density of each species equals their ΛCDM counterpart, *i.e.* $\dot{\phi}_i = \phi_i = 0$. The cosmological parameters are fixed by the Planck bestfit values [139]. The energy densities for the species are shown on the top panel of Fig. 3.1, for ΛCDM ($\beta = 0$),

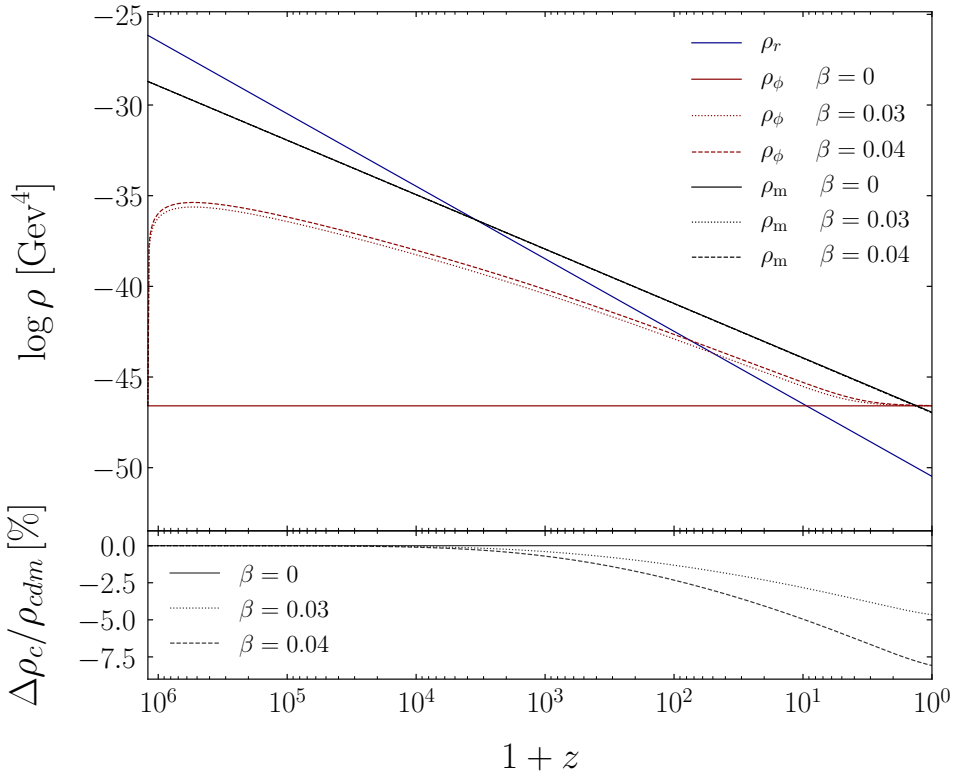

Figure 3.1: Top panel: evolution of the energy densities, ρ, for different values of the coupling (see legend), along redshift, in regard to the model presented in Sec.3.2. Bottom panel: deviation on the energy density of dark matter relative to the uncoupled case ($\beta = 0$), *i.e.* $\Delta\rho_c = \rho_c - \rho_{cdm}$.

$\beta = 0.03$ and $\beta = 0.04$. Note that the behaviour of ρ_ϕ also encodes the dynamics of the potential V, and $\dot{\phi}^2$, since these are both linear functions of $\dot{\phi}^2$ (see Eqs.(3.2.9) and (3.2.10)). From our choice of initial conditions we find that $\beta\dot{\phi} > 0$, which implies that the flow of energy always happens from dark matter into the quintessence field ϕ, throughout the cosmic history. This is concordant with the fact that, as mentioned earlier, the energy share of dark matter (dark energy) today is lower (higher), than in standard ΛCDM. Particularly, the value of the energy density of dark matter today is, using Eq. (3.2.11), $\rho_c^0 = \rho_{cdm}^0 - \dot{\phi}_0^2$, where, using Eq. (3.2.6), $\dot{\phi}_0 = \rho_{cdm}^0(1 - e^{-\kappa\beta\phi_0})$. This trend is depicted on the bottom panel of Fig. 3.1, where the relative difference $\Delta\rho_c = \rho_c - \rho_{cdm}$ is plotted for different values of β. For a coupling strength of $\beta = 0.03$, the density of DM today is approximately 5% smaller than in the ΛCDM case. Naturally, as the dark matter species is granting energy to dark energy, the matter-radiation equality will happen latter in the cosmic history. However, this effect if negligible for the chosen values of β, since at this epoch the differences from ΛCDM are consistently less than 0.3%. On the other hand, the epoch at which dark energy starts to dominate happens manifestly earlier. This can be observed in Fig. 3.2, where the relative energy densities (cosmic abundances) are

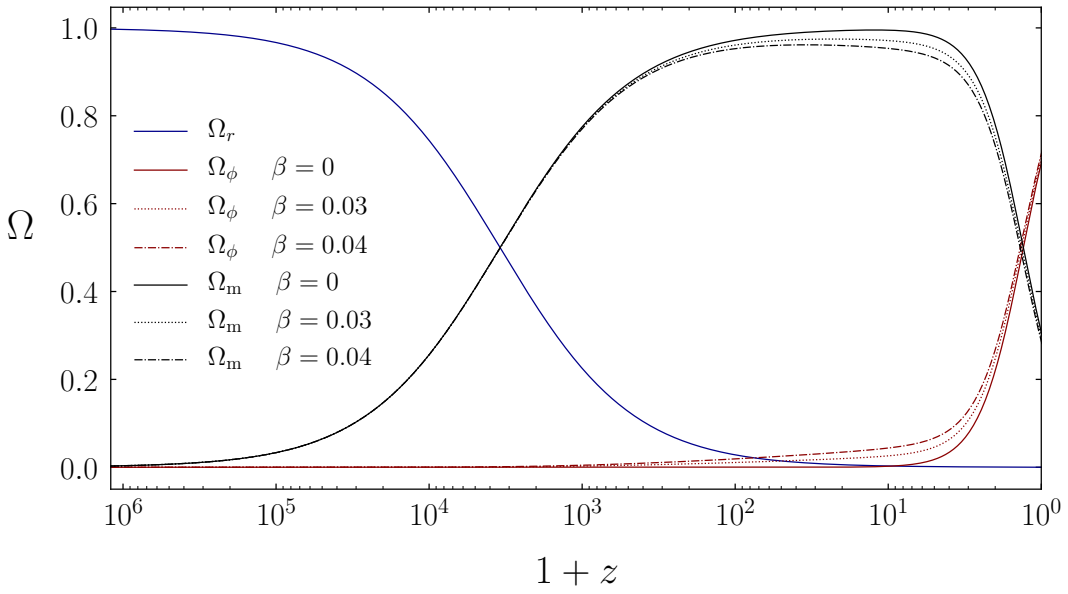

Figure 3.2: Evolution of the relative energy densities (cosmic abundances), Ω, for different values of the coupling (see legend), along redshift, in regard to the model presented in Sec.3.2.

depicted for each species and different values of β. The matter-dark energy transition happens around 317 Myr and 562 Myr earlier, for $\beta = 0.03$ and $\beta = 0.04$, respectively, in contrast with standard ΛCDM. Note that the evolution of cosmic time is left unchanged in the present model, since the Hubble rate is the same as in the standard model of cosmology, *i.e.* $t = \int da/aH$. Thus, the age of the Universe is left unaltered by varying β.

The dynamics of the equation of state parameter for the field, w_ϕ, is depicted in Fig. 3.3. The behaviour of w_ϕ at early and late times can easily be understood through the balance of two terms: $\dot{\phi}^2$ and ρ_Λ. Note that by taking the time derivative of Eq. (3.2.7) one finds that the pressure of the quintessence field is also constant, $p_\phi = p_\Lambda = -\rho_\Lambda$. Now, using Eq. (3.2.10), the equation of state can be written as

$$w_\phi = \frac{p_\phi}{\rho_\phi} = -\frac{\rho_\Lambda}{\rho_\Lambda + \dot{\phi}^2}\,. \tag{3.2.15}$$

At early times $\dot{\phi}^2 \gg \rho_\Lambda$ (see Fig. 3.1 remembering that $\rho_\phi = \rho_\Lambda + \dot{\phi}^2$), thus Eq. (3.2.15) gives $w_\phi \approx 0$ in this regime. On the other hand, for $\dot{\phi}^2 \ll \rho_\Lambda$, at late times, we have $w_\phi \approx -1$. However, the dynamics of ϕ strongly depends on the choice of the coupling β. Hence, the epoch at which each term starts to dominate is strongly influenced by β. For larger values of β, the time taken by ϕ to depart from $w_\phi \approx 0$ is prolonged since $\dot{\phi}$ takes higher values with increasing β. This is depicted in Fig. 3.3. One special feature of this model is that the rate at which the universe

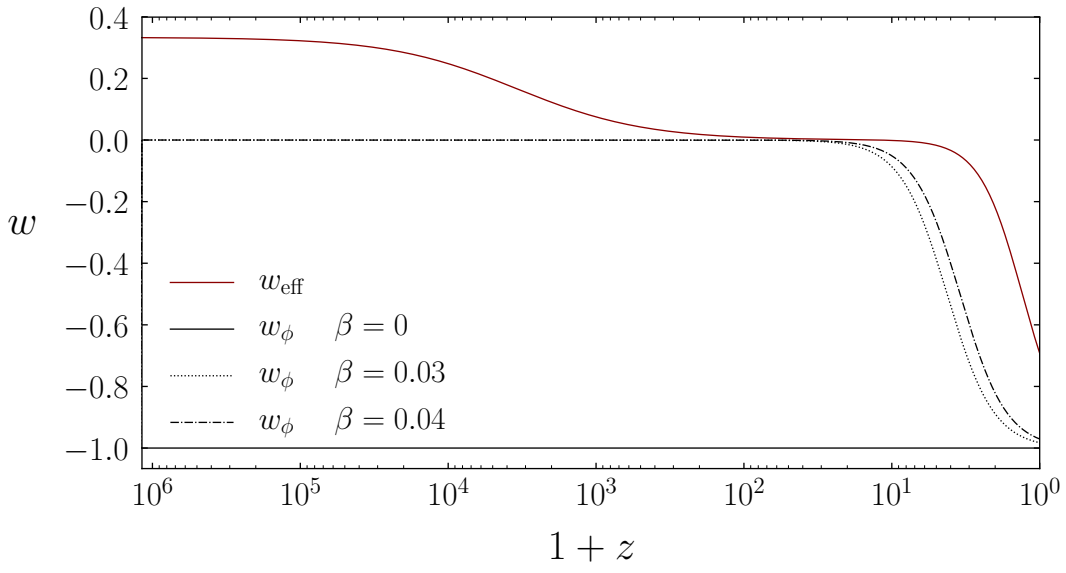

Figure 3.3: Evolution of the equation of state parameters, $w_{\rm eff}$ and w_ϕ, along redshift, for different coupling values (see legend), in regard to the model presented in Sec.3.2.

accelerates is always the same as in ΛCDM, independently of when DE starts to dominate. As already been mentioned, $p_\phi = p_\Lambda$. Now, as stated in the last chapter, the deceleration parameter is related to the effective equation of state $w_{\rm eff}$, which does not change in the current model since, from Eqs. (3.2.10), (3.2.11) and the derivative of Eq. (3.2.7),

$$w_{\rm eff} = \frac{\sum_i p_i}{\sum_i \rho_i} = \frac{p_\phi + p_r}{\rho_\phi + \rho_c + \rho_b + \rho_r} = \frac{p_\Lambda + p_r}{\rho_\Lambda + \cancel{\dot{\phi}^2} + \rho_{cdm} - \cancel{\dot{\phi}^2} + \rho_b + \rho_r} = w_{\rm eff}^{\Lambda\rm CDM} . \quad (3.2.16)$$

The behaviour of $w_{\rm eff}$ is also depicted in red in Fig. (3.3), and since there are no novelties (apart from its invariance with β) in contrast with ΛCDM we do not focus on a detailed interpretation. During radiation domination it follows the trend of $w_{\rm eff} \approx w_r = 1/3$, for the matter dominated epoch $w_{\rm eff} \approx w_m = 0$, and $w_{\rm eff} \approx w_\Lambda = -1$ at late times.

3.3 Perturbations and the σ_8 tension

For the background study, we have assumed our Universe to be described by the homogeneous and isotropic FLRW line element. However, we know that the Universe must be described by a far more complex picture. In this section, we study the linear matter perturbations for this model in the longitudinal gauge, also called Newtonian gauge, (see section 8 of Ref. [140]). We will additionally dive into the study of formation of structure processes. Thus, our main focus is the

behaviour of matter (dark matter + baryons) perturbations at late times (after matter-radiation equality) and small scales (this will be quantified along this section). Therefore we will neglect radiation fluids and other baryonic effects.

We begin by considering scalar perturbations along FLRW in the Newtonian gauge (also called longitudinal gauge) with line element given by,

$$ds^2 = -(1+2\Psi)dt^2 + a(t)^2(1-2\Phi)\delta_{ij}dx^i dx^j\,, \tag{3.3.1}$$

where Ψ and Φ are the standard Bardeen potentials [141]. We also define the dimensionless density contrast for the i-th species,

$$\delta_i = \frac{\delta\rho_i}{\bar{\rho}_i}\,. \tag{3.3.2}$$

Analogous to the metric, the matter content is perturbed by expanding the variables as the sum of background plus a small perturbation:

$$\phi(\vec{x},t) = \phi_i(t) + \delta\phi(\vec{x},t)\,, \tag{3.3.3}$$

$$\rho_i(\vec{x},t) = \rho_i(t) + \delta\rho_i(\vec{x},t)\,, \tag{3.3.4}$$

$$p_i(\vec{x},t) = p_i(t) + \delta p_i(\vec{x},t)\,. \tag{3.3.5}$$

We may compute the components of the energy-momentum tensors of the species through Eq. (2.4.1) at first order,

$$\delta T^{(i)\mu}_{\ \ \nu} = (\delta\rho_i + \delta p_i)u^{(i)\mu}u^{(i)}_{\ \ \nu} + \delta p_i\delta^\mu_\nu + (\rho_i + p_i)\left(\delta u^{(i)\mu}u^{(i)}_{\ \ \nu} + u^{(i)\mu}\delta u^{(i)}_{\ \ \nu}\right)\,, \tag{3.3.6}$$

where $\delta u^{(i)}_{\ \ \mu}$ is the perturbation of the four velocity vector of the i-species, *i.e.* $u^{(i)}_{\ \ \mu} = a(-1, v^{(i)}_{\ \ j})$, with v_j being the peculiar velocity (spacial perturbation). where j denotes runs the spacial components only.

It is useful to work in Fourier space, where we expand the fluctuations as a sum of plain waves, *i.e.* $\delta\phi(\vec{x},\tau) \to e^{i\vec{k}\cdot\vec{x}}\delta\phi_k(\tau)$, and therefore $\nabla^2\delta\phi(\vec{x},\tau) \to -e^{i\vec{k}\cdot\vec{x}}k^2\delta\phi_k(\tau)$. In this setting, the linearised Einstein equations are:

$$\frac{k^2}{a^2}\Phi + 3H\left(\dot{\Phi} + H\Psi\right) = -4\pi G \sum_i \delta\rho_i \,, \tag{3.3.7}$$

$$k^2\left(\dot{\Phi} + H\Psi\right) = 4\pi G a \sum_i \rho_i(1+w_i)\theta_i \,, \tag{3.3.8}$$

$$\ddot{\Phi} + H\left(\dot{\Psi} + 3\dot{\Phi}\right) + \Psi\left(3H^2 + 2\dot{H}\right) + \frac{k^2}{3a^2}(\Phi - \Psi) = 4\pi G \sum_i \delta p_i \,, \tag{3.3.9}$$

$$\Phi = \Psi \,. \tag{3.3.10}$$

The first equation (3.3.7) gives the energy constraint, $\delta G^0_0 = 8\pi G \delta T^0_0$, where the field perturbations are written as

$$\delta\rho_\phi = \dot{\phi}\dot{\delta\phi} - \Psi\dot{\phi}^2 + V_\phi \delta\phi \,, \tag{3.3.11}$$

$$\delta p_\phi = \dot{\phi}\dot{\delta\phi} - \Psi\dot{\phi}^2 - V_\phi \delta\phi \,. \tag{3.3.12}$$

Equation (3.3.8), computed from $\nabla \cdot \sum_i \delta G^0_i = 8\pi G \nabla \cdot \sum_i T^0_i$, gives the momentum constraint, where we have defined the velocity divergence $\theta = \nabla_i v^i$. The trace of the spacial components (pressure perturbations), $\sum_i \delta G^i_i = 8\pi G \sum_i T^i_i$, yields Eq. (3.3.9). Finally, the shear propagation, $\sum_{i,j} \delta G^i_j = 8\pi G \sum_{i,j} \delta T^i_j$ $(i \neq j)$, is described by Eq. (3.3.10), and since we have assumed all the species to be described as perfect fluids at the linear level, there is no generation of anisotropic stress, $\delta T^i_j = 0$ $(i \neq j)$.

The evolution equations of the dark matter density contrast, δ_c, and velocity divergence, θ_c, can be found through the first order time and spacial component of Eq. (3.1.16), respectively, and read:

$$\dot{\delta}_c - 3\dot{\Phi} + \frac{\theta_c}{a} + \kappa\beta\dot{\delta\phi} = 0 \,, \tag{3.3.13}$$

$$\dot{\theta}_c + \theta_c\left(H - \kappa\beta\dot{\phi}\right) + \frac{k^2}{a}\left(\kappa\beta\dot{\delta\phi} - \Psi\right) = 0 \,. \tag{3.3.14}$$

The first order equation of motion for the quintessence field can be found by the $\nu = 0$ components of Eq. (3.1.15),

$$\ddot{\delta\phi} + 3H\dot{\delta\phi} + V_{\phi\phi}\delta\phi + \frac{k^2}{a^2}\delta\phi + 2\Psi V_\phi - \dot{\phi}\left(\dot{\Psi} + 3\dot{\Phi}\right) - \kappa\beta\rho_c\left(2\Psi + \delta_c\right) = 0 \,. \tag{3.3.15}$$

We can now derive Eq. (3.3.13), using Eqs. (3.3.10) and (3.3.14), and obtain a second order

equation for the dark matter perturbations,

$$\ddot{\delta}_c - 3\ddot{\Phi} + \frac{k^2}{a^2}\Phi - \kappa\beta\frac{k^2}{a^2}\delta\phi + \kappa\beta\delta\ddot{\phi} + \left(\dot{\delta}_c - 3\dot{\Phi} + \kappa\beta\delta\dot{\phi}\right)\left(2H - \kappa\beta\dot{\phi}\right) = 0\,. \tag{3.3.16}$$

As mentioned above, our aim is to study the influence of the coupling on the evolution of matter perturbations (CDM + baryons) and on formation of structure processes. Thus we are interested in the perturbations that are deep inside the Hubble horizon, $(k/a)^2 \gg H^2$, but that are nevertheless still large enough such that the linear regime is valid. This is called the small scale limit or the Newtonian limit [93]. Through the second Einstein equation, Eq. (3.3.8), we note that on such a limit, we may neglect the term $\left(\dot{\Phi} + H\Psi\right)$, since it goes with the inverse of k^2. Therefore, inserting this relation Eq. (3.3.7) we get,

$$\frac{k^2}{a^2}\Phi \approx -\frac{4\pi G}{k^2}\sum_i \rho_i\delta_i\,. \tag{3.3.17}$$

Accordingly, the Newtonian limit amounts to neglecting Φ and its derivatives. In addition, we average out rapid oscillations of $\delta\phi$ (by setting $\delta\ddot{\phi} \approx \delta\dot{\phi} \approx 0$) [96, 142], and finally we assume that the potential V may be neglected, since it only affects late times, when the Universe starts to accelerate [96]. Note that with these assumptions, the dark energy perturbations fully decouple from the evolution of the dark matter components, and the Klein-Gordon Eq. (3.3.15) gives the relation,

$$\frac{k^2}{a^2}\delta\phi \approx \kappa\beta\rho_c\delta_c\,. \tag{3.3.18}$$

Finally, using Eqs. (3.3.17), (3.3.18) in Eq. (3.3.16), we find that the dark matter fluctuations in the small scale limit, evolve as [143],

$$\ddot{\delta}_c + \dot{\delta}_c\left(2H - \kappa\beta\dot{\phi}\right) - \frac{\kappa^2}{2}\rho_c\delta_c\left(1 + 2\beta^2\right) - \frac{\kappa^2}{2}\rho_b\delta_b = 0\,. \tag{3.3.19}$$

Note that Eq. (3.3.19) has an additional friction term proportional to $\kappa\beta\dot{\phi}$ and the source term is modified by the emergence of an effective gravitational constant $G_{\rm eff}/G = 1 + 2\beta^2$. This latter effect expresses the nature of a fifth force arising, mediated by the scalar degree of freedom [144, 145]. We can write the effective potential felt by the dark matter particles, following the modified Poisson equation,

$$\nabla^2\Phi_{\rm eff} \approx 4\pi G\rho_c\delta_c\left(1 + 2\beta^2\right)\,. \tag{3.3.20}$$

This expresses the fact that the dark matter particles feel a stronger gravitational force, as $G_{\rm eff} > G$, (this is always true for conformal couplings of the form $\Omega = e^{-\beta\phi}$).

Let us emphasise that the process of deriving Eq. (3.3.19) is a standard known procedure which can easily be found in the literature [93, 96, 144, 146]. In this present model, the evolution of matter perturbations with a non-interacting dark matter component, setting $\beta = 0$ (which implies $\dot{\phi} = 0$), exactly mimics the linear evolution of matter fluctuations on small scales for ΛCDM. This is a special feature of this model due to the fixing of the background, Eq. (3.2.7). In the Newtonian limit, baryons evolve following

$$\ddot{\delta}_b + 2H\dot{\delta}_b - \frac{\kappa^2}{2}\rho_c\delta_c - \frac{\kappa^2}{2}\rho_b\delta_b = 0\,. \tag{3.3.21}$$

Equations (3.3.19) and (3.3.21) can be rewritten using derivatives with respect to $N = \ln a$, as

$$\delta_c'' + \delta_c'\left(2 + \frac{H'}{H} - \kappa\beta\phi'\right) - \frac{3}{2}\delta_c\Omega_c\left(1 + 2\beta^2\right) - \frac{3}{2}\Omega_b\delta_b = 0\,, \tag{3.3.22}$$

$$\delta_b'' + \delta_b'\left(2 + \frac{H'}{H}\right) - \frac{3}{2}\delta_c\Omega_c - \frac{3}{2}\Omega_b\delta_b = 0 \tag{3.3.23}$$

We follow to numerically evolve Eqs. (3.3.22) and (3.3.23), together with the background equation of motion for the quintessence field, Eq. (3.2.13). Since we want to present the results regarding the total matter perturbations, we define the quantity,

$$\delta_m = \frac{\rho_c\delta_c + \rho_b\delta_b}{\rho_c + \rho_b}\,, \tag{3.3.24}$$

and present the results accordingly.

The initial conditions for the density contrast are taken well within the validity of the linear regime, $\delta(t_i) < 10^{-3}$ [144]. The evolution of the total matter (CDM + baryons) density contrast for different values of the coupling is depicted in Fig. 3.4. We note that the perturbations are suppressed for higher values of β. This can be understood through two competing effects. As mentioned before, stronger couplings lead to an enhanced scalar force on the dark matter particles, ($G_{\rm eff} = (1 + 2\beta^2)G > G$), and thus one would expect a higher level of clustering (larger δ_m values). On the other hand, we have seen from the background analysis, that in order to mimic a ΛCDM background, the amount of matter must decrease at late times. This latter effect leads to a smaller source term (the prefactor of δ_c) in Eq. (3.3.22), since at high z we have $\Omega_c(1 + 2\beta^2) < \Omega_{cdm}$ resulting on a slower growth of the matter fluctuations as β increases. It

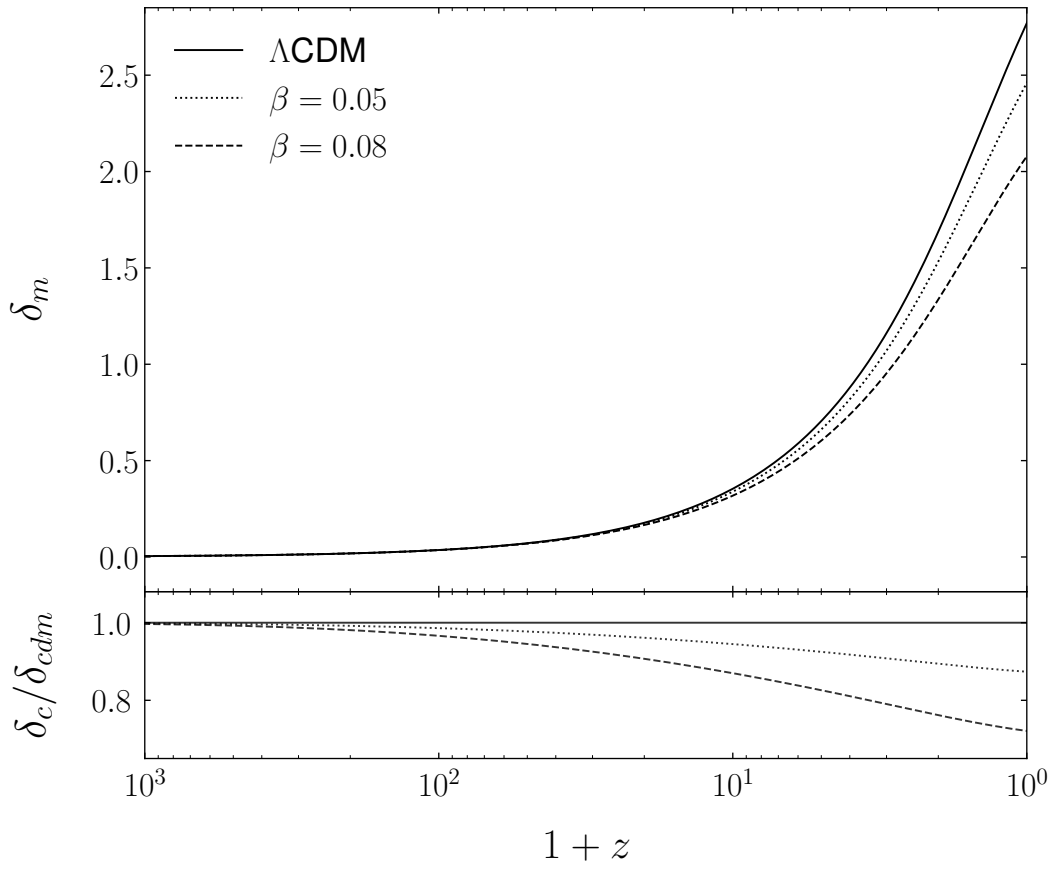

Figure 3.4: Top: evolution of the total matter (CDM + baryons) density contrast for different values of the coupling. Bottom: Difference of the dark matter perturbation in comparison with the uncoupled model (ΛCDM).

should also be noted that there is an additional friction term, $-\kappa\beta\phi'$ in Eq. (3.3.22), which, as stated in the background analysis, is always negative (since $\beta\phi' > 0$). Thus, large couplings lead to less friction sourcing the growth. This effect, however, is subdominant in contrast with the suppression due to the aforementioned decrease of the energy density of matter. This is one of the main results of this model: the clustering of matter is suppressed by the coupling.

One useful quantity to characterise the growth of matter fluctuations is the *growth rate*,

$$f := \frac{d\ln\delta_m}{d\ln a} = \frac{\delta_m'}{\delta_m}\,. \tag{3.3.25}$$

By observing the spatial distribution of galaxies in a cluster one may directly extract useful cosmological quantities that can be used to probe the growth of matter perturbations, and thus formation of structure processes. If one plots the distribution of galaxies in redshift space, instead of a function of their distance, there is an additional effect besides the usual Doppler shift caused

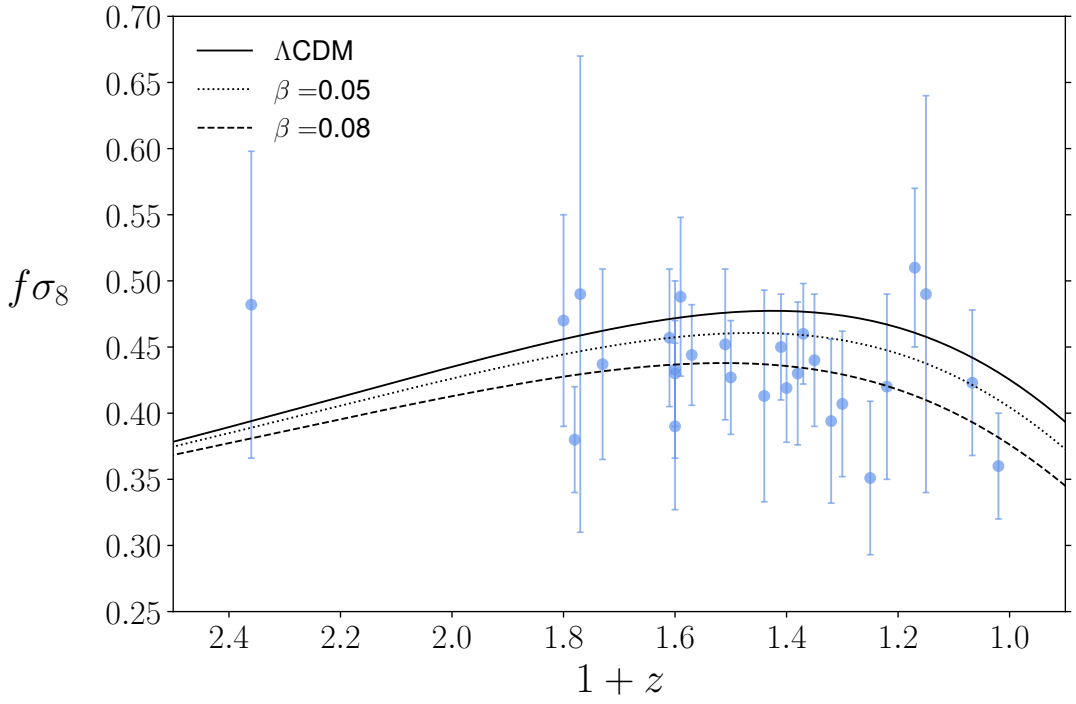

Figure 3.5: Function $f\sigma_8$ for ΛCDM (solid line) and different values of β (see legend) fixing a value of $\sigma_8(0) = 0.818$ [139]. The observational data points are taken from Refs. [148–162] and are summarised in Table II of Ref. [163].

by the expansion. This effect is known as *redshift space distortions* (RSD) [147] and is caused by the peculiar velocities of these galaxies (an additional Doppler shift), that results in making the image of a cluster appear distorted. One quantity which can be directly extracted by RSD data is

$$f\sigma_8(N) = \sigma_8 \frac{\delta'_m(N)}{\delta_m(0)}\,, \tag{3.3.26}$$

where $\sigma_8 := \sigma_8(0)$ is the present amplitude of the matter power spectrum at the scale of $8h^{-1}$Mpc [8]. Note that since $f\sigma_8$ is intimately related with the growth rate of matter perturbations, we expect to obtain smaller values of $f\sigma_8$ with stronger interactions in the dark sector, for a fixed σ_8. This effect is indeed verified through the curves on Fig. 3.5.

There have been proposals to solve or alleviate the σ_8 tension by assuming alternatives to the standard model, *e.g.* modified gravity [126, 127]. These models admit distinct evolutions of the matter perturbations, thus possibly obtaining σ_8 values in concordance with observations. We follow to test how this model behaves when tested against RSD data in the light of the σ_8 tension.

We wish to study how the $f\sigma_8$ parameter behaves, when varying the coupling and σ_8, in terms of agreement with observational data of RSD. To this end we consider a set of 27 data

Table 3.1: Best fit values for β and σ_8, number of fitted parameters (dof) and respective χ^2 and $\tilde{\chi}^2$ values.

Model	β	σ_8	dof	χ^2	$\tilde{\chi}^2$
ΛCDM	0	0.750 ± 0.024	1	11.4413	0.4400
Coupled quintessence	$0.079^{+0.059}_{-0.067}$	$0.818^{+0.115}_{-0.088}$	2	11.0946	0.4438

points [148–164] which can be found in Table II of Ref. [163] and are plotted in Fig. 3.5. A likelihood analysis is then performed, by letting β and σ_8 as free parameters. We compute the likelihood,

$$L = A \exp\left(-\chi^2/2\right) , \tag{3.3.27}$$

where A is a normalization constant and the chi squared, χ^2, is given by

$$\chi^2 = (d_i - t_i)^T C_{ij}^{-1} (d_j - t_j) , \tag{3.3.28}$$

t_i, t_i and C_{ij} being the vector of data points, theory and the covariance matrix. It is also useful to compute the reduced chi squared, $\tilde{\chi}^2$, which takes into account the number of free parameters, $\tilde{\chi}^2 = \chi^2/\text{dof}$, where the number of degrees of freedom equals the number of data points minus the number of fitted parameters, *i.e.* $\text{dof} = N_d - N_f$.

The best fit values are summarised in Tab. 3.1 and in Fig. 3.6 the contour regions on the two parameter space are shown, together with the respective marginalised curves. The value $\sigma_8 = 0.75 \pm 0.024$ found for ΛCDM (with σ_8 as the only free parameter) is known to be in tension with the Planck 2015 measurements [139], $\sigma_8^0 = 0.82 \pm 0.014$. However, for the coupled quintessence model, we find a best fit of $0.818^{+0.115}_{-0.088}$ with $\beta = 0.079^{+0.059}_{-0.067}$. This value for σ_8 is well within the Planck 1σ constraints, and therefore alleviates this tension. The best fit for the coupling actually proposes a slower growth for the perturbations, which curiously does not include ΛCDM ($\beta = 0$) within the 1σ error. With these best-fit values for β, the present value of total matter is constrained as $\Omega_m = \Omega_c + \Omega_b = 0.237^{+0.069}_{-0.081}$. The coupled quintessence model gives a slightly better value for the chi squared test in comparison with the standard model. However, if we take into account the fact that coupled quintessence introduces one more parameter than ΛCDM - the coupling β - the value of $\tilde{\chi}^2$ slightly favours ΛCDM.

It should be noted that our best fit value found for β, is close to the likelihood peak observed in Ref. [165] for $\beta = 0.066 \pm 0.018$, through an analysis combining data from the Planck CMB

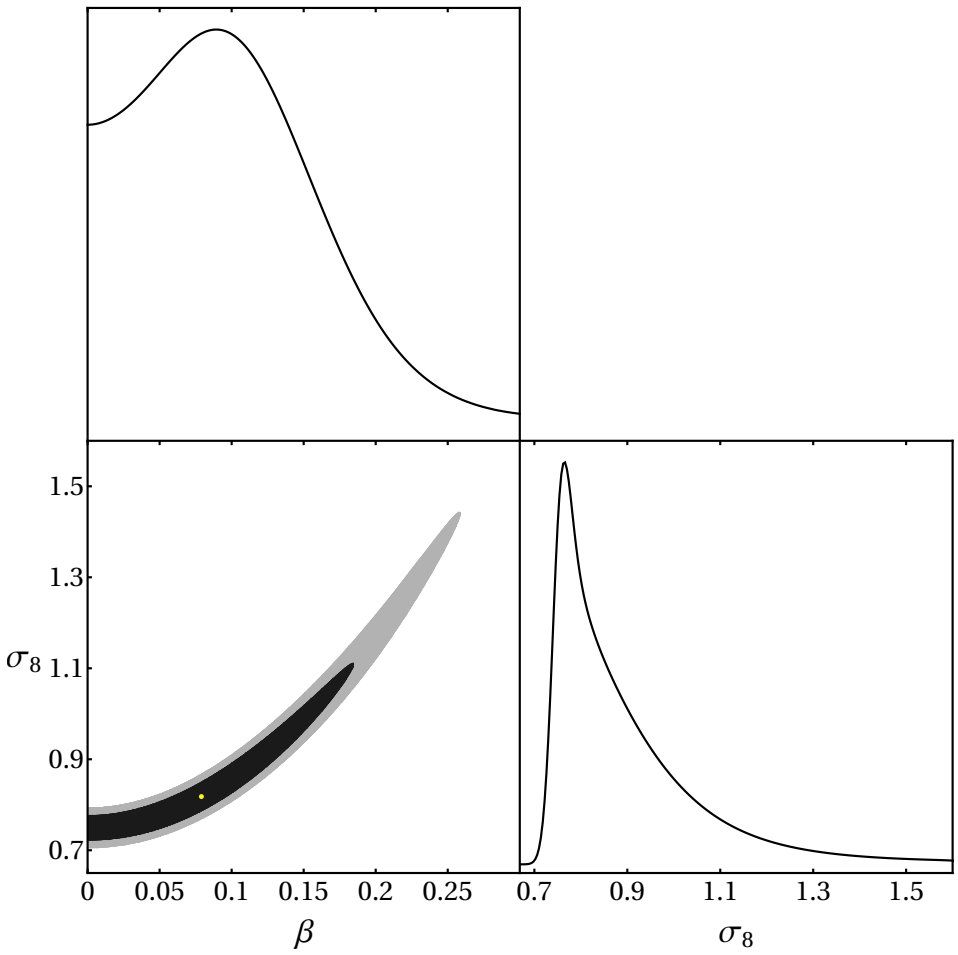

Figure 3.6: Constraints on β and σ_8: 1σ and 2σ regions and respective marginalised curves for the coupled quintessence model. A dot denotes the best fit value on the two parameter space.

and the Hubble Space Telescope computation of H_0. However, in Ref. [165] the background was not chosen to mimic a ΛCDM evolution. For a concrete comparison one should analyse the CMB data anew.

Through weak lensing, it is possible to put bounds on a particular combination of the σ_8 and Ω_m^0 parameters. These have been constrained in Ref. [167] in the KiDS-450 survey. A bound of $S_8 := \sigma_8\sqrt{\Omega_m^0/0.3} = 0.745 \pm 0.039$ was found, in 2.3σ tension with CMB experiments. This result was attained by propagating the observations in redshift bins from $z = 0.1$ to $z = 0.9$ to present time, assuming a ΛCDM cosmology. We may rescale this value to the current model by

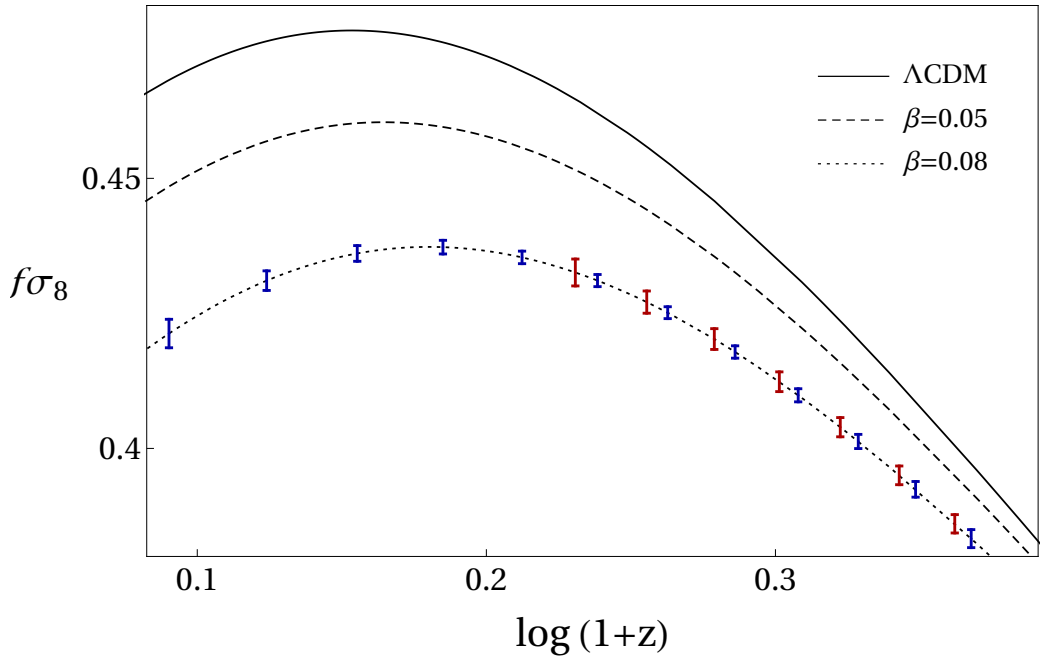

Figure 3.7: Error bars corresponding to the generated mock data regarding the future SKA (blue) and Euclid (red) missions [166]. The curves presented are the same as in Fig. 3.5.

proceeding as follows. The value of S_8 at a given redshift $\bar{z}$ in KiDS is,

$$S_{8(s)}(\bar{z}) = \sigma_8\, g_s(\bar{z}) \sqrt{\frac{\Omega_{m(s)}(\bar{z})}{0.3}} \tag{3.3.29}$$

$$= S_{8(s)} g_s(\bar{z}) \sqrt{\frac{\Omega_{m(s)}(\bar{z})}{\Omega^0_{m(s)}}}\,, \tag{3.3.30}$$

where an s subscript denotes ΛCDM quantities, $S_{8(s)}$ is the KiDS' value and g_s is the standard growth function, $g = \delta_m/\delta_m(0)$. Through $S_8(\bar{z})$ we can now find a rough estimate on the KiDS prediction for coupled quintessence as,

$$S_8 = S_{8(s)} \frac{g_s(\bar{z})}{g(\bar{z})} \sqrt{\frac{\Omega_{m(s)}(\bar{z})}{\Omega_m(\bar{z})}} \sqrt{\frac{\Omega^0_m}{\Omega^0_{m(s)}}}\,. \tag{3.3.31}$$

Taking the average value of $\bar{z} = 0.5$, we find $S_8 \approx 0.72 \pm 0.038$. Regarding σ_8 for our model,

$$\sigma_8 = S_{8(s)} \frac{g_s(\bar{z})}{g(\bar{z})} \sqrt{\frac{\Omega_{m(s)}(\bar{z})}{\Omega_m(\bar{z})}} \sqrt{\frac{0.3}{\Omega^0_{m(s)}}}\,, \tag{3.3.32}$$

we obtain a value of $\sigma_8 \approx 0.81 \pm 0.02$. This value is in good agreement with the value obtained above from RSD data, and also with the Planck constraint $\sigma_8 = 0.82 \pm 0.014$ [139]. This

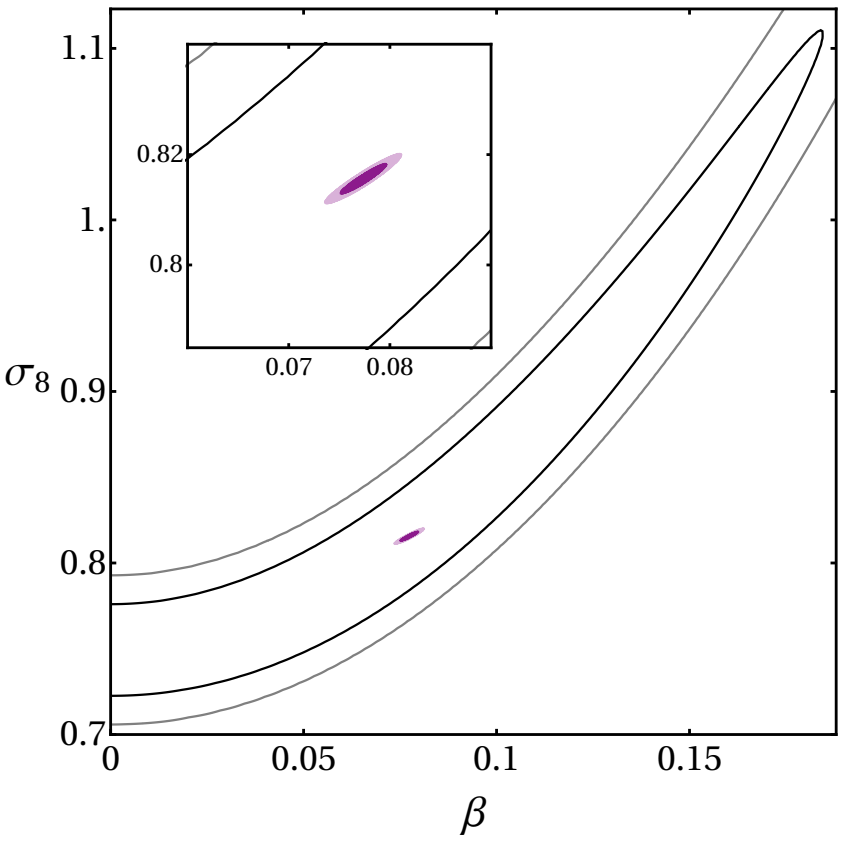

Figure 3.8: Forecast on the future constraints for β and σ_8 from the mock data generated for SKA and Euclid missions. The two lines represent the 1σ and 2σ regions (darker to lighter), present in Fig. 3.6, and the two small ellipses show the 1σ and 2σ regions expected from the points of Fig. 3.7.

confirms that coupled quintessence grants a clustering rate in full agreement with observations. On the other hand, recent data from the first year of the Dark Energy Survey (DES) has alleviated the tension with Planck [168]. Through a combined analysis of galaxy clustering and weak gravitational lensing, covering an area of 1321 deg^2 on the first year, DES found the value of $S_8 = 0.783^{+0.021}_{-0.025}$ assuming a ΛCDM cosmology. This is within the 1σ region of Planck, and thus alleviates the tension in comparison with the KiDS-450 data (lensing only). Considering this DES value for S_8, we find for our model, using Eqs. (3.3.31) and (3.3.32), $S_8 \approx 0.757 \pm 0.020$ and $\sigma_8 \approx 0.85 \pm 0.02$. This is outside the 1σ region of the Planck value, and does not agree with our σ_8 value obtained from the RSD data above. Therefore, our best fit model is slightly disfavoured if we consider instead the DES data.

Future missions, in particular SKA[1] and Euclid[2] are expected to measure $f\sigma_8$ with a much higher level of precision [166] in contrast with current observations. In order to shed some light

[1]https://www.skatelescope.org
[2]https://sci.esa.int/web/euclid

on the performance of these surveys, we generate mock data around the fiducial value $\beta = 0.08$ corresponding to the best fit for the coupled model. These are shown in Fig. 3.7. With this data, we carried out a similar statistical analysis, for which the results are presented in Fig. 3.8. The 1σ errors for σ_8 and β are estimated as $\pm\, 1.5 \times 10^{-3}$ and $\pm\, 1.8 \times 10^{-3}$, respectively. We can observe that the two ellipsis, corresponding to 1σ and 2σ regions, are much smaller than the present constraints by RSD data. This suggests that we will have significantly better constraints for $f\sigma_8$ and also other parameters of interacting dark energy models.

3.4 Spherical collapse and number counts

As we saw in the last section, the linear evolution of matter perturbations is of great importance in cosmology, since it can provide direct observables, such as the growth rate and the σ_8 parameter, which can be directly linked to observational data. However, certain phenomena can only be captured by diving into the nonlinear regime (see Sec. 8 of Ref. [169]). Such is the case of formation of structure processes. Apart from N-body simulations [170–173], the spherical collapse model [169, 174–176] has been shown to be a useful semianalytic method to track the dynamics of the overdensities in the initial stages of their nonlinear regime. By considering models which deviate from the standard ΛCDM, significant modifications on the dynamics governing the nonlinear evolution might emerge. Here, the spherical collapse of matter fluctuations and the number of bound objects formed within a certain mass range at a given redshift [177] are investigated. We will focus on how the interaction in the dark sector may influence these processes.

Spherical collapse in dynamical dark energy models has already been extensively studied throughout the literature [178–181]. The analysis of the standard minimally coupled quintessence scenario was conducted in Ref. [182], where the impact of assuming different types of scalar field potentials on the spherical collapse parameters was analysed. The presence of scalar perturbations on the collapse was also carefully analysed, assuming that dark energy clusters alongside with matter. In Ref. [183] it was shown that collapse in models with a coupling within the dark sector can leave imprints on the cluster number density. A meticulous examination of the collapse for different dark energy models was carried out in Ref. [184]. The authors have found that departures from ΛCDM may occur, and that these effects can be enhanced by assuming inhomogeneities in the dark energy component. The analysis of a time varying dark energy-dark matter coupling was explored in Ref. [172]. The specific form of the interaction naturally has

an impact on the background dynamics. Resorting to N-body simulations, it was found that the formation of cosmic structures and the nonlinear demeanour of matter perturbations are therefore strongly dependent on the background evolution. Here, we explore the spherical collapse for the coupled quintessence model presented in the previous section, in which the background Hubble expansion follows a ΛCDM evolution.

Before we start, it should be mentioned that in order to simplify the analysis and the numerical calculations, baryons will be neglected. At this level it is fair to assume that baryons evolve as dust. Thus, the main effect of considering a baryonic component is to add an uncoupled species of matter, thus diluting the overall impact of the coupling. That is, the reference value for the parameters may change slightly, but in general the main conclusions remain unaltered.

Let us consider a CDM density perturbation, $\delta = \delta\rho_c/\rho_c \ll 1$. At first, this perturbation will grow along with its own expanding background at a slower rate, since it counteracts the expansion due to its own self gravity. When the size of this perturbation reaches the order of unity the linear regime is broken and the evolution starts to be dominated by the nonlinear terms. At some point, when the region has assembled a significant amount of mass, the perturbation collapses on its own gravity to form a bound system. Thus, in order to have a grasp on the mechanisms driving formation of structures we need to dive into the nonlinear regime [96, 185].

Considering that the overdense region has a radius r, it first grows in size with the Hubble expansion, and only later, depending on the scale, does it departs from the background expansion and collapses, *i.e.* $r \to 0$ as $\delta \to \infty$. The *spherical collapse model* [169, 174, 186] is an approach to trace the evolution of the matter flucuations on the primary phases of their nonlinear regime. It focuses on the evolution of a certain overdense spherical and nonrotating region with radius $r(t)$. Birkhoff's theorem [187] guarantees that the evolution of this "bubble" radius, depends solely on its enclosed mass. Therefore, we can model this region as a subuniverse with total mass $\rho_c + \delta\rho_c$ and "scale factor" r,

$$\left(\frac{\dot{r}}{r}\right)^2 = \frac{\kappa^2}{3}\sum_i(\rho_i + \delta\rho_i) - \frac{K}{r^2}\,, \tag{3.4.1}$$

where the sum runs over all the i-th species. The presence of a curvature term simply manifests that the spherical patch is positively curved as its density is larger than its critical (background) one due to the existence of the overdensity $\delta\rho_c$ [144]. Note that the background quantity ρ_c

evolves according to the standard Friedmann equation,

$$\left(\frac{\dot{a}}{a}\right)^2 = \frac{\kappa^2}{3}\sum_i \rho_i \,. \tag{3.4.2}$$

The main assumption of the spherical collapse model is that δ follows a top hat (or step) function [16], where $\delta = \delta\rho_c/\rho_c$ inside the spherical region, and $\delta = 0$ outside. Assuming that initially the scale factors r and a are equal, i.e. $r_{in} = a_{in}$, and that the mass of the background CDM particles is the same as that on the spherical overdense region, we may write [144]

$$1 + \delta = (1 + \delta_{in})\left(\frac{a}{r}\right)^3 , \tag{3.4.3}$$

where $\delta_{in} = \delta(z_{in})$ is the initial density contrast for the CDM component. From Eq. (3.4.3) it becomes clear that the divergence of the density contrast, $\delta \to \infty$, happens as the region collapses, $r \to 0$.

In Ref. [144] the second order equation for the evolution of perturbations in coupled quintessence, in the small scale regime, were derived from the full set of nonlinear hydrodynamical equations (see also Refs. [178, 188]), and reads,

$$\ddot{\delta} + \dot{\delta}\left(2H - \kappa\beta\dot{\phi}\right) - \frac{\kappa^2}{2}\rho_c\,\delta\,(1+\delta)\left(1+2\beta^2\right) - \frac{4}{3}\frac{\dot{\delta}^2}{1+\delta} = 0\,. \tag{3.4.4}$$

Note that by linearising Eq. (3.4.4) we recover the first order equation (3.3.19) (without the baryons source term). The deviations from standard ΛCDM are the same as mentioned in the last section for the linear case: an extra fifth force term and an additional contribution to the frictional term which weakens the overall damping effect. The balance of these two effects has a direct impact on the growth rate of the matter perturbations [39, 93]. Recall that in this work, the background is fixed in order to reproduce ΛCDM. Hence, we may reformulate Eq. (3.4.4), using Eq. (3.2.11),

$$\ddot{\delta} + \dot{\delta}\left(2H - \kappa\beta\dot{\phi}\right) - \frac{\kappa^2}{2}\left(\rho_{cdm} - \dot{\phi}^2\right)\,\delta\,(1+\delta)\left(1+2\beta^2\right) - \frac{4}{3}\frac{\dot{\delta}^2}{1+\delta} = 0\,, \tag{3.4.5}$$

which can be written in terms of derivatives with respect to N as

$$\delta'' + \delta'\left(2 + \frac{H'}{H} - \kappa\beta\phi'\right) - \frac{3}{2}\left(\Omega_{cdm} - \frac{\kappa^2}{3}\phi'^2\right)\delta\,(1+\delta)\left(1+2\beta^2\right) - \frac{4}{3}\frac{\delta'^2}{1+\delta} = 0\,, \tag{3.4.6}$$

where H'/H becomes,

$$\frac{H'}{H} = -\frac{1}{2}\left(3 + \Omega_r - 3\,\Omega_\Lambda\right) \,. \tag{3.4.7}$$

We follow to numerically evolve Eqs. (3.4.6), along with the background Eq. (3.2.13), and explore how the dynamical behaviour of the spherical collapse is influenced by the coupling parameter β.

The collapse of the matter density contrast

The numerical simulations start deep inside the radiation dominaton era, at $N_{in} = -14$ ($z_{in} \approx 10^6$). Regarding the initial conditions for the density contrast, we take $\dot{\delta}_{in} = 0$ and $\delta_{in} < 10^{-3}$, well within the validity of the linear regime at early times [144]. We fix the parameters using the latest Planck 2018 values [8], $\Omega^0_{cdm} = 0.311$, $\Omega^0_r h^2 = 4.1 \times 10^{-4}$ and $\Omega_\Lambda = 1 - \Omega_c - \Omega_r$. As previously discussed, for symmetry reasons, we consider scenarios with $\beta \geqslant 0$ only.

As mentioned in the previous section, in order to mimic the same background as ΛCDM, with increasing β, the amount of CDM is always lower or equal to the one of DE, which consequently leads to a slower growth of the linear matter fluctuations. This effect can be observed in Fig. 3.9 (gray lines).

The black curves in Fig. 3.9 depict the evolution of the nonlinear density contrast of matter for different coupling values. As the perturbation grows with the expansion, it eventually departs from the linear regime, and the nonlinear terms starts to rule the evolution. When a sufficient amount of density contrast is gathered within the spherical region, the collapse occurs, that is $\delta \to \infty$. As the growth of the matter fluctuation is suppressed for higher values of the coupling β, the perturbation takes longer to assemble the critical amount of matter for the collapse to happen. Therefore, as we observe in Fig. 3.9, the collapse befalls latter for larger values of β.

One quantity that is very useful to characterise the spherical collapse is the *critical density contrast*. It is defined as the value of the linear density contrast δ_L when its nonlinear counterpart diverges, *i.e.* when $\delta_{NL} \to \infty$. Running the simulations until δ_{NL} diverges, we can extract the redshift value at the collapse, z_c, as well as the corresponding linear density contrast $\delta_c := \delta_L(z = z_c)$. We can then obtain the collapse at different redshifts by varying the initial condition δ_{in}, therefore obtaining different values for z_c and δ_c. The results for δ_c vs z_c are presented in Fig. 3.10, where the uncoupled case ($\beta = 0$) is plotted in solid (red) as a reference. As antecipated, we observe that increasing the value of the coupling leads to higher values of δ_c.

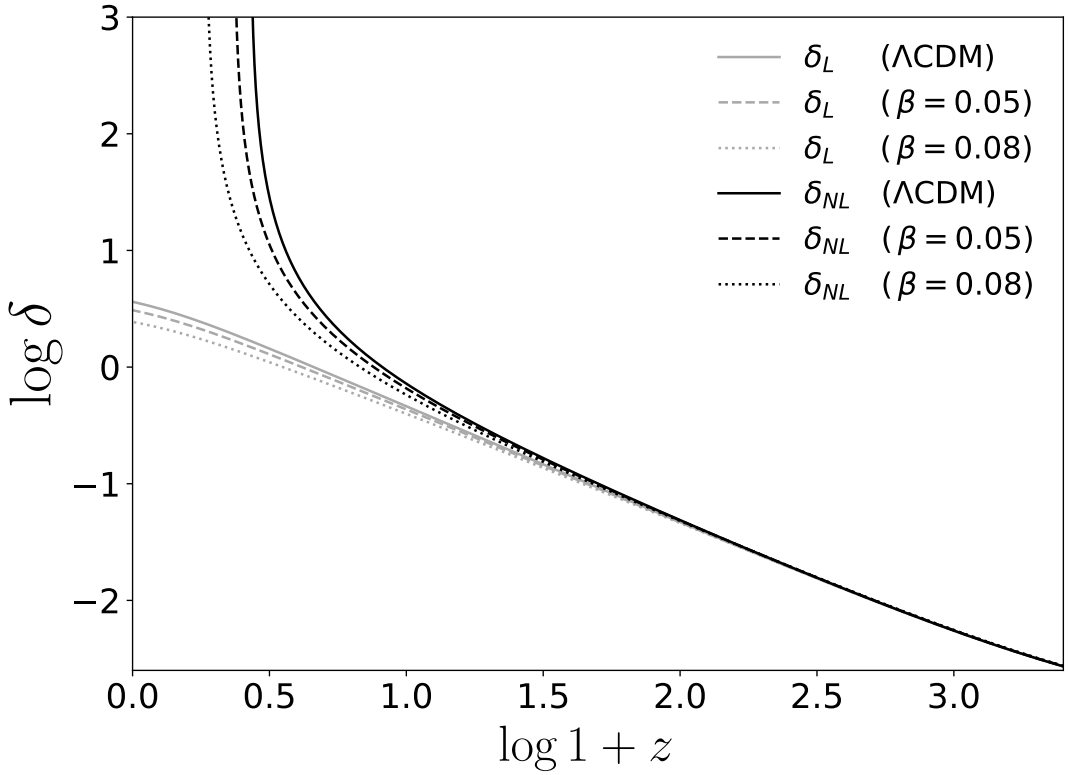

Figure 3.9: Linear (gray), δ_L, and nonlinear (black), δ_{NL}, CDM density contrast versus redshift. Solutions of Eqs. (3.2.13) and (3.4.6) for $\beta = 0$ (solid), $\beta = 0.05$ (dashed) and $\beta = 0.08$ (dotted) with $\delta_{in} = 9 \times 10^{-4}$.

This can be explianed by the fact that, a slower growth rate should require a greater value of the density contrast in order for the collapse to take place. An opposite effect was found in Ref. [67] in the context of disformal couplings [62, 189].

Press-Schechter formula

The linear density contrast at the collapse is of paramount importance in characterizing formation of structure processes. The reason is that it enters directly in the *Press-Schechter* formula [190], widely used to calculate the number density of collapsed objects over a volume, in a given mass range, and at a specific time in the cosmic history. This formula stands upon the assumption that the matter density field follows a Gaussian distribution [191]. To be more precise, the prediction for the comoving number density of collapsed objects with mass between M and $M + dM$ is [191–193]

$$\frac{dn}{dM} = -\sqrt{\frac{2}{\pi}}\frac{\tilde{\rho}_c(z)}{M}\frac{\delta_c(z)}{\sigma(z,M)}\frac{d\ln\sigma(z,M)}{dM}\exp\left[-\frac{\delta_c(z)^2}{2\sigma(z,M)^2}\right], \tag{3.4.8}$$

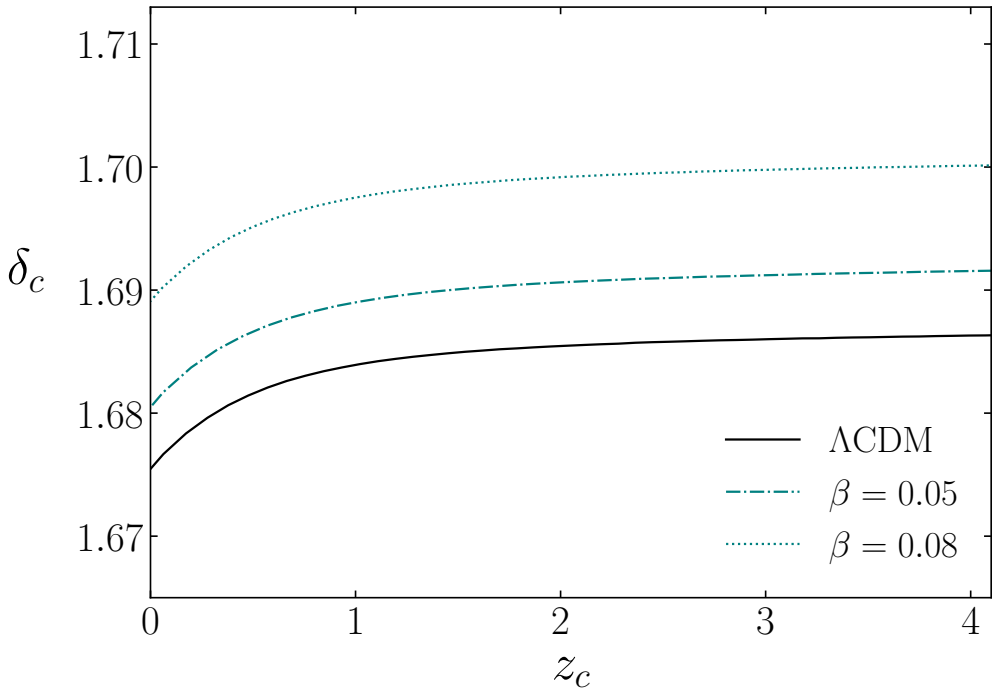

Figure 3.10: Linear density contrast at collapse, δ_c, versus redshift of the collapse, z_c, for $\beta = 0$ (solid), $\beta = 0.05$ (dashed) and $\beta = 0.08$ (dotted).

with $\tilde{\rho}_c := a^3\rho_c$ being the comoving matter density [177, 192], and $\sigma(z, M)$ the variance corresponding to the rms density fluctuation in a sphere of radius R, enclosing a mass M. This variance can be expressed in terms of the growth factor $g(z) := \delta(z)/\delta(0)$, at the fixed scale of $R = R_8 = 8h^{-1}$Mpc [184], as

$$\sigma(z, M) = \sigma(0, M_8)\left(\frac{M}{M_8}\right)^{-\gamma/3} g(z)\,, \tag{3.4.9}$$

where $M_8 = 6 \times 10^{14}\Omega_c h^{-1} M_\odot$ is the mass within the sphere (of radius R_8), where $M_\odot$ denotes the solar mass, and, following the notation of Ref. [184],

$$\gamma = (0.3\Gamma + 0.2)\left[2.92 + \frac{1}{3}\log\left(\frac{M}{M_8}\right)\right]\,, \tag{3.4.10}$$

with $\Gamma = \Omega_c h$ [67] and $\sigma_8 := \sigma(0, M_8) = 0.811$ [8]. It is possible to convert the number density Eq. (3.4.8) into an effective number of objects with masses within $M_{\rm inf} < M < M_{\rm sup}$ per redshift and square degree,

$$\mathcal{N} := \frac{dN}{dz} = \int_{1\text{deg}^2} d\Omega \frac{dV}{dz\, d\Omega} \int_{M_{\rm inf}}^{M_{\rm sup}} \frac{dn}{dM} dM\,, \tag{3.4.11}$$

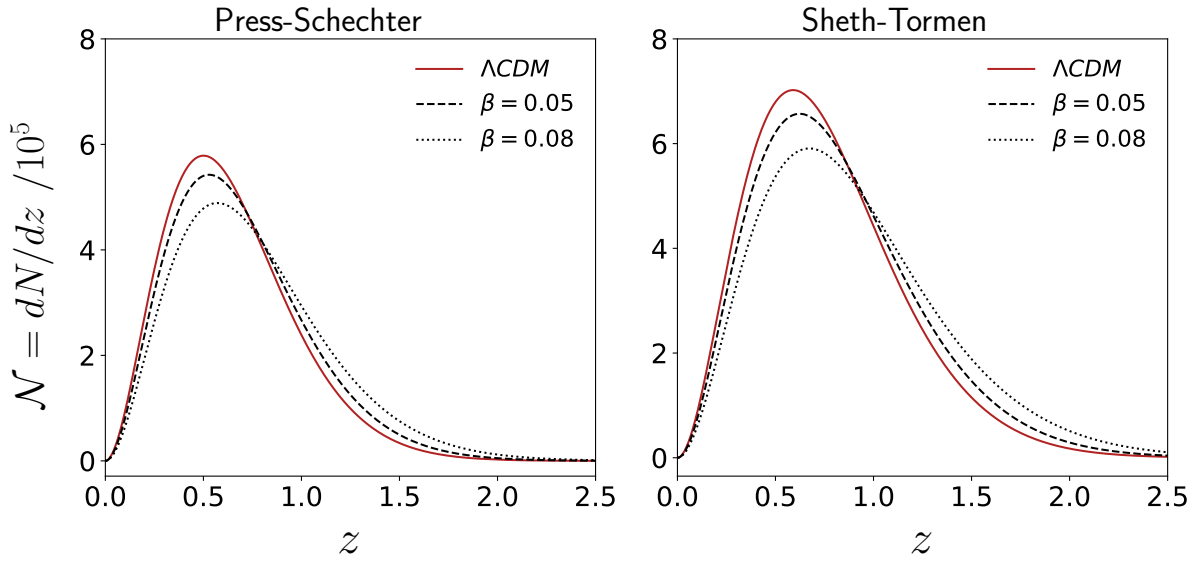

Figure 3.11: Comoving number of dark matter halos with masses within $10^{14}h^{-1}M_\odot < M < 10^{16}h^{-1}M_\odot$ for the Press-Schechter (left panel) and the Sheth-Tormen (right panel) mass functions, with $\beta = 0$ (solid), $\beta = 0.05$ (dashed) and $\beta = 0.08$ (dotted).

where

$$\frac{dV}{dz\,d\Omega} = \frac{c\,r(z)^2}{H(z)} = \frac{c}{H(z)}\left[\int_0^z \frac{c}{H(x)}dx\right]^2 \tag{3.4.12}$$

is the comoving volume element and $r(z)$ the comoving distance. A novel feature of this model, is that the comoving volume element, Eq. (3.4.12), does not depend on the value of the coupling β, in contrast with standard dynamical dark energy models [67, 184, 192, 194]. This is ascribed to the fact that Eq. (3.4.12) solely depends on the redshift evolution of H, which is in general dependent on the coupling, but not in this case, as it has been tailored to mimic a ΛCDM evolution.

At this point, the main goal is to investigate how the number of dark matter halos formed is influenced by the dark interaction, quantified by β. To do so, we consider masses within the galaxy cluster range, *i.e.* $10^{14}\,h^{-1}M_\odot < M < 10^{16}\,h^{-1}M_\odot$ [184]. The results for the comoving number counts of DM halos for $\beta = 0$, $\beta = 0.05$ and $\beta = 0.08$ are shown on the left panel of Fig. 3.11. Increasing β has the effect of suppressing (enhancing) the number counts at low (high) redshifts. This can be explained as the balance of two effects. On one hand, since the ΛCDM model has higher values of δ_c/σ, compared to the coupled models, the mass function Eq. (3.4.8) will take smaller values through the exponential term. On the other hand, the background matter energy density $\tilde{\rho}_c$ is also higher for ΛCDM (recall that the density of matter today decreases with increasing β), which results on an increase of the mass function. This latter effect is dominant

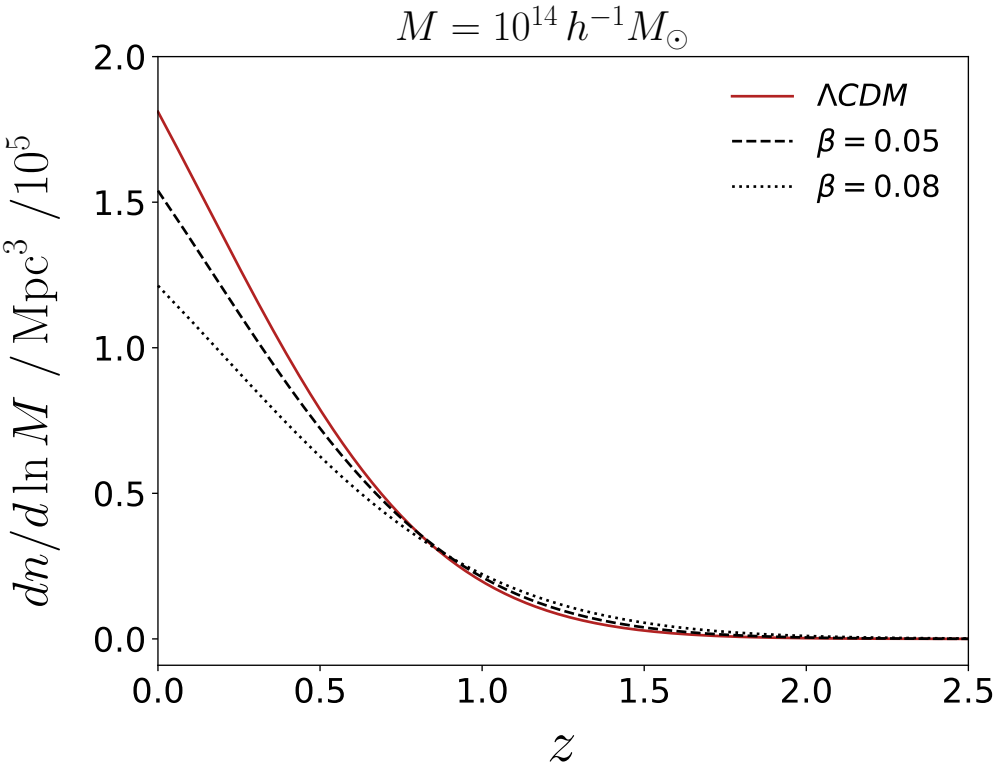

Figure 3.12: Press-Schechter mass function, Eq. (3.4.8), for $M = 10^{14}\,h^{-1}M_\odot$ with $\beta = 0$ (solid), $\beta = 0.05$ (dashed) and $\beta = 0.08$ (dotted).

at lower redshifts, whereas the first dominates at high z, causing the crossover between the curves for the expected number of clusters $\mathcal{N}$ that can be seen in Fig. 3.12. A similar demeanor was attained in Ref. [184], however due to a completely different cause: the suppression of the Press-Schechter function at later times is induced by deviations in the volume element (which here remains invariant) when varying the equation of state parameter for the dark energy fluid.

Another useful quantity is the integrated number of objects in the full sky up to redshift z. This can be computed by integration of Eq. (3.11), that is,

$$N = \int_{1\mathrm{deg}^2} d\Omega \int_{M_{\mathrm{inf}}}^{M_{\mathrm{sup}}} \int_0^z \frac{dn}{dM}\frac{dV}{d\bar{z}\,d\Omega} dM d\bar{z}\,. \tag{3.4.13}$$

The results are presented in Fig. 3.13. We notice that the interaction with $\beta = 0.05$ leads to larger integrated number of dark matter halos at higher redshifts. At the same time, for larger values of β the suppression of the mass function at low z is considerably more pronounced, ultimately causing the total number of halos to remain below ΛCDM even for higher redshifts.

Throughout this analysis we have assumed all parameters, aside from the coupling β, to be fixed, since our aim was to focus solely on the role of the interaction on the cosmological matters

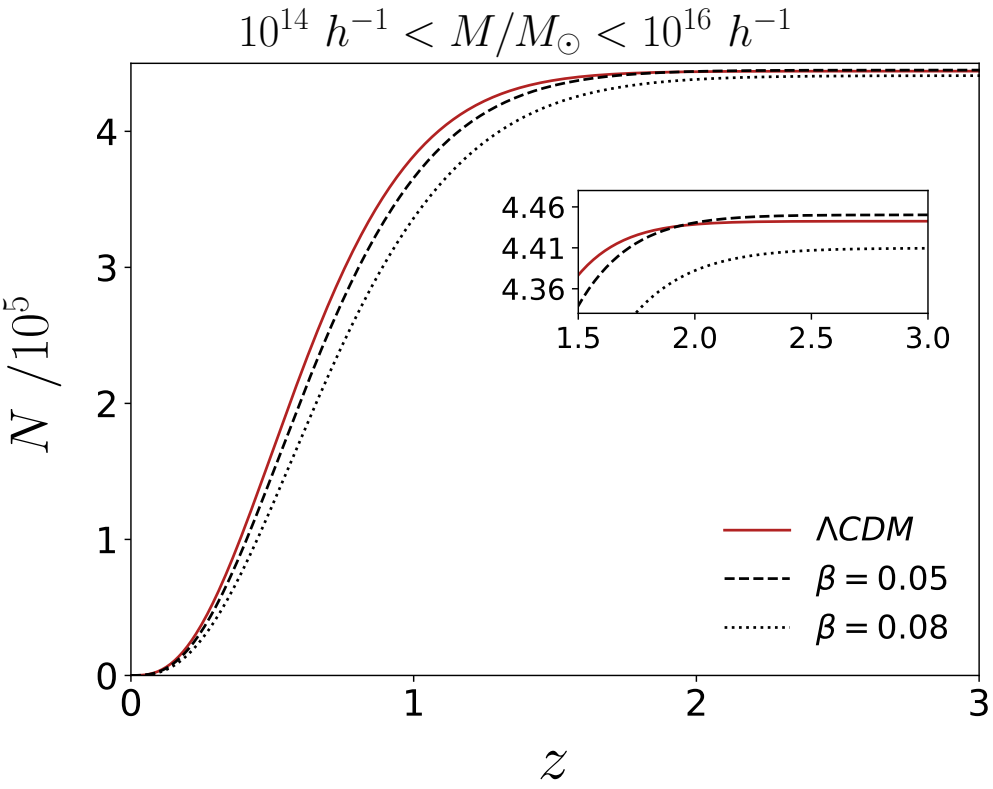

Figure 3.13: Integrated number of dark matter halos with masses within $10^{14}h^{-1}M_\odot < M < 10^{16}h^{-1}M_\odot$. Solution of Eq. (3.4.13) with $\beta = 0$ (solid), $\beta = 0.05$ (dashed) and $\beta = 0.08$ (dotted).

addressed. However, we have verified that, for example, by allowing σ_8 to vary, a degeneracy between the free parameters arises. With increasing (decreasing) σ_8 the expected number count significantly increases (decreases). This effect can be indeed very sensitive to variations in σ_8. We illustrate this trend in Fig. 3.14. Ultimately, one should constrain the β and σ_8 parameters simultaneously, and in general we expect these to be correlated. In Ref. [183] an interacting dark energy-dark matter model was considered. The analysis is first conducted for a fixed $\sigma_8 = 0.8$ and, further on, the authors show that it is possible to tune the σ_8 parameter such that all models yield the same number density of halos at $z = 0$ (in such case, different models may acquire different values of σ_8).

Sheth-Tormen mass function

The pioneering model put forward by Press and Schechter is very advantageous in capturing a general picture of the number of bound objects in the Universe. Nonetheless, from N-body simulations, the PS formalism is known [195] to predict a higher abundance of dark matter

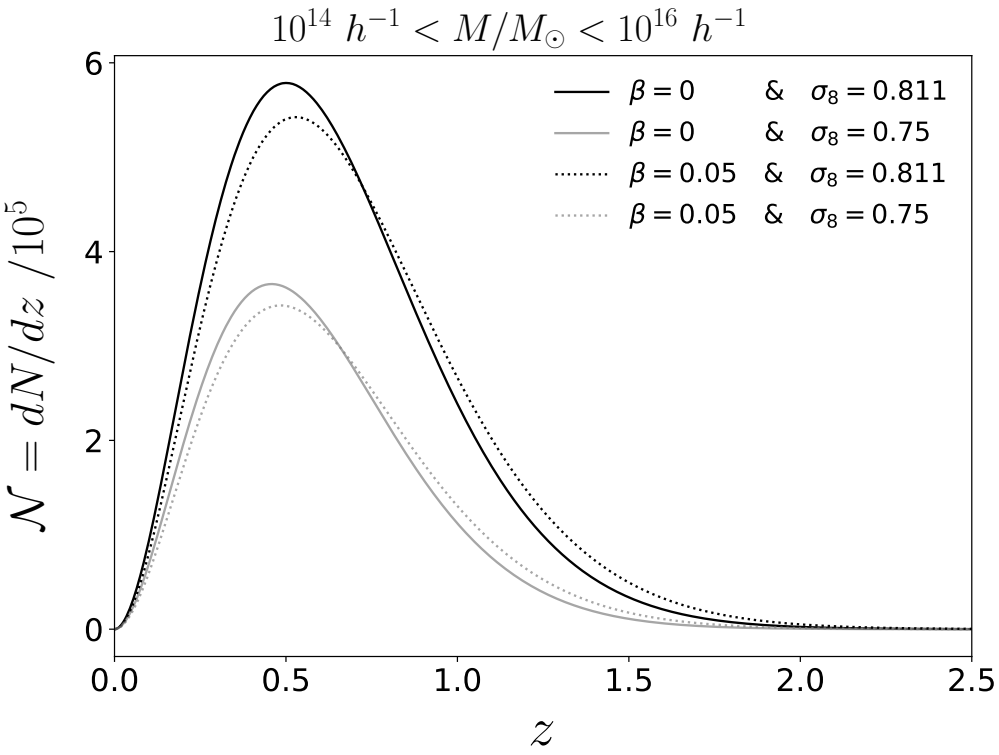

Figure 3.14: Comoving number of dark matter halos with masses within $10^{14}h^{-1}M_\odot < M < 10^{16}h^{-1}M_\odot$ calculated from the Press-Schechter mass function for the uncoupled case (solid) and $\beta = 0.05$ (dotted) with $\sigma_8 = 0.811$ (black) and $\sigma_8 = 0.75$ (gray).

halos at low z and a lower abundance at high redshifts. Sheth and Tormen [196] formulated a modification of the PS formalism, assuming an ellipsoidal model for the collapse of the density contrast region, resulting in a modified mass function which is in better agreement with simulations [197]. In this subsection, the results for the number of dark matter halos from the PS analysis are compared with the ones obtained using the Sheth-Tormen mass function.

The Sheth-Tormen (ST) mass function can be written as

$$\frac{dn}{dM} = -A\sqrt{\frac{2a}{\pi}}\frac{\tilde{\rho}_c(z)}{M}\left[1+\left(\frac{\sigma(z,M)^2}{\delta_c(z)^2}\right)^p\right]\frac{\delta_c(z)}{\sigma(z,M)}\frac{d\ln\sigma(z,M)}{dM}\exp\left[-\frac{a\delta_c(z)^2}{2\sigma(z,M)^2}\right], \tag{3.4.14}$$

with a and p being parameters fitted by numerical simulations and A a normalization constant. For details we refer the reader to Refs. [195, 196]. Following Refs. [195, 198], we adopt the values $(a, p, A) = (0.707, 0.3, 0.322)$, well in agreement with numerical simulations. The standard Press-Schechter mass function is recovered for the choice $(a, p, A) = (1, 0, 1/2)$.

The comoving number count of dark matter halos for the Sheth-Tormen mass functions, for for different values of the coupling, is displayed on the right panel of Fig. 3.11. The influence

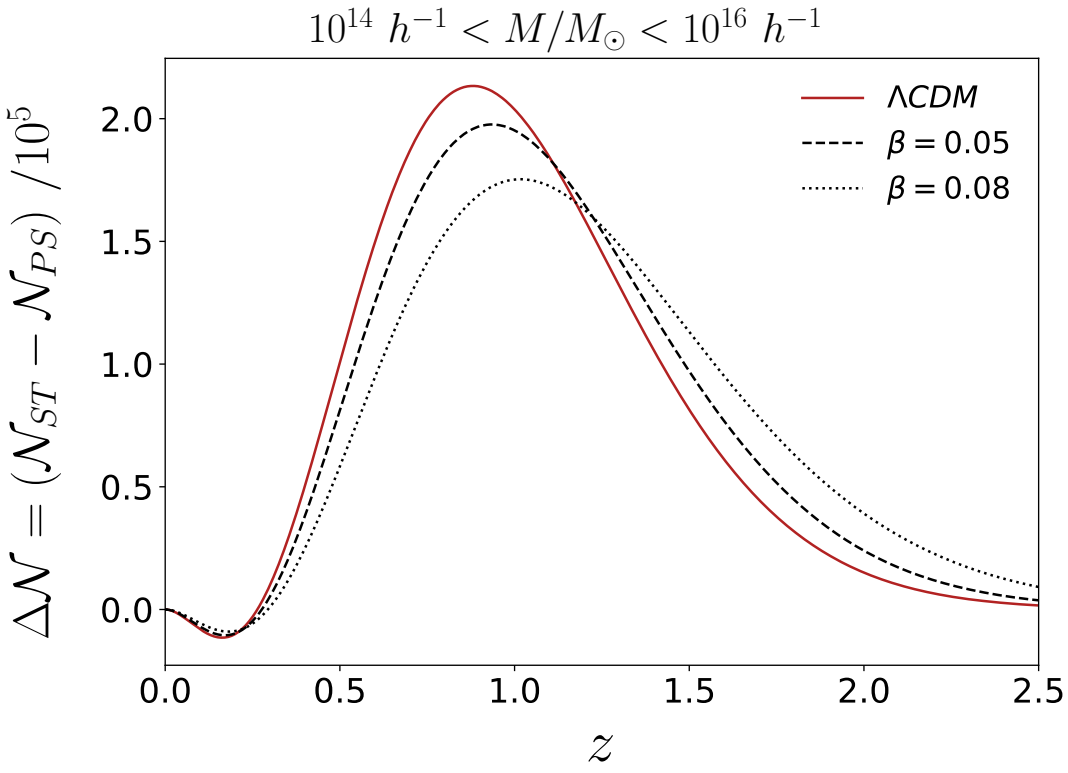

Figure 3.15: Difference of the comoving number of dark matter halos with masses within $10^{14}h^{-1}M_\odot < M < 10^{16}h^{-1}M_\odot$, between the ST Eq. (3.4.14) and the PS mass function Eq. (3.4.8), for $\beta = 0$ (solid), $\beta = 0.05$ (dashed) and $\beta = 0.08$ (dotted).

of the coupling follows the same trend as in the PS formalism, however, more pronounced: for example, the suppression of the number counts at low z can be prolonged up to higher redshifts. This fact is already known [195]; the ST mass function suppresses (enhances) the number of objects at low (high) redshifts when compared to the PS formalism. This effect can be better identified in Fig. 3.15 where we show the number difference between the PS and the ST number prediction. The discrepancy between the two mass functions peaks at around $z \sim 1$ with a difference reaching $\sim 2 \times 10^5$ clusters (for ΛCDM).

Although the ST formalism seems to be in better agreement with numerical simulations of the distribution of halos when compared to the standard PS, N-body simulations have been able to find improved fitting mass functions [199] for a wide plethora of cosmologies. It is important to notice however, that for the scope of this work either the PS or the ST functions attend our purposes.

3.5 Observing $\mathcal{N}$ with eROSITA and the SPT

In this section we shed some light on the predicted number of cluster-sized objects for two different surveys and comment on the possibility to distinguish between theoretical models. Notice that prior studies have implemented a similar analysis for different theoretical models, such as disformally coupled [67], thawing [195] and freezing [198] models of dark energy.

The 10 meter South Pole Telescope [200], stationed in Antarctica, is conducting a survey of galaxy clusters on the southern hemisphere sky. Currently, it is operating with its third-generation camera, SPT-3G, however, here the focus is on the estimate with regard to its first survey SPT-SZ [201]. This mission covered an area of 2500 deg^2 (corresponding to a fraction of the sky of $f_{\rm sky} \approx 0.06$) throught the Sunyaev-Zel'dovich (SZ) Effect [202], from 2007 until 2011. The details regarding the observational strategy can be found in Ref. [203] and the criteria used for cluster selection, determination of redshift and other characteristics of the survey can be found in Ref. [201]. Cosmological constraints from the SPT-SZ survey were conducted in Ref. [204], considering a sample of clusters at $z > 0.25$. Our aim here is to estimate the effect of the coupling parameter on the number of observed galaxy clusters, *i.e.* on $\mathcal{N}$.

According to the SPT-SZ survey criteria [204], the detection significance parameter ξ can be used as an estimate for the cluster mass. Specifically, the cluster mass is calculated using the unbiased significance ζ, related to ξ through $\zeta = \sqrt{\langle\xi\rangle^2 - 3}$. The mass scaling relation can be parametrised as

$$\zeta = A \left(\frac{M}{3 \times 10^{14} M_{\odot} h^{-1}} \right)^B \left(\frac{E(z)}{E(0.6)} \right)^C , \tag{3.5.1}$$

with $E(z) = H(z)/H(0)$. The parameters A, B and C are ultimately fitted by the data. Here, we employ the values $(A, B, C) = (3.531, 1.661, 0.733)$ (SPT+Planck+WP+BAO [204]). Imposing the selection criteria employed in the SPT-SZ survey of $\xi > 5$, we follow to numerically solve Eq.(3.4.11) with the integration being performed from the lower bound $M_{\rm inf} = \max[M_l, 10^{14} M_{\odot}]$, where M_l is the mass limit obtained by solving Eq. (3.5.1) for M. Recall that, as the SPT only covers a limiting fraction of the sky, the result has to be multiplied by this fraction, *i.e.* $f_{\rm sky} = 0.06$, to only capture the objects within that region. The integration is performed with the upper bound of $M_{\rm sup} = 10^{16} M_{\odot}$ as no structures are expected to form with larger masses. Nonetheless, we have verified that increasing this upper bound does not affect the results.

The estimated number of galaxy clusters for the SPT-SZ survey as a function of redshift is reported on the left panel of Fig. 3.16, using the Press-Schechter mass function, for ΛCDM and

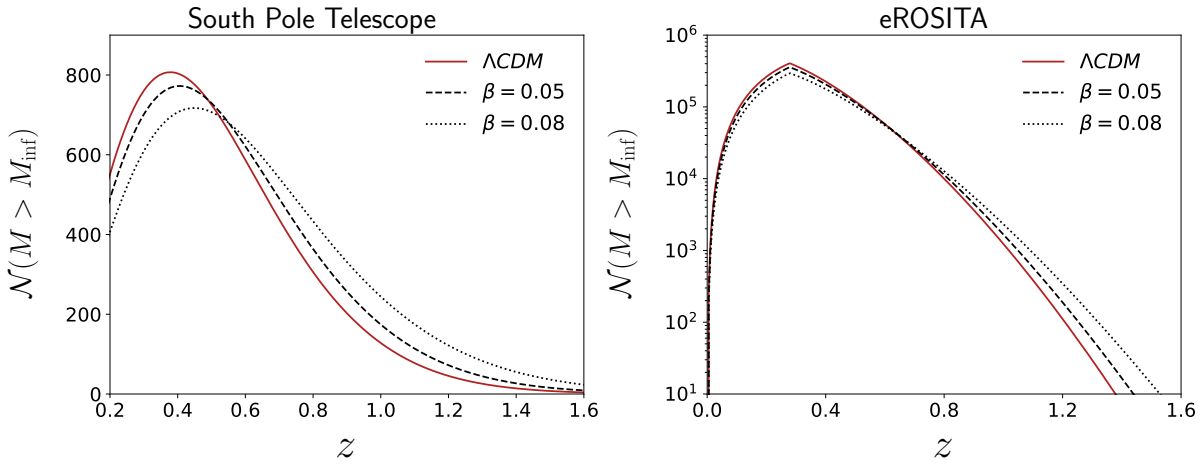

Figure 3.16: Estimate on the number of galaxy clusters for the SPT SZ survey (left) and expected number of clusters along redshift for the eROSITA (right), for $\beta = 0$ (solid), $\beta = 0.05$ (dashed) and $\beta = 0.08$ (dotted).

different values of the coupling. The values obtained for ΛCDM are of the same order as the ones predicted by Refs. [204, 205]. The number of detected galaxy clusters is expected to peak at $z \approx 0.4$ with $\mathcal{N} \approx 800$. This number however is slightly suppressed for nonzero couplings. This explicitly shows how an interaction between the dark species leaves an evident imprint in the spectrum of $\mathcal{N}$.

It is also fruitful to analyse whether the differences for the coupled models to the standard ΛCDM remain within the sensitivity range in which the survey will be able to discriminate. This difference is depicted on the left panel of Fig. 3.17. There is a clear discrepancy on the number counts predicted by ΛCDM and interacting models. This difference peaks at around $z \approx 0.3$, with $\Delta\mathcal{N} \approx 150$ for $\beta = 0.08$ and $\Delta\mathcal{N} \approx 60$ for $\beta = 0.05$. These values lie above the estimated SPT uncertainty $\Delta\mathcal{N} \approx 50$ [206, 207]. Therefore, in principle it would be possible to discriminate between ΛCDM and coupled quintessence models with the SPT-SZ survey. Note however that this holds only if one assumes all the remaining cosmological parameters to be fixed. As mentioned before, the values of $\mathcal{N}$ strongly rely on the value of σ_8, as seen in Fig.3.14.

The last survey addressed here is the X-ray telescope eROSITA, launched on the 13th of July, 2019. It covers a much wider fraction of the sky, $f_{\rm sky} = 0.485$ when compared with the SPT. The limiting mass that eROSITA will be able to detect can be inferred by its limiting energy flux. In the band $[0.5, 2.0]$ KeV this is $f_{lim} = 3.3 \times 10^{-14}$ erg s^{-1} cm^{-2}. To convert these values to a mass limit, in order to perform the integration of the expected number counts, we follow the method of Refs. [208, 209]. Particularly, the relation between bolometric X-ray luminosity and

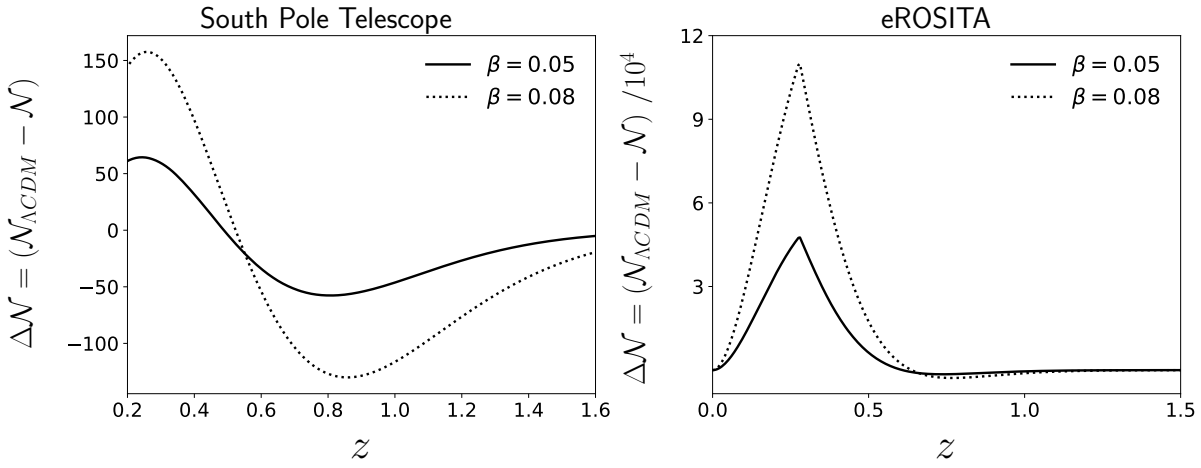

Figure 3.17: Difference on the expected number of galaxy clusters from ΛCDM, for the SPT (left) and eROSITA (right) surveys, for $\beta = 0.05$ (dashed) and $\beta = 0.08$ (dotted).

mass is

$$L(M, z) = 3.087 \times 10^{44} \left[\frac{M\, E(z)}{10^{15} h^{-1} M_\odot} \right]^{1.554} h^{-2} \,. \tag{3.5.2}$$

Analogously to the SPT case, we are then able to find the limiting mass by solving Eq. (3.5.2) for M, with the luminosity function given by $L = 4\pi d_L^2 f_{\rm lim} c_b$. The parameter c_b is a band correction needed to convert a bolometric luminosity into the eROSITA energy band [209, 210]. In this work we consider the value $c_b \approx 1.5$. This value was verified to yield values for the limiting mass versus redshift in concordance with previous studies [210].

The results for the expected halo number counts are reported on the right panel of Fig. 3.16 and the differences on the halo counts relative to the standard ΛCDM are shown on the right panel of Fig. 3.17. Clearly, eROSITA is expected to measure a much higher number of clusters than the South Pole Telescope, peaking at around $z \approx 0.28$, with the differences relative to ΛCDM, at this redshift, being $\Delta\mathcal{N} \approx 47\,000$ and $\Delta\mathcal{N} \approx 110\,000$ for $\beta = 0.05$ and $\beta = 0.08$, respectively. As for the SPT, these values are well over the expected eROSITA sensitivity of $\Delta\mathcal{N} \approx 500$ [198, 211], suggesting the possibility to distinguish between models with eROSITA. It is important to notice that the numbers computed for $\mathcal{N}$ with $\beta = 0$ (ΛCDM) are, as expected, consistent with previous studies in the literature [67, 208].

As a final remark, we should comment on the fact that the forecast analysis applied in this section was conducted using the PS mass function. We have nonetheless numerically verified that the ellipsoidal collapse model of Sheth-Tormen yields equivalent conclusions for the spherical model, with the values for $\Delta\mathcal{N}$ being remarkably close to the ones reported for PS in Fig. 3.17.

Chapter 4

The σ_8 tension in the light of Q-gravity

These disquisitions reminded him of the answer he once got from a little boy whom he met coming home from school. Nekhludoff asked him if he had learned his spelling.

"I have", answered the boy.

"Well, then, tell me, how do you spell 'leg'?"

"A dog's leg, or what kind of leg?"

From *Ressurection*,

by Leo Tolstoy

This chapter is based on Ref. [212].

Up to this point, this thesis has only been concerned with models of modified gravity in the context of dark energy, through the inclusion of an extra scalar degree of freedom, in the form of a scalar field in the matter sector. In this section, however, we present a modified gravity model, or, more precisely, an *alternative* gravity model (this will be clarified further ahead), on a flat space, encompassing the standard ΛCDM species. In this framework, gravitational phenomena are not ascribed to curvature, but to another geometrical property of the spacetime instead: *nonmetricity*. This model will be presented - as the title suggests - in the context of the σ_8 tension, previously addressed in Sec. 3.3. But let's not get ahead of ourselves. What exactly is nonmetricity? And what does the Q in this chapter's title stands for?

Let $\mathcal{S}\left[\mathbf{g}, \phi, \nabla\phi\right]$ be an action over a smooth manifold $\mathcal{M}$, where $\mathbf{g}$ is a metric and ϕ denotes the matter fields. This connection specifies a way of joining nearby tangent spaces, say at $T_p\mathcal{M}$ and $T_{p+\epsilon}\mathcal{M}$, thus allowing the parallel transport of vectors to be defined. Locally, its action on a contravariant tensor is

$$\nabla_\mu V^\nu = \partial_\mu V^\nu + \Gamma^\nu{}_{\mu\alpha} V^\alpha \,, \tag{4.0.1}$$

with $\Gamma^{\nu}{}_{\mu\alpha}$ being the connection coefficients, which fully determine the connection and express how the basis for $T_p\mathcal{M}$ changes along nearby points $\in \mathcal{M}$. The covariant nature of ∇ is encoded in the commutation relation

$$\big[\nabla_\mu, \nabla_\nu\big] V^\alpha = R^\alpha{}_{\beta\mu\nu} V^\beta - T^\beta{}_{\mu\nu} \nabla_\beta V^\alpha \,, \tag{4.0.2}$$

where

$$R^\alpha{}_{\beta\mu\nu} := 2\partial_{[\mu}\Gamma^\alpha{}_{\nu]\beta} + 2\Gamma^\alpha{}_{[\mu|\lambda|}\Gamma^\lambda{}_{\nu]\beta} \,, \tag{4.0.3}$$

$$T^\beta{}_{\mu\nu} := 2\Gamma^\beta{}_{[\mu\nu]} \,, \tag{4.0.4}$$

are the curvature and torsion which, unlike Γ, are tensors. Notice that, by introducing a connection, we naturally endow $\mathcal{M}$ with two geometrical objects - curvature and torsion - which characterise the affine structure of the manifold. The geometrical meaning of such objects can be understood as follows. Take a vector and parallel transport it along a closed loop. When the vector returns to its initial position, if it is not pointing to where it initially was (it is rotated), then the manifold is curved (and this rotation is indeed quantified by the Riemann tensor). Now take two vectors and parallel transport them along each other. If the parallelogram they form does not close, it means the manifold has torsion. A very clarifying illustration of these effects can be found in Ref. [213].

Now let us remember that the manifold was endowed with a (pseudo Riemannian) metric $\mathbf{g}$. The notions of length and angles are intimately connected to this object,

$$||\mathbf{v}||^2 = \mathbf{g}(\mathbf{v}, \mathbf{v}) \,, \qquad\qquad \cos\alpha = \frac{\mathbf{g}(\mathbf{v}, \mathbf{u})}{||\mathbf{v}||\ ||\mathbf{u}||} \,, \tag{4.0.5}$$

and its covariant derivative defines a tensor,

$$Q_{\alpha\mu\nu} := \nabla_\alpha g_{\mu\nu} \,, \tag{4.0.6}$$

called the *nonmetricity*, which describes the failure of the connection to be metric compatible. The objects ∇ and $\mathbf{g}$ completely describe the affine structure of $\mathcal{M}$, and their geometrical properties are encoded into the *curvature, torsion* and *nonmetricity* tensors. The geometrical meaning of $Q_{\alpha\mu\nu}$ can be easily understood. Given a vector $\vec{v}$ (ore more precisely, any section of

the vector bundle), we say that it is parallel transported along a curve $\gamma : \mathbb{R} \to \mathcal{M}$, if

$$t^\mu \nabla_\mu v^\alpha = 0\,, \tag{4.0.7}$$

where t^μ stands for the components of the unit vector tangent to γ. If we inspect the change of the vector's length along this curve, we find,

$$\begin{aligned} t^\mu \nabla_\mu ||\vec{v}||^2 &= t^\mu \nabla_\mu g(\vec{v},\vec{v}) = t^\mu \nabla_\mu (g_{\alpha\beta} v^\alpha v^\beta) \\ &= 2 g_{\alpha\beta} v^\alpha \underbrace{t^\mu \nabla_\mu v^\beta}_{=0} + t^\mu v^\alpha v^\beta \nabla_\mu g_{\alpha\beta} \\ &= t^\mu v^\alpha v^\beta Q_{\mu\alpha\beta}\,, \end{aligned} \tag{4.0.8}$$

that is, the change of the length of the vector is quantified by the nonmetricity. Thus, $Q_{\alpha\mu\nu}$ measures changes in lengths. In standard GR, the so called metricity condition, $Q_{\alpha\mu\nu} = 0$, guarantees the invariance of a vector's length over parallel transport.

Besides the metricity condition, in GR vanishing torsion is also assumed. These two conditions can be relaxed by choosing different connection coefficients on $\mathcal{M}$. This boils down to assuming different ways of joining nearby fibers, alternative ways of defining the differentiation of vectors; one for each choice of Γ. There are many distinct ways of defining differentiation on the manifold, with each choice of ∇, corresponding to different connection coefficients, $\Gamma^\nu{}_{\mu\alpha}$ (encoding how the vector basis change at different points of $\mathcal{M}$), that, together with the metric g, fully characterise the affine structure of $\mathcal{M}$.

The most general connection can be decomposed into the elements [214] (see Appendix B)

$$\Gamma^\lambda{}_{\mu\nu} = \tilde{\Gamma}^\lambda{}_{\mu\nu} + K^\lambda{}_{\mu\nu} + L^\lambda{}_{\mu\nu}\,, \tag{4.0.9}$$

where

$$\tilde{\Gamma}^\lambda{}_{\mu\nu} = \frac{1}{2} g^{\lambda\alpha} \left(\partial_\mu g_{\alpha\nu} + \partial_\nu g_{\alpha\mu} - \partial_\alpha g_{\mu\nu}\right) \tag{4.0.10}$$

are the familiar Levi-Civita coefficients,

$$K^\lambda{}_{\mu\nu} = \frac{1}{2} g^{\lambda\alpha} \left(T_{\alpha\mu\nu} + T_{\nu\alpha\mu} + T_{\mu\alpha\nu}\right) \tag{4.0.11}$$

is known as the *contorsion* and

$$L^{\lambda}{}_{\mu\nu} = \frac{1}{2} g^{\lambda\alpha} \left(Q_{\alpha\mu\nu} - Q_{\nu\alpha\mu} - Q_{\mu\alpha\nu} \right) \tag{4.0.12}$$

is the *disformation*. Note that the latter two objects stem from torsion and nonmetricity, respectively. The contorsion tensor is antisymmetric with respect to the first and last indices, $K_{\lambda\mu\nu} = -K_{\nu\mu\lambda}$, whereas the disformation is symmetric on the last two indices, $L_{\lambda\mu\nu} = L_{\lambda\nu\mu}$.

The universal character of the equivalence principle led Einstein to formulate a geometric theory of gravity, general relativity. GR stands upon the presumption that gravity is ascribed solely to the curvature of spacetime (through the invariant R), assuming vanishing torsion and nonmetricty (thus setting $\Gamma = \tilde{\Gamma}$), with this being the widely accepted interpretation of gravity. Nonetheless, it has been shown [213] that different methods for geometrising gravity may lead to the same elemental theory. By considering different connection coefficients, it is possible to write actions based on invariants constructed from either nonmetricity or torsion, that, nonetheless, reproduce the same standard GR cosmology, on a flat spacetime ($R^{\alpha}{}_{\beta\mu\nu} = 0$), and with the same two degrees of freedom of the massless graviton. This has been dubbed the Geometrical Trinity of Gravity [213]. Even though the dynamics of each theory is exactly the same, these different formulations yield completely distinct and rich interpretations for the source of gravitational phenomena.

Since the nonmetricity tensor has three indices, any invariant object constructed from it needs to be, at least, of quadratic order [215],

$$Q := -\frac{1}{4} Q_{\alpha\mu\nu} Q^{\alpha\mu\nu} + \frac{1}{2} Q_{\alpha\mu\nu} Q^{\mu\nu\alpha} + \frac{1}{4} Q_{\mu} Q^{\mu} - \frac{1}{2} Q_{\mu} \tilde{Q}^{\mu} \,, \tag{4.0.13}$$

where

$$Q_{\mu} := Q_{\mu}{}^{\alpha}{}_{\alpha} \qquad \text{and} \qquad \tilde{Q}^{\mu} := Q_{\alpha}{}^{\mu\alpha} \,, \tag{4.0.14}$$

are the two independent traces of $Q_{\alpha\mu\nu}$. The coefficients multiplying each term in Eq. (4.0.13) are chosen such that the action $\mathcal{S} = \int \omega_g Q / 16\pi G$ leads back to the same dynamics of GR. This model is known as Symmetric Teleparallel Equivalent of GR [213]. This section deals with modified $f(Q)$ gravity [216–218], also known as Symmetric Teleparallel Gravity (STG) [219–223]. Note however, that this framework has already been proposed in previous works, together with applications to cosmology [224]. In Ref. [225], the authors have introduced a coupling betwen the non-metricity scalar Q and the matter sector, thus breaking the covariant

conservation of the energy-momentum tensor, and have also analysed the dynamical behaviour of scenarios with specific coupling functions (see also Ref. [226]). Models assuming the existence of a scalar field nonminimally coupled to nonmetricity, called the scalar-nonmetricity theories of gravity, were proposed in Refs. [227, 228]. There, the authors have explored the similarities of these theories with scalar-torsion and scalar-curvature models. An equivalence between the solutions of $F(Q)$ and the metric teleparallel $F(T)$ models on a flat Friedmann cosmology was also found. The authors also explored conformal transformations under this setting (see also Ref. [229]). The propagation of tensor modes in Symmetric Teleparallel Gravity has been studied in Refs. [230–233], focusing on the possible new parity-violating signatures [234, 235]. The modified Newtonian limit in $F(Q)$ gravity in the light of dark matter phenomenology was investigated in Refs. [236, 237].

4.1 Model

Let us consider the following action minimally coupled to gravity,

$$\mathcal{S} = \int \omega_g \left[-\frac{1}{16\pi G} F(Q) + \mathcal{L}_m(\phi, \nabla\phi) \right] , \tag{4.1.1}$$

where $\mathcal{L}_m$ stand for the matter fields' Lagrangian density. The field equations and geometrical interpretation on this flat and torsion-free setting were thoroughly explored in Ref. [213]. Considering an homogeneous and isotropic FLRW line element, given by Eq. (2.2.2), the nonmetricity invariant, Eq. (4.0.13), becomes simply $Q = 6H^2$. The field equations arising from Eq. (2.1.1), considering a pressureless matter component and a cosmological constant Λ (Λ+CDM), are [215]:

$$2F_Q H^2 - \frac{1}{6}F = \frac{8\pi G}{3}\rho_m + \frac{\Lambda}{3} , \tag{4.1.2}$$

$$\left(12H^2 F_{QQ} + F_Q\right)\dot{H} = -4\pi G\rho_m , \tag{4.1.3}$$

where ρ_m and Λ denote the energy density of matter and the cosmological constant, respectively, and we use the notation $F_Q := \partial F/\partial Q$.

We follow an approach similar to the one in Sec. 3, by focusing on the specific cases of $F(Q)$ cosmology in which the background is constructed so as to mimic the ΛCDM dynamics in general relativity. At perturbative level, as it will be seen, deviations arise. The main aim, is to

see if this linear deviations can provide a way to alleviate the σ_8 tension.

Through the field equations, Eq. (4.1.2), we note that a ΛCDM evolution is attained by setting the left hand side of Eq. (4.1.2) equal to H^2, which gives the solution [217]:

$$F(Q) = Q + M\sqrt{Q} + C\,, \tag{4.1.4}$$

with M and C being constants with dimensions of mass and mass^2, respectively. This choice holds the familiar Friedmann equation

$$H^2 = \frac{8\pi G}{3}\rho_m + \frac{\Lambda}{3} + \frac{C}{6}\,, \tag{4.1.5}$$

and the matter fields are then set to follow,

$$\dot{\rho}_m + 3H\rho_m = 0\,. \tag{4.1.6}$$

For details we refer the reader to Ref. [217]. Kindly note that C behaves as a cosmological constant. Hence, Λ can be entirely introduced in the gravitational Lagrangian by setting $C = 2\Lambda$ in Eq. (4.1.4) (on such case $\mathcal{L}_m = \mathcal{L}_{cdm}$), or in the matter Lagrangian, fixing in this case $C = 0$ and $\mathcal{L}_m = \mathcal{L}_{cdm} + 2\Lambda$.

Equation (4.1.4) is interesting since it introduces a free parameter M without having any influence whatsoever on the background evolution. On the other hand, at the perturbative level, this will lead to different predictions for the growth of fluctuations, that can be used to constrain the model against observational data, as we will shown.

The evolution of the first order matter overdensities, denoted simply by δ, in the small scales limit, were derived in Ref. [217], and can be written as,

$$\ddot{\delta} + 2H\dot{\delta} - \frac{4\pi G}{F_Q}\,\rho_m\,\delta = 0\,. \tag{4.1.7}$$

Notice that, in Eq. (4.1.7), the only difference from standard GR is a running gravitational constant, $G_{\rm eff}/G = 1/F_Q$, sourced by the nonmetricity (here mediated by M). Equation (4.1.7) reduces to pure GR by setting $M = 0$ in Eq. (4.1.4). Notice that since we are interested in the behaviour of matter fluctuations at small scales and late times, radiation may be neglected. It should be mentioned that, in models of Teleparallel gravity, the equation governing the growth of matter fluctuations, has exactly the same form as Eq. (4.1.7), with $F_Q \to F_T$.

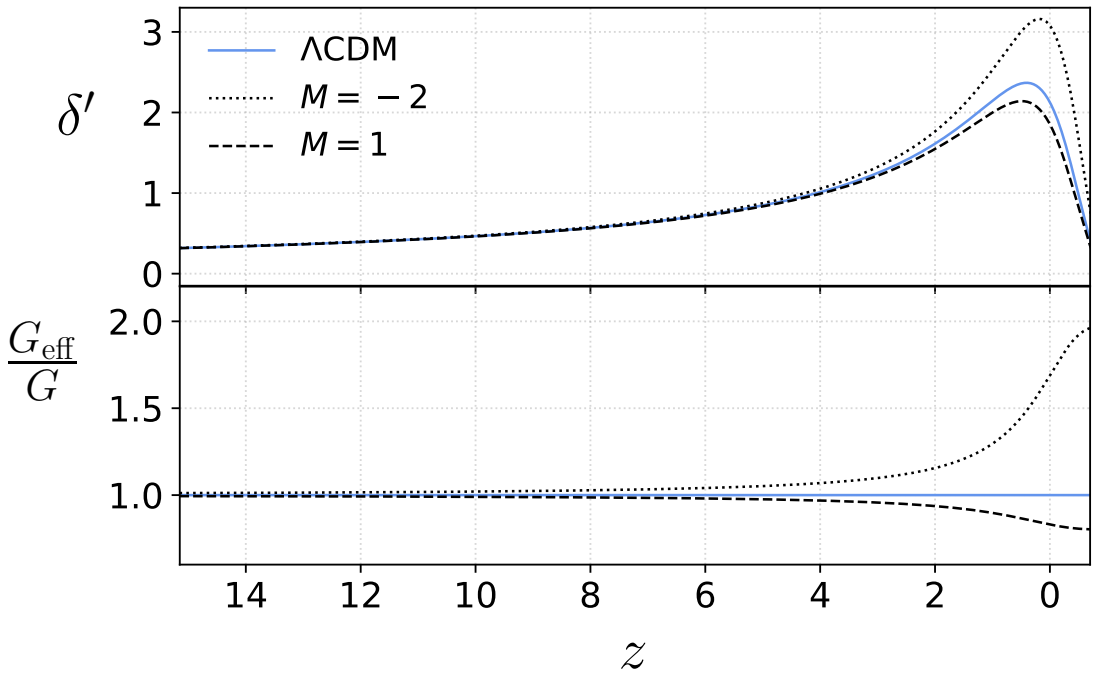

Figure 4.1: Top panel: derivative of the density contrast, δ', for $M = -2$ (dotted), ΛCDM (solid) and $M = 1$ (dashed). M values are in H_0 units. Bottom: Deviations on the effective gravitational constant with respect to ΛCDM, for the same values of the coupling.

Rewriting Eq. (4.1.7) in terms of derivatives with respect to the number of e-folds $N = \ln a$, and with $F(Q)$ as given by Eq. (4.1.4), we obtain

$$\delta'' + \delta' \left(2 + \frac{H'}{H}\right) - \frac{3\sqrt{6}H}{2\sqrt{6}H + M}\Omega_m \delta = 0\,. \tag{4.1.8}$$

Although the background of this model remains unaltered by varying M, the matter perturbations are suppressed for $M > 0$ and enhanced for $M < 0$, depending on the corrective force term in Eq. (4.1.8). This trend is depicted in Fig. 4.1. We note that the deviations on the matter overdensities become clear at latter times, when H becomes of the order of M, and the effective gravitational constant deviates from its GR counterpart. It is useful to express M in units of H_0, and hereafter we will always present our results accordingly.

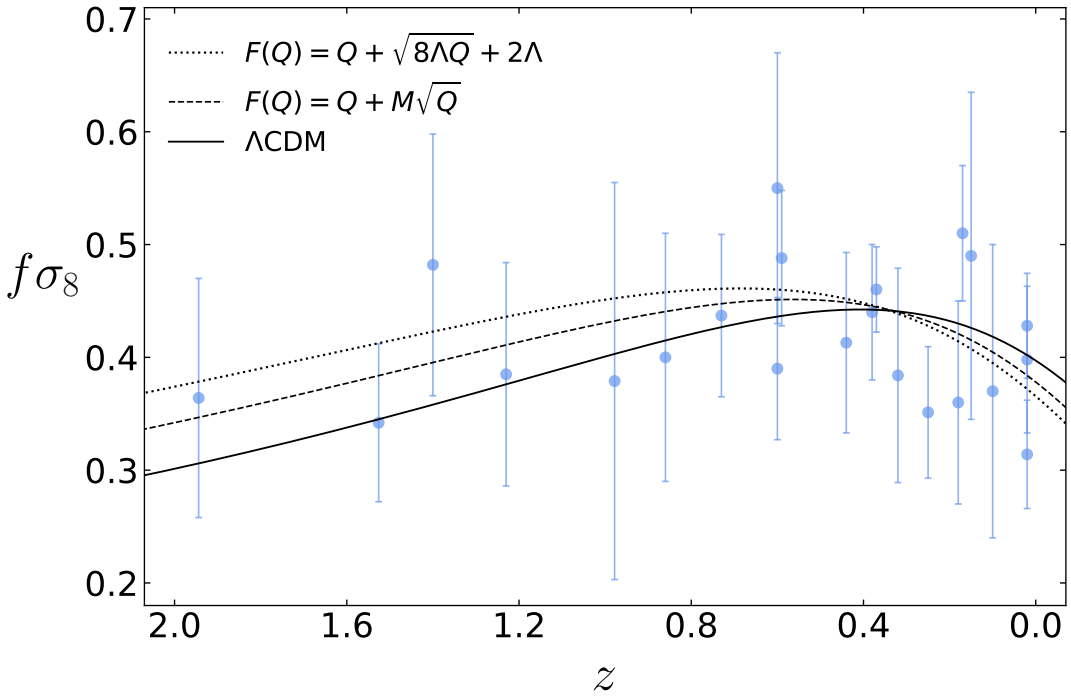

Figure 4.2: Evolution of $f\sigma_8$ given the best fit values for ΛCDM (solid), $F(Q) = Q + M\sqrt{Q}$ (dashed) and $M^2 = 8\Lambda$ (dotted). Data points can be found in Table I of Ref. [238].

4.2 Analysis and results

In this section, the numerical evolution of the matter perturbations, Eq. (4.1.8), is performed, together with a likelihood analysis considering RSD data, akin to the study conducted in Chapter 3.3. To do so, we adopt a set consisting of 22 data points, referenced in Table I of Ref. [238].[1] In Ref. [26], the authors built a robust subsample of 18 independent data points, dubbed 'Gold-2017' growth dataset, from a total dataset of 34 data points for $f\sigma_8$. The validity of this dataset – with four new data points added – was analysed through a Bayesian model comparison and by performing cross-checks to confirm its sensitivity [238]. It was concluded that the data points presented in Table I of Ref. [238] are indeed internally robust. Accordingly, we resort to the observational values for $f\sigma_8$, which have already been exploited in other studies [239, 240]. The data points and respective redshifts z are presented in Fig. 4.2.

Since we wish to compare $F(Q)$ predictions against the standard ΛCDM, we follow to fix the relevant parameters to the latest Planck 2018 bestfit results [8]. We consider three case studies. First, the scenario where both M and σ_8 are free parameters. Secondly, $M = 0$, as it by doing so, the theory is reduced to pure ΛCDM, both at the background and linear levels. The third case,

[1]Note that the data points used in this section are different than the ones used in the coupled quintessence model of 3.3. This because, at the time that Ref. [124] was being performed, the work in Ref. [238] had not yet been published and we were not aware of the results of Ref. [26].

$M^2 = 8\Lambda$, can be understood by assuming that the Lagrangian for the gravitational sector $F(Q)$ admits an expansion of the form,

$$F(Q) = \left(\sqrt{Q} + \frac{M}{2}\right)^2 = Q + M\sqrt{Q} + \frac{M^2}{4}\,, \tag{4.2.1}$$

where, as we can see, the cosmological constant was shifted into the gravity sector – absorbed into $F(Q)$ –, and we identify $M^2 = 8\Lambda$. The Friedmann equation derived from Eq. (4.2.1) is,

$$H^2 = \frac{8\pi G}{3}\rho_m + \frac{M^2}{24}\,, \tag{4.2.2}$$

where the relation between the cosmological constant and the mass scale M can be fully appreciated, and is equivalent to fixing $C = M^2/4$ in Eq. (4.1.5). Thus, we have $M^2 = 24H_0^2\Omega_\Lambda^0$, which, in terms of the latest Planck 2018 [8] values, yields $M = 4.0544$. Hence, we can write the third case as,

$$F(Q) = Q + \sqrt{8\Lambda Q} + 2\Lambda\,, \tag{4.2.3}$$

where only the background is set to follow a ΛCDM evolution and not the perturbations, as $M \neq 0$.

In Refs. [26, 238], the observations of the data points are conducted assuming a fiducial cosmological model (different values of Ω_m^0) in order to estimate the distances to the sources. The values for Ω_m^0 are listed in the fourth column of Table I in Ref. [238]. Accordingly, following the procedure described in Ref. [241], we apply a correction to the theoretical values of $f\sigma_8$, through the ratio,

$$r(N) = \frac{H^{\rm obs}D_A^{\rm obs}}{H^{\rm th}D_A^{\rm th}}\,, \tag{4.2.4}$$

between the fiducial cosmology adopted in the observations and the theoretical values we are testing. Here, D_A is the angular diameter distance, *i.e.*

$$D_A = \frac{1}{1+z}\int_0^z \frac{1}{H(z')}dz'\,. \tag{4.2.5}$$

A likelihood analysis is then performed, allowing M and σ_8 to be free parameters. The likelihood is calculated through Eq. (3.3.27), with the chi squared test, Eq. (3.3.28) corrected according to the ratio in Eq. (4.2.4),

$$\chi^2 = \left[d_i - r(N_i)\,t_i\right]^T C_{ij}^{-1}\left[d_j - r(N_j)\,t_j\right]\,. \tag{4.2.6}$$

Table 4.1: Best fit values for M (in units of H_0) and σ_8, number of fitted parameters (N_{fp}) and respective χ^2 and AIC_c values.

Model	M	σ_8	χ^2	$\tilde{\chi}^2$	ΔAIC_c
ΛCDM	0	0.7535 ± 0.0280	13.1227	0.6249	0.5951
$F(Q) = Q + M\sqrt{Q}$	$2.0331^{+3.8212}_{-1.9596}$	$0.8326^{+0.1386}_{-0.0630}$	11.9960	0.5998	1.9003
$F(Q) = Q + \sqrt{8\Lambda Q} + 2\Lambda$	4.0544	0.8987 ± 0.0332	12.5276	0.5966	0

Through the computation of the χ^2 and the reduced $\tilde{\chi}^2$ we obtain a basic estimate of how much a model is preferred by the data. Nonetheless, there exist more rigorous criteria available for comparing models. A widely used test in the literature, the Akaike Information Criterion (AIC) [242], takes into account the number of fitted parameters, N_{fp}, [239, 240],

$$AIC = -2\ln\left(L_{\max}\right) + 2N_{fp}\,, \tag{4.2.7}$$

where $L_{\max}$ is the maximum of the likelihood function, given by Eq. (3.3.27). In the presence of a small sample size, the AIC can be corrected as

$$AIC_c = AIC + 2\frac{N_{fp}\left(N_{fp}+1\right)}{N_d - N_{fp} - 1}\,. \tag{4.2.8}$$

Note that the correction, *i.e.* the last term in the equation above, becomes superfluous as $N_d \to \infty$. Clearly, the model with smaller AIC_c is favoured. However, we will focus on the deviations $\Delta AIC_c = AIC_c - AIC_c^{\min}$ from the model with a minimum value for AIC_c. Models with $\Delta AIC_c \leq 2$, $4 \leq \Delta AIC_c \leq 7$ and $\Delta AIC_c \geq 10$ are said to have substantial support, considerably less support and essentially no support, respectively [243]. Thus, in addition to the χ^2 and $\tilde{\chi}^2$ conditions, the AIC_c test will also be used for model selection.

In Table. 4.1, the best fit values are listed along with the respective statistical uncertainties. The evolution of $f\sigma_8$ for the best fit parameters for each model is depicted in Fig. 4.3. The value of $\sigma_8 = 0.7535 \pm 0.0280$, found for ΛCDM, suggests a lower clustering level in contrast with the latest Planck 2018 value $\sigma_8 = 0.811 \pm 0.006$ [8]. This tension is illustrated in the first panel of Fig. 4.4 where the Planck likelihood (approximated as a Gaussian) has been included for reference (in red). Note that none of the statistical tests suggest ΛCDM as the preferred model. On the other hand, the introduction of one additional parameter, M, *i.e.* taking $F(Q) = Q + M\sqrt{Q}$, yields a best fit of $M = 2.0331^{+3.8212}_{-1.9596} \neq 0$, which curiously does not include ΛCDM ($M = 0$)

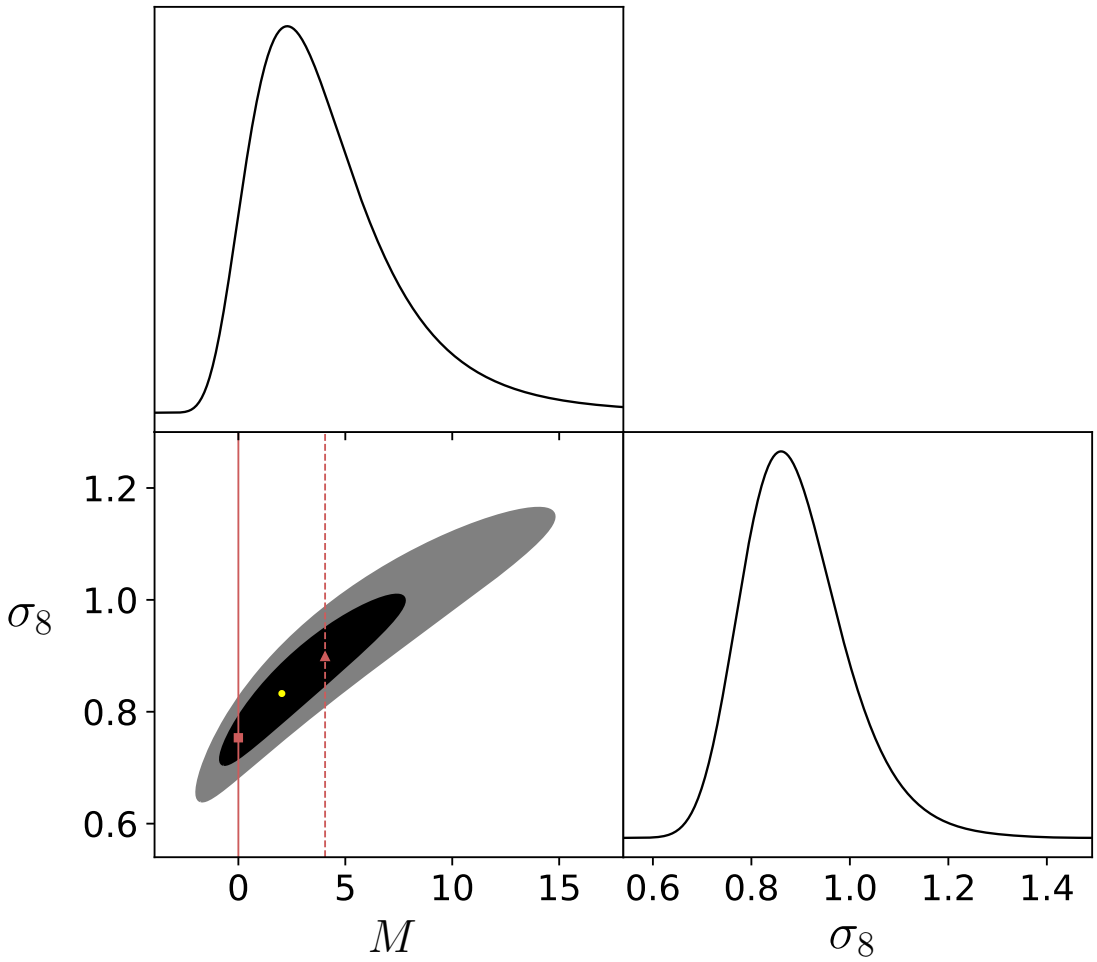

Figure 4.3: Constraints on M and σ_8: contours for the 1σ and 2σ regions, with the respective marginalised curves for $F(Q) = Q + M\sqrt{Q}$. A circle denotes the best fit value. The vertical lines denote the reference models: ΛCDM (solid) with a square marker on the best fit and for $M^2 = 8\Lambda$ (dashed) with a triangle marker on the best fit.

at 1σ level, and $\sigma_8 = 0.8326^{+0.1386}_{-0.0630}$. Hence, it can be stated that RSD data favours a slower growth (as $M > 0$) of the matter perturbations for $F(Q)$ gravity, in comparison with standard ΛCDM. Note that the Planck 2018 best fit is well within the 1σ region of the marginalised values for σ_8 (see last panel of Fig. 4.4). This suggests that it is possible to solve this tension within this alternate gravity framework. However, this σ_8 value has a relatively larger uncertainty in comparison with the other two models, due to its degeneracy with M. This is the price to pay for adding one more parameter. With this extra free parameter, the χ^2 test favours this model. On the other hand, this is not concordant with the weighted chi squared and the AIC_c test. The Lagrangian $F(Q) = Q + \sqrt{8\Lambda Q} + 2\Lambda$ shows a best fit of $\sigma_8 = 0.8987 \pm 0.0332$. This value is also in tension with Planck observations, although in the opposite side, comparing with ΛCDM. Curiously, both the χ^2 and AIC_c tests favour this model, $F(Q) = Q + \sqrt{8\Lambda Q} + 2\Lambda$, with only one fitted parameter. The contour regions and respective marginalised curves are presented in

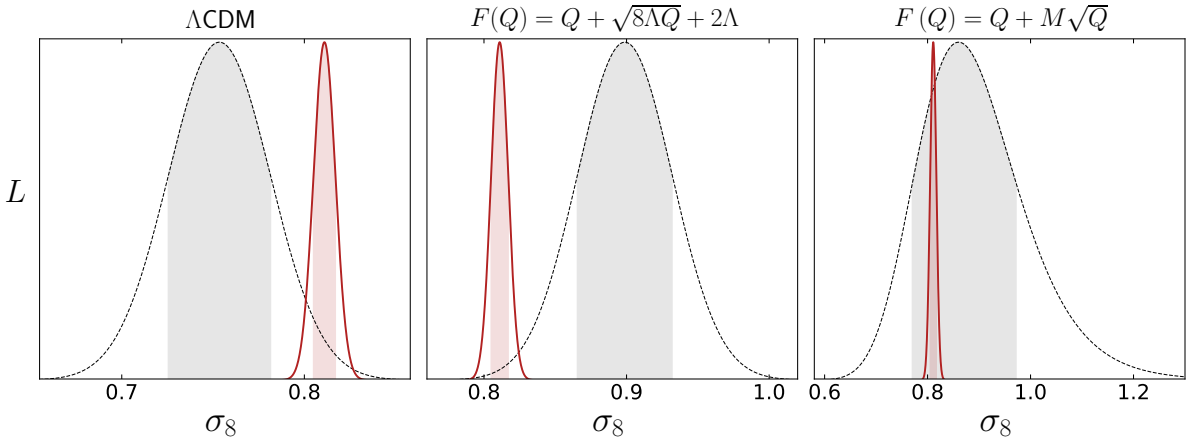

Figure 4.4: Likelihood for σ_8 (curves) and respective 1σ interval (shaded region), for the models (dashed lines) labelled on top of each panel. Planck reference in solid red lines.

Fig. 4.3 for $F(Q) = Q + M\sqrt{Q}$, together with the best fit values for the two reference models: ΛCDM (solid red vertical line) and $F(Q) = Q + \sqrt{8\Lambda Q} + 2\Lambda$ (dashed red vertical line). It is possible to identify a positive correlation between M and σ_8, which can be easily explained. As mentioned earlier, increasing values of M result in a slower growth of the overdensities, and thus a larger value for σ_8 is required to compensate the dynamics of $f\sigma_8$ and better fit the data. Nevertheless, it is important to note that the values for the AIC_c test are all relatively close to each other, therefore there is no strong evidence for a preferred model.

By combining multiple observations, it should be possible to set further constraints on Q-gravity at smaller scales. Such studies have already been done in the context of Teleparallel gravity with appealing results. Interesting possibilities include observations of deformations in black hole shadows [244], and low-z experimental data on weak gravitational fields through weak lensing effects [245].

Chapter 5

Exotic fluids in gravitation: 3-form Wormholes

Not how the world is, is the mystical, but that it is.

From *Tractatus Logico-Philosophicus*,

by Ludwig Wittgenstein

This chapter is based on Ref. [246].

In Chapters 2 and 3 we have considered models which regard the exotic source of the theory as a scalar field. Here we will deal with higher order spin fields, in particular three-form fields, and explore their exotic nature in the realm of gravitation. It is important to emphasize what has been done thus far in the literature with 3-forms.

Differential three-form fields [247, 248] have already been studied in various contexts and seem to yield viable solutions to several cosmological scenarios such as the late time acceleration of the Universe [249–251], primordial inflation [252–256], reheating [255], generation of cosmological magnetic fields [257], among others. The dynamics of self-interacting three-forms were explored in Refs. [247, 248], where it was shown that a minimally coupled canonical theory can naturally produce a variety of homogeneous and isotropic background dynamics, including scaling and phantom crossing. The background dynamics and cosmological perturbations of self-interacting three-forms were investigated in Ref. [251]. It was also shown that the phase space of cosmological solutions includes inflating attractors and saddle points useful to describe three-form driven inflation and dark energy scenarios. Inflationary models in extra dimensional braneworld scenarios inhabited by a single 3-form, confined to a 4D brane, were studied in

Ref. [258], by means of dynamical systems techniques. The dynamical study was complemented by testing the perturbation observables, tensor to scalar ratio and spectral index, against the Planck data. The study of screening mechanisms with three-forms can be found in Ref. [259]. The authors have considered a single three-form field conformally coupled to the matter sector, and showed that it is possible to obtain a thin-shell solution where the field interactions are only short range. Hawking and Turok showed that one can naturally explain the vanishing cosmological constant problem through the inclusion of a 4-form, constructed from a three-form field potential [260].

On a four dimensional spacetime, it is known that a 3-form field admits a dual scalar field representation [261, 262]. For instance, nonquadratic 3-form self-interactions lead to a noncanonical kinetic term on the equivalent scalar field representation. Nevertheless, this mapping however is nontrivial, and for several self-interactions, or the inclusion of any nonminimal coupling, the dual representation breaks down [251]. However, this is not problematic, and, on the contrary, suggests that three-form fields can provide new physics through richer cosmological settings, certainly worth exploring. Note that even in the cases where the dual description exists, it is often quite complicated to deal with, being much more efficient and intuitive to work in the form-representative framework.

In this section, we will employ the use of 3-forms to wormhole geometries. Before we move to the mathematical details, some words with regard to wormholes and their historical background should be mentioned.

Wormholes [263, 264] are shortcuts joining different regions of the Universe (or different Universes) and have been a matter of discussion for more than a century. The study of these (so far) hypothetical objects can be traced back to 1916 [265], when Flamm was examining the interior solution of the Schwarzschild solution (a few months after Schwarzschild's seminal paper [266]). Nearly two decades later, the famous Einstein-Rosen bridge solution was put forward [267] by Albert Einstein and Nathan Rosen, coining the possibility of the existence of "bridges" connecting different regions of spacetime. Again, two decades later, John Wheeler studied the topological structure of spacetime, in particular the multiply-connected spacetime, and proposed the geon concept [268]. Considering solutions to the interacting Maxwell-Einstein equations, Wheeler hypothesized the existence of tunnels connecting two separate regions, which he baptized as geons. In 1957, Misner and Wheeler [269], thoroughly explored the geon concept, focusing on non-trivial topologies of spacetime, to elaborate models of electrical charges at the

classical level. This work was among the first studies intimately merging geometrical concepts of spacetime and physics, and it is believed to be the earliest mention of the term *wormhole*. The renaissance of wormhole physics was not until 1988 [263], with the influential work by Michael Morris and Kip Thorne: "*Wormholes in spacetime and their use for interstellar travel: A tool for teaching General Gelativity*". They discuss the traversability conditions for travelling through a wormhole by holding its throat open with some sort of exotic matter. Other works regading wormholes should be mentioned, in particular the "drainhole" traversability concepts proposed by Ellis in 1973 [270] and, independently, by Bronnikov [271]. Wormholes are valid solutions to the Einstein field equations. Their existence, however, remains a speculation. For further details the reader is referenced to Refs. [264, 272]

As we will show, a fundamental ingredient for constructing traversable wormholes is the violation of the classical energy conditions near the throat [263, 264, 272–275], hinting at the possibility of the existence of exotic matter (matter that violates the energy conditions), needed to sustain the wormhole. For example, classical minimally coupled canonical scalar fields are known to not obey this property [264]. However, by introducing a nonminimal coupling of the scalar source to curvature [275], the scalar field can violate the energy conditions, and thus sustain the wormhole. This has also been explored in the context of modified gravity [276]. In particular, the "ordinary matter fields" threading the wormhole may obey the energy conditions, with the higher order curvature terms - interpreted as an effective fluid - sustaining the wormhole, by acting as the exotic source. This has been studied in several modified gravity models such as in $f(R)$ gravity [277], Weyl gravity [278], modified teleparallel gravity [279], curvature-matter couplings [280, 281], Einstein-Gauss-Bonnet gravity [282], hybrid metric-Palatini theory [283, 284], among others. Here we show how this behaviour can *de facto* be obtained, resorting to a single 3-form field.

5.1 Wormholes and energy conditions

The line element describing a static and spherically symmetric (non-charged and non-rotating) wormhole geometry can be written as [272]:

$$ds^2 = -e^{2\Phi(r)}dt^2 + \frac{dr^2}{1-b(r)/r} + r^2\left(d\theta^2 + \sin^2\theta d\phi^2\right) . \tag{5.1.1}$$

Here, $\Phi(r)$ is the redshift function, related to the gravitational redshift. To see this, one may compute the shift on the wavelength of a signal sent by someone going through the wormhole to someone outside:

$$\frac{\Delta\lambda}{\lambda} = e^{-\Phi} - 1 \approx -\Phi\,. \tag{5.1.2}$$

Thus, one requires that $|\Phi| \ll 1$, such that the proper time of the infalling person matches the one of the observer. Besides that, note that Eq. (5.1.2) diverges as $\Phi \to -\infty$, expressing the presence of an event horizon. Therefore, one needs to assume Φ to be finite in the entire domain of r, in order to avoid the presence of event horizons, hence rendering the wormhole traversable [277, 285]. Another effect that is characterised by the redshift function is the gravitational attraction of the wormhole over an observer [272]. One way to check this is by writing the radial component of the four acceleration, $a^\mu = u^\nu \nabla_\nu u^\mu$, of a static observer with four-velocity $u^\mu = dx^\mu/d\tau = (e^{-\Phi}, 0, 0, 0)$,

$$a^r = \Phi' \left(1 - \frac{b}{r}\right)\,, \tag{5.1.3}$$

where a prime denotes a derivative with respect to the radial coordinate r. This gives the radial acceleration that an observer needs to maintain in order to remain at rest and not be "sucked in" (or reppeled) by the wormhole. A wormhole is therefore attractive if $\Phi' > 0$ and repulsive for $\Phi' < 0$ [272]. Having said this, in order to be humanely possible to travel throughout (at least at present times), both Φ and Φ' need to be small. The $b(r)$ function in Eq. (5.1.1) is known as the shape function, since it depicts the form of the wormhole, as it will be shown next . Both the metric functions depend solely on the radial coordinate r. Since the g_{rr} component of the metric in Eq. (5.1.1) triggers a singularity, we require the proper radial distance, $l(r) = \pm \int_{r_0}^{r} [1 - b(r)/r]^{-1/2} dr$, to be finite in its entire domain [263]. In addition, we assume a flat spacetime far away from the wormhole, such that $b(r) \to 0$ and $\Phi(r) \to 0$ as $r \to \infty$, to obtain an appropriate asymptotically flat Minkowski limit.

One very useful method that helps us to visualise curved spacetimes as a 3D picture, is via *embedding diagrams* [286]. Here, this will help us not only to visualise the wormhole spacetime, but also to extract important information regarding the properties of the shape function $b(r)$. To this end, let us write the metric Eq. (2.2.2) at a fixed time t and sliced at $\theta = \pi/2$ as,

$$ds^2 = \frac{dr^2}{1 - \frac{b}{r}} + r^2 d\phi^2\,, \tag{5.1.4}$$

and embed it into a 3D Euclidean space, in cylindrical coordinates (r, ϕ, z),

$$ds^2 = dz^2 + dr^2 + r^2 d\phi^2 = \left[1 + \left(\frac{dz}{dr}\right)^2\right] dr^2 + r^2 d\phi^2 \,, \tag{5.1.5}$$

since in Euclidean space the surface has equation $z = z(r)$. Observing Eq. (5.1.4) and Eq. (5.1.5), we identify the embedding surface (also called lift function) as,

$$dz = \pm \left(\frac{r}{b} - 1\right)^{-1/2} dr \,, \tag{5.1.6}$$

where the $\pm$ signs represent two different regions of the Universe. Note that the r coordinate in Eq. (5.1.6) runs from a minimum, corresponding to the throat of the wormhole, at $r = b(r) = r_0$, where the lift function is vertical, *i.e.* $dz/dr \to \infty$, to infinity, $b(r) \leqslant r$. As one moves away from the throat, space becomes flat, $dz/dr \to 0$ as $r \to \infty$. Now, for the solution to represent a wormhole, we need the end of the throat to open "outwards", that is, as it is common use to say, the throat flares out. This effect is related with the second derivative,

$$\frac{d^2 r}{dz^2} > 0 \quad \Rightarrow \quad b'(r) < \frac{b(r)}{r} \,, \tag{5.1.7}$$

which, at the throat, implies $b'(r_0) < 1$. These three conditions: $b(r) \leqslant r$, $b(r_0) = r_0$ and $b'(r) < b(r)/r$, are the so called *flare out conditions* [263, 264, 272–275]. In Fig. 5.1 a picture of a 2π rotation around the z axis of the surface Eq. (5.1.6), for $b = r_0^2/r$ (note that this choice obeys the flare out conditions) can be found.

We will now see how the flare out conditions, together with the Einstein field equations, result on the violation of the classical energy conditions. But, what are these so called energy conditions? The Einstein field equations relate the geometry of spacetime with the distribution of matter. They do not, however, tell us anything about the global nature of the matter fields *per se*. The *classical energy conditions* [272] are a set of identities which are evoked in order to sensibly associate the Einstein equations with our physical reality.

The *null energy condition* (NEC) states that, for every future oriented null vector k^μ, the relation,

$$T_{\mu\nu} k^\mu k^\nu \geqslant 0 \,, \tag{5.1.8}$$

must hold. Considering that the world line of an observer (or family of observers) can be expressed through a timelike vector V^μ, the *weak energy condition* (WEC) implies both the NEC

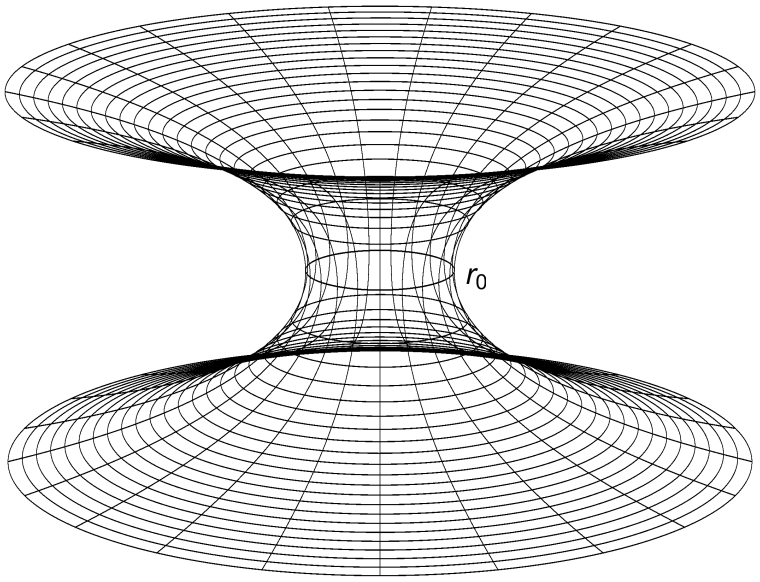

Figure 5.1: Rotation of the surface $z(r)$ given by Eq. (5.1.6) with the choice of the shape function $b = r_0^2/r$.

and, in addition, that the energy density measured by this observer is always non-negative, *i.e.*

$$T_{\mu\nu}V^\mu V^\nu \geqslant 0\,. \tag{5.1.9}$$

The *dominant energy condition* (DEC) implies both the NEC and WEC and, furthermore, imposes that the energy density cannot be found to flow superluminal (propagates in a causal way),

$$F^\mu F_\mu \leqslant 0\,, \tag{5.1.10}$$

where $F^\mu := -T^\mu_\nu V^\nu$. Finally, the *strong energy condition* (SEC) implies the NEC and a relation which takes into account the trace of the energy-momentum tensor, $T := g_{\mu\nu}T^{\mu\nu}$,

$$\left(T_{\mu\nu} - \frac{1}{2}T g_{\mu\nu}\right) V^\mu V^\nu \geqslant 0\,. \tag{5.1.11}$$

Both the weak and strong energy conditions automatically satisfy the null, but the strong does not, in general, imply the weak (for example the case of a scalar field with a positive potential can violate the strong and still verify the weak [287]). The implications then read,

$$\text{DOMINANT} \;\rightarrow\; \text{WEAK} \;\rightarrow\; \text{NULL} \;\leftarrow\; \text{STRONG}. \tag{5.1.12}$$

For an energy-momentum tensor with components described as $T_{\mu\nu} = \text{diag}(\rho, p_1, p_2, p_3)$ (the physical interpretation of the components will be made clear ahead), the conditions are summarised in Tab.5.1.

Table 5.1: Energy conditions for a fluid with $T_{\mu\nu} = \text{diag}(\rho, p_1, p_2, p_3)$.

DOMINANT	$(\forall j\colon\ \rho \geqslant \lvert p_j \rvert) \wedge$ WEAK
WEAK	$(\rho \geqslant 0) \wedge$ NULL
NULL	$\forall j\colon\ \rho + p_j \geqslant 0$
STRONG	$(\rho + \sum_j p_j \geqslant 0) \wedge$ NULL

Note that, through the Einstein equations, one may find the analogous conditions for the geometry sector. This is related with conditions on the congruence of curves [287]. For example, the condition entailing the attractive character of gravity,

$$R_{\mu\nu}V^\mu V^\nu \geqslant 0\,, \tag{5.1.13}$$

for any timelike vector V^μ, with $R_{\mu\nu}$ being the Ricci tensor, is the geometry counterpart of the SEC, Eq. (5.1.11), since we may write the field equations as

$$R_{\mu\nu} = 8\pi G\left(T_{\mu\nu} - \frac{1}{2}T g_{\mu\nu}\right)\,, \tag{5.1.14}$$

which ensure the focussing of timelike geodesics [272, 287]. The geometrical part of the energy conditions are an essential tool to understand the intuitive picture of gravitational phenomena and the Penrose–Hawking singularity theorems. One may have a glimpse of this feature by writing the Raychaudhuri equation (in the absence of shear and vorticity),

$$\dot{\theta} = -\frac{1}{3}\theta^2 - R_{\mu\nu}V^\mu V^\nu\,, \tag{5.1.15}$$

where θ denotes the expansion. The idea now is that, since for $R_{\mu\nu}V^\mu V^\nu \geqslant 0$ the expansion decreases, then two separated observers that only feel gravity will get closer to each other. So, as was stated through the SEC, or more precisely through Eq. (5.1.13), this condition asserts the mere fact that gravity is attractive. The reader is referred to Ref. [288] for a review on

energy conditions, in particular to the Table 1, where all the classical energy conditions are listed, together with their geometrical and perfect fluid counterparts.

Now let us write the Einstein field equations for GR+matter, with action

$$\mathcal{S} = \int \omega_g \frac{R}{16\pi G} + \mathcal{S}_m \left[g_{\mu\nu}, \psi, \nabla\psi \right] , \tag{5.1.16}$$

assuming the wormhole metric Eq. (5.1.1) and an energy-momentum tensor for the matter sector described by an anisotropic distribution of matter:

$$T_{\mu\nu} = (\rho + p) u_\mu u_\nu + p g_{\mu\nu} - (\tau + p) \chi_\mu \chi_\nu \, , \tag{5.1.17}$$

where u_μ is the four velocity, $\chi^\mu = \sqrt{1 - b/r}\delta^\mu_r$ is the unit spacelike vector on the radial direction, ρ denotes the energy density, τ the radial tension (the negative of the radial pressure) measured along the direction of χ^μ, and p is the transversal component of the pressure, orthogonal to χ^μ. Equation (5.1.17) simply yields

$$T^\mu_\nu = \mathrm{diag} \left(-\rho, -\tau, p, p \right) \, . \tag{5.1.18}$$

The field equations are then:

$$\rho = \frac{1}{8\pi G} \frac{b'}{r^2} \, , \tag{5.1.19}$$

$$\tau = \frac{1}{8\pi G} \left[\frac{b}{r^3} - \frac{2}{r} \left(1 - \frac{b}{r} \right) \Phi' \right] \, , \tag{5.1.20}$$

$$p = \frac{1}{8\pi G} \left(1 - \frac{b}{r} \right) \left[\Phi'' + \Phi'^2 - \frac{b'r - b}{2r(r-b)} \left(\Phi' + \frac{1}{r} \right) + \frac{\Phi'}{r} \right] \, . \tag{5.1.21}$$

Now, if we evaluate the quantity $\rho - \tau$ near the throat (as $r \to r_0$), remembering that $b(r_0) = r_0$, we obtain

$$(\rho - \tau)|_{r_0} = \frac{1}{8\pi G} \frac{1}{r^2} \left(b' - \frac{b}{r} \, , \right) \tag{5.1.22}$$

which, from the flare out condition $b' < b/r$, gives $\rho - \tau = \rho + p_r < 0$. This implies that, in order to sustain the wormhole, the matter content needs to violate the null energy condition near the throat. And, because all the other classical energy conditions stand upon the NEC, all the energy conditions are violated on the vicinity of the throat. This expresses the fact that, in order to maintain a wormhole open, an exotic source is required such that the radial tension holding

the throat open is larger than the energy density sourcing its gravitational collapse (closure of the throat).

Here, we will show that a 3-form field can indeed act as the exotic source (violating all the energy conditions) and sustain a wormhole open, while allowing the "ordinary" matter fields threading the wormhole to obey all of the energy conditions. A brief introduction to 3-forms is now presented in the next section.

5.2 3-forms

In formal terms, differential forms are smooth sections[1] of the kth exterior power of the cotangent bundle $T^*\mathcal{M} \xrightarrow{\pi} \mathcal{M}$. When performing calculus on manifolds, these tensor fields have an enormous importance, since their algebraic structure allows us to construct diffeomorphism invariant objects on smooth manifolds, and carry out integration on a coordinate-free fashion. Pioneered by Élie Cartan, they are also the central objects of De Rham cohomology, linking the topological and differentiable structures of manifolds. Since the topological anatomy of a manifold has a strong impact on the solutions for (differentiable) equations defined within it, it is only reasonable to assume that differential forms play a fundamental role in physics, particularly while formulating (gauge) field theories in a form-representative framework. One might regard three-forms simply as rank-3 totally antisymmetric covariant tensors. In such case, one might think of the standard Levi-Civita tensor, $\epsilon_{\alpha\mu\nu}$, defined in the cross product, $(\vec{u} \times \vec{v})_\alpha = \epsilon_{\alpha\mu\nu} u^\mu v^\nu$, as a 3-form.

Relative to a coordinate chart (U, Φ), with $U \subset \mathcal{M}$ and $\Phi = (x_1, ..., x_n)$, we may express locally a k-form, $\mathbf{A} \in \mathbf{\Omega^k}(\mathcal{M})$, over U, through the linear combination $\mathbf{A} = A_{1\,...\,k} dx^1 \wedge \ldots \wedge dx^k$, where the dx^i are the basis for the cotangent space $T^*_p\mathcal{M}$ at each $p \in U$. See Refs. [3–5] for textbooks on differential geometry applied to physics. In this current work, we will focus on a single differentiable[2] 3-form field $\mathbf{A} \in \Omega^3(\mathcal{M})$, in a 4-dimensional spacetime with action

$$\mathcal{S}_A = -\int \omega_g \left[\frac{1}{48} F^{\alpha\beta\gamma\delta} F_{\alpha\beta\gamma\delta} + V(A^{\alpha\beta\gamma} A_{\alpha\beta\gamma}) \right] , \tag{5.2.1}$$

where we have assumed a self interacting potential V, function of the invariant $A^{\alpha\beta\gamma} A_{\alpha\beta\gamma} =: A^2$.

[1] A section α, of a bundle $\mathcal{A} \xrightarrow{\beta} \mathcal{B}$ is a smooth map $\sigma : \mathcal{O} \to \mathcal{A}$, with $\mathcal{O} \subset \mathcal{B}$, such that $\beta \circ \alpha = \mathrm{id}$. See Ref. [3]

[2] By differentiable we simply imply that, for any chart, the coeficients $A_{\alpha\beta\gamma}$ are all $\mathcal{C}^\infty$ relative to the chart basis.

The first kinetic term,

$$-\frac{1}{48}\int \omega_g F^{\alpha\beta\gamma\delta}F_{\alpha\beta\gamma\delta} = -\frac{1}{2}\int \mathbf{F}\wedge\star\mathbf{F}\,, \tag{5.2.2}$$

encompasses the strength tensor $\mathbf{F}=\mathbf{dA}$, which generalises Maxwell's 2-form from classical electromagnetism, it has components $F_{\alpha\beta\gamma\delta}=4\nabla_{[\alpha}A_{\beta\gamma\delta]}$, and is a closed form, $\mathbf{dF}=0$. Because the action Eq. (5.2.1) contains a general potential function, $V(A^2)$, gauge invariance may be broken. It is possible however to restore this symmetry through the introduction of a Stückelberg form [251, 252].

5.3 Model

The total action for our theory minimally coupled to Einstein's gravity, can thus be penned as

$$\mathcal{S}=\frac{1}{16\pi G}\int \omega_g R+\mathcal{S}_m\left[g_{\mu\nu},\psi,\nabla\psi\right]+\mathcal{S}_A\left[g_{\mu\nu},\mathbf{A},\mathbf{F}\right]\,, \tag{5.3.1}$$

where G is Newton's constant, R the curvature scalar and $\mathcal{S}_m$ stands for an anisotropic distribution of matter threading our spactime, with, following Eq. (5.1.18), $T^{(m)}_{\mu\nu}=\mathrm{diag}\left(\rho_m,-\tau_m,p_m,p_m\right)$

To find the dynamics governing this model, we start by varying the action Eq. (5.3.1) with respect to the three-form, and find the following equations of motion:

$$E_{\alpha\beta\gamma}=\nabla_\mu F^{\mu}{}_{\alpha\beta\gamma}-12\frac{\partial V}{\partial(A^2)}A_{\alpha\beta\gamma}=0\,. \tag{5.3.2}$$

The energy-momentum tensor relative to the 3-form reads,

$$\begin{aligned}T^{(A)}_{\mu\nu}&=-2\frac{\delta\mathcal{L}_A}{\delta g^{\mu\nu}}+g_{\mu\nu}\mathcal{L}_A\\&=\frac{1}{6}\left(F\circ F\right)_{\mu\nu}+6\frac{\partial V}{\partial(A^2)}\left(A\circ A\right)_{\mu\nu}+\mathcal{L}_A\,g_{\mu\nu}\,,\end{aligned} \tag{5.3.3}$$

where we have introduced the notation $\left(F\circ F\right)_{\mu\nu}=F_{\mu\alpha\beta\gamma}F_{\nu}{}^{\alpha\beta\gamma}$ and $\mathcal{L}_A$ is the field's Lagrangian density, *i.e.* $\mathcal{S}_A=\int\omega_g\,\mathcal{L}_A$. Kindly note, however, that the equations of motion Eqs. (5.3.2) could equivalently be deduced from the contracted Bianchi identities [289],

$$\nabla_\mu T^{(A)\,\mu}{}_{\nu}=\frac{1}{6}F_{\nu\alpha\beta\gamma}E^{\alpha\beta\gamma}=0\,. \tag{5.3.4}$$

The modified field equations can be computed by varying Eq. (5.3.1) with respect to $g^{\mu\nu}$, leading to

$$\frac{1}{8\pi G}G_{\mu\nu} = T^{(m)}_{\mu\nu} + T^{(A)}_{\mu\nu} =: T^{(\text{eff})}_{\mu\nu}\,, \tag{5.3.5}$$

where it was introduced an effective energy-momentum tensor, $T^{(\text{eff})}_{\mu\nu}$.

At the time of this work, theories employing three-form fields in cosmological models were mostly conducted on FLRW universes, e.g., in models of dark energy [249–251] and of inflation [252–256, 258], where the 3-form is constructed as a function of cosmic time t (at the background level). Here, however, since we are standing upon a static and spherically symmetric model, we are interested on a radial dependence only. Therefore, we may associate the 3-form components with a scalar function, say $\zeta(r)$, solely dependent on the radial coordinate r. Due to the antisymmetric nature of the three-form, once $\zeta(r)$ is known, all of the other components are fully determined.

We will choose an ansatz for the 3-form, through its Hodge dual 1-form (vector) B^δ [252], via the Hodge star operator[3], $\star : \Omega^p(X) \to \Omega^{n-p}(X)$, which maps p-forms into $(n-p)$-forms, through:

$$(\star A)^{\alpha_1\ldots\alpha_{n-p}} = \frac{1}{p!}\frac{1}{\sqrt{-g}}\,\epsilon^{\alpha_1\ldots\alpha_{n-p}\beta_1\ldots\beta_p}A_{\beta_1\ldots\beta_p}, \tag{5.3.6}$$

with A being a $p-$form and ϵ denotes the $n-$dimensional Levi-Civita symbol. For our present study, with $n = 4$ and $p = 3$, Eq. (5.3.6) produces a vector,

$$B^\delta := (\star A)^\delta = \frac{1}{3!}\frac{1}{\sqrt{-g}}\,\epsilon^{\delta\alpha\beta\gamma}A_{\alpha\beta\gamma}\,. \tag{5.3.7}$$

Inverting Eq. (5.3.7), we can express the components of the three-form in terms of its dual

$$A_{\alpha\beta\gamma} = \sqrt{-g}\,\epsilon_{\alpha\beta\gamma\delta}B^\delta\,. \tag{5.3.8}$$

We then choose a convenient parametrization of $\mathbf{B}$, given the line element Eq. (5.1.1), as the radially directed vector with components

$$B^\mu = \zeta(r)\chi^\mu\,, \tag{5.3.9}$$

(remember that $\chi^\mu = \sqrt{1-b/r}\delta^\mu_r$), which depends on a suitable scalar function $\zeta(r)$ afore-

[3]Where $\Omega^p(X)$ being the vector space of p-forms on an n-dimensional smooth manifold X

mentioned. Accordingly, the field equations can be expressed entirely in terms of $\zeta(r)$ which significantly simplifies the analysis. From Eq. (5.3.8), the contraction A^2 is

$$A^2 := A^{\alpha\beta\gamma}A_{\alpha\beta\gamma} = -6B^\mu B_\mu = -6\,\zeta(r)^2\,, \tag{5.3.10}$$

and we can write the kinetic term in the Lagrangian Eq. (5.2.1) as

$$-\frac{1}{48}F^2 = -\frac{1}{2}F_{0123}F^{0123} = \frac{1}{2}(\nabla_\mu B^\mu)^2\,. \tag{5.3.11}$$

For simplicity, let us introduce

$$F^2 := F^{\alpha\beta\gamma\delta}F_{\alpha\beta\gamma\delta} = -6\Upsilon\,, \tag{5.3.12}$$

where Υ is defined for convenience as

$$\Upsilon = 4\left(1-\frac{b}{r}\right)\left[\zeta\left(\Phi' + \frac{2}{r}\right) + \zeta'\right]^2\,. \tag{5.3.13}$$

Υ expresses the kinetic energy of the three-form, and vanishes at the throat, $\Upsilon|_{r_0} = 0$.

Note that by introducing the Hodge dual $\mathbf{B} = \star\mathbf{A}$, one may write the three-form Lagrangian in a vector structure form as [254]:

$$\begin{aligned}\mathcal{L}_A &= -\frac{1}{48}F^2 - V(A^2)\\ &= \frac{1}{2}\left(\nabla_\mu B^\mu\right)^2 - V(B^2)\,,\end{aligned} \tag{5.3.14}$$

explicitly showing how this theory might be recast into a vector-tensor theory at the background level (see appendix A of Ref. [254]).

The components of the gravitational field equations Eq. (5.3.5) are (setting $8\pi G = 1$ for simplicity):

$$\rho_{\rm eff} = \rho_m + \rho_{\rm A} = \frac{b'}{r^2}\,, \tag{5.3.15}$$

$$\tau_{\rm eff} = \tau_m + \tau_{\rm A} = \frac{b}{r^3} - \frac{2}{r}\left(1-\frac{b}{r}\right)\Phi'\,, \tag{5.3.16}$$

$$p_{\rm eff} = p_m + p_{\rm A} = \left(1-\frac{b}{r}\right)\left[\Phi'' + \Phi'^2 - \frac{b'r-b}{2r(r-b)}\left(\Phi' + \frac{1}{r}\right) + \frac{\Phi'}{r}\right]\,, \tag{5.3.17}$$

where the energy density, radial tension and pressure of the three-form field are, respectively,

$$T^{(\mathrm{A})}{}_{t}^{t} = -\rho_{\mathrm{A}} = -\frac{1}{8}\Upsilon - V + \zeta V_{\zeta}\,, \tag{5.3.18}$$

$$T^{(\mathrm{A})}{}_{r}^{r} = -\tau_{\mathrm{A}} = -\frac{1}{8}\Upsilon - V\,, \tag{5.3.19}$$

$$T^{(\mathrm{A})}{}_{\theta}^{\theta} = p_{\mathrm{A}} = T^{(\mathrm{A})}{}_{\phi}^{\phi} = -\frac{1}{8}\Upsilon - V + \zeta V_{\zeta}\,, \tag{5.3.20}$$

with $V_{\zeta} = \partial V/\partial\zeta$. Note that in the absence of a potential in the Lagrangian Eq. (5.2.1), the three-form source plays the role of a cosmological constant with an equation of state $w = p_{\mathrm{A}}/\rho_{\mathrm{A}} = -1$ [250, 251]. This was used by Hawking and Turok [260] to explain the cosmological constant problem.

Diffeomorphism invariance renders the field equations covariant. The Bianchi identities yield the following continuity equation, through $\nabla_{\mu}T^{(\mathrm{eff})}{}_{\nu}^{\mu} = 0$,

$$\tau'_{\mathrm{eff}} + \frac{2}{r}\left(\tau_{\mathrm{eff}} + p_{\mathrm{eff}}\right) + \Phi'\left(\tau_{\mathrm{eff}} - \rho_{\mathrm{eff}}\right) = 0\,, \tag{5.3.21}$$

which can be equally deduced by taking the radial derivative of Eq. (5.3.16) and using Eqs. (5.3.15) and (5.3.17).

The equations of motion for the 3-form, Eq. (5.3.2) can now be written as a single differential equation for the scalar function ζ, *i.e.*,

$$\begin{aligned}\zeta''\left(\frac{b}{r} - 1\right) + \frac{\zeta'}{2r}\left[3\,\frac{b}{r} - 4 + b' + 2\Phi'\,r\left(\frac{b}{r} - 1\right)\right]\\ \frac{\zeta}{2r^2}\left[r\,\Phi'\left(b' - \frac{b}{r}\right) + 4 + 2\,b' + 2\,r^2\,\Phi''\left(\frac{b}{r} - 1\right) - 6\,\frac{b}{r}\right] + V_{\zeta} = 0\,.\end{aligned} \tag{5.3.22}$$

The main objective of this work is to show that it is possible to attain wormhole solutions in which the 3-form is the responsible source for holding the throat of the wormhole open, violating the NEC and WEC. These solutions also show that it is possible for the ordinary matter fields threading the wormhole to obey the energy conditions throughout the spacetime continuum. Therefore, we will find solutions where matter obeys the conditions

$$\rho_m \geqslant 0\,, \quad \rho_m - \tau_m \geqslant 0 \quad \text{and} \quad \rho_m + p_m \geqslant 0\,, \tag{5.3.23}$$

near the throat.

5.4 Solutions

Note that our gravitational setting has a set of four independent equations, Eqs. (5.3.15)-(5.3.17) and (5.3.22), for seven unknown variables, *i.e.* Φ, b, ρ_m, τ_m, p_m, ζ and V. Thus, we have up to three assumptions to make. Similarly to previous works [278, 284, 290], we will proceed by specifying the redshift and shape functions, and assume a specific ansatz for ζ or for the potential, and then solve the equations.

5.4.1 Case I

Following Ref. [284], let us write the metric functions as:

$$b(r) = r_0 \left(\frac{r_0}{r}\right)^{\beta}, \qquad \Phi(r) = \Phi_0 \left(\frac{r_0}{r}\right)^{\alpha}, \tag{5.4.1}$$

and the function ζ,

$$\zeta(r) = \zeta_0 \left(\frac{r_0}{r}\right)^{\gamma}, \tag{5.4.2}$$

with $\beta > -1$, $\alpha > 0$ and $\gamma > 0$. Note that Eq. (5.4.2) assumes the value $\zeta = \zeta_0$ at the throat of the wormhole, and tends to zero at spatial infinity.

Inserting (5.4.1) and (5.4.2) into Eq. (5.3.22), the latter becomes a first order differential equation for the potential $V(r)$, which holds the following analytical solution,

$$\begin{aligned} V = \frac{\zeta_0^2 \gamma}{2r^2} \Bigg\{ \left[1 - \left(\frac{r_0}{r}\right)^{\beta+1}\right](\gamma - 2) + \Phi_0\, \alpha \left(\frac{r_0}{r}\right)^{\alpha} \Bigg[1 + \frac{\alpha}{\alpha + 2\,(1+\gamma)} \\ - \left(\frac{r_0}{r}\right)^{\beta+1} \frac{3 + \beta + 2\,(\alpha+\gamma)}{3 + \beta + \alpha + 2\gamma}\Bigg]\Bigg\} + C\,, \end{aligned} \tag{5.4.3}$$

where C is a constant.

The energy densities (left panel) together with the NEC profile (right panel) are depicted in Fig. 5.2, for a particular solution, with the potential given by Eq. (5.4.3). The ordinary matter component does not violate the NEC nor the WEC. This implies that the responsible for sustaining the wormhole is the three-form field, where all the exoticity is confined within it, and the matter fields inhabit the wormhole while satisfying the classical energy conditions. This shows the main virtue of this model.

The case of vanishing redshift function, $\Phi_0 = 0$ and $\gamma = 2$, is an interesting case since it gives a constant potential $V = C$, which is readily found from Eq. (5.4.3). In such case, although

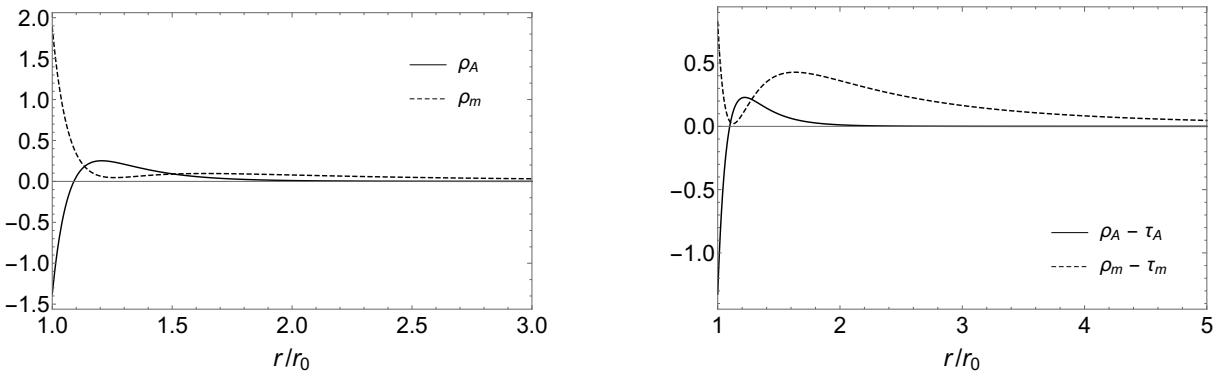

Figure 5.2: Energy densities (left panel) and NEC profile (right panel) for the form field (solid) and for the matter sources (dashed), regarding the specific choice given by Eqs. (5.4.1)-(5.4.2) with $\beta = -1/2$, $\Phi_0 = -6.3$, $\alpha = 1$, $\zeta_0 = 1$, $\gamma = 3$ and $C = 0$.

ζ depends on the radial coordinate, its kinetic term given by Eq. (5.3.13) vanishes, thus the energy density of the form field is constant, given by $\rho_{\rm A} = V = C$. Curiosusly, this implies that the field mimics a cosmological constant [291]. This feature is not present with classical non-constant scalar fields. This is ascribed to the fact that the kinetic term of the three-form, Eq. (5.3.13), depends on both ζ' and ζ itself (in contrast with canonical scalar fields where the kinetic term depends solely on the field derivative, and not explicitly on the field itself). Thus, the terms ζ' and ζ can mutually cancel. For $C \geqslant 0$ the 3-form field does not violate the NEC nor the WEC, however the matter fields in this case are exotic (violate the energy conditions). Nonetheless, this expresses the fact that it is possible for a three-form to mimic a cosmological constant without violating the energy conditions.

5.4.2 Case II

Let us now turn our attention to the metric functions given by (5.4.1) but instead with an ansatz for the potential V with a quadratic form,

$$V(\zeta) = \zeta^2 + C\,. \tag{5.4.4}$$

In this case, Eq. (5.3.22) becomes a second order differential equation for ζ where analytical solutions were not found, therefore, numerical methods are applied. The results are reported in Fig. 5.3, for the case $b = r_0^2/r$ (left panel) and $b = \sqrt{r_0 r}$ (right panel), with different choices for the parameters. It is possible to recreate a similar behaviour, where the matter fields do not violate classical energy conditions and it is the 3-form to sustain the throat of the wormhole open.

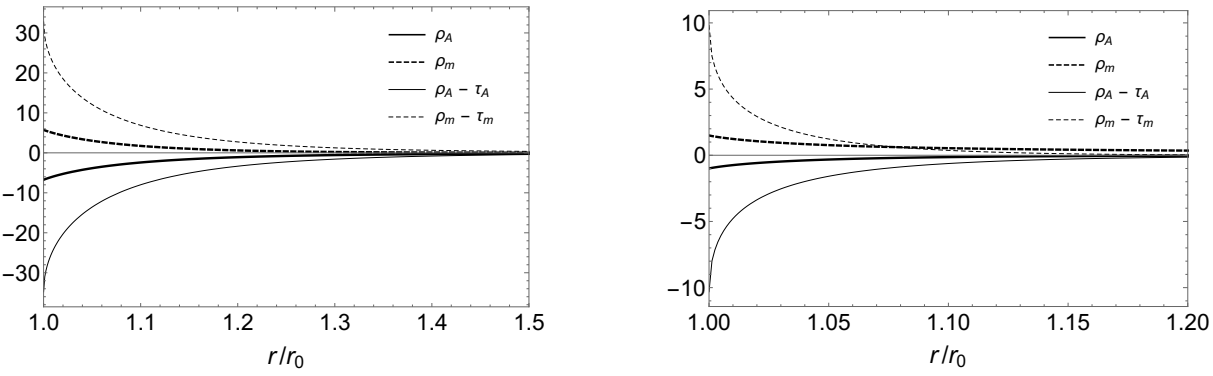

Figure 5.3: Energy densities (thick) and NEC profiles (thin) for the form field (solid) and the matter sources (dashed) for the choices in Eqs. (5.4.1)-(5.4.2) and Eq. (5.4.4) and . Left panel: $\beta = 1$, $\Phi_0 = -1$, $\alpha = 1$ and $C = -0.1$. Right panel: $\beta = -1/2$, $\Phi_0 = -2$, $\alpha = 1$ and $C = 0$.

The behaviour of the ζ functions, solutions to the numerical integration of Eq. (5.3.22) with the potential given by Eq. (5.4.4), are shown in Fig. 5.4. The field smoothly decays, vanishing as $r \to \infty$, and takes non-zero values near the throat of the wormhole. In the vicinity of r_0, the choice $b = \sqrt{r_0 r}$, ζ presents a faster decrease, thus clustering the energy density of the three form closer to the throat.

An interesting solution is the one of zero tidal force, i.e., $\Phi(r) = 0$. Assuming that the wormhole follows the shape function given by $b(r) = r_0^2/r$, and taking a constant potential $V = V_0$, Eq. (5.3.22) becomes

$$\zeta'' r^2 \left[\left(\frac{r}{r_0}\right)^2 - 1\right] + \zeta' r \left[2\left(\frac{r}{r_0}\right)^2 - 1\right] - 2\zeta \left[\left(\frac{r}{r_0}\right)^2 - 2\right] = 0\,, \tag{5.4.5}$$

which indeed bears the following analytical solution

$$\zeta(r) = \frac{C_1}{r^2} + C_2 \sqrt{\left(\frac{r}{r_0}\right)^2 - 1}\left[1 + 2\left(\frac{r_0}{r}\right)^2\right]\,, \tag{5.4.6}$$

C_1 and C_2 being constants. On such setting, the energy density of the 3-form remains constant,

$$\rho_{\rm A} = \frac{9}{2}\left(\frac{C_2}{r_0}\right)^2 + V_0\,. \tag{5.4.7}$$

Note that Eq. (5.4.7) has the same form of a specific solution found in (5.4.3), when setting $C_2 = 0$. However, in (5.4.3), with a specific assumption regarding the form of ζ, the energy density depended solely on V_0. Here it attains a general form for the field profile, where in the absence of a potential, $V_0 = 0$, the 3-form behaves as a cosmological constant when $C_2 \neq 0$.

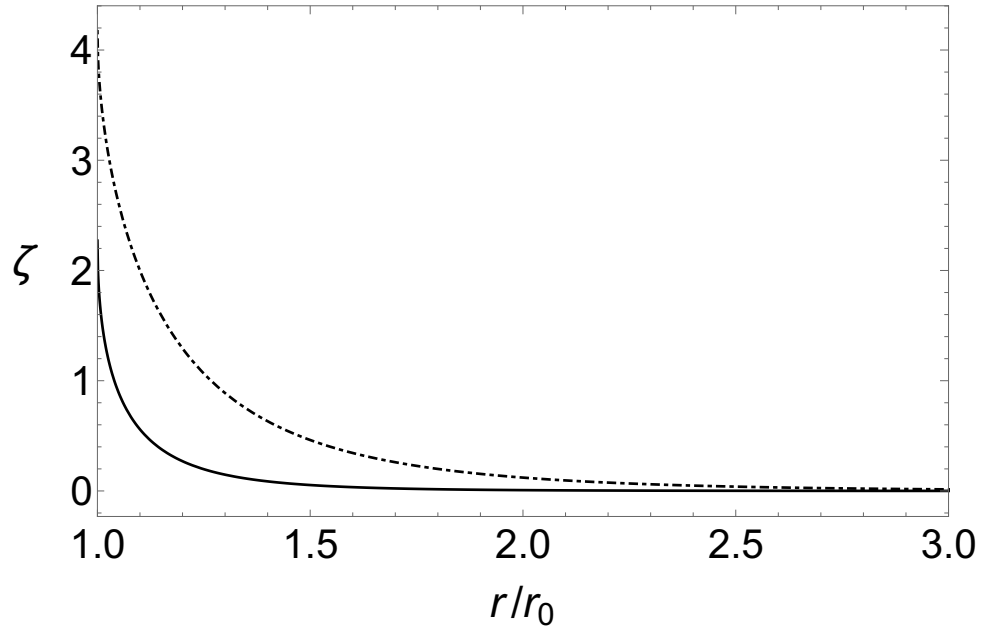

Figure 5.4: Solutions for $\zeta(r)$, regarding the two solutions of Eqs. (5.4.1)-(5.4.2) and Eq. (5.4.4) for: $\beta = -1/2$, $\Phi_0 = -2$, $\alpha = 1$ and $C = 0$ (solid) and $\beta = 1$, $\Phi_0 = -1$, $\alpha = 1$ and $C = -0.1$ (dot dashed).

Nonetheless, we impose the condition $C_2 = 0$ so that $\zeta \to 0$ as $r \to \infty$.

In wormhole physics, one aspect of great importance is the one with regard to the stability of these objects. For future work, it would be interesting to conduct a similar analysis as considered in Refs. [292, 293] however employing 3-form fields.

Another possibility for future research is to consider wormhole geometries evolving with time: searching for background solutions conformally related to the respective static line element [294–297]. These are of particular interest since it was already shown that, on such framework, these time evolving geometries exhibit brief intervals of time where the weak energy condition is satisfied.

Chapter 6

Bouncing cosmology in modified Gauss-Bonnet gravity

"I wanted to run after him, but remembered that it is ridiculous to run after one's wife's lover in one's socks; and I did not wish to be ridiculous but terrible."

From *The Kreutzer Sonata*,

by Leo Tolstoy

This chapter is based on Ref. [298].

Let us now turn our attention to the very early Universe. One of the problems of standard general relativity is the presence of a singularity ($\rho \to \infty$ as $a \to 0$) at the initial time. GR alone cannot accurately describe such enormous energy scales, thus no acceptable answer exists hitherto for such phenomenon. In such high energy regimes, it is expected for quantum effects to have a significant role in spacetime physics. However, a satisfying theory merging quantum mechanics and general relativity is still to be constructed, although efforts in this direction have been made [299].

On the other hand, an effective description of Loop Quantum Cosmology (LQC) [300, 301] makes possible for one to write the dynamics of a given cosmology in a classical fashion but incorporating leading order quantum corrections. The predictions of this theory overlap with GR at low energies while at high density regimes, where quantum effects are expected to play a role, they significantly depart from the classical theory [302–304]. In the light of LQC, the Big Bang singularity in replaced by a quantum bounce [305–311]. To help us understand this, let us commence by writing the Friedmann equation emerging from this effective description of Loop

Quantum Cosmology [312, 313]:

$$H^2 = \frac{\kappa^2}{3}\rho\left(1 - \frac{\rho}{\rho_c}\right), \tag{6.0.1}$$

where here $\rho_c = \sqrt{3}/(32\pi^2\gamma^3)$ is the critical energy density at the bounce, with γ being the Barbero–Immirzi parameter. From Eq. (6.0.1), it is evident that the Universe undergoes a cosmic bounce when $\rho = \rho_c$.

Here, we deal with bouncing scenarios within modified gravity models [314, 315]. Note that the gravitational action for such theories usually contain higher order derivatives, thus propagate extra degrees of freedom. The focus of this work are modified Gauss–Bonnet $f(R, \mathcal{G})$ gravity models, where $\mathcal{G}$ is the Gauss–Bonnet term and R the curvature scalar. It is to be noted that these models can be equivalently written as a scalar tensor theory with two extra dynamical scalar fields [316] (in contrast with $f(R)$ where only one scalar field is required).

Among the literature, researchers have framed Gauss-Bonnet gravity within several cosmological scenarios, such as primordial inflation [317, 318] and dark energy [317, 319, 320]. Lagrangians containing terms of the form $\mathcal{G}^\alpha/R^\beta$ have been discussed [321] in the context of future singularities and some proposals to avoid these. Scalar and tensor perturbations in $f(R, \mathcal{G})$ and their stability were studied in Refs. [316, 322, 323]. It was shown in Ref. [324] that a double inflationary setting naturally arise on such modified gravity framework.

In this chapter, we will see how it is possible to avoid the presence of extra degrees of freedom, by means of the so-called order reduction technique [325–327], first applied to Gravitation in 1985. This technique consists of expressing the geometrical objects in terms of the matter fields at their lowest order on the perturbation expansion. Thus, the model is framed within an effective field theory approach where the field equations contain only up to second order derivatives. By effective field theory, it is meant that we treat our theory not as fundamental but to be valid only at some energy regime. It might however come from a low energy limit of a more fundamental theory.

It is possible to summarize this work by asking the following question: Can the Friedmann equation emerging from an effective description of LQC, Eq. (6.0.1), be derived from an effective modified gravity theory? If the answer is affirmative, then what is the most general form of the Lagrangian under these conditions? Previous works have proven this to be possible in $f(R)$ [328] and $f(\mathcal{G})$ [329] gravity. Here we resort to the same approach but in the context of $f(R, \mathcal{G})$ models. It is to be noted, that different methods than the one employed in this work have

been used to reproduce this desired Friedmann equation for many modified gravity theories. As an example, in Ref. [330], the specific Lagrangian for $f(R)$ was numerically reconstructed on *a Palatini* approach, by directly imposing that the Friedmann equation should match the one from LQC. In Ref. [331], an Hamiltonian analysis was applied to reconstruct the covariant action for a specific class of scalar tensor theories, called mimetic gravity, for homogeneous and isotropic backgrounds.

6.1 Model

On a 4-dimensional spacetime, the action for modified Gauss-Bonnet gravity can be written as

$$\mathcal{S} = \frac{1}{2\kappa^2}\int \omega_g \big[R + f(R,\mathcal{G})\big] + \mathcal{S}_m(g_{\mu\nu},\psi,\nabla\psi)\,, \tag{6.1.1}$$

where $\mathcal{S}_m$ portray the matter action and

$$\mathcal{G} = R^2 - 4R^{\mu\nu}R_{\mu\nu} + R^{\mu\nu\alpha\beta}R_{\mu\nu\alpha\beta}\,, \tag{6.1.2}$$

is the Gauss-Bonnet term, a topological invariant whose presence in the action is only non-trivial in more than 4 spacetime dimensions (see Section 8.4 of Ref. [332]).

By varying the action with respect to the metric field, one finds the following modified field equations

$$\begin{aligned} R_{\mu\nu} - \frac{1}{2}g_{\mu\nu}R - \frac{1}{2}g_{\mu\nu}f + f_{,R}R_{\mu\nu} + (g_{\mu\nu}\,\Box - \nabla_\mu\nabla_\nu)\,f_{,R} + f_{,\mathcal{G}}\,\big(2RR_{\mu\nu} - 4R_\mu{}^\alpha R_{\nu\alpha} \\ +2R_{\mu\alpha\beta\gamma}R_\nu{}^{\alpha\beta\gamma} - 4R_{\mu\alpha\nu\beta}R^{\alpha\beta}\big) + \big(2\,g_{\mu\nu}R\,\Box - 2R\,\nabla_\mu\nabla_\nu + 4R_\mu{}^\alpha\,\nabla_\alpha\nabla_\nu \\ +4R_\nu{}^\alpha\,\nabla_\alpha\nabla_\mu - 4g_{\mu\nu}R^{\alpha\beta}\,\nabla_\alpha\nabla_\beta - 4R_{\mu\nu}\,\Box + 4R_\mu{}^\alpha{}_\nu{}^\beta\,\nabla_\alpha\nabla_\beta\big)\,f_{,\mathcal{G}} = \kappa^2 T_{\mu\nu}\,, \end{aligned} \tag{6.1.3}$$

where the notation $f_{,R} := \partial f/\partial R$, $f_{,\mathcal{G}} := \partial f/\partial\mathcal{G}$ has been defined, and

$$T_{\mu\nu} := -\frac{2}{\sqrt{-g}}\frac{\delta\mathcal{S}_m}{\delta g^{\mu\nu}}\,. \tag{6.1.4}$$

The Riemann tensor can be decomposed into a traceless, semi-traceless and scalar parts,

respectively, as (see Chapter 3 of Ref. [333]):

$$R_{\mu\nu\alpha\beta} = \ C_{\mu\nu\alpha\beta} + \frac{1}{2}\left(g_{\mu\alpha}R_{\beta\nu} + g_{\nu\beta}R_{\alpha\mu} - g_{\mu\beta}R_{\alpha\nu} - g_{\nu\alpha}R_{\beta\mu}\right) + \frac{1}{6}\left(g_{\mu\beta}g_{\alpha\nu} - g_{\mu\alpha}g_{\beta\nu}\right)R\,, \tag{6.1.5}$$

with $C_{\mu\nu\alpha\beta}$ being the Weyl tensor components. At this point, we assume that the Weyl tensor vanishes, *i.e.* $C_{\mu\nu\alpha\beta} = 0$. This assumption holds by requiring that our spacetime is conformally flat (see Section 6.13 of Ref. [334]), *i.e.*, if every point in the manifold contains a neighbourhood which can be mapped to a flat space by means of a conformal transformation. This condition is true on a Friedmann-Lemaître-Robertson-Walker background, in which our study will be based. Therefore, the Riemann tensor components simplify to

$$R_{\mu\nu\alpha\beta} = \ \frac{1}{2}\left(g_{\mu\alpha}R_{\beta\nu} + g_{\nu\beta}R_{\alpha\mu} - g_{\mu\beta}R_{\alpha\nu} - g_{\nu\alpha}R_{\beta\mu}\right) + \frac{1}{6}\left(g_{\mu\beta}g_{\alpha\nu} - g_{\mu\alpha}g_{\beta\nu}\right)R\,, \tag{6.1.6}$$

and the Gauss–Bonnet invariant becomes,

$$\mathcal{G} = \frac{2}{3}R^2 - 2R_{\mu\nu}R^{\mu\nu}\,. \tag{6.1.7}$$

It is possible to avoid the spurious degrees of freedom arising on such theories by employing the order reduction technique [325–327]. Following the strategy described in Refs. [328, 329], the function $f(R,\mathcal{G})$ is then parametrized as

$$f(R,\mathcal{G}) = \epsilon\varphi(R,\mathcal{G})\,, \tag{6.1.8}$$

where the dimensionless parameter ϵ controls the deviations from general relativity. The solutions are then perturbatively close to GR, namely $\epsilon\varphi \ll R$. This procedure is germane with the fact that we wish to enclosure $f(R,\mathcal{G})$ gravity within an effective field theory approach. Therefore, only the lowest order terms in ϵ will be considered, so that the higher order field equations contain up to second order derivatives of the metric, thus avoiding the propagation of any additional degrees of freedom.

The order reduction technique simply consists of replacing all the $\mathcal{O}(\epsilon)$ terms in the field equations by their lowest order ($\epsilon = 0$) counterparts. For this reason, we express the geometrical quantities R, $R_{\mu\nu}$, $R_{\mu\nu\alpha\beta}$, and $\mathcal{G}$, in terms of the matter fields, at the lowest order in the perturbative expansion. The expressions for the order reduced curvature scalar and Ricci tensor

can be found by evaluating Eq. (6.1.3) and its trace, with f as defined in Eq. (6.1.8), for $\epsilon = 0$, resulting in:

$$R^T = -\kappa^2 T\,, \tag{6.1.9}$$

$$R^T_{\mu\nu} = \kappa^2 T_{\mu\nu} - \frac{\kappa^2}{2} g_{\mu\nu} T\,, \tag{6.1.10}$$

where a T superscript simply denotes the order reduced quantities. The Riemann tensor in Eq. (6.1.6), and the Gauss–Bonnet term in Eq. (6.1.7) can now be expressed at the lowest order as,

$$R^T_{\mu\nu\alpha\beta} = \; -\frac{\kappa^2}{2}\left(g_{\mu\beta}T_{\alpha\nu} + g_{\nu\alpha}T_{\beta\mu} - g_{\mu\alpha}T_{\beta\nu} - g_{\nu\beta}T_{\alpha\mu}\right) - \frac{1}{3}\left(g_{\mu\alpha}g_{\nu\beta} - g_{\mu\beta}g_{\alpha\nu}\right)\kappa^2 T\,, \tag{6.1.11}$$

$$\mathcal{G}^T = \; \frac{2}{3}\kappa^4 T^2 - 2\kappa^4 T_{\mu\nu}T^{\mu\nu}\,. \tag{6.1.12}$$

We may now replace each order-ϵ term by its corresponding order reduced analogue in the field equations, arriving at

$$\begin{aligned} R_{\mu\nu} - \frac{1}{2}g_{\mu\nu}R + \epsilon\Bigg[&-\frac{1}{2}g_{\mu\nu}\varphi^T + \varphi^T_{,R}R^T_{\mu\nu} + \left(g_{\mu\nu}\,\Box - \nabla_\mu\nabla_\nu\right)\varphi^T_{,R} + \varphi^T_{,\mathcal{G}}\left(2R^T R^T_{\mu\nu} - 4R^T_{\mu}{}^{\alpha}R^T_{\nu\alpha}\right. \\ &+2R^T_{\mu\alpha\beta\gamma}R^{T\;\alpha\beta\gamma}_{\nu} - 4R^T_{\mu\alpha\nu\beta}R^{T\;\alpha\beta}\Big) + \Big(2\,g_{\mu\nu}R^T\,\Box - 2R^T\,\nabla_\mu\nabla_\nu + 4R^{T\;\alpha}_{\mu}\,\nabla_\alpha\nabla_\nu + 4R^{T\;\alpha}_{\nu}\,\nabla_\alpha\nabla_\mu \\ &\left.-4g_{\mu\nu}R^{T\;\alpha\beta}\,\nabla_\alpha\nabla_\beta - 4R^T_{\mu\nu}\,\Box + 4R^{T\alpha}_{\mu\;\;\nu\;\;\beta}\,\nabla_\alpha\nabla_\beta\Big)\,\varphi_{,\mathcal{G}}\right] = \kappa^2 T_{\mu\nu}\,, \end{aligned} \tag{6.1.13}$$

in which the derivatives are taken with respect to the lowest order quantities, *i.e.*, $\varphi^T_{,R} = \partial\varphi^T/\partial R^T$, with $\varphi^T = \varphi^T(R^T, \mathcal{G}^T)$.

Note that Eq. (6.1.13) is simply GR plus order-ϵ terms. The latter will only be significant near the bounce. The requirement $\epsilon\varphi \ll R$ is, indeed, a necessary condition for the whole procedure to be well posed [328, 329]. This guarantees that the corrective terms are dealt with within an effective field theory approach, where $R \ll \rho_c \sim l_p^{-2}$ (l_p being the Planck scale). This will be verified *a posteriori*, by the solutions found.

We now assume a flat FLRW geometry, given by Eq. (2.2.2), and a perfect fluid form for the energy-momentum tensor of matter,

$$T_{\mu\nu} = (\rho + p)\,u_\mu u_\nu + p\,g_{\mu\nu}\,. \tag{6.1.14}$$

In addition, we consider a barotropic equation of state for the pressure, *i.e.*,

$$p = w\rho\,, \tag{6.1.15}$$

with $w \in [-1, 1]$ being a constant. Naturally, the standard continuity equation,

$$\dot{\rho} = -3H\,(1+w)\,\rho\,, \tag{6.1.16}$$

holds.

The order reduced scalars R^T and $\mathcal{G}^T$, at the background level, can now be written as:

$$R^T = (1-3w)\,\kappa^2\rho\,, \tag{6.1.17}$$

$$\mathcal{G}^T = -\frac{4}{3}\,(1+3w)\,\kappa^4\rho^2\,. \tag{6.1.18}$$

Consistently, we will search for solutions where both R and $\mathcal{G}$ do not vanish, since it is our aim to formulate an $f(R,\mathcal{G})$ gravity model. Nonetheless, the general solutions will be analysed in the limit where both these objects are zero. Accordingly, henceforth we will assume $w \neq \pm 1/3$. Relativistic fluids, such as radiation, are then automatically excluded from our study.

From the 0-0 component of the reduced field equations in Eq. (6.1.13), we compute the modified Friedmann equation:

$$6H^2+2\kappa^2\rho+\epsilon\left[\varphi^T+6H\dot{\varphi}^T_R+\kappa^2\rho(1+3w)\varphi^T_R+8H\kappa^2\rho\,\dot{\varphi}^T_{\mathcal{G}}+\frac{4}{3}\kappa^4\rho^2(1+3w)\,\varphi^T_{\mathcal{G}}\right]=0\,. \tag{6.1.19}$$

Using the chain rule, alongside with Eq. (6.1.16) and Eqs. (6.1.17)-(6.1.18), we may express the time derivative of φ^T in terms of derivatives with respect to $\mathcal{G}^T$ and R^T:

$$\dot{\varphi}^T = \frac{\partial\varphi^T}{\partial R^T}\frac{\partial R^T}{\partial\rho}\dot{\rho}+\frac{\partial\varphi^T}{\partial\mathcal{G}^T}\frac{\partial\mathcal{G}^T}{\partial\rho}\dot{\rho} = -3H\kappa^2\rho(1+w)(1-3w)\varphi^T_R+8H\kappa^4\rho^2(1+3w)(1+w)\varphi^T_{\mathcal{G}}\,. \tag{6.1.20}$$

Thus, the Friedmann equation, Eq. (6.1.19), turns into

$$H^2 = \frac{\kappa^2\rho}{3}-\frac{\epsilon}{3}\left[\frac{1}{2}\varphi^T+\frac{2}{3}(1+3w)\kappa^4\rho^2\varphi^T_{\mathcal{G}}+\frac{32}{3}(1+3w)(1+w)\kappa^8\rho^4\varphi^T_{\mathcal{G}\mathcal{G}}+\frac{1}{2}(1+3w)\kappa^2\rho\varphi^T_R\right.$$
$$\left.-3(1-3w)(1+w)\kappa^4\rho^2\varphi^T_{RR}+4(1+9w)(1+w)\kappa^6\rho^3\varphi^T_{R\mathcal{G}}\right]. \tag{6.1.21}$$

6.2 Solutions

Here, we will find analytical solutions for the $f(R,\mathcal{G})$ function, such that the effective Friedmann equation of a bouncing Universe is recovered, that is,

$$H^2 = \frac{\kappa^2}{3}\rho\left(1-\frac{\rho}{\rho_c}\right)\,. \tag{6.2.1}$$

Since the characteristic scale of our study is given by ρ_c, for dimensionality reasons we define the following dimensionless quantities[329]:

$$\bar{R}^T = \frac{R^T}{\rho_c}\,,\;\; \bar{\mathcal{G}}^T = \frac{\mathcal{G}^T}{\rho_c^2}\,,\;\; \bar{\rho} = \frac{\rho}{\rho_c} \;\text{ and }\; \bar{\varphi}^T = \frac{\varphi^T}{\rho_c}\,, \tag{6.2.2}$$

so that we can directly impose that the right-hand side of Eq. (6.1.21) matches the one we wish to obtain, that is, Eq. (6.2.1). This results on a differential equation for $\bar{\varphi}^T(\bar{R}^T,\bar{\mathcal{G}}^T)$, expressed in terms of the dimensionless variables:

$$\begin{aligned}&\frac{1}{2}\bar{\varphi}^T + \frac{2}{3}(1+3w)\kappa^4\bar{\rho}^2\bar{\varphi}^T_{\bar{\mathcal{G}}} + \frac{32}{3}(1+3w)(1+w)\kappa^8\bar{\rho}^4\bar{\varphi}^T_{\bar{\mathcal{G}}\bar{\mathcal{G}}} + \frac{1}{2}(1+3w)\kappa^2\bar{\rho}\bar{\varphi}^T_{\bar{R}}\\ &-3(1-3w)(1+w)\kappa^4\bar{\rho}^2\bar{\varphi}^T_{\bar{R}\bar{R}} + 4(1+9w)(1+w)\kappa^6\bar{\rho}^3\bar{\varphi}^T_{\bar{R}\bar{\mathcal{G}}} = \frac{\kappa^2\bar{\rho}^2}{\epsilon}\,,\end{aligned} \tag{6.2.3}$$

which is a non-linear second-order partial differential equation for a two variable function. We will then proceed in the following manner: by assuming a specific ansatz for $\bar{\varphi}^T$ which satisfies Eq. (6.2.3), we investigate under which conditions is the Lagrangian able to reproduce a bouncing Universe. Note that, while in previous works regarding $f(R)$ [328] and $f(\mathcal{G})$ [329] gravity, the EoS parameter w was kept at a fixed value, here we allow it to be arbitrary. Henceforth we omit the superscript T for convenience.

We begin by assuming the simplest form for $\bar{\varphi}$, that is, a power law, to be an ansatz for the differential equation Eq. (6.2.3):

$$\bar{\varphi}(\bar{R},\bar{\mathcal{G}}) = c_1\,|\bar{\mathcal{G}}|^{\alpha}|\bar{R}|^{\beta}\,, \tag{6.2.4}$$

with α, β and c_1 being real constants. Note that from Eqs. (6.1.17) and (6.1.18), depending on the value of w, the scalars R and $\mathcal{G}$ may become negative. Hence, without loss of generality, and to avoid the emergence of complex solutions, we write the ansatz in terms of the modulus of the scalars, with powers $\{\alpha,\beta\}\in\mathbb{R}$ (this, however, becomes superfluous for $\{\alpha,\beta\}\in\mathbb{Z}$).

It is important to state that this specific power law Lagrangian has already been considered in the literature in the context of primordial inflation [324], dark energy [321, 335] and stability of cosmological solutions [336]. The specific choice $(\alpha, \beta) = (0, 2)$ has been shown [328] to successfully reproduce a bounce within an $f(R)$ gravity setting under the same order reduction technique.

Inserting Eq. (6.2.4) on the left-hand side of Eq. (6.2.3), and using Eqs. (6.1.17)-(6.1.18), one finds

$$\bar{\rho}^{2\alpha+\beta} \propto \bar{\rho}^2 \,. \tag{6.2.5}$$

In order for the above relation to hold, we need $2\alpha + \beta = 2$, or equivalently, $\beta = 2 - 2\alpha$. The constant c_1 can be found from the constraint that Eq. (6.2.3) must be valid with the ansatz in Eq. (6.2.4):

$$c_1 = \frac{2}{9}\frac{3^\alpha}{4^\alpha}\frac{1}{(1-\alpha)\epsilon\kappa^2}\frac{|1-3w|^{2\alpha}|1+3w|^{-\alpha}}{(w+1)(3w-1)} \,. \tag{6.2.6}$$

Therefore, we attain a family of solutions as,

$$\mathcal{L}_g = R + \frac{C_1}{\rho_c}\,|\mathcal{G}|^\alpha |R|^{2-2\alpha} \,, \tag{6.2.7}$$

with $C_1 = \epsilon\, c_1$.

Note that the cases $\alpha = 1$ or $w = -1$ are imediatly excluded, as these do not yield a cosmological bounce. With $\alpha = 0$, the solution found for $f(R)$ gravity (with $w = 1$) in Ref. [328] is generalized to arbitrary values of w:

$$\mathcal{L}_g = R + \frac{2}{9(w+1)(3w-1)\kappa^2\rho_c}R^2 \,. \tag{6.2.8}$$

Recall that the values $w = \pm 1/3$ were ruled out *a priori*, which renders Eq. (6.2.8) non-singular. The particular case $w = 1/3$ yields $R^T = 0$, from which we demand that $\alpha = 1$ such that $\varphi \neq 0$. However, this choice does not feature a cosmological bounce since it leaves $\varphi \propto G$, a mere topological term. On the other hand, $w = -1/3$ ($\mathcal{G}^T = 0$) is, indeed, valid provided that $\alpha = 0$ and, according to Eq. (6.2.8), the correction to the Friedmann equation stems from an R^2 term.

By taking the ansatz $\bar{\varphi}(\bar{R}, \bar{\mathcal{G}}) = \bar{R}\Psi(\bar{\mathcal{G}})$, and solving Eq. (6.2.3) for Ψ, it is possible to verify that we obtain a solution where the bounce is induced by Eq. (6.2.7) with $\alpha = 1/2$.

We now wish to construct an ansatz which encapsulates the solution found in the framework

of $f(\mathcal{G})$ gravity [329]. This suggests searching for $\bar{\varphi}$ functions of the form:

$$\bar{\varphi}(\bar{R},\bar{\mathcal{G}}) = c_2\,\bar{\mathcal{G}}\ln(|\bar{\mathcal{G}}|^{\beta}|\bar{R}|^{\gamma})\,, \tag{6.2.9}$$

where β, γ and c_2 are real-valued constants.

Similarly to the previous case, we have defined $\bar{\varphi}$ in terms of the modulus of the scalar invariants to guarantee that the solutions are real-valued and well-defined. Curiously, the term multiplying the logarithm in Eq. (6.2.9) should be exactly $\mathcal{G}$ (for $w \neq -1$) and not some combination of different powers of R and $\mathcal{G}$. This is intimately related to the structure of the differential equation, Eq. (6.2.3), and the specific factors which are required to cancel out the dependence on the logarithm in the Friedmann equation. Equation (6.2.9) can be manipulated such that the powers inside the logarithm appear merely as multiplicative factors. Thus β and γ have no influence in any way on the exponent of ρ in the modified Friedmann equation.

Inserting the expression for $\bar{\varphi}$, Eq. (6.2.9), in the differential equation, Eq. (6.2.3), gives

$$c_2 = \frac{3}{2}\frac{1}{\epsilon\kappa^2}\frac{1-3w}{\beta(-11+24w+27w^2)+\gamma(-1+30w+27w^2)}\,. \tag{6.2.10}$$

Note that the values of β, γ and w must be such that the denominator of the last expression is non-zero. Finally, the gravitational Lagrangian for this specific solution is:

$$\mathcal{L}_g = R + \frac{C_2}{\rho_c}\,\mathcal{G}\ln\frac{|\mathcal{G}|^{\beta}|R|^{\gamma}}{\rho_c^{2\beta+\gamma}}\,, \tag{6.2.11}$$

with $C_2 = \epsilon\, c_2$. Solving Eq. (6.2.3) for $\bar{\varphi}(\bar{R},\bar{\mathcal{G}}) = \bar{\mathcal{G}}\Psi(\bar{R})$ gives a bouncing solution, driven by the corrective term in Eq. (6.2.11) with $\beta = 0$. Additionally, the solution presented in [329] is generalized to arbitrary values of w by setting $\gamma = 0$:

$$\mathcal{L}_g = R - \frac{3}{2\,(11+9w)\,\kappa^2\rho_c}\mathcal{G}\ln\frac{|\mathcal{G}|}{\rho_c^2}\,. \tag{6.2.12}$$

The choice $w = 1/3$ ($R^T = 0$) is valid, as long as $\gamma = 0$, leading to Eq. (6.2.12). On the other hand, $w = -1/3$ ($\mathcal{G}^T = 0$) is naturally not allowed by the ansatz in Eq. (6.2.9).

It is curious to observe that, only for the particular choice of $w = -1$, is it possible to have a general combination of powers of R and $\mathcal{G}$ multiplying the logarithm, and still obtain valid solutions for the differential equation, Eq. (6.2.3). Hence, exclusively for the case $w = -1$, we

may extend the gravitational Lagrangian into:

$$\mathcal{L}_g = R - \frac{6^\delta}{4}\frac{1}{\kappa^2\rho_c(2\beta+\gamma)}\,|\mathcal{G}|^\delta|R|^{2-2\delta}\ln\frac{|\mathcal{G}|^\beta|R|^\gamma}{\rho_c^{2\beta+\gamma}}\,, \tag{6.2.13}$$

where $\{\beta,\gamma,\delta\}\in\mathbb{R}$ such that $2\beta+\gamma\neq 0$.

To wrap up this chapter, we summarize the main results. We have found that it is possible to obtain the modified Friedmann, equation emerging from an effective description of LQC, through the following general gravitational Lagrangian

$$\mathcal{L}_g = R + \frac{\mathcal{A}}{\rho_c}\,|\mathcal{G}|^\alpha|R|^{2-2\alpha} + \frac{\mathcal{B}}{\rho_c}\,\mathcal{G}\ln\frac{|\mathcal{G}|^\beta|R|^\gamma}{\rho_c^{2\beta+\gamma}}\,, \tag{6.2.14}$$

where $\{\mathcal{A},\mathcal{B},\alpha,\beta,\gamma\}\in\mathbb{R}$ are arbitrary parameters. The modified Friedmann equation emerging from the Lagrangian in Eq. (6.2.14) *via* the order reduction technique is:

$$H^2 = \frac{\kappa^2}{3}\rho\left[1-\left(\frac{\mathcal{A}}{C_1}+\frac{\mathcal{B}}{C_2}\right)\frac{\rho}{\rho_c}\right]. \tag{6.2.15}$$

The additional constraint $\mathcal{A}/C_1+\mathcal{B}/C_2=1$ has to be satisfied (hence, only four parameters are, indeed, free).

Notice that, in order to reproduce the term $\propto\rho^2$ in the Friedmann equation, the solutions have to satisfy $\epsilon\varphi\sim R^2/\rho_c$ (since $\mathcal{G}\sim R^2$). Therefore, as previously mentioned in Sec. 6.1, it is now a simple task to verify that the necessary condition for the validity of the order reduction approach, *i.e.* $\epsilon\varphi\ll R$, leads to $R\ll\rho_c$, since $\epsilon\varphi\sim R^2/\rho_c\ll R\;\Rightarrow\;R\ll\rho_c$.

Chapter 7

Final remarks

"Cher enfant!" he cried, suddenly overcome by a rush of emotion, "my dear young friend" (he put both hands on my head), "I bless you and your destiny. Let us always be as true-hearted as today... as kind-hearted and good as possible, let us love all that is fair and good...in all its varied forms...Well, enfin... enfin rendons grâce...et je te benis!"

From *A Raw Youth*,
by Fyodor Dostoevsky

And so we reach the end of this thesis. We will not extend ourselves much more, but rather just summarize the main results and briefly mention some words with respect to the future challenges of cosmology. To that end, the action of the particular models that were studied are first exposed, followed by some words stating the main results.

- **Kinetically coupled quintessence:**

$$\mathcal{S} = \int \omega_g \left[\frac{R}{2\kappa^2} + X - V_0 e^{-\kappa\lambda\phi} + (\kappa^2 X)^\alpha \tilde{\mathcal{L}}_c \right] + \mathcal{S}_m(g_{\mu\nu}, \psi, \nabla\psi) \tag{7.0.1}$$

  In Chapter. 2, we have seen that this specific action for a canonical scalar field kinetically coupled to dark matter admits viable cosmological solutions, allowing for an early regime which may alleviate the cosmic coincidence problem. Through a dynamical system analysis, we have shown that the scaling regime is only possible due to the emergence of two new transient scaling critical points. During the scaling regime, the scalar source behaves as a stiff fluid, with $w_\phi = 1$. In this particular model, when the coupling is switched on, dark matter has a higher energy density throughout the cosmic history and

transfers energy into the dark energy field ϕ. As a consequence, with higher values of the coupling, the matter-radiation equality is shifted towards earlier times in the cosmic history. Similarly, dark energy starts to dominate earlier, when compared to the uncoupled case, even though the Universe starts to accelerate at later times and at a slower rate. Finally, from the Planck data it was possible to find an upper bound for the coupling of $\alpha \leqslant 0.0036$.

- **Coupled quintessence with a ΛCDM background:**

$$\mathcal{S} = \int \omega_g \left[\frac{R}{2\kappa^2} + X - V(\phi)\right] + \mathcal{S}_c(e^{-\kappa\beta\phi} g_{\mu\nu}, \psi, \nabla\psi) + \mathcal{S}_m(g_{\mu\nu}, \varphi, \nabla\varphi) \qquad (7.0.2)$$

This particular action, for a canonical scalar field conformally coupled to a pressureless dark matter component, was studied in Chapter. 3, with a unique trait: the background expansion is imposed in such a way so as to follow exactly the same evolution as in the standard model, *i.e.* $H = H_s$. As a consequence, when the interaction is present, $\beta \neq 0$, dark matter transfers energy to the quintessence field, resulting in lower present values for the energy density of dark matter, as compared to standard ΛCDM. The presence of an additional fifth force triggers a slower evolution rate for the first order perturbations of the dark matter fluid, thus having a direct impact on the formation of structures. Through a likelihood analysis, it was shown that, when tested against redshift space distortions data, this model is able to alleviate the present tension between CMB experiments and RSD measurements, which is also concordant with the weak lensing KiDS-450 survey data. We have found a best fit of $\beta = 0.079 \neq 0$ and $\sigma_8 = 0.818$. At the second order level in the perturbations we have studied the collapse of a spherical perturbation and the cluster number counts under this model. We have seen that, since the growth rate of CDM fluctuations is slower for larger couplings, the collapse of the matter density contrast happens later in the cosmic history. The comoving number of dark matter halos formed is suppressed (enhanced) at low (high) redshifts when the coupling is present, due to the interplay between two terms in the mass function. This effect is present for both the Press-Schechter and Sheth-Tormen mass functions but, however, it is more pronounced in the latter. It is to be noted that an exceptional feature of this model is the fact that the comoving volume element stays unaltered by the dark interaction, since it only depends on H, which was fixed *a priori* to be the same as in ΛCDM. Finally, we have carried out

a forecast regarding the detected number of clusters for two surveys conducted by the eROSITA mission and the South Pole Telescope. In both cases, the predicted number of objects is well within the sensitivity of the instruments, hinting at the possibility of observationally discriminating between ΛCDM and a model with nonzero coupling.

- **Modified $F(Q)$ gravity with a GR background:**

$$\mathcal{S} = -\frac{1}{2\kappa^2}\int \omega_g \left(Q + M\sqrt{Q} + C\right) + \mathcal{S}_m(g_{\mu\nu}, \psi, \nabla\psi) \tag{7.0.3}$$

In Chapter. 4, we have presented a model where gravity is mediated solely by the non-metricity, more precisely, the scalar invariant Q in Eq. (7.0.3), given by Eq. (4.0.13), in a flat and torsion-free spacetime. Analogously to the previous chapter, we study the $F(Q)$ model presented above, with the additional assumption that the background expansion evolution must match to the ΛCDM one. We have shown that, at linear order differences arise, with the matter perturbations being suppressed for $M > 0$ and enhanced for $M < 0$. This effect can also be understood by defining an effective gravitational constant $G_{\text{eff}} = G\left[1 + M/\left(2\sqrt{Q}\right)\right]$. In this study we have tested three particular models given by the action above against a set of 22 data points of redshift space distortions. We found that the preferred model is the one with $M = \sqrt{8\Lambda}$ and $C = 2\Lambda$, suggesting that RSD data favours a model with a lower clustering rate. Employing the Akaike Information Criterion, we found that all of the specific cases considered seem to have substantial support. A positive correlation between M and σ_8 was found, that is, increasing the value of M results in a slower growth rate for the overdensities, and thus a larger value for σ_8 is required to compensate the evolution of $f\sigma_8$ and better fit the data. From the likelihood analysis, the best fit model with $M = 2.0331$ is capable of alleviating the σ_8 tension between the high level of clustering from CMB experiments in contrast with large scale observations.

- **Wormhole geometries supported by 3-form fields:**

$$\mathcal{S} = \int \omega_g \left[\frac{R}{2\kappa^2} - \frac{1}{48}F^{\alpha\beta\gamma\delta}F_{\alpha\beta\gamma\delta} - V(A^{\alpha\beta\gamma}A_{\alpha\beta\gamma})\right] + \mathcal{S}_m(g_{\mu\nu}, \psi, \nabla\psi) \tag{7.0.4}$$

In Chapter. 5, we have derived the equations describing a single 3-form field minimally coupled to Einstein gravity for a static and spherically symmetric spacetime in the presence of an ordinary anisotropic distribution of matter. The 3-form field was constructed

specifically for this particular background metric, with an ansatz expressed in terms of a useful radial scalar function $\zeta(r)$. We have derived a general analytical function for the 3-form self interaction, assuming a general form for the metric functions, and that the field goes with the inverse of the radius r. By assuming a quadratic potential for the 3-form, we were able to arrive at additional numerical solutions. The novelty found in both the analytical and numerical solutions, is the fact that the 3-form field is able to act as the exotic source, violating the classical energy conditions (NEC and WEC), while holding the throat of the wormhole open. In this way, the ordinary matter fields threading the wormhole are able to coexist with the 3-form, without violating any energy conditions. This can also be achieved in the context of modified gravity, with non-canonical scalar fields, or with canonical scalar fields with a nonminimal coupling to curvature.

- **Bouncing solutions in $f(R,\mathcal{G})$ gravity:**

$$\mathcal{S}=\int\omega_g\left[\frac{R}{2\kappa^2}+\frac{\mathcal{A}}{\rho_c}\left|\mathcal{G}\right|^{\alpha}\left|R\right|^{2-2\alpha}+\frac{\mathcal{B}}{\rho_c}\,\mathcal{G}\ln\frac{\left|\mathcal{G}\right|^{\beta}\left|R\right|^{\gamma}}{\rho_c^{2\beta+\gamma}}\right]+\mathcal{S}_m(g_{\mu\nu},\psi,\nabla\psi) \tag{7.0.5}$$

In Chapter. 6, we have formally derived the covariant action given above for modified Gauss-Bonnet gravity, where $\mathcal{G}$ is the Gauss–Bonnet invariant, that reproduce the Friedmann equation of a bouncing Universe predicted by an effective description of Loop Quantum Cosmology. To do so, we adopted an effective field theory approach, and resorted to a method called order reduction technique, which allows one to find solutions which are perturbatively close to GR, while disposing of the extra degrees of freedom present in higher order theories of gravity. This work generalises and encompasses previous studies in the literature, conducted upon the same method and purpose, for $f(R)$ and $f(\mathcal{G})$ models.

The ΛCDM model has been able to explain most astrophysical and cosmological data with great success. However, it still fails to answer some key concepts such as [337]: what is the nature of dark energy and dark matter? Did an inflationary period took place in the early Univese? In addition, we still need to understand the reason for the discrepancy between observations with regard to H_0 and σ_8 when considering different datasets. Is this tension of a statistical nature? Does it hint towards modifications of the standard model? It is therefore of paramount importance to extract the maximum possible scientific information from cosmological

measurements to improve our understanding of the source of systematic uncertainties and deepen our knowledge with regard to the physics of non-linear scales. In the upcoming years, several missions will be launched, that will focus on trying to answer some of these puzzles. In particular, gravitational wave standard sirens [338, 339] are expected to put further constraints on H_0 in an model-independent approach. The space-based Euclid mission [145] will study the nature of dark energy and dark matter through gravitational lensing and galaxy clustering. Radio-interferometers such as the Square Kilometre Array [340, 341] will shed some light on interacting dark energy and modified gravity, through the measurement of the 21 cm HI emission line of galaxies, with up to 10 times more sensitivity than current radio-interferometers. For more details and references addressing the next decade chalenges of observational cosmology and prospects of answering some of our present conundrums, please see Refs. [20, 21, 337, 342].

Bibliography

[1] D. Lovelock. The Einstein tensor and its generalizations. *J. Math. Phys.*, 12:498–501, 1971.

[2] D. Lovelock. The four-dimensionality of space and the einstein tensor. *J. Math. Phys.*, 13:874–876, 1972.

[3] M. Fecko. *Differential geometry and Lie groups for physicists*. Cambridge University Press, 3 2011.

[4] C.J. Isham. *Modern differential geometry for physicists*. 10 1999.

[5] T. Frankel. *The geometry of physics: An introduction*. 1997.

[6] Robert M. Wald. *General Relativity*. Chicago Univ. Pr., Chicago, USA, 1984.

[7] M. Ostrogradsky. Mémoires sur les équations différentielles, relatives au problème des isopérimètres. *Mem. Acad. St. Petersbourg*, 6(4):385–517, 1850.

[8] N. Aghanim et al. Planck 2018 results. VI. Cosmological parameters. 2018.

[9] Matthew Colless et al. The 2dF Galaxy Redshift Survey: Spectra and redshifts. *Mon. Not. Roy. Astron. Soc.*, 328:1039, 2001.

[10] F. Zwicky. Die Rotverschiebung von extragalaktischen Nebeln. *Helv. Phys. Acta*, 6:110–127, 1933.

[11] K.C. Freeman. On the disks of spiral and SO Galaxies. *Astrophys. J.*, 160:811, 1970.

[12] Albert Einstein. Cosmological Considerations in the General Theory of Relativity. *Sitzungsber. Preuss. Akad. Wiss. Berlin (Math. Phys.)*, 1917:142–152, 1917.

[13] Edwin Hubble. A relation between distance and radial velocity among extra-galactic nebulae. *Proc. Nat. Acad. Sci.*, 15:168–173, 1929.

[14] Adam G. Riess et al. Observational evidence from supernovae for an accelerating universe and a cosmological constant. *Astron. J.*, 116:1009–1038, 1998.

[15] S. Perlmutter et al. Measurements of Omega and Lambda from 42 high redshift supernovae. *Astrophys. J.*, 517:565–586, 1999.

[16] Luca Amendola and Shinji Tsujikawa. *Dark Energy: Theory and Observations*. Cambridge University Press, 1 2015.

[17] Steven Weinberg. The Cosmological constant problems. In *Sources and detection of dark matter and dark energy in the universe. Proceedings, 4th International Symposium, DM 2000, Marina del Rey, USA, February 23-25, 2000*, pages 18–26, 2000.

[18] Ivaylo Zlatev, Li-Min Wang, and Paul J. Steinhardt. Quintessence, cosmic coincidence, and the cosmological constant. *Phys. Rev. Lett.*, 82:896–899, 1999.

[19] Licia Verde, Tommaso Treu, and Adam G. Riess. Tensions between the early and late universe. *Nature Astronomy*, 3(10):891–895, Sep 2019.

[20] Eleonora Di Valentino et al. Cosmology Intertwined II: The Hubble Constant Tension. 8 2020.

[21] Eleonora Di Valentino et al. Cosmology Intertwined III: $f\sigma_8$ and S_8. 8 2020.

[22] Adam G. Riess, Stefano Casertano, Wenlong Yuan, Lucas M. Macri, and Dan Scolnic. Large Magellanic Cloud Cepheid Standards Provide a 1% Foundation for the Determination of the Hubble Constant and Stronger Evidence for Physics beyond ΛCDM. *Astrophys. J.*, 876(1):85, 2019.

[23] Marian Douspis, Laura Salvati, and Nabila Aghanim. On the Tension between Large Scale Structures and Cosmic Microwave Background. *PoS*, EDSU2018:037, 2018.

[24] Richard A. Battye, Tom Charnock, and Adam Moss. Tension between the power spectrum of density perturbations measured on large and small scales. *Phys. Rev.*, D91(10):103508, 2015.

[25] Edward Macaulay, Ingunn Kathrine Wehus, and Hans Kristian Eriksen. Lower Growth Rate from Recent Redshift Space Distortion Measurements than Expected from Planck. *Phys. Rev. Lett.*, 111(16):161301, 2013.

[26] Savvas Nesseris, George Pantazis, and Leandros Perivolaropoulos. Tension and constraints on modified gravity parametrizations of $G_{\rm eff}(z)$ from growth rate and Planck data. *Phys. Rev.*, D96(2):023542, 2017.

[27] Spyros Basilakos and Savvas Nesseris. Conjoined constraints on modified gravity from the expansion history and cosmic growth. *Phys. Rev.*, D96(6):063517, 2017.

[28] Shahab Joudaki et al. CFHTLenS revisited: assessing concordance with Planck including astrophysical systematics. *Mon. Not. Roy. Astron. Soc.*, 465(2):2033–2052, 2017.

[29] James S. Bullock and Michael Boylan-Kolchin. Small-Scale Challenges to the ΛCDM Paradigm. *Ann. Rev. Astron. Astrophys.*, 55:343–387, 2017.

[30] Shin'ichi Nojiri and Sergei D. Odintsov. Introduction to modified gravity and gravitational alternative for dark energy. *eConf*, C0602061:06, 2006. [Int. J. Geom. Meth. Mod. Phys.4,115(2007)].

[31] Thomas P. Sotiriou and Valerio Faraoni. f(R) Theories Of Gravity. *Rev. Mod. Phys.*, 82:451–497, 2010.

[32] Antonio De Felice and Shinji Tsujikawa. f(R) theories. *Living Rev. Rel.*, 13:3, 2010.

[33] Timothy Clifton, Pedro G. Ferreira, Antonio Padilla, and Constantinos Skordis. Modified Gravity and Cosmology. *Phys. Rept.*, 513:1–189, 2012.

[34] Edmund J. Copeland, Andrew R Liddle, and David Wands. Exponential potentials and cosmological scaling solutions. *Phys. Rev.*, D57:4686–4690, 1998.

[35] Takeshi Chiba, Takahiro Okabe, and Masahide Yamaguchi. Kinetically driven quintessence. *Phys. Rev.*, D62:023511, 2000.

[36] Christof Wetterich. The Cosmon model for an asymptotically vanishing time dependent cosmological 'constant'. *Astron. Astrophys.*, 301:321–328, 1995.

[37] Bruno J. Barros. Kinetically coupled dark energy. *Phys. Rev.*, D99(6):064051, 2019.

[38] Luca Amendola. Coupled quintessence. *Phys. Rev.*, D62:043511, 2000.

[39] Alexander Leithes, Karim A. Malik, David J. Mulryne, and Nelson J. Nunes. Linear Density Perturbations in Multifield Coupled Quintessence. *Phys. Rev.*, D95(12):123519, 2017.

[40] Arpine Piloyan, Valerio Marra, Marco Baldi, and Luca Amendola. Linear Perturbation constraints on Multi-coupled Dark Energy. *JCAP*, 1402:045, 2014.

[41] Shinji Tsujikawa. Dark energy: investigation and modeling. 370(2010):331–402, 2011.

[42] Rong-Gen Cai and Anzhong Wang. Cosmology with interaction between phantom dark energy and dark matter and the coincidence problem. *JCAP*, 0503:002, 2005.

[43] Winfried Zimdahl and Diego Pavon. Interacting quintessence. *Phys. Lett.*, B521:133–138, 2001.

[44] Luca Amendola. Scaling solutions in general nonminimal coupling theories. *Phys. Rev.*, D60:043501, 1999.

[45] Tomi Koivisto. Growth of perturbations in dark matter coupled with quintessence. *Phys. Rev.*, D72:043516, 2005.

[46] Rachel Bean and Joao Magueijo. Dilaton derived quintessence scenario leading naturally to the late time acceleration of the universe. *Phys. Lett.*, B517:177–183, 2001.

[47] Glennys R. Farrar and P. James E. Peebles. Interacting dark matter and dark energy. *Astrophys. J.*, 604:1–11, 2004.

[48] Michael Doran and Joerg Jaeckel. Loop corrections to scalar quintessence potentials. *Phys. Rev.*, D66:043519, 2002.

[49] Adalto R. Gomes and Luca Amendola. The general form of the coupled Horndeski Lagrangian that allows cosmological scaling solutions. *JCAP*, 1602:035, 2016.

[50] Ali H. Chamseddine and Viatcheslav Mukhanov. Mimetic Dark Matter. *JHEP*, 11:135, 2013.

[51] L. Sebastiani, S. Vagnozzi, and R. Myrzakulov. Mimetic gravity: a review of recent developments and applications to cosmology and astrophysics. *Adv. High Energy Phys.*, 2017:3156915, 2017.

[52] Liuyuan Shen, Yicen Mou, Yunlong Zheng, and Mingzhe Li. Direct couplings of mimetic dark matter and their cosmological effects. *Chin. Phys.*, C42(1):015101, 2018.

[53] Sunny Vagnozzi. Recovering a MOND-like acceleration law in mimetic gravity. *Class. Quant. Grav.*, 34(18):185006, 2017.

[54] A. Pourtsidou, C. Skordis, and E. J. Copeland. Models of dark matter coupled to dark energy. *Phys. Rev.*, D88(8):083505, 2013.

[55] J. David Brown. Action functionals for relativistic perfect fluids. *Class. Quant. Grav.*, 10:1579–1606, 1993.

[56] Christian G. Boehmer, Nicola Tamanini, and Matthew Wright. Interacting quintessence from a variational approach Part II: derivative couplings. *Phys. Rev.*, D91(12):123003, 2015.

[57] Christian G. Boehmer, Nicola Tamanini, and Matthew Wright. Interacting quintessence from a variational approach Part I: algebraic couplings. *Phys. Rev.*, D91(12):123002, 2015.

[58] Jibitesh Dutta, Wompherdeiki Khyllep, and Nicola Tamanini. Scalar-Fluid interacting dark energy: cosmological dynamics beyond the exponential potential. *Phys. Rev.*, D95(2):023515, 2017.

[59] Tomi S. Koivisto, Emmanuel N. Saridakis, and Nicola Tamanini. Scalar-Fluid theories: cosmological perturbations and large-scale structure. *JCAP*, 1509:047, 2015.

[60] L. N. Granda. Non-minimal Kinetic coupling to gravity and accelerated expansion. *JCAP*, 1007:006, 2010.

[61] L. N. Granda. Dark energy from scalar field with Gauss Bonnet and non-minimal kinetic coupling. *Mod. Phys. Lett.*, A27:1250018, 2012.

[62] Jacob D. Bekenstein. The Relation between physical and gravitational geometry. *Phys. Rev.*, D48:3641–3647, 1993.

[63] Miguel Zumalacarregui, Tomi S. Koivisto, and David F. Mota. DBI Galileons in the Einstein Frame: Local Gravity and Cosmology. *Phys. Rev.*, D87:083010, 2013.

[64] M. Zumalacarregui, T. S. Koivisto, D. F. Mota, and P. Ruiz-Lapuente. Disformal Scalar Fields and the Dark Sector of the Universe. *JCAP*, 1005:038, 2010.

[65] C. van de Bruck and J. Morrice. Disformal couplings and the dark sector of the universe. *JCAP*, 1504:036, 2015.

[66] Carsten van de Bruck, Jurgen Mifsud, José P. Mimoso, and Nelson J. Nunes. Generalized dark energy interactions with multiple fluids. *JCAP*, 1611(11):031, 2016.

[67] Stharporn Sapa, Khamphee Karwan, and David F. Mota. Spherical collapse and cluster number counts in dark energy models disformally coupled to dark matter. *Phys. Rev.*, D98(2):023528, 2018.

[68] C. Armendariz-Picon, Viatcheslav F. Mukhanov, and Paul J. Steinhardt. Essentials of k essence. *Phys. Rev.*, D63:103510, 2001.

[69] Pedro F. Gonzalez-Diaz. K-essential phantom energy: Doomsday around the corner? *Phys. Lett.*, B586:1–4, 2004.

[70] Robert J. Scherrer. Purely kinetic k-essence as unified dark matter. *Phys. Rev. Lett.*, 93:011301, 2004.

[71] Eugeny Babichev, Viatcheslav Mukhanov, and Alexander Vikman. k-Essence, superluminal propagation, causality and emergent geometry. *JHEP*, 02:101, 2008.

[72] Luis P. Chimento. Extended tachyon field, Chaplygin gas and solvable k-essence cosmologies. *Phys. Rev.*, D69:123517, 2004.

[73] Roland de Putter and Eric V. Linder. Kinetic k-essence and Quintessence. *Astropart. Phys.*, 28:263–272, 2007.

[74] Marco Baldi. Multiple Dark Matter as a self-regulating mechanism for dark sector interactions. *Annalen Phys.*, 524:602–617, 2012.

[75] Luca Amendola and Domenico Tocchini-Valentini. Stationary dark energy: The Present universe as a global attractor. *Phys. Rev.*, D64:043509, 2001.

[76] German Olivares, F. Atrio-Barandela, and D. Pavon. Matter density perturbations in interacting quintessence models. *Phys. Rev.*, D74:043521, 2006.

[77] Songbai Chen, Bin Wang, and Jiliang Jing. Dynamics of interacting dark energy model in Einstein and Loop Quantum Cosmology. *Phys. Rev.*, D78:123503, 2008.

[78] Claudia Quercellini, Marco Bruni, Amedeo Balbi, and Davide Pietrobon. Late universe dynamics with scale-independent linear couplings in the dark sector. *Phys. Rev.*, D78:063527, 2008.

[79] Marek Szydłowski and Aleksander Stachowski. Does the diffusion dark matter-dark energy interaction model solve cosmological puzzles? *Phys. Rev.*, D94(4):043521, 2016.

[80] Fabiola Arevalo, Anna Paula Ramos Bacalhau, and Winfried Zimdahl. Cosmological dynamics with non-linear interactions. *Class. Quant. Grav.*, 29:235001, 2012.

[81] Ana Nunes, Jose P. Mimoso, and Tiago C. Charters. Scaling solutions from interacting fluids. *Phys. Rev.*, D63:083506, 2001.

[82] Burin Gumjudpai, Tapan Naskar, M. Sami, and Shinji Tsujikawa. Coupled dark energy: Towards a general description of the dynamics. *JCAP*, 0506:007, 2005.

[83] Takeshi Chiba, Antonio De Felice, and Shinji Tsujikawa. Cosmological Scaling Solutions for Multiple Scalar Fields. *Phys. Rev.*, D90(2):023516, 2014.

[84] M. Shahalam, S. D. Pathak, Shiyuan Li, R. Myrzakulov, and Anzhong Wang. Dynamics of coupled phantom and tachyon fields. *Eur. Phys. J.*, C77(10):686, 2017.

[85] Sudipta Das and Abdulla Al Mamon. Cosmic acceleration in non-canonical scalar field model - An interacting scenario. *Astrophys. Space Sci.*, 355(2):371–380, 2015.

[86] H. Farajollahi and A. Salehi. A New approach in stability analysis: case study: tachyon cosmology with non-minimally coupled scalar field-matter. *Phys. Rev.*, D83:124042, 2011.

[87] Ryotaro Kase and Shinji Tsujikawa. Scalar-Field Dark Energy Nonminimally and Kinetically Coupled to Dark Matter. *Phys. Rev. D*, 101(6):063511, 2020.

[88] Ryotaro Kase and Shinji Tsujikawa. Weak cosmic growth in coupled dark energy with a Lagrangian formulation. *Phys. Lett. B*, 804:135400, 2020.

[89] Luca Amendola and Shinji Tsujikawa. Scaling solutions and weak gravity in dark energy with energy and momentum couplings. *JCAP*, 06:020, 2020.

[90] L. Gabriel Gomez and Yeinzon Rodriguez. Coupled Multi-Proca Vector Dark Energy. 4 2020.

[91] Olivier Minazzoli and Tiberiu Harko. New derivation of the Lagrangian of a perfect fluid with a barotropic equation of state. *Phys. Rev.*, D86:087502, 2012.

[92] T. Harko. The matter Lagrangian and the energy-momentum tensor in modified gravity with non-minimal coupling between matter and geometry. *Phys. Rev.*, D81:044021, 2010.

[93] Valeria Pettorino and Carlo Baccigalupi. Coupled and Extended Quintessence: theoretical differences and structure formation. *Phys. Rev.*, D77:103003, 2008.

[94] Luca Amendola, Tiago Barreiro, and Nelson J. Nunes. Multifield coupled quintessence. *Phys. Rev.*, D90(8):083508, 2014.

[95] T. Damour, G. W. Gibbons, and C. Gundlach. Dark matter, time-varying g, and a dilaton field. *Phys. Rev. Lett.*, 64:123–126, Jan 1990.

[96] Luca Amendola. Linear and non-linear perturbations in dark energy models. *Phys. Rev.*, D69:103524, 2004.

[97] David Anderson and Nicolás Yunes. Solar System constraints on massless scalar-tensor gravity with positive coupling constant upon cosmological evolution of the scalar field. *Phys. Rev.*, D96(6):064037, 2017.

[98] Sean M. Carroll. Quintessence and the rest of the world. *Phys. Rev. Lett.*, 81:3067–3070, 1998.

[99] N. Chandrachani Devi, Sudhakar Panda, and Anjan A Sen. Solar System Constraints on Scalar Tensor Theories with Non-Standard Action. *Phys. Rev.*, D84:063521, 2011.

[100] Orfeu Bertolami, Riccardo March, and Jorge Páramos. Solar System constraints to nonminimally coupled gravity. *Phys. Rev.*, D88:064019, 2013.

[101] Valerio Faraoni and Nicolas Lanahan-Tremblay. Comments on 'Solar System constraints to general f(R) gravity'. *Phys. Rev.*, D77:108501, 2008.

[102] Stephen C. Davis. Solar System Constraints on Gauss-Bonnet Dark Energy. *AIP Conf. Proc.*, 957:379–382, 2007.

[103] Zong Kuan Guo, Yun-Song Piao, and Yuan-Zhong Zhang. Cosmological scaling solutions and multiple exponential potentials. *Phys. Lett.*, B568:1–7, 2003.

[104] T. Barreiro, Edmund J. Copeland, and N. J. Nunes. Quintessence arising from exponential potentials. *Phys. Rev.*, D61:127301, 2000.

[105] Sebastian Bahamonde, Christian G. Böhmer, Sante Carloni, Edmund J. Copeland, Wei Fang, and Nicola Tamanini. Dynamical systems applied to cosmology: dark energy and modified gravity. *Phys. Rept.*, 775-777:1–122, 2018.

[106] Luca Amendola, Radouane Gannouji, David Polarski, and Shinji Tsujikawa. Conditions for the cosmological viability of f(R) dark energy models. *Phys. Rev. D*, 75:083504, 2007.

[107] J. Wainwright and G.F.R. Ellis. *Dynamical Systems in Cosmology*. Cambridge University Press, 2005.

[108] Lawrence Perko. *Differential Equations and Dynamical Systems*. Springer-Verlag, Berlin, Heidelberg, 1991.

[109] Edmund J. Copeland, M. Sami, and Shinji Tsujikawa. Dynamics of dark energy. *Int. J. Mod. Phys.*, D15:1753–1936, 2006.

[110] Ines S. Albuquerque, Noemi Frusciante, Nelson J. Nunes, and Shinji Tsujikawa. New scaling solutions in cubic Horndeski theories. *Phys. Rev.*, D98(6):064038, 2018.

[111] Julien Lesgourgues. The cosmic linear anisotropy solving system (class) i: Overview, 2011.

[112] Diego Blas, Julien Lesgourgues, and Thomas Tram. The cosmic linear anisotropy solving system (class). part ii: Approximation schemes. *Journal of Cosmology and Astroparticle Physics*, 2011(07):034–034, Jul 2011.

[113] Julien Lesgourgues. The cosmic linear anisotropy solving system (class) iii: Comparision with camb for lambdacdm, 2011.

[114] Julien Lesgourgues and Thomas Tram. The cosmic linear anisotropy solving system (class) iv: efficient implementation of non-cold relics. *Journal of Cosmology and Astroparticle Physics*, 2011(09):032–032, Sep 2011.

[115] Carsten van de Bruck, Jurgen Mifsud, and Jack Morrice. Testing coupled dark energy models with their cosmological background evolution. *Phys. Rev. D*, 95(4):043513, 2017.

[116] Christof Wetterich. Phenomenological parameterization of quintessence. *Phys. Lett.*, B594:17–22, 2004.

[117] P. A. R. Ade et al. Planck 2015 results. XIV. Dark energy and modified gravity. *Astron. Astrophys.*, 594:A14, 2016.

[118] Tanvi Karwal and Marc Kamionkowski. Dark energy at early times, the Hubble parameter, and the string axiverse. *Phys. Rev.*, D94(10):103523, 2016.

[119] Vivian Poulin, Tristan L. Smith, Tanvi Karwal, and Marc Kamionkowski. Early Dark Energy Can Resolve The Hubble Tension. 2018.

[120] Guido Risaliti and Elisabeta Lusso. Cosmological constraints from the Hubble diagram of quasars at high redshifts. *Nat. Astron.*, 2018.

[121] Pau Amaro Seoane et al. The Gravitational Universe. 2013.

[122] Chiara Caprini and Nicola Tamanini. Constraining early and interacting dark energy with gravitational wave standard sirens: the potential of the eLISA mission. *JCAP*, 1610(10):006, 2016.

[123] Nicola Tamanini, Chiara Caprini, Enrico Barausse, Alberto Sesana, Antoine Klein, and Antoine Petiteau. Science with the space-based interferometer eLISA. III: Probing the expansion of the Universe using gravitational wave standard sirens. *JCAP*, 1604(04):002, 2016.

[124] Bruno J. Barros, Luca Amendola, Tiago Barreiro, and Nelson J. Nunes. Coupled quintessence with a ΛCDM background: removing the σ_8 tension. *JCAP*, 1901:007, 2019.

[125] Bruno J. Barros, Tiago Barreiro, and Nelson J. Nunes. Spherical collapse in coupled quintessence with a ΛCDM background. *Phys. Rev.*, D101(2):023502, 2020.

[126] Henrik Nersisyan, Adrian Fernandez Cid, and Luca Amendola. Structure formation in the Deser-Woodard nonlocal gravity model: a reappraisal. *JCAP*, 04:046, 2017.

[127] Luca Amendola, Yves Dirian, Henrik Nersisyan, and Sohyun Park. Observational Constraints in Nonlocal Gravity: the Deser-Woodard Case. *JCAP*, 03:045, 2019.

[128] M. Nakahara. *Geometry, topology and physics*. 2003.

[129] C. Brans and R.H. Dicke. Mach's principle and a relativistic theory of gravitation. *Phys. Rev.*, 124:925–935, 1961.

[130] Valerio Faraoni. *Cosmology in scalar tensor gravity*, volume 139. 2004.

[131] Luca Amendola and Valeria Pettorino. Beyond self-acceleration: force- and fluid-acceleration. *Phys. Lett. B*, 802:135214, 2020.

[132] Marieke Postma and Marco Volponi. Equivalence of the Einstein and Jordan frames. *Phys. Rev. D*, 90(10):103516, 2014.

[133] Valerio Faraoni and Salvatore Capozziello. *Beyond Einstein Gravity*, volume 170. Springer, Dordrecht, 2011.

[134] M. Gasperini and G. Veneziano. The Pre - big bang scenario in string cosmology. *Phys. Rept.*, 373:1–212, 2003.

[135] James E. Lidsey, David Wands, and Edmund J. Copeland. Superstring cosmology. *Phys. Rept.*, 337:343–492, 2000.

[136] T. Damour, G. W. Gibbons, and C. Gundlach. Dark Matter, Time Varying G, and a Dilaton Field. *Phys. Rev. Lett.*, 64:123–126, 1990.

[137] David H. Weinberg, Michael J. Mortonson, Daniel J. Eisenstein, Christopher Hirata, Adam G. Riess, and Eduardo Rozo. Observational Probes of Cosmic Acceleration. *Phys. Rept.*, 530:87–255, 2013.

[138] Mahnaz Asghari, Jose Beltrán Jiménez, Shahram Khosravi, and David F. Mota. On structure formation from a small-scales-interacting dark sector. *JCAP*, 2019(04):042, 2019.

[139] P. A. R. Ade et al. Planck 2015 results. XIII. Cosmological parameters. *Astron. Astrophys.*, 594:A13, 2016.

[140] David H. Lyth and Andrew R. Liddle. *The primordial density perturbation: Cosmology, inflation and the origin of structure*. 2009.

[141] James M. Bardeen. Gauge Invariant Cosmological Perturbations. *Phys. Rev. D*, 22:1882–1905, 1980.

[142] Tomi Koivisto. Growth of perturbations in dark matter coupled with quintessence. *Phys. Rev.*, D72:043516, 2005.

[143] Luca Amendola and Domenico Tocchini-Valentini. Baryon bias and structure formation in an accelerating universe. *Phys. Rev.*, D66:043528, 2002.

[144] Nico Wintergerst and Valeria Pettorino. Clarifying spherical collapse in coupled dark energy cosmologies. *Phys. Rev.*, D82:103516, 2010.

[145] Luca Amendola et al. Cosmology and fundamental physics with the Euclid satellite. *Living Rev. Rel.*, 16:6, 2013.

[146] Luca Amendola, Tiago Barreiro, and Nelson J. Nunes. Multifield coupled quintessence. *Phys. Rev.*, D90(8):083508, 2014.

[147] N. Kaiser. Clustering in real space and in redshift space. *Mon. Not. Roy. Astron. Soc.*, 227:1–27, 1987.

[148] S. de la Torre et al. The VIMOS Public Extragalactic Redshift Survey (VIPERS). Galaxy clustering and redshift-space distortions at z=0.8 in the first data release. *Astron. Astrophys.*, 557:A54, 2013.

[149] Hiroyuki Okada et al. The Subaru FMOS Galaxy Redshift Survey (FastSound). II. The Emission Line Catalog and Properties of Emission Line Galaxies. *Publ. Astron. Soc. Jap.*, 68(33, id.47):17, 2016.

[150] L. Guzzo et al. A test of the nature of cosmic acceleration using galaxy redshift distortions. *Nature*, 451:541–545, 2008.

[151] Chia-Hsun Chuang et al. The clustering of galaxies in the SDSS-III Baryon Oscillation Spectroscopic Survey: single-probe measurements from CMASS anisotropic galaxy clustering. *Mon. Not. Roy. Astron. Soc.*, 461(4):3781–3793, 2016.

[152] C. Blake, S. Brough, M. Colless, C. Contreras, W. Couch, S. Croom, D. Croton, T. M. Davis, M. J. Drinkwater, K. Forster, D. Gilbank, M. Gladders, K. Glazebrook, B. Jelliffe, R. J. Jurek, I.-h. Li, B. Madore, D. C. Martin, K. Pimbblet, G. B. Poole, M. Pracy,

R. Sharp, E. Wisnioski, D. Woods, T. K. Wyder, and H. K. C. Yee. The WiggleZ Dark Energy Survey: joint measurements of the expansion and growth history at $z < 1$. *"Mon. Not. Roy. Astron. Soc.",*, 425:405–414, September 2012.

[153] Max Tegmark et al. Cosmological Constraints from the SDSS Luminous Red Galaxies. *Phys. Rev.*, D74:123507, 2006.

[154] Héctor Gil-Marín et al. The clustering of galaxies in the SDSS-III Baryon Oscillation Spectroscopic Survey: RSD measurement from the LOS-dependent power spectrum of DR12 BOSS galaxies. *Mon. Not. Roy. Astron. Soc.*, 460(4):4188–4209, 2016.

[155] R. Tojeiro, W. J. Percival, J. Brinkmann, J. R. Brownstein, D. J. Eisenstein, M. Manera, C. Maraston, C. K. McBride, D. Muna, B. Reid, A. J. Ross, N. P. Ross, L. Samushia, N. Padmanabhan, D. P. Schneider, R. Skibba, A. G. Sánchez, M. E. C. Swanson, D. Thomas, J. L. Tinker, L. Verde, D. A. Wake, B. A. Weaver, and G.-B. Zhao. The clustering of galaxies in the SDSS-III Baryon Oscillation Spectroscopic Survey: measuring structure growth using passive galaxies. *Mon. Not. Roy. Astron. Soc.*, 424:2339–2344, August 2012.

[156] Siddharth Satpathy et al. The clustering of galaxies in the completed SDSS-III Baryon Oscillation Spectroscopic Survey: On the measurement of growth rate using galaxy correlation functions. *Mon. Not. Roy. Astron. Soc.*, 469(2):1369–1382, 2017.

[157] L. Samushia, W. J. Percival, and A. Raccanelli. Interpreting large-scale redshift-space distortion measurements. *"Mon. Not. Roy. Astron. Soc.",*, 420:2102–2119, March 2012.

[158] C. Blake, S. Brough, M. Colless, C. Contreras, W. Couch, S. Croom, T. Davis, M. J. Drinkwater, K. Forster, D. Gilbank, M. Gladders, K. Glazebrook, B. Jelliffe, R. J. Jurek, I.-H. Li, B. Madore, D. C. Martin, K. Pimbblet, G. B. Poole, M. Pracy, R. Sharp, E. Wisnioski, D. Woods, T. K. Wyder, and H. K. C. Yee. The WiggleZ Dark Energy Survey: the growth rate of cosmic structure since redshift z=0.9. *"Mon. Not. Roy. Astron. Soc.",*, 415:2876–2891, August 2011.

[159] Will J. Percival et al. The 2dF Galaxy Redshift Survey: Spherical harmonics analysis of fluctuations in the final catalogue. *Mon. Not. Roy. Astron. Soc.*, 353:1201, 2004.

[160] Cullan Howlett, Ashley Ross, Lado Samushia, Will Percival, and Marc Manera. The clustering of the SDSS main galaxy sample – II. Mock galaxy catalogues and a measurement of the growth of structure from redshift space distortions at $z = 0.15$. *Mon. Not. Roy. Astron. Soc.*, 449(1):848–866, 2015.

[161] F. Beutler, C. Blake, M. Colless, D. H. Jones, L. Staveley-Smith, G. B. Poole, L. Campbell, Q. Parker, W. Saunders, and F. Watson. The 6dF Galaxy Survey: $z \approx 0$ measurements of the growth rate and σ_8. *"Mon. Not. Roy. Astron. Soc.",*, 423:3430–3444, July 2012.

[162] Yong-Seon Song and Will J. Percival. Reconstructing the history of structure formation using Redshift Distortions. *JCAP*, 0910:004, 2009.

[163] Imanol Albarran, Mariam Bouhmadi-López, and João Morais. Cosmological perturbations in an effective and genuinely phantom dark energy Universe. *Phys. Dark Univ.*, 16:94–108, 2017.

[164] M. J. Hudson and S. J. Turnbull. The Growth Rate of Cosmic Structure from Peculiar Velocities at Low and High Redshifts. *Astrophys. J.*, 751:L30, June 2012.

[165] Valeria Pettorino. Testing modified gravity with Planck: the case of coupled dark energy. *Phys. Rev.*, D88:063519, 2013.

[166] Alvise Raccanelli et al. Measuring redshift-space distortions with future SKA surveys. 2015.

[167] H. Hildebrandt et al. KiDS-450: Cosmological parameter constraints from tomographic weak gravitational lensing. *Mon. Not. Roy. Astron. Soc.*, 465:1454, 2017.

[168] T. M. C. Abbott et al. Dark Energy Survey year 1 results: Cosmological constraints from galaxy clustering and weak lensing. *Phys. Rev.*, D98(4):043526, 2018.

[169] Andrew R. Liddle and David H. Lyth. The Cold dark matter density perturbation. *Phys. Rept.*, 231:1–105, 1993.

[170] Elise Jennings. *Simulations of Dark Energy Cosmologies*. Springer-Verlag Berlin Heidelberg, 2012.

[171] Andrea V. Maccio, Claudia Quercellini, Roberto Mainini, Luca Amendola, and Silvio A. Bonometto. N-body simulations for coupled dark energy: Halo mass function and density profiles. *Phys. Rev.*, D69:123516, 2004.

[172] Marco Baldi. Time dependent couplings in the dark sector: from background evolution to nonlinear structure formation. *Mon. Not. Roy. Astron. Soc.*, 411:1077, 2011.

[173] C. De Boni, K. Dolag, S. Ettori, L. Moscardini, V. Pettorino, and C. Baccigalupi. Hydrodynamical simulations of galaxy clusters in dark energy cosmologies – I. General properties. *Monthly Notices of the Royal Astronomical Society*, 415(3):2758–2772, 08 2011.

[174] James E. Gunn and J. Richard Gott, III. On the Infall of Matter into Clusters of Galaxies and Some Effects on Their Evolution. *Astrophys. J.*, 176:1–19, 1972.

[175] F. Pace, J.-C. Waizmann, and M. Bartelmann. Spherical collapse model in dark-energy cosmologies. *Monthly Notices of the Royal Astronomical Society*, 406(3):1865–1874, 08 2010.

[176] T. Padmanabhan. *Structure Formation in the Universe*. Cambridge University Press, 1999.

[177] Andrew R. Liddle, David H. Lyth, Robert K. Schaefer, Q. Shafi, and Pedro T. P. Viana. Pursuing parameters for critical density dark matter models. *Mon. Not. Roy. Astron. Soc.*, 281:531, 1996.

[178] Francesco Pace, Lauro Moscardini, Robert Crittenden, Matthias Bartelmann, and Valeria Pettorino. A comparison of structure formation in minimally and non-minimally coupled quintessence models. *Mon. Not. Roy. Astron. Soc.*, 437(1):547–561, 2014.

[179] Morgan Le Delliou and Tiago Barreiro. Interacting dark energy collapse with matter components separation. *JCAP*, 1302:037, 2013.

[180] N. Nazari-Pooya, M. Malekjani, F. Pace, and D. Mohammad-Zadeh Jassur. Growth of spherical overdensities in scalar-tensor cosmologies. *Mon. Not. Roy. Astron. Soc.*, 458(4):3795–3807, 2016.

[181] David F. Mota. Probing Dark Energy at Galactic and Cluster Scales. *JCAP*, 0809:006, 2008.

[182] D. F. Mota and C. van de Bruck. On the Spherical collapse model in dark energy cosmologies. *Astron. Astrophys.*, 421:71–81, 2004.

[183] Jian-Hua He, Bin Wang, Elcio Abdalla, and Diego Pavon. The Imprint of the interaction between dark sectors in galaxy clusters. *JCAP*, 1012:022, 2010.

[184] Nelson J. Nunes, A. C. da Silva, and N. Aghanim. Number counts in homogeneous and inhomogeneous dark energy models. *Astron. Astrophys.*, 450:899–907, 2006.

[185] Morgan Le Delliou. Dynamical quintessence fields Press-Schechter mass function: Detectability and effect on dark haloes. *JCAP*, 0601:021, 2006.

[186] Nelson J. Nunes and D. F. Mota. Structure formation in inhomogeneous dark energy models. *Mon. Not. Roy. Astron. Soc.*, 368:751–758, 2006.

[187] G. D. Birkhoff and R. E. Langer. *Relativity and modern physics*. Harvard University Press, 1923.

[188] Stefano Savastano, Luca Amendola, Javier Rubio, and Christof Wetterich. Primordial dark matter halos from fifth-forces. 2019.

[189] Miguel Zumalacárregui and Juan García-Bellido. Transforming gravity: from derivative couplings to matter to second-order scalar-tensor theories beyond the Horndeski Lagrangian. *Phys. Rev.*, D89:064046, 2014.

[190] William H. Press and Paul Schechter. Formation of galaxies and clusters of galaxies by selfsimilar gravitational condensation. *Astrophys. J.*, 187:425–438, 1974.

[191] Pedro T. P. Viana and Andrew R. Liddle. The Cluster abundance in flat and open cosmologies. *Mon. Not. Roy. Astron. Soc.*, 281:323, 1996.

[192] Marc Manera and D. F. Mota. Cluster number counts dependence on dark energy inhomogeneities and coupling to dark matter. *Mon. Not. Roy. Astron. Soc.*, 371:1373, 2006.

[193] Ewan R. M. Tarrant, Carsten van de Bruck, Edmund J. Copeland, and Anne M. Green. Coupled quintessence and the halo mass function. *Phys. Rev. D*, 85:023503, Jan 2012.

[194] F. Pace, J. C. Waizmann, and M. Bartelmann. Spherical collapse model in dark energy cosmologies. *Mon. Not. Roy. Astron. Soc.*, 406:1865, 2010.

[195] N. Chandrachani Devi, T. Roy Choudhury, and Anjan A. Sen. Constraining Thawing Dark Energy using Galaxy Cluster Number Counts. *Mon. Not. Roy. Astron. Soc.*, 432:1513–1524, 2013.

[196] Ravi K. Sheth and Giuseppe Tormen. Large scale bias and the peak background split. *Mon. Not. Roy. Astron. Soc.*, 308:119, 1999.

[197] Darren Reed, Richard Bower, Carlos Frenk, Adrian Jenkins, and Tom Theuns. The halo mass function from the dark ages through the present day. *Mon. Not. Roy. Astron. Soc.*, 374:2–15, 2007.

[198] N. Chandrachani Devi, J. E. Gonzalez, and J. S. Alcaniz. Constraining thawing and freezing models with cluster number counts. *JCAP*, 1406:055, 2014.

[199] Suman Bhattacharya, Katrin Heitmann, Martin White, Zarija Lukic, Christian Wagner, and Salman Habib. Mass Function Predictions Beyond LCDM. *Astrophys. J.*, 732:122, 2011.

[200] J. E. Carlstrom et al. The 10 Meter South Pole Telescope. *Publ. Astron. Soc. Pac.*, 123:568–581, 2011.

[201] L. E. Bleem et al. Galaxy Clusters Discovered via the Sunyaev-Zel'dovich Effect in the 2500-square-degree SPT-SZ survey. *Astrophys. J. Suppl.*, 216(2):27, 2015.

[202] R. A. Sunyaev and Ya. B. Zeldovich. The Observations of relic radiation as a test of the nature of X-Ray radiation from the clusters of galaxies. *Comments Astrophys. Space Phys.*, 4:173–178, 1972.

[203] K. K. Schaffer et al. The First Public Release of South Pole Telescope Data: Maps of a 95-square-degree Field from 2008 Observations. *Astrophys. J.*, 743:90, 2011.

[204] T. de Haan et al. Cosmological Constraints from Galaxy Clusters in the 2500 square-degree SPT-SZ Survey. *Astrophys. J.*, 832(1):95, 2016.

[205] S. Bocquet et al. Cluster Cosmology Constraints from the 2500 deg^2 SPT-SZ Survey: Inclusion of Weak Gravitational Lensing Data from Magellan and the Hubble Space Telescope. *Astrophys. J.*, 878(1):55, 2019.

[206] K. Vanderlinde et al. GALAXY CLUSTERS SELECTED WITH THE SUNYAEV ZELDOVICH EFFECT FROM 2008 SOUTH POLE TELESCOPE OBSERVATIONS. *The Astrophysical Journal*, 722(2):1180–1196, sep 2010.

[207] K. Story et al. South Pole Telescope Detections of the Previously Unconfirmed Planck Early SZ Clusters in the Southern Hemisphere. *Astrophys. J.*, 735(2):L36, 2011.

[208] S. Basilakos, M. Plionis, and J. A. S. Lima. Confronting Dark Energy Models using Galaxy Cluster Number Counts. *Phys. Rev.*, D82:083517, 2010.

[209] C. Fedeli, L. Moscardini, and S. Matarrese. The clustering of galaxy clusters in cosmological models with non-Gaussian initial conditions: Predictions for future surveys. *Mon. Not. Roy. Astron. Soc.*, 397:1125–1137, 2009.

[210] C. Fedeli, L. Moscardini, and M. Bartelmann. Observing the clustering properties of galaxy clusters in dynamical-dark energy cosmologies. *Astron. Astrophys.*, 500:667–679, 2009.

[211] A. Merloni et al. eROSITA Science Book: Mapping the Structure of the Energetic Universe. 2012.

[212] Bruno J. Barros, Tiago Barreiro, Tomi Koivisto, and Nelson J. Nunes. Testing $F(Q)$ gravity with redshift space distortions. *Phys. Dark Univ.*, 30:100616, 2020.

[213] Jose Beltrán Jiménez, Lavinia Heisenberg, and Tomi S. Koivisto. The Geometrical Trinity of Gravity. *Universe*, 5(7):173, 2019.

[214] Friedrich W. Hehl, J.Dermott McCrea, Eckehard W. Mielke, and Yuval Ne'eman. Metric affine gauge theory of gravity: Field equations, Noether identities, world spinors, and breaking of dilation invariance. *Phys. Rept.*, 258:1–171, 1995.

[215] Jose Beltrán Jiménez, Lavinia Heisenberg, and Tomi Koivisto. Coincident General Relativity. *Phys. Rev.*, D98(4):044048, 2018.

[216] Ruth Lazkoz, Francisco S. N. Lobo, María Ortiz-Baños, and Vincenzo Salzano. Observational constraints of $f(Q)$ gravity. *Phys. Rev.*, D100(10):104027, 2019.

[217] Jose Beltrán Jiménez, Lavinia Heisenberg, Tomi Sebastian Koivisto, and Simon Pekar. Cosmology in $f(Q)$ geometry. 2019.

[218] Jianbo Lu, Xin Zhao, and Guoying Chee. Cosmology in symmetric teleparallel gravity and its dynamical system. *Eur. Phys. J.*, C79(6):530, 2019.

[219] James M. Nester and Hwei-Jang Yo. Symmetric teleparallel general relativity. *Chin. J. Phys.*, 37:113, 1999.

[220] Muzaffer Adak, M. Kalay, and Ozcan Sert. Lagrange formulation of the symmetric teleparallel gravity. *Int. J. Mod. Phys. D*, 15:619–634, 2006.

[221] Muzaffer Adak. The Symmetric teleparallel gravity. *Turk. J. Phys.*, 30:379–390, 2006.

[222] Muzaffer Adak, Ozcan Sert, Mestan Kalay, and Murat Sari. Symmetric Teleparallel Gravity: Some exact solutions and spinor couplings. *Int. J. Mod. Phys.*, A28:1350167, 2013.

[223] Muzaffer Adak. Gauge Approach to The Symmetric Teleparallel Gravity. *Int. J. Geom. Meth. Mod. Phys.*, 15(12):1850198, 2018.

[224] Konstantinos F. Dialektopoulos, Tomi S. Koivisto, and Salvatore Capozziello. Noether symmetries in Symmetric Teleparallel Cosmology. *Eur. Phys. J.*, C79(7):606, 2019.

[225] Tiberiu Harko, Tomi S. Koivisto, Francisco S. N. Lobo, Gonzalo J. Olmo, and Diego Rubiera-Garcia. Coupling matter in modified Q gravity. *Phys. Rev.*, D98(8):084043, 2018.

[226] Yixin Xu, Guangjie Li, Tiberiu Harko, and Shi-Dong Liang. $f(Q,T)$ gravity. *Eur. Phys. J. C*, 79(8):708, 2019.

[227] Laur Järv, Mihkel Rünkla, Margus Saal, and Ott Vilson. Nonmetricity formulation of general relativity and its scalar-tensor extension. *Phys. Rev.*, D97(12):124025, 2018.

[228] Mihkel Rünkla and Ott Vilson. Family of scalar-nonmetricity theories of gravity. *Phys. Rev.*, D98(8):084034, 2018.

[229] Viktor Gakis, Martin Krˇ sšák, Jackson Levi Said, and Emmanuel N. Saridakis. Conformal gravity and transformations in the symmetric teleparallel framework. *Phys. Rev. D*, 101(6):064024, 2020.

[230] Aindriú Conroy and Tomi Koivisto. The spectrum of symmetric teleparallel gravity. *Eur. Phys. J.*, C78(11):923, 2018.

[231] Ismail Soudi, Gabriel Farrugia, Viktor Gakis, Jackson Levi Said, and Emmanuel N. Saridakis. Polarization of gravitational waves in symmetric teleparallel theories of gravity and their modifications. *Phys. Rev.*, D100(4):044008, 2019.

[232] Manuel Hohmann. Polarization of gravitational waves in general teleparallel theories of gravity. *Astron. Rep.*, 62(12):890–897, 2018.

[233] Manuel Hohmann, Christian Pfeifer, Jackson Levi Said, and Ulbossyn Ualikhanova. Propagation of gravitational waves in symmetric teleparallel gravity theories. *Phys. Rev.*, D99(2):024009, 2019.

[234] Aindriú Conroy and Tomi Koivisto. Parity-Violating Gravity and GW170817 in Non-Riemannian Cosmology. *JCAP*, 12(12):016, 2019.

[235] Wen Zhao, Tao Zhu, Jin Qiao, and Anzhong Wang. Waveform of gravitational waves in the general parity-violating gravities. *Phys. Rev. D*, 101(2):024002, 2020.

[236] Mordehai Milgrom. Noncovariance at low accelerations as a route to MOND. *Phys. Rev.*, D100(8):084039, 2019.

[237] Fabio D'Ambrosio, Mudit Garg, and Lavinia Heisenberg. Non-linear extension of non-metricity scalar for MOND. 4 2020.

[238] Bryan Sagredo, Savvas Nesseris, and Domenico Sapone. Internal Robustness of Growth Rate data. *Phys. Rev.*, D98(8):083543, 2018.

[239] Amine Bouali, Imanol Albarran, Mariam Bouhmadi-López, and Taoufik Ouali. Cosmological constraints of phantom dark energy models. *Phys. Dark Univ.*, 26:100391, 2019.

[240] Bryan Sagredo, Javier Silva Lafaurie, and Domenico Sapone. Comparing Dark Energy models with Hubble versus Growth Rate data. 2018.

[241] Lavrentios Kazantzidis and Leandros Perivolaropoulos. Evolution of the $f\sigma_8$ tension with the Planck15/ΛCDM determination and implications for modified gravity theories. *Phys. Rev.*, D97(10):103503, 2018.

[242] H. Akaike. A new look at the statistical model identification. *IEEE Transactions on Automatic Control*, 19(6):716–723, December 1974.

[243] Kenneth P. Burnham and David R. Anderson. Multimodel inference: Understanding aic and bic in model selection. *Sociological Methods & Research*, 33(2):261–304, 2004.

[244] Chunlong Li, Sheng-Feng Yan, Lingqin Xue, Xin Ren, Yi-Fu Cai, Damien A. Easson, Ye-Fei Yuan, and Hongsheng Zhao. Testing the equivalence principle via the shadow of black holes. *Phys. Rev. Res.*, 2:023164, 2020.

[245] Zhaoting Chen, Wentao Luo, Yi-Fu Cai, and Emmanuel N. Saridakis. New test on General Relativity using galaxy-galaxy lensing with astronomical surveys. 7 2019.

[246] Bruno J. Barros and Francisco S.N. Lobo. Wormhole geometries supported by three-form fields. *Phys. Rev. D*, 98(4):044012, 2018.

[247] Pitayuth Wongjun. Generalized Three-Form Field. *J. Phys. Conf. Ser.*, 883(1):012002, 2017.

[248] Tomi S. Koivisto and Nelson J. Nunes. Three-form cosmology. *Phys. Lett.*, B685:105–109, 2010.

[249] João Morais, Mariam Bouhmadi-López, K. Sravan Kumar, João Marto, and Yaser Tavak. Interacting 3-form dark energy models: distinguishing interactions and avoiding the Little Sibling of the Big Rip. *Phys. Dark Univ.*, 15:7–30, 2017.

[250] Tomi S. Koivisto and Nelson J. Nunes. Coupled three-form dark energy. *Phys. Rev.*, D88(12):123512, 2013.

[251] Tomi S. Koivisto and Nelson J. Nunes. Inflation and dark energy from three-forms. *Phys. Rev.*, D80:103509, 2009.

[252] Tomi S. Koivisto, David F. Mota, and Cyril Pitrou. Inflation from N-Forms and its stability. *JHEP*, 09:092, 2009.

[253] K. Sravan Kumar, David J. Mulryne, Nelson J. Nunes, João Marto, and Paulo Vargas Moniz. Non-Gaussianity in multiple three-form field inflation. *Phys. Rev.*, D94(10):103504, 2016.

[254] Antonio De Felice, Khamphee Karwan, and Pitayuth Wongjun. Stability of the 3-form field during inflation. *Phys. Rev.*, D85:123545, 2012.

[255] Antonio De Felice, Khamphee Karwan, and Pitayuth Wongjun. Reheating in 3-form inflation. *Phys. Rev.*, D86:103526, 2012.

[256] K. Sravan Kumar, J. Marto, Nelson J. Nunes, and P. Vargas Moniz. Inflation in a two 3-form fields scenario. *JCAP*, 1406:064, 2014.

[257] Tomi S. Koivisto and Federico R. Urban. Three-magnetic fields. *Phys. Rev. D*, 85:083508, 2012.

[258] Bruno J. Barros and Nelson J. Nunes. Three-form inflation in type II Randall-Sundrum. *Phys. Rev.*, D93(4):043512, 2016.

[259] Tiago Barreiro, Ugo Bertello, and Nelson J. Nunes. Screening three-form fields. *Phys. Lett.*, B773:417–421, 2017.

[260] Neil Turok and S. W. Hawking. Open inflation, the four form and the cosmological constant. *Phys. Lett.*, B432:271–278, 1998.

[261] David J. Mulryne, Johannes Noller, and Nelson J. Nunes. Three-form inflation and non-Gaussianity. *JCAP*, 12:016, 2012.

[262] Cristiano Germani and Alex Kehagias. P-nflation: generating cosmic Inflation with p-forms. *JCAP*, 03:028, 2009.

[263] M. S. Morris and K. S. Thorne. Wormholes in space-time and their use for interstellar travel: A tool for teaching general relativity. *Am. J. Phys.*, 56:395–412, 1988.

[264] Matt Visser. *Lorentzian wormholes: From Einstein to Hawking*. 1995.

[265] L. Flamm. Beitrage zur Einsteinschen Gravitationstheorie. *Phys. Z.*, 17(448), 1916.

[266] Karl Schwarzschild. Über das Gravitationsfeld eines Massenpunktes nach der Einsteinschen Theorie. *Sitzungsberichte der Königlich Preußischen Akademie der Wissenschaften (Berlin*, pages 189–196, January 1916.

[267] A. Einstein and N. Rosen. The particle problem in the general theory of relativity. *Phys. Rev.*, 48:73–77, Jul 1935.

[268] J. A. Wheeler. Geons. *Phys. Rev.*, 97:511–536, 1955.

[269] Charles W. Misner and John A. Wheeler. Classical physics as geometry: Gravitation, electromagnetism, unquantized charge, and mass as properties of curved empty space. *Annals Phys.*, 2:525–603, 1957.

[270] H. G. Ellis. Ether flow through a drainhole - a particle model in general relativity. *J. Math. Phys.*, 14:104–118, 1973.

[271] K. A. Bronnikov. Scalar-tensor theory and scalar charge. *Acta Phys. Polon.*, B4:251–266, 1973.

[272] Francisco S. N. Lobo. Wormholes, Warp Drives and Energy Conditions. *Fundam. Theor. Phys.*, 189:pp.–, 2017.

[273] Francisco S. N. Lobo. Energy conditions, traversable wormholes and dust shells. *Gen. Rel. Grav.*, 37:2023–2038, 2005.

[274] Erik Curiel. A Primer on Energy Conditions. *Einstein Stud.*, 13:43–104, 2017.

[275] Carlos Barcelo and Matt Visser. Scalar fields, energy conditions, and traversable wormholes. *Class. Quant. Grav.*, 17:3843–3864, 2000.

[276] Tiberiu Harko, Francisco S. N. Lobo, M. K. Mak, and Sergey V. Sushkov. Modified-gravity wormholes without exotic matter. *Phys. Rev.*, D87(6):067504, 2013.

[277] Francisco S. N. Lobo and Miguel A. Oliveira. Wormhole geometries in f(R) modified theories of gravity. *Phys. Rev.*, D80:104012, 2009.

[278] Francisco S. N. Lobo. General class of wormhole geometries in conformal Weyl gravity. *Class. Quant. Grav.*, 25:175006, 2008.

[279] Christian G. Boehmer, Tiberiu Harko, and Francisco S. N. Lobo. Wormhole geometries in modified teleparralel gravity and the energy conditions. *Phys. Rev.*, D85:044033, 2012.

[280] Nadiezhda Montelongo Garcia and Francisco S. N. Lobo. Wormhole geometries supported by a nonminimal curvature-matter coupling. *Phys. Rev.*, D82:104018, 2010.

[281] Nadiezhda Montelongo Garcia and Francisco S. N. Lobo. Nonminimal curvature-matter coupled wormholes with matter satisfying the null energy condition. *Class. Quant. Grav.*, 28:085018, 2011.

[282] Mohammad Reza Mehdizadeh, Mahdi Kord Zangeneh, and Francisco S. N. Lobo. Einstein-Gauss-Bonnet traversable wormholes satisfying the weak energy condition. *Phys. Rev.*, D91(8):084004, 2015.

[283] João Luís Rosa, José P.S. Lemos, and Francisco S.N. Lobo. Wormholes in generalized hybrid metric-Palatini gravity obeying the matter null energy condition everywhere. *Phys. Rev. D*, 98(6):064054, 2018.

[284] Salvatore Capozziello, Tiberiu Harko, Tomi S. Koivisto, Francisco S. N. Lobo, and Gonzalo J. Olmo. Wormholes supported by hybrid metric-Palatini gravity. *Phys. Rev.*, D86:127504, 2012.

[285] Luke M. Butcher. Traversable Wormholes and Classical Scalar Fields. *Phys. Rev.*, D91(12):124031, 2015.

[286] Stanislav Hledik, Zdenek Stuchlik, and Alois Cipko. Visualizing spacetimes via embedding diagrams. In *11th Marcel Grossmann Meeting on General Relativity*, pages 2299–2301, 1 2007.

[287] S. W. Hawking and G. F. R. Ellis. *The Large Scale Structure of Space-Time*. Cambridge Monographs on Mathematical Physics. Cambridge University Press, 2011.

[288] Eleni-Alexandra Kontou and Ko Sanders. Energy conditions in general relativity and quantum field theory. *Classical and Quantum Gravity*, May 2020.

[289] Pitayuth Wongjun. Perfect fluid in Lagrangian formulation due to generalized three-form field. *Phys. Rev. D*, 96(2):023516, 2017.

[290] Francisco S. N. Lobo. Phantom energy traversable wormholes. *Phys. Rev.*, D71:084011, 2005.

[291] Jose' P. S. Lemos, Francisco S. N. Lobo, and Sergio Quinet de Oliveira. Morris-Thorne wormholes with a cosmological constant. *Phys. Rev.*, D68:064004, 2003.

[292] Burkhard Kleihaus and Jutta Kunz. Rotating Wormholes. *Fundam. Theor. Phys.*, 189:35–61, 2017.

[293] Burkhard Kleihaus and Jutta Kunz. Rotating Ellis Wormholes in Four Dimensions. *Phys. Rev.*, D90:121503, 2014.

[294] Sayan Kar and Deshdeep Sahdev. Evolving Lorentzian wormholes. *Phys. Rev.*, D53:722–730, 1996.

[295] Aaron V. B. Arellano and Francisco S. N. Lobo. Evolving wormhole geometries within nonlinear electrodynamics. *Class. Quant. Grav.*, 23:5811–5824, 2006.

[296] Francisco S. N. Lobo. Exotic solutions in General Relativity: Traversable wormholes and 'warp drive' spacetimes. In *Classical and Quantum Gravity Research, 1-78, (2008), Nova Sci. Pub. ISBN 978-1-60456-366-5*. 2007.

[297] K. A. Bronnikov. Nonlinear electrodynamics, regular black holes and wormholes. *Int. J. Mod. Phys.*, D27(06):1841005, 2018.

[298] Bruno J. Barros, Elsa M. Teixeira, and Daniele Vernieri. Bouncing cosmology in $f(R, \mathcal{G})$ gravity by order reduction. *Annals Phys.*, 419:168231, 2020.

[299] Claus Kiefer. *Quantum Gravity*. Oxford University Press, New York, 2nd ed edition, 2007.

[300] Martin Bojowald. Loop quantum cosmology. *Living Rev. Rel.*, 8:11, 2005.

[301] Abhay Ashtekar and Parampreet Singh. Loop Quantum Cosmology: A Status Report. *Class. Quant. Grav.*, 28:213001, 2011.

[302] Shinji Tsujikawa, Parampreet Singh, and Roy Maartens. Loop quantum gravity effects on inflation and the CMB. *Class. Quant. Grav.*, 21:5767–5775, 2004.

[303] Martin Bojowald, James E. Lidsey, David J. Mulryne, Parampreet Singh, and Reza Tavakol. Inflationary cosmology and quantization ambiguities in semiclassical loop quantum gravity. *Phys. Rev. D*, 70:043530, 2004.

[304] Parampreet Singh and Alexey Toporensky. Big crunch avoidance in K=1 semiclassical loop quantum cosmology. *Phys. Rev. D*, 69:104008, 2004.

[305] Martin Bojowald. Absence of singularity in loop quantum cosmology. *Phys. Rev. Lett.*, 86:5227–5230, 2001.

[306] Martin Bojowald, Roy Maartens, and Parampreet Singh. Loop quantum gravity and the cyclic universe. *Phys. Rev. D*, 70:083517, 2004.

[307] Abhay Ashtekar, Tomasz Pawlowski, and Parampreet Singh. Quantum Nature of the Big Bang: Improved dynamics. *Phys. Rev.*, D74:084003, 2006.

[308] Robert H. Brandenberger. The Matter Bounce Alternative to Inflationary Cosmology. 6 2012.

[309] S.D. Odintsov and V.K. Oikonomou. Matter Bounce Loop Quantum Cosmology from $F(R)$ Gravity. *Phys. Rev. D*, 90(12):124083, 2014.

[310] S.D. Odintsov and V.K. Oikonomou. Big-Bounce with Finite-time Singularity: The $F(R)$ Gravity Description. *Int. J. Mod. Phys. D*, 26(08):1750085, 2017.

[311] S.D. Odintsov and V.K. Oikonomou. Deformed Matter Bounce with Dark Energy Epoch. *Phys. Rev. D*, 94(6):064022, 2016.

[312] Victor Taveras. Corrections to the Friedmann Equations from LQG for a Universe with a Free Scalar Field. *Phys. Rev.*, D78:064072, 2008.

[313] Kinjal Banerjee, Gianluca Calcagni, and Mercedes Martin-Benito. Introduction to loop quantum cosmology. *SIGMA*, 8:016, 2012.

[314] Salvatore Capozziello and Mauro Francaviglia. Extended Theories of Gravity and their Cosmological and Astrophysical Applications. *Gen. Rel. Grav.*, 40:357–420, 2008.

[315] S. Nojiri, S.D. Odintsov, and V.K. Oikonomou. Modified Gravity Theories on a Nutshell: Inflation, Bounce and Late-time Evolution. *Phys. Rept.*, 692:1–104, 2017.

[316] Antonio De Felice and Teruaki Suyama. Vacuum structure for scalar cosmological perturbations in Modified Gravity Models. *JCAP*, 0906:034, 2009.

[317] S. D. Odintsov, V. K. Oikonomou, and S. Banerjee. Dynamics of inflation and dark energy from $F(R, G)$ gravity. *Nucl. Phys.*, B938:935–956, 2019.

[318] S.D. Odintsov, V.K. Oikonomou, and F.P. Fronimos. Rectifying Einstein-Gauss-Bonnet Inflation in View of GW170817. 3 2020.

[319] M. Alimohammadi and A. Ghalee. Remarks on generalized Gauss-Bonnet dark energy. *Phys. Rev.*, D79:063006, 2009.

[320] E. Elizalde, R. Myrzakulov, V. V. Obukhov, and D. Saez-Gomez. LambdaCDM epoch reconstruction from F(R,G) and modified Gauss-Bonnet gravities. *Class. Quant. Grav.*, 27:095007, 2010.

[321] Kazuharu Bamba, Sergei D. Odintsov, Lorenzo Sebastiani, and Sergio Zerbini. Finite-time future singularities in modified Gauss-Bonnet and F(R,G) gravity and singularity avoidance. *Eur. Phys. J.*, C67:295–310, 2010.

[322] Antonio De Felice, Jean-Marc Gerard, and Teruaki Suyama. Cosmological perturbation in f(R,G) theories with a perfect fluid. *Phys. Rev.*, D82:063526, 2010.

[323] Antonio De Felice and Takahiro Tanaka. Inevitable ghost and the degrees of freedom in f(R,G) gravity. *Prog. Theor. Phys.*, 124:503–515, 2010.

[324] Mariafelicia De Laurentis, Mariacristina Paolella, and Salvatore Capozziello. Cosmological inflation in $F(R, \mathcal{G})$ gravity. *Phys. Rev.*, D91(8):083531, 2015.

[325] L. Bel and H. Sirousse Zia. Regular reduction of relativistic theories of gravitation with a quadratic Lagrangian. *Phys. Rev.*, D32:3128–3135, 1985.

[326] Jonathan Z. Simon. Higher Derivative Lagrangians, Nonlocality, Problems and Solutions. *Phys. Rev.*, D41:3720, 1990.

[327] Jonathan Z. Simon. No Starobinsky inflation from selfconsistent semiclassical gravity. *Phys. Rev.*, D45:1953–1960, 1992.

[328] Thomas P. Sotiriou. Covariant Effective Action for Loop Quantum Cosmology from Order Reduction. *Phys. Rev.*, D79:044035, 2009.

[329] Inês Terrucha, Daniele Vernieri, and José P. S. Lemos. Covariant action for bouncing cosmologies in modified Gauss–Bonnet gravity. *Annals Phys.*, 404:39–46, 2019.

[330] Gonzalo J. Olmo and Parampreet Singh. Effective Action for Loop Quantum Cosmology a la Palatini. *JCAP*, 0901:030, 2009.

[331] David Langlois, Hongguang Liu, Karim Noui, and Edward Wilson-Ewing. Effective loop quantum cosmology as a higher-derivative scalar-tensor theory. *Class. Quant. Grav.*, 34(22):225004, 2017.

[332] David Lovelock and Hanno Rund. *Tensors, differential forms, and variational principles*. Dover Books on Mathematics. Dover, New York, NY, 1989. Originally published: New York : Wiley, 1975.

[333] Sean M. Carroll. *Spacetime and Geometry*. Cambridge University Press, 7 2019.

[334] R. d'Inverno. *Introducing Einstein's relativity*. 1992.

[335] M. Alimohammadi and A. Ghalee. The Phase-space of generalized Gauss-Bonnet dark energy. *Phys. Rev.*, D80:043006, 2009.

[336] Alvaro de la Cruz-Dombriz and Diego Saez-Gomez. On the stability of the cosmological solutions in $f(R, G)$ gravity. *Class. Quant. Grav.*, 29:245014, 2012.

[337] Eleonora Di Valentino et al. Cosmology Intertwined I: Perspectives for the Next Decade. 8 2020.

[338] Eleonora Di Valentino, Daniel E. Holz, Alessandro Melchiorri, and Fabrizio Renzi. The cosmological impact of future constraints on H_0 from gravitational-wave standard sirens. *Phys. Rev. D*, 98(8):083523, 2018.

[339] Hsin-Yu Chen, Maya Fishbach, and Daniel E. Holz. A two per cent Hubble constant measurement from standard sirens within five years. *Nature*, 562(7728):545–547, 2018.

[340] Mario G. Santos et al. Cosmology from a SKA HI intensity mapping survey. *PoS*, AASKA14:019, 2015.

[341] Philip Bull, Stefano Camera, Alvise Raccanelli, Chris Blake, Pedro G. Ferreira, Mario G. Santos, and Dominik J. Schwarz. Measuring baryon acoustic oscillations with future SKA surveys. 1 2015.

[342] Eleonora Di Valentino et al. Cosmology Intertwined IV: The Age of the Universe and its Curvature. 8 2020.

Appendix A

Kinetically coupled dark energy

Let us consider the action Eq. (2.1.1). By Hamilton's principle, the dynamics of ϕ will be such that the action is minimized,

$$\delta\mathcal{S} = \delta S_\phi + \delta S_m = \int \omega_g \frac{\delta P(\phi, X)}{\delta\phi}\delta\phi + \int \omega_g \frac{\delta\left[f(\phi, X)\tilde{\mathcal{L}}_m\right]}{\delta\phi}\delta\phi = 0\,, \tag{A.0.1}$$

with $X = -(1/2)g^{\alpha\beta}\nabla_\alpha\phi\nabla_\beta\phi$.

Let us consider the first term, which is a standard k-essence action,

$$\delta S_\phi = \int \omega_g \frac{\delta P(\phi, X)}{\delta\phi}\delta\phi = \int \omega_g \left[\frac{\partial P(\phi, X)}{\partial\phi}\delta\phi + \frac{\partial P(\phi, X)}{\partial X}\frac{\partial X}{\partial(\nabla_\mu\phi)}\delta(\nabla_\mu\phi)\right]\,. \tag{A.0.2}$$

Noting that,

$$\frac{\partial X}{\partial(\nabla_\mu\phi)} = -\frac{1}{2}g^{\alpha\beta}\left(\delta^\mu_\alpha\nabla_\beta\phi + \delta^\mu_\beta\nabla_\alpha\phi\right) = -g^{\mu\alpha}\nabla_\alpha\phi\,, \tag{A.0.3}$$

we have

$$\begin{aligned}\delta S_\phi &= \int \omega_g \left[\frac{\partial P(\phi, X)}{\partial\phi}\delta\phi + \frac{\partial P(\phi, X)}{\partial X}\frac{\partial X}{\partial(\nabla_\mu\phi)}\delta(\nabla_\mu\phi)\right] \\ &= \int \omega_g \left[P_{,\phi}\delta\phi - P_{,X}g^{\mu\alpha}\nabla_\alpha\phi\delta(\nabla_\mu\phi)\right]\,.\end{aligned} \tag{A.0.4}$$

Using the relation $\delta(\nabla_\mu\phi) = \nabla_\mu(\delta\phi)$ and integrating the last term by parts

$$\begin{aligned}\delta S_\phi &= \int \omega_g \left[P_{,\phi}\delta\phi - P_{,X}g^{\mu\alpha}\nabla_\alpha\phi\,\delta(\nabla_\mu\phi)\right] \\ &= \int \omega_g \left[P_{,\phi}\delta\phi - \nabla_\mu\left(P_{,X}g^{\mu\alpha}\nabla_\alpha\phi\,\delta\phi\right) + \nabla_\mu\left(P_{,X}g^{\mu\alpha}\nabla_\alpha\phi\right)\delta\phi\right]\,.\end{aligned} \tag{A.0.5}$$

Assuming now that the field vanishes at the boundary (*i.e.* at infinity), using Stokes theorem, the middle term vanishes. Hence

$$\begin{aligned}\delta S_\phi &= \int \omega_g \left[P_{,\phi} + \nabla_\mu \left(P_{,X} g^{\mu\alpha}\nabla_\alpha\phi\right)\right]\delta\phi \\ &= \int \omega_g \left[P_{,\phi} + \left(P_{,X,\phi}\nabla_\mu\phi + P_{,XX}\nabla_\mu X\right) g^{\mu\alpha}\nabla_\alpha\phi + P_{,X} g^{\mu\alpha}\nabla_\mu\nabla_\alpha\phi\right]\delta\phi\,,\end{aligned} \tag{A.0.6}$$

where we have used the metricity condition $\nabla_\mu g^{\mu\alpha} = 0$. Now,

$$\nabla_\mu X = -\frac{1}{2} g^{\gamma\beta}\left(\nabla_\mu\nabla_\gamma\phi\nabla_\beta\phi + \nabla_\gamma\phi\nabla_\mu\nabla_\beta\phi\right) = -g^{\gamma\beta}\nabla_\gamma\phi\nabla_\mu\nabla_\beta\phi\,, \tag{A.0.7}$$

where we have used that fact that the metric is symmetric, *i.e.* $g^{\gamma\beta} = g^{\beta\gamma}$. Noting that $g^{\mu\alpha}\nabla_\mu\nabla_\alpha\phi = \Box\phi$, being $\Box$ the d'Alembert operator, we may write,

$$\begin{aligned}\delta S_\phi &= \int \omega_g \left(P_{,\phi} + P_{,X\phi} g^{\mu\alpha}\nabla_\mu\phi\nabla_\alpha\phi - P_{,XX} g^{\gamma\beta} g^{\mu\alpha}\nabla_\alpha\phi\nabla_\gamma\phi\nabla_\mu\nabla_\beta\phi + P_{,X}\Box\phi\right)\delta\phi \\ &= \int \omega_g \left(P_{,\phi} + P_{,X}\Box\phi - 2P_{,X\phi}X - P_{,XX}\partial^\alpha\phi\,\partial_\beta\phi\,\nabla_\alpha\partial^\beta\phi\right)\delta\phi\,.\end{aligned} \tag{A.0.8}$$

The second term in Eq. (A.0.1) gives

$$\begin{aligned}\delta S_m &= \int \omega_g \frac{\delta\left[f(\phi,X)\tilde{\mathcal{L}}_m\right]}{\delta\phi}\delta\phi = \int \omega_g \left[f_{,\phi}\,\delta\phi\tilde{\mathcal{L}}_m + f_{,X}\frac{\partial X}{\partial(\nabla_\mu\phi)}\delta(\nabla_\mu\phi)\tilde{\mathcal{L}}_m\right] \\ &= \int \omega_g \left[f_{,\phi}\,\delta\phi\tilde{\mathcal{L}}_m - f_{,X} g^{\mu\alpha}\nabla_\alpha\phi\,\delta(\nabla_\mu\phi)\tilde{\mathcal{L}}_m\right]\,,\end{aligned} \tag{A.0.9}$$

which integrating by parts the last term results in

$$\delta S_m = \int \omega_g \left[f_{,\phi}\,\delta\phi\tilde{\mathcal{L}}_m - \nabla_\mu\left(f_{,X} g^{\mu\alpha}\nabla_\alpha\phi\,\delta\phi\,\tilde{\mathcal{L}}_m\right) + \nabla_\mu\left(f_{,X} g^{\mu\alpha}\nabla_\alpha\phi\,\tilde{\mathcal{L}}_m\right)\delta\phi\right]\,. \tag{A.0.10}$$

Using Stokes theorem the middle term vanishes,

$$\delta S_m = \int \omega_g \left\{\tilde{\mathcal{L}}_m\left[f_{,\phi} + \nabla_\mu\left(f_{,X} g^{\mu\alpha}\nabla_\alpha\phi\right)\right]\delta\phi + f_{,X} g^{\mu\alpha}\nabla_\alpha\phi\nabla_\mu\tilde{\mathcal{L}}_m\,\delta\phi\right\}\,. \tag{A.0.11}$$

Noting that the first term inside square brackets is equal to the one in Eq. (A.0.6), with $P \to f$,

we can, analogously, substitute it using the result Eq. (A.0.8)

$$\delta S_m = \int \omega_g \left\{ \tilde{\mathcal{L}}_m \left[f_{,\phi} + f_{,X}\Box\phi - 2f_{,X\phi}X - f_{,XX}\partial^\alpha\phi\,\partial_\beta\phi\,\nabla_\alpha\partial^\beta\phi \right] + f_{,X}\partial^\mu\phi\nabla_\mu\tilde{\mathcal{L}}_m \right\} \delta\phi\,. \tag{A.0.12}$$

Gathering the results for the variation of both the scalar and matter Lagrangians, Eqs. (A.0.8) and (A.0.12), and substituting on Eq. (A.0.1), assuming that the action is stationary for every variation $\delta\phi$, gives the equation of motion for the scalar field ϕ:

$$\begin{aligned} &P_{,\phi} + P_{,X}\Box\phi - 2P_{,X\phi}X - P_{,XX}\partial^\alpha\phi\,\partial_\beta\phi\,\nabla_\alpha\partial^\beta\phi = \\ &-\tilde{\mathcal{L}}_m \left(f_{,\phi} + f_{,X}\Box\phi - 2f_{,X\phi}X - f_{,XX}\partial^\alpha\phi\,\partial_\beta\phi\,\nabla_\alpha\partial^\beta\phi \right) - f_{,X}\partial^\mu\phi\nabla_\mu\tilde{\mathcal{L}}_m\,. \end{aligned} \tag{A.0.13}$$

Defining $\mathcal{L}_m = f\tilde{\mathcal{L}}_m$, the term

$$\begin{aligned} \nabla_\mu\tilde{\mathcal{L}}_m &= \nabla_\mu\left(\frac{\mathcal{L}_m}{f}\right) = \frac{\nabla_\mu\mathcal{L}_m}{f} - \mathcal{L}_m\left(\frac{f_{,\phi}}{f^2}\nabla_\mu\phi + \frac{f_{,X}}{f^2}\nabla_\mu X\right) \\ &= \frac{\nabla_\mu\mathcal{L}_m}{f} - \mathcal{L}_m\left(\frac{f_{,\phi}}{f^2}\nabla_\mu\phi - \frac{f_{,X}}{f^2}g^{\gamma\beta}\nabla_\gamma\phi\nabla_\mu\nabla_\beta\phi\right) \\ &= \frac{\nabla_\mu\mathcal{L}_m}{f} + \frac{\mathcal{L}_m}{f}\left(\frac{f_{,X}}{f}\partial_\alpha\phi\nabla_\mu\partial^\alpha\phi - \frac{f_{,\phi}}{f}\partial_\mu\phi\right)\,, \end{aligned} \tag{A.0.14}$$

which substituting into the rhs of Eq. (A.0.13), gives, finally

$$P_{,\phi} + P_{,X}\Box\phi - 2P_{,X\phi}X - P_{,XX}\partial^\alpha\phi\,\partial_\beta\phi\,\nabla_\alpha\partial^\beta\phi = \mathcal{L}_m\,Q\,, \tag{A.0.15}$$

where the coupling term is

$$\begin{aligned} Q = &-\mathcal{L}_m\left(\frac{f_{,\phi}}{f} + \frac{f_{,X}}{f}\Box\phi - 2\frac{f_{,X\phi}}{f}X - \frac{f_{,XX}}{f}\partial^\alpha\phi\,\partial_\beta\phi\,\nabla_\alpha\partial^\beta\phi\right) \\ &-\frac{f_{,X}}{f}\partial^\mu\phi\nabla_\mu\mathcal{L}_m - \frac{f_{,X}}{f}\partial^\mu\phi\mathcal{L}_m\left(\frac{f_{,X}}{f}\partial_\alpha\phi\nabla_\mu\partial^\alpha\phi - \frac{f_{,\phi}}{f}\partial_\mu\phi\right) \\ = &-\frac{f_{,\phi}}{f} - \frac{f_{,X}}{f}\left[\Box\phi + \partial^\alpha\phi\left(\frac{\nabla_\alpha\mathcal{L}_m}{\mathcal{L}_m} + \frac{f_{,X}}{f}\partial_\beta\phi\nabla_\alpha\partial^\beta\phi - \frac{f_{,\phi}}{f}\partial_\alpha\phi\right)\right] \\ &+ 2\frac{f_{,X\phi}}{f}X + \frac{f_{,XX}}{f}\partial^\alpha\phi\partial_\beta\phi\nabla_\alpha\partial^\beta\phi\,, \end{aligned} \tag{A.0.16}$$

or

$$P_{,\phi} + P_{,X}\Box\phi - 2P_{,X\phi}X - P_{,XX}A = \mathcal{L}_m\,Q\,, \tag{A.0.17}$$

where

$$Q = -\frac{f_{,\phi}}{f} - \frac{f_{,X}}{f}\left(\Box\phi + \partial^\alpha\phi\frac{\nabla_\alpha\mathcal{L}_m}{\mathcal{L}_m} + \frac{f_{,X}}{f}A + 2\frac{f_{,\phi}}{f}X\right) + 2\frac{f_{,X\phi}}{f}X + \frac{f_{,XX}}{f}A\,, \quad \text{(A.0.18)}$$

with $A := \partial^\alpha\phi\partial_\beta\phi\nabla_\alpha\partial^\beta\phi$.

A.1 FLRW background

Assuming an homogeneous quintessence field $\phi = \phi(t)$, we may write, at background level, assuming a FLRW metric:

$$X = -\frac{1}{2}g^{\alpha\beta}\partial_\alpha\phi\partial_\beta\phi = -\frac{1}{2}g^{00}\partial_0\phi\partial_0\phi = \frac{1}{2}\dot\phi^2 \quad \text{(A.1.1)}$$

$$\Box\phi = g^{\alpha\beta}\nabla_\alpha\partial_\beta\phi = g^{\alpha\beta}\partial_\alpha\partial_\beta\phi - g^{\alpha\beta}\Gamma^\gamma_{\alpha\beta}\partial_\gamma\phi = g^{00}\partial_0\partial_0\phi - \overbrace{g^{ii}}^{=1/a^2}\underbrace{\Gamma^0_{ii}}_{=a\dot a}\partial_0\phi$$

$$= -\ddot\phi - 3H\dot\phi \quad \text{(A.1.2)}$$

$$A = \partial^\alpha\phi\partial_\beta\phi\left(\partial_\alpha\partial^\beta\phi + \Gamma^\beta_{\alpha\mu}\partial^\mu\phi\right) = \partial^0\phi\partial_0\phi\left(\partial_0\partial^0\phi + \underbrace{\Gamma^0_{00}}_{=0}\partial^0\phi\right) = \dot\phi^2\ddot\phi \quad \text{(A.1.3)}$$

Thus, the equations of motion Eq. (A.0.17) become

$$P_{,\phi} - P_{,X}\left(\ddot\phi + 3H\dot\phi\right) - P_{,X\phi}\dot\phi^2 - P_{,XX}\dot\phi^2\ddot\phi = \mathcal{L}_m Q\,, \quad \text{(A.1.4)}$$

with

$$Q = -\frac{f_{,\phi}}{f} - \frac{f_{,X}}{f}\left(-\ddot\phi - 3H\phi + \dot\phi\frac{\dot{\mathcal{L}}_m}{\mathcal{L}_m} + \frac{f_{,X}}{f}\dot\phi^2\ddot\phi + \frac{f_{,\phi}}{f}\dot\phi^2\right) + \frac{f_{,X\phi}}{f}\dot\phi^2 + \frac{f_{,XX}}{f}\dot\phi^2\ddot\phi\,. \quad \text{(A.1.5)}$$

Appendix B

Connection decomposition

In standard GR, the Levi-Civita connection, $\tilde{\Gamma}$, is defined such as it is metric compatible, i.e.

$$\tilde{\nabla}\mathbf{g} = 0, \tag{B.0.1}$$

and torsion vanishes (it is torsion-free),

$$T(X,Y) = \tilde{\nabla}_X Y - \tilde{\nabla}_Y X - [X,Y] = 0, \tag{B.0.2}$$

for any vector fields X and Y, $[X,Y]$ denoting the Lie Bracket of X and Y (also a vector field). The condition Eq. (B.0.1) is refered to as *metricity condition*. The uniqueness of this connection, satisfying the properties Eqs. (B.0.1)-(B.0.2), is given by the *fundamental theorem of Riemannian geometry*. This is actually the connection which requires the least amount of geometrical structure to be defined, as it is completely determined by the metric $\mathbf{g}$. Regarding non-Riemannian geometries, we may introduce a generic connection ∇ on $T\mathcal{M}$. We can write the connections on a vector V^μ as,

$$\tilde{\nabla}_\mu V^\nu = \partial_\mu V^\nu + \tilde{\Gamma}^\nu{}_{\mu\alpha} V^\alpha, \tag{B.0.3}$$

$$\nabla_\mu V^\nu = \partial_\mu V^\nu + \Gamma^\nu{}_{\mu\alpha} V^\alpha, \tag{B.0.4}$$

where $\tilde{\Gamma}$ and Γ are the coefficients of the Levi-Civita and the general connection, respectively. We can now compute

$$\begin{aligned}\left(\nabla_\mu - \tilde{\nabla}_\mu\right) V^\nu &= \cancel{\partial_\mu V^\nu} + \Gamma^\nu{}_{\mu\alpha} V^\alpha - \cancel{\partial_\mu V^\nu} - \tilde{\Gamma}^\nu{}_{\mu\alpha} V^\alpha \\ &= \left(\Gamma^\nu{}_{\mu\alpha} - \tilde{\Gamma}^\nu{}_{\mu\alpha}\right) V^\alpha \\ &=: N^\nu{}_{\mu\alpha} V^\alpha. \end{aligned} \tag{B.0.5}$$

The object

$$N^\nu{}_{\mu\alpha} := \Gamma^\nu{}_{\mu\alpha} - \tilde{\Gamma}^\nu{}_{\mu\alpha}, \tag{B.0.6}$$

is a tensor, called the *distortion*, and represents the amount that ∇ deviates from its Levi-Civita part $\tilde{\nabla}$.

The *nonmetricity tensor* $Q_{\lambda\mu\nu}$ is defined as the covariant derivative of the metric tensor, and it can be written in terms of the distortion,

$$\begin{aligned} Q_{\lambda\mu\nu} &:= \nabla_\lambda g_{\mu\nu} \\ &= \partial_\lambda g_{\mu\nu} - \Gamma^\sigma{}_{\lambda\mu} g_{\sigma\nu} - \Gamma^\sigma{}_{\lambda\nu} g_{\mu\sigma} \\ &= \partial_\lambda g_{\mu\nu} - \left(N^\sigma{}_{\lambda\mu} + \tilde{\Gamma}^\sigma{}_{\lambda\mu}\right) g_{\sigma\nu} - \left(N^\sigma{}_{\lambda\nu} + \tilde{\Gamma}^\sigma{}_{\lambda\nu}\right) g_{\mu\sigma} \\ &= \overbrace{\cancel{\partial_\lambda g_{\mu\nu} - \tilde{\Gamma}^\sigma{}_{\lambda\mu} g_{\sigma\nu} - \tilde{\Gamma}^\sigma{}_{\lambda\nu} g_{\mu\sigma}}}^{\text{since } \tilde{\nabla}_\lambda g_{\mu\nu} = 0} - N^\sigma{}_{\lambda\mu} g_{\sigma\nu} - N^\sigma{}_{\lambda\nu} g_{\mu\sigma} \\ &= -N_{\nu\lambda\mu} - N_{\mu\lambda\nu}, \end{aligned} \tag{B.0.7}$$

where it was used Eq. (B.0.5). Note that the nonmetricity tensor is symmetric on the last two indices, i.e. $Q_{\lambda\mu\nu} = Q_{\lambda\nu\mu}$.

The *torsion tensor*, $T_{\lambda\mu\nu}$, is defined as the antisymmetric part of the connection, and can also be written in terms of the distortion,

$$\begin{aligned} T_{\lambda\mu\nu} &:= \Gamma_{\lambda\mu\nu} - \Gamma_{\lambda\nu\mu} \\ &= \Gamma_{\lambda\mu\nu} - \Gamma_{\lambda\nu\mu} - \tilde{\Gamma}_{\lambda\mu\nu} + \overbrace{\tilde{\Gamma}_{\lambda\mu\nu}}^{= -\tilde{\Gamma}_{\lambda\nu\mu}} \\ &= N_{\lambda\mu\nu} - N_{\lambda\nu\mu}, \end{aligned} \tag{B.0.8}$$

using the definition on Eq. (B.0.5). The torsion tensor is antisymmetric on the last two indices,

i.e. $T_{\lambda\mu\nu} = -T_{\lambda\nu\mu}$.

With some basic algebra, using only Eqs. (B.0.7) and (B.0.8), we can write the distortion as,

$$\begin{aligned}
N_{\lambda\mu\nu} &= \frac{1}{2}\left(T_{\lambda\mu\nu} + N_{\lambda\nu\mu}\right) + \frac{1}{2}\left(-Q_{\mu\lambda\nu} - N_{\nu\mu\lambda}\right) \\
&= \frac{1}{2}\left(T_{\lambda\mu\nu} - N_{\nu\mu\lambda}\right) + \frac{1}{2}\left(-Q_{\mu\lambda\nu} + N_{\lambda\nu\mu}\right) \\
&= \frac{1}{2}\left(T_{\lambda\mu\nu} - T_{\nu\mu\lambda} - N_{\nu\lambda\mu}\right) + \frac{1}{2}\left(-Q_{\mu\lambda\nu} - Q_{\nu\lambda\mu} - N_{\mu\nu\lambda}\right) \\
&= \frac{1}{2}\left(T_{\lambda\mu\nu} - T_{\nu\mu\lambda} - N_{\mu\nu\lambda}\right) + \frac{1}{2}\left(-Q_{\mu\lambda\nu} - Q_{\nu\lambda\mu} - N_{\nu\lambda\mu}\right) \\
&= \frac{1}{2}\left(T_{\lambda\mu\nu} - T_{\nu\mu\lambda} - T_{\mu\nu\lambda} - \cancel{N_{\mu\lambda\nu}}\right) + \frac{1}{2}\left(-Q_{\mu\lambda\nu} - Q_{\nu\lambda\mu} + Q_{\lambda\nu\mu} + \cancel{N_{\mu\lambda\nu}}\right) \\
&= \underbrace{\frac{1}{2}\left(T_{\lambda\mu\nu} + T_{\nu\lambda\mu} + T_{\mu\lambda\nu}\right)}_{\text{Contorsion}} + \underbrace{\frac{1}{2}\left(Q_{\lambda\mu\nu} - Q_{\nu\lambda\mu} - Q_{\mu\lambda\nu}\right)}_{\text{Disformation}}.
\end{aligned} \tag{B.0.9}$$

Finally, we can write the general affine connection coefficients, using Eqs. (B.0.6) and (B.0.9), as

$$\boxed{\Gamma^{\lambda}{}_{\mu\nu} = \tilde{\Gamma}^{\lambda}{}_{\mu\nu} + K^{\lambda}{}_{\mu\nu} + L^{\lambda}{}_{\mu\nu}} \tag{B.0.10}$$

where

$$K^{\lambda}{}_{\mu\nu} := \frac{1}{2} g^{\lambda\alpha}\left(T_{\alpha\mu\nu} + T_{\nu\alpha\mu} + T_{\mu\alpha\nu}\right) \tag{B.0.11}$$

is known as the *contorsion* and

$$L^{\lambda}{}_{\mu\nu} := \frac{1}{2} g^{\lambda\alpha}\left(Q_{\alpha\mu\nu} - Q_{\nu\alpha\mu} - Q_{\mu\alpha\nu}\right) \tag{B.0.12}$$

the *disformation*. The contorsion tensor is antisymmetric with respect to the first and last index, $K_{\lambda\mu\nu} = -K_{\nu\mu\lambda}$, whereas the disformation is symmetric on the last two indices, $L_{\lambda\mu\nu} = L_{\lambda\nu\mu}$.